DEVELOPING FAST AND EFFICIENT MOLECULAR DIAGNOSTIC TOOLS FOR HUMAN INVASIVE CANDIDIASIS

By

Mohd Hanif bin Jainlabdin

Thesis submitted for the degree of Doctor of Philosophy

School of Biological Sciences

Royal Holloway, University of London

March 2019

DECLARATION OF AUTHORSHIP

I, Mohd Hanif bin Jainlabdin, hereby declare that the work carried out and presented in this thesis is my own.

Signature: 

Date: 31/05/2019

ACKNOWLEDGEMENTS

I would like to express my gratitude to my supervisor, Dr Jorge Tovar-Torres for the continuous support of my PhD research, for his patience, motivation, and immense knowledge. His expertise was invaluable in the formulating of the research topic and methodology in particular. Without his guidance and persistent help, this thesis would not have been possible.

I would like to thank my advisors, Professor Simon Cutting and Dr Shobana Dissanayeke for their encouragement and, insightful comments.

My sincere thanks also go to Dr Ambalika Batra, and Dr Christopher Pull for their wonderful collaboration and guidance in a statistical analysis of data.

I thank my fellow lab mates in the School of Biological Sciences, Ucheoma Ugoji, Noor Sharif, Ravinder Bhardwaj, James March, Alaa Hussien-Ali, Ilda Hassan and the former project students, Atia Jakfar and, Amrita Chudasama who were of great support in deliberating over our problems and findings, as well as providing happy distraction to rest my mind outside of my research.

A special thanks to my family. My wife, Diana has been incredibly supportive of me throughout this entire process and has made countless sacrifices to help me get to this point. My joyful daughters, Chqyra and Chqish, their cooperation, and motivation has given me the strength to continue the work until completion. I owe a special thanks to my mother-in-law, father-in-law, and my mother, for all of the sacrifices that they have made on my behalf.

Last, but not least, I am much indebted to my father, the late Mr Jainlabdin Mohd Ismail. I dedicate this thesis to him.

ABSTRACT

Infection with yeasts of the genus *Candida* can cause invasive human candidiasis in hospitalised immunosuppressed patients. Mortality rates are high due to the lack of specific clinical signs of infection and of reliable diagnostic tools. Early diagnosis could facilitate implementation of accurate treatment and save lives but currently used diagnostic methods based on microbial culture and taxonomic identification are time-consuming, cumbersome and non-specific. To address this problem, this research explores the potential of two different biomarker detection platforms as simple nucleic acid biosensors for the diagnosis of invasive candidiasis. These include Multiplex Probe Amplification (MPA) and Multi-component Nucleic Acid Enzymes (MNAzymes). In all cases assay specificity is conferred by diagnostic probes and amplification primers designed from the internal transcribed spacer (ITS) and D1/D2 domains of the ribosomal DNA locus. A single-tube MPA assay was developed which relies on multiple-biomarker probe pairs with unique melting temperature profiles. Specific probe hydrolysis during amplification leads to measurable change(s) in post-amplification melting profiles compared with the negative control. Nine *Candida* species associated with invasive candidiasis were targeted by the MPA-*Candida* assay, including antifungal-resistant *C. auris*, *C. glabrata* and *C. krusei*. A unique internal control certifies assay functionality and avoids false-negative results. The MPA-*Candida* assay can also be coupled with an independent pan-fungal assay, exhibiting detection limits of 10-100 genomic copies. *In vitro* characterisation of the assay and its evaluation against a standardised *Candida* panel and a commercially available *Candida* diagnostic kit are reported. The MPA-*Candida* assay was further optimised to incorporate a pan-fungal biomarker for a single-tube reaction in either two or three fluorescence detection channels. Finally, the engineering and characterisation of an isothermal MNAzyme assay for *Candida* diagnosis was also investigated. Here, homology-dependent self-assembly of a hydrolytic MNAzyme is driven by a synthetic single-stranded oligonucleotide complementary to the target biomarker. Catalytic activity is monitored by hydrolysis of dual-labelled substrate probe, which is detectable in a qPCR instrument. In conclusion, the development of effective diagnostic tools for invasive candidiasis could save thousands of lives and find clinical, epidemiological and outbreak control applications.

TABLE OF CONTENTS

LIST OF FIGURES

CHAPTER 1

CHAPTER 2

CHAPTER 3

CHAPTER 5

CHAPTER 6

LIST OF TABLES

CHAPTER 1

CHAPTER 2

CHAPTER 3

CHAPTER 4

CHAPTER 5

CHAPTER 6

ABBREVIATIONS

a.u.	arbitrary unit
$A_{260/280}$	absorbance 260/280 nm ratio
AF	assembly facilitator
AFc	assembly facilitator component
AI	assembly inhibitor
AIDS	acquired immune deficiency syndrome
AMR	antimicrobial resistance
ANCOVA	analysis of covariance
ANOVA	analysis of variance
BAL	bronchoalveolar lavage
BDG	β-D-glucan
BHQ	black hole quencher
BLAST	basic local alignment search tool
bp	base pair
CAGTA	*Candida albicans* germ tube antibody
CFU	colony-forming unit
CI	confidence interval
C_p	heat capacity
CT	computed tomography
C_t	threshold cycle
CV	coefficient of variation
dNTP	deoxyribonucleotide triphosphate
E	efficiency
EDTA	ethylenediaminetetraacetic acid
EIA	enzyme immunoassay

ELISA	enzyme-linked immunosorbent assay
EORTC	European Organization of Research and Treatment of Cancer
FAM	6-carboxy-fluorescein
FDA	Food and Drug Administration
FISH	fluorescent *in situ* hybridisation
FPCRI	fungal PCR initiative
GM	galactomannan
HEX	hexachloro-fluorescein
HIV	human immunodeficiency virus
HPLC	high performance liquid chromatography
HPV	human papilloma virus
HSCT	haematopoietic stem cell transplantation
Hwp1	hyphal wall protein 1 gene
IC	internal control
ICU	intensive care unit
IFI	invasive fungal infection
IGS	intergenic spacer
IPA	invasive pulmonary aspergillosis
ISHAM	International Society for Human and Animal Mycology
ISO	International Organisation for Standardisation
ITS	internal transcribed spacer
JOE	2,7- dimethoxy-4,5-dichloro-6-carboxyfluorescein
K_{cat}	catalytic constant
KCl	potassium chloride
K_m	Michaelis-Menten constant
K_{obs}	observed rate constant

L	litre
LAMP	loop-mediated isothermal amplification
LB	Luria-Bertani
LSU	large subunit
M	molar
MALDI-TOF	matrix-assisted laser desorption-ionisation time of flight (mass spectrometry)
MCM7	mini-chromosome maintenance protein gene
$MgCl_2$	magnesium chloride
MIC	minimum inhibitory concentration
MNAzymes	multi-component nucleic acid enzymes
MPA	multiplex probe amplification
MSG	mycoses study group
mtCytB	mitochondrial cytochrome B gene
N/A	not applicable
NaCl	sodium chloride
NCPF	national collection of pathogenic fungi
ND	not detected
NDC	no DNA control
ng	nanogram
NMR	nuclear magnetic resonance
NPV	negative predictive value
ns	not significance
ODI	optical density index
Partzyme	partial enzyme
PCO	partially-complementary oligonucleotide

PCR	polymerase chain reaction
PNA	peptide nucleic acid
ppt	precipitation
PTZ	piperacillin/tazobactam
qPCR	quantitative polymerase chain reaction
R^2	coefficient of determination
rDNA	ribosomal DNA
RFLP	restriction fragment length polymorhism
RPA	recombinase polymerase amplification
RPM	revolutions per minute
RPR1	ribonuclease P RNA gene
RT	real-time
RuO	research use only
S.O.C	super optimal broth with catabolite repression
SD	standard deviation
SDA	Sabouraud dextrose agar
SDS	sodium dodecyl sulphate
SERRS	surface-enhanced resonance Raman spectroscopy
SIBA	strand invasion based amplification
Sub	substrate
T2MR	T2 magnetic resonance
TBE	tris-borate-EDTA
TEF	translation elongation factor
THO	target-hybridising oligonucleotide
T_m	melting temperature
Tris-HCl	tris hydrochloride

UK	United Kingdom
USA	United States of America
UV	ultraviolet
V_{max}	maximum velocity
WCD	whole-genome duplication
YPD	yeast peptone-dextrose

CHAPTER 1: Introduction

1.1 Invasive fungal infections (IFIs)

IFIs are serious infections caused by various fungal species, often life threatening to patients with impaired immune systems. Filamentous fungi are normally ubiquitous in the environment and yeasts exist as part of human normal micro flora. Whilst almost any fungus has the potential to cause invasive disease, *Candida*, *Pneumocystis, Aspergillus* and *Cryptococcus* are the most significant genera causing death in humans. The latest estimates on the global burden of IFIs show 700,000 cases of invasive candidiasis, 500,000 cases of *Pneumocystis jirovecii* pneumonia, 250,000 cases of invasive aspergillosis and, 223,100 cases of cryptococcal meningitis complicating Human Immunodeficiency Virus infection and Acquired Immune Deficiency Syndrome (HIV/AIDS) (Bongomin *et al.*, 2017). Although the incidence related to superficial infections are much higher, invasive infections result in higher morbidity and mortality rates among hospitalised patients (Webb *et al.*, 2018; Brown *et al.*, 2012). The trends of IFIs in the public health are expected to increase largely because of the expanding susceptible host and the use of immune suppressive agents that predispose the patients to the fungal infections (Casadevall, 2018). Concerted actions from public awareness, effective hospital infection controls and surveillance programmes are important to curb the problem.

Several reasons have been proposed for the increase in fungal infections, including the use of immunosuppressive agents and chemotherapy for cancer treatments, broad-spectrum antibiotics, prosthetic devices and grafts, and more aggressive surgery. The *Candida* spp., *Cryptococcus* spp., *Aspergillus* spp. and other emerging pathogens, such as the *Fusarium* spp. and Zygomycetes are largely opportunists, causing infection when host the defence mechanisms are breached.

Moreover, the infections related to the endemic dimorphic fungi, *Histoplasma capsulatum*, *Blastomyces dermatitidis*, *Coccidioides immitis*, are opportunistic in nature and highly prevalent in immunocompromised individuals, such as HIV/AIDS patients, transplant recipients or those taking steroids (Nosanchuk, 2016). Pulmonary involvement may prevail during onset of infection but clinical signs and symptoms such as fever, cough, chest pain and respiratory failure are non-specific and may be the sole manifestation (Person, Kontoyiannis & Alexander, 2011). The human innate and adaptive immune responses are important to control invasive fungal infections. The host cells express germ-line pattern recognition receptors (PRRs) present in monocytes, macrophages, dendritic cells, B-cells, T-cells and endothelial cells, which are responsible in recognising fungal pathogen-associated molecular patterns (PAMPs) (Blanco & Garcia, 2008). Impaired immune functions especially among cancer patients or those receiving haematopoietic stem cell transplantation (HSCT) were reported with high mortality rates, of which more than 50% were associated with IFIs (Ma *et al.*, 2018). Furthermore, mortality rates in neutropenic patients with candidiasis are approximately 50% and may approach 100% for those with invasive aspergillosis, fusariosis, or trichosporonosis (Odabasi *et al.*, 2004). These statistics have drawn special attention to fungal infections leading to better management of these infections.

Current epidemiological trends recognise *Candida* species as the most common fungal pathogen isolated from the blood of immunocompromised patients and an important cause of nosocomial infections (Wisplinghoff *et al.*, 2014). Despite the availability of antifungal drugs, *Candida* species infections are reported with mortality rates as high as 60% in candidaemia (De Rosa *et al.*, 2015; Bassetti *et al.*, 2018). An increase of up to 20% mortality rates has been demonstrated in invasive candidiasis for every 12 hours delay of initiation of an effective antifungal therapy (Morell et al.

2005). Late or no treatment of invasive candidiasis are independent predictors of death (Denning 2003). Therefore, improvements from the current state of diagnosis which is based on the microbiological cultures and an effective administration of antifungal therapy are pivotal for a better management of *Candida* infections.

1.2 Human pathogenic *Candida* species

Yeast of the genus *Candida* is a normal commensal of the human skin, gastrointestinal and genitourinary tracts but, the infections on the mucosal surfaces caused by this species are extremely frequent. Although many *Candida* species exist, only a small number are pathogenic to humans. Up to 90% of all *Candida* infections are caused by *C. albicans*, *C. glabrata*, *C. parapsilosis*, *C. tropicalis* and *C. krusei* (Guinea, 2014; Ng *et al.*, 2015). Less frequent pathogenic *Candida* species include *C. dubliniensis*, *C. guilliermondii*, *C. lusitaniae*, *C. rugosa*, *C. orthopsilosis* and *C. metapsilosis*, and emerging of rare species have been reported as infectious agent (Turner & Butler, 2014). A newly emerging *C. auris*, multidrug-resistant yeast, has caused nosocomial outbreaks in the United Kingdom (UK) and multiple countries across five continents (Rhodes *et al.*, 2018). In the UK, there was an estimated 6,500 cases of invasive candidiasis with one third of the manifestations in the bloodstream infections (Public Health England, 2017).

C. albicans remains the human major fungal pathogen and the most common cause of systemic fungal infections among immunocompromised patients (Guinea, 2014). *C. albicans* is usually susceptible to azole antifungals, however, overuse of the drugs in therapy and prophylaxis has led to a rise in non-*albicans* species (Ruhnke, 2014). In many hospitals, *C. glabrata* is the second most cause of candidaemia after *C. albicans* (Colomba *et al.*, 2014; Pfaller & Castanheira, 2016; Public Health

England, 2017). Increasing incidences related to *C. glabrata* is alarming as the species is well-known for its reduced susceptibility to antifungal drugs (azoles and echinocandins).

C. krusei is another clinically significant species, although less common in candidaemia cases in the UK, it is intrinsically resistance to fluconazole and is highly prevalent among patients with recent exposure to fluconazole (Pfaller et al. 2008). It is also noted that *C. krusei* showed resistance to flucytosine and reduced susceptibility to other antifungal drugs. The Minimum Inhibitory Concentration (MIC) of *C. krusei* towards fluconazole is significantly higher (64 μg/mL) compared to *C. albicans* towards the same antifungal drug (2 μg/mL) (Badiee *et al.*, 2017). It is therefore not surprising that *C. krusei* is associated with a higher mortality rate than *C. albicans* (Abbas *et al.*, 2000). *C. krusei* is frequently recovered from patients with haematological malignancies complicated with neutropenia and transplant recipients.

C. parapsilosis, is a member of the skin microbiota, often associated with catheter-related candidaemia and can efficiently colonise prosthetic devices. This species produces slime as a virulence factor enabling it to persist and survive on the environmental surfaces and the skin of healthcare workers (Welsh *et al.*, 2017). Of note, this species is also reported at the second rank after *C. albicans* causing candidaemia in some centres in the United States of America (USA) (Wisplinghoff *et al.*, 2014). It is more prevalent among early age patients, whereas the opposite is true for *C. glabrata.*

C. tropicalis has also gained importance due to its high prevalence (41.6%) among patients in the intensive care unit (ICU) across hospitals in India (Chakrabarti *et al.*, 2015). The number is also highly recorded in the Central and South America countries (Zuza-Alves, Silva-Rocha & Chaves, 2017). In the UK, *C. tropicalis* was recorded as low (3%) causing bloodstreams infections (Public Health England, 2017).

The risk factors include immunocompromised patients with leukaemia, receiving chemotherapy for cancer treatments and prolonged hospitalisation in the ICU (Leung *et al.*, 2002).

Recently, multidrug-resistant *C. auris* has caused outbreaks of bloodstream and wound infections in healthcare settings around the world (Schelenz *et al.*, 2016; Rhodes *et al.*, 2018). The species was first identified in Japan as a cause of ear infection in an elderly patient (Satoh et al. 2009). *C. auris* has been misidentified as *C. haemulonii*, a less virulent *Candida* species, by most commercial identification systems (Centres for Disease Control and Prevention, 2018). Improving the diagnosis of *C. auris* is essential to support clinical decision making, and to provide timely prescription of therapeutics drugs to patients (Sexton *et al.*, 2018).

1.3 Cell biology of yeasts and phylogenetics

Yeasts are single-celled fungi that reproduce asexually by the process of septation and separation of daughter cells, either by budding (blastoconidia formation) or binary fission (Brooks *et al.*, 2013). Yeasts are different from most fungi which are multicellular (moulds) and exist as filament-like hyphae, which can grow and form a mycelial map. Human fungal pathogens, including *Candida* species, *Cryptococcus* species and *Histoplasma* species produce yeast cells that propagate during infection through budding formation (Kauffman *et al.*, 2003). Meanwhile, *Penicillium marneffei* yeast cells can divide by fission to form two uninucleate cells, and these cells can further propagate by binary fission (Vanittanakom *et al.*, 2006). The release of yeast cells in the human bloodstream will allow rapid dissemination in the host and organs, causing systemic and deep-seated fungal infections.

Some of the yeasts such as *H. capsulatum*, *B. dermatitidis* and, *C. immitis* are categorised as dimorphic for their ability to form hyphae under certain environmental conditions. Notably, *C. albicans* is called a polymorphic fungus, as it can form several morphologies from the budding yeast cells, pseudohyphae and hyphae (Gow & Yadav, 2017). The term pseudohyphae describes an elongated budding yeast cell that remains attached after cytokinesis which forms branches of yeast cells with a constriction between the cells (da Silva Dantas *et al.*, 2016). Due to its medical importance, *C. albicans* is the most studied yeast within its genus. The cell wall of *C. albicans* plays pivotal roles in pathogenesis; as the first structure that comes into contact and maintains its adherence to the host cells, this is responsible for the invasion of the host cells and, carries important antigenic determinants of the fungus for host recognition (Ruiz-Herrera *et al.*, 2006). Figure 1.1 illustrates the fungal cell wall composed of an inner polysaccharide surfaces of β-glucans and chitin and an outer surface of mannoproteins which are bound to the inner surface through the lateral chains of β-1,6-glucan or 1,3-glucan (Gow *et al.*, 2012). Notably, except for *Cryptococcus*, which is composed of the glucuronoxylomannan and galactoxylomannan polysaccharides capsule (Nalintya, Kiggundu & Meya, 2017; Nelson & Lodge, 2006).

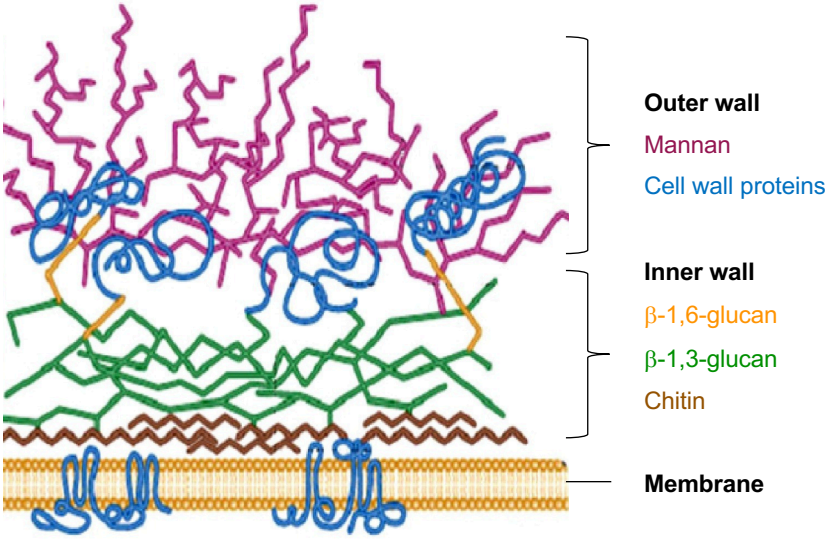

Figure 1. 1 Schematic representation of the molecular structure of the *C. albicans* cell wall. The figure adapted from Gow *et al.*, (2012).

The metabolism of *C. albicans* is adaptable to niche-specific conditions, facilitating cell growth within the host during infections (Martin *et al.*, 2011). The critical characteristics of *C. albicans* as a pathogen are its adaptability to use a variety of micronutrients (da Silva Dantas *et al.*, 2016), the active manipulation of the environmental pH and its adaptation to stresses (Brown *et al.*, 2014; Hube, 2009).

The *Candida* genus is diverse, and its taxonomy classification was previously based on morphological features and sexual reproduction (Guarro, Gené & Stchigel, 1999). The advancement of DNA based taxonomy has broadened the understanding of the relationship between the *Candida* species and the fungal kingdom. Systematic DNA sequence analysis by the recognition of fungal DNA barcoding serves to define fungal species relationships and their evolution (Robert *et al.*, 2011; Schoch *et al.*, 2012). The genomic data ascertained the classification of the *Candida* species belonged in the phylum Ascomycota and the important order of Saccharomycetales (Hibbett *et al.*, 2007). Phylogenetic analysis also demonstrated that *C. glabrata* belongs to the WCD (whole-genome duplication) clade which is relatively closer to

Saccharomyces cerevisiae than to *C. albicans* and *C. dubliniensis*, *C. parapsilosis*, or *C. tropicalis*, which are classified in the CTG clade (CTG codon codes for serine, rather than leucine) (Brunke & Hube, 2013; Turner & Butler, 2014). A non-exhaustive list of *Candida* species in approximate order of phylogenetic relationship is demonstrated in Table 1.1.

Table 1. 1 Classification of *Candida* pathogenic species according to phylogenetic analysis. The table adapted from Brunke & Hube, (2013).

***Candida* species**	**Teleomorphic/sexual name**	**Ploidy**
CTG clade species		
C. albicans		Diploid
C. dubliniensis		Diploid
C. tropicalis		Diploid
C. parapsilosis		Diploid
C. orthopsilosis		Diploid
C. metapsilosis		Diploid
C. famata	*Debaryomyces hansenii*	Haploid
C. lusitaniae	*Clavispora lusitaniae*	Haploid
C. guilliermondii	*Meyerozyma guilliermondii; Pichia guilliermondii*	Haploid
WCD clade species		
C. krusei	*Issatchenkia orientalis; Pichia kudriavzevii*	Haploid
C. glabrata		Haploid
C. kefyr	*Kluyveromyces marxianus*	Haploid
C. norvegensis	*Pichia norvegensis*	Haploid
C. inconspicua	*Pichia cactophila*	Haploid
C. lypolytica	*Yarrowia lipolytica*	Haploid

*CTG clade, the CTG codon exchange from leucine to serine; WCD, the species that have undergone whole-genome duplication. Haploid represents isolates exist in stable haploids; diploids may also be formed.

1.4 Traditional diagnostic methods for fungal infections

1.4.1 Blood cultures and histopathology

Blood culture is considered the "gold standard" for the diagnosis of invasive candidiasis, particularly when candidaemia is suspected (De Pauw *et al.*, 2008). Positive culture results can yield a specific aetiological agent and allows for susceptibility testing (Kozel & Wickes, 2014). However, autopsy results suggest that blood cultures are 50% less sensitive for cases with proven invasive candidiasis (Clancy & Nguyen, 2013). Therefore, negative blood cultures do not rule out invasive candidiasis. A more extended time period for cultures positivity which typically can take 24 to 72 hours further complicated the use of blood culture for early diagnosis of invasive candidiasis (Pfaller & Castanheira, 2016). Fully automated blood culture systems such as the BACTEC® (Becton–Dickinson Diagnostic Systems, USA) and the BacT/Alert® (BioMérieux, France) are routinely performed in healthcare facilities (Pryce *et al.*, 2006). The alert sign from the blood culture system for the positive results signals the subculture of the broth onto the solid mycological media for further identification (Horvath *et al.*, 2004). The isolation and identification of the *Candida* species can be performed in parallel on chromogenic media. The principle for the use of the media is the formation of different coloured colonies with varied morphology which result from the cleavage of chromogenic substrates by species-specific enzymes (Alam *et al.*, 2014). The CHROMagar *Candida* is one of the chromogenic agars that are commercially available and could provide faster identification of major *Candida* species (Nadeem, Hakim & Kazmi, 2010).

Positive blood cultures for invasive aspergillosis is rare and hence have a little value as a diagnostic tool, even in cases of widely disseminated disease (Barton, 2013). A positive culture result may represent environmental contamination or colonisation,

especially when the samples are from a non-sterile site therefore; overall interpretation is necessary by considering the patient's risk factors (Ostrosky-Zeichner, 2012). Interestingly, the study conducted by Kontoyiannis *et al.*, (2000), to differentiate between true bloodstream aspergillosis and a contamination issue in their institution, found that the false-positive results for the *Aspergillus* species do occur due to culture media contamination. However, it is also important to recognise that positive culture results in a high-risk patient may suggest the presence of infection (Kauffman *et al.*, 2011). *Aspergillus* species also are slow-growing fungi and can take several days to weeks to sporulate on an appropriate selective media (Borman & Johnson, 2014). Also, cultures and microscopic morphology lack specificity and identification of the species, is laborious to perform and require specialised expertise (Reyes-Montes *et al.*, 2018). Histopathology of the clinical specimens has the advantage of detecting fungal elements from the targeted biopsies including the host response or tissue necrosis (Arvanitis *et al.*, 2014). However, histopathologic analysis is not always suitable for all patient groups, for example, patients with severe thrombocytopenia tend to have a high possibility of bleeding complications thus, preventing the use of biopsy or other invasive techniques (Oz & Kiraz, 2011).

1.4.2 *Candida albicans* Germ Tube Antibody (CAGTA) and antibody (anti-mannan), antigen (mannan) detection

The CAGTA test is based on the detection of specific IgG antibodies against the antigens located on the surfaces of the *C. albicans* germ tubes by indirect immunofluorescence (Martín-Mazuelos *et al.*, 2017). The test has reported a sensitivity of 91.3%, and a specificity of 68.1% for the diagnosis of invasive candidiasis among critically-ill patients (Trovato *et al.*, 2019). The test sensitivity can be lower for detection of non-*albicans Candida* (Clancy & Nguyen, 2018a). The test has shown

clinical utility for reducing the mortality rates in ICU patients with positive CAGTA assay that allowed appropriate antifungal treatment (Zaragoza *et al.*, 2009). The sensitivity of CAGTA assay is not affected by the prior intake of antifungal drugs or *Candida* colonisation, demonstrating it as a useful serological biomarker for diagnosis of the invasive candidiasis in ICU settings (Bassetti *et al.*, 2018). The combination of the CAGTA and β-D-glucan tests as a diagnostic tool has shown a higher sensitivity of 97% in a population studied (Martínez-Jiménez *et al.*, 2015).

Other serological biomarkers available for diagnosis of the invasive candidiasis are the mannan antigen and anti-mannan antibody detections (Duettmann *et al.*, 2016). Optimal result can be achieved from the combination of these two biomarkers. The combination of the mannan and anti-mannan antibody detections has a sensitivity of 83% and a specificity of 86% in patients with *Candida* species infections (Clancy & Nguyen, 2018b). The high Negative Predictive Values (NPV) of the test is useful to guide clinical decisions regarding the need for antifungal therapy in immunocompromised patients (Ellis *et al.*, 2009). Other than *Candida* immunogenic detection, the increased level of the metabolic products from the *Candida* species such as enolase or D-arabinitol/creatine ratio has been demonstrated in patients with invasive candidiasis (Ostrosky-Zeichner, 2012). D-arabinitol is produced by most of the *Candida* species with exceptions for *C. krusei* and *C. glabrata*. However, an elevated D-arabinitol/creatine ratio level is observed in patients with renal failure. Fungal antigens and metabolites are usually cleared rapidly from the immunocompromised patient's body leading to false negative results of the antibody tests. (Alam *et al.*, 2014).

1.4.3 Galactomannan (GM) detection for *Aspergillus*

GM is the main polysaccharide component of the cell wall of the *Aspergillus* species, which is released into the bloodstream during hyphae growth (Taghizadeh-Armaki *et al.*, 2017). The antigen GM is detectable from serum, bronchoalveolar lavage (BAL) and cerebrospinal fluid (CSF) and can be considered specific for the diagnosis of invasive aspergillosis (Eigl *et al.*, 2017). However, other fungal species, *Penicillium* spp., *Fusarium* spp. may also contain a smaller amount of GM and can lead to a false-positive test to invasive aspergillosis (Barton, 2013). The sandwich enzyme-linked immunosorbent assay (ELISA) Platelia® *Aspergillus* (Bio-Rad, USA) is the most commonly used test for GM antigen quantification and is included in the European Organization of Research and Treatment of Cancer/Mycoses Study Group (EORTC/MSG) as a mycological criterion of probable invasive aspergillosis (De Pauw *et al.*, 2008). The recommended cut-off value is an optical density index (ODI) of ≥0.5 for a positive result in serum GM detection (Zhou *et al.*, 2017; De Pauw *et al.*, 2008).

The sensitivity and specificity of the GM assay ranges from 71-75% and 80-89% for invasive aspergillosis and the value can vary considerably due to factors such as the patient population, host factors, nutrition of the patient, and most importantly it can be affected by prior treatment (Zhou *et al.*, 2017; Hsu *et al.*, 2014). The main utility of the GM test is in the high-risk haemato-oncological patients especially with the combination test with Computed Tomography (CT) imaging, in the early diagnosis of invasive aspergillosis (Ruhnke *et al.*, 2018). The result agreement between the GM test from BAL and PCR tests have highly supported the diagnosis of pulmonary aspergillosis (Reinwald *et al.*, 2012). One of the significant problems with the GM assay are false positive results. The use of the β-lactam antibiotics such as piperacillin/tazobactam (PTZ) in patients was reported for false-positive detections in the Platelia GM assay (Alhambra *et al.*, 2007). It has been suggested that the GM was

passed to the PTZ through the production of piperacillin as a fermentation product of the *Penicillium* species that also contain GM in the cell wall (Vergidis *et al.*, 2014). False-positive results are frequent in neonates and children colonised by *Bifidobacterium* spp. (Arendrup, Fisher & Zaoutis, 2009). In contrast, the sensitivity of the GM test is negatively affected by the prior use of azole drugs as a preventive treatment (Barton, 2013).

1.4.4 β-D-glucan (BDG) for pan-fungal detection

BDG is a polysaccharide component of fungal cell walls found in most fungal pathogens (Kolomeyer *et al.*, 2018). Due to its universal presence in the fungal species but not in humans, bacteria, or viruses, BDG detection is useful for a pan-fungal diagnostic test (Theel & Doern, 2013). The BDG test is routine in hospitals for surveillance and diagnosis of invasive candidiasis, invasive aspergillosis and *Pneumocystis* pneumonia but, not for cryptococcosis and mucormycosis (Pfaller & Castanheira, 2016; Passos *et al.*, 2017). Detection of the BDG is not reliable for the *Cryptococcus* spp. and the *Mucor* sp., as the amount of the component, is more variable and rarely detected by the BDG assay (Ostrosky-Zeichner, 2012).

The BDG assay is based on the activation of a coagulation cascade, which uses purified components from horseshoe crabs (Hope, Walsh & Denning, 2005). The assay was developed to detect glucan and measure transformation of a chromogenic substrate which is quantifiable by a spectrophotometer (Azoulay *et al.*, 2016). One of the BDG assays, the Fungitell (Associates of Cape Code, USA) is FDA-approved (Food and Drug Administration) for use on serum and the test was included in the EORTC/MSG mycological criteria for classification of probable invasive fungal infection (De Pauw *et al.*, 2008). The meta-analysis conducted by Karageorgopoulos *et al.*, (2011) included 16 studies which reported that the overall sensitivity and

specificity of BDG assays is 76.8% and 85.3% and respectively. The test showed high NPV of 94% (with a 10% prevalence of IFI) and is practical to exclude the fungal disease from other infections (Azoulay *et al.*, 2016). However, given the fact that the fungi are ubiquitous in the environment, the false positive of the test is common (Hsu *et al.*, 2014).

1.4.5 Antigen detection and lateral-flow assay for cryptococcosis

Cryptococcosis is an infection caused by *C. neoformans* and *C. gatti* (Mada & Alam, 2019). The major capsular polysaccharide of *Cryptococcus* spp. termed as glucuronoxylomannan, is released into blood and CSF during the course of cryptococcal meningitis (Nalintya, Kiggundu & Meya, 2017). The detection of the cryptococcal polysaccharide antigen in CSF or serum has been included as a standard method in the diagnosis of cryptococcal meningitis (De Pauw *et al.*, 2008). Latex agglutination testing and enzyme immunoassay (EIA) techniques have been used widely for cryptococcal antigen detection, both demonstrate excellent performance, with 97% sensitivity for the test on CSF (Marchetti *et al.*, 2012). A lateral-flow format of the immunoassay detection of cryptococcal antigen has demonstrated a performance comparable to those of EIA and latex agglutination on CSF and serum samples (Arvanitis *et al.*, 2014). The lateral-flow assay uses gold-conjugated, monoclonal antibodies impregnated onto an immunochromatographic test strip to detect the GXM antigen for all four *C. neoformans* serotypes (Nalintya, Kiggundu & Meya, 2017). The cryptococcal antigen lateral-flow assay is rapid, highly accurate, and has the ability to be performed on different clinical samples including urine samples, making it very promising as a point-of-care diagnostic method (McMullan *et al.*, 2012; Mpoza *et al.*, 2018).

1.5 Molecular diagnostic methods for *Candida* infections

1.5.1 T2 Magnetic Resonance (T2MR)

The T2 *Candida* assay (T2 Biosystems, USA), a recent FDA-cleared diagnostic test for clinical use, has introduced a novel method for detecting *Candida* species directly from the patient's blood sample (Clancy & Nguyen, 2018c). The technology is based on nuclear magnetic resonance (NMR) spectroscopy and has been widely applied in chemistry and radiology (Arvanitis *et al.*, 2014). In brief, a blood sample in the EDTA (Ethylenediaminetetraacetic acid) collection tube is loaded into a fully automated instrument platform, T2DX, to provide a sample-to-answer diagnostic test. It lyses the yeast cells by mechanical bead-beating, amplifies the target sequence from the multicopy internal transcribed spacer region 2 (ITS2) of the fungal ribosomal DNA (rDNA) and finally detects amplified DNA using magnetic resonance technology (Mylonakis *et al.*, 2015). Specifically, *Candida* DNA amplified in blood hybridises to nanoparticles coated with target-complementary oligonucleotide probes. The nanoparticles aggregate into clusters which alter T2 magnetic resonance (MR) signals producing a 'signature'. The signature is then statistically compared to a known database to identify the target of interest, in this case, the *Candida* species. The flow of the T2MR is illustrated in Figure 1.2. In a preliminary study, the T2MR assay can identify the five major *Candida* species at a sensitivity of 91.1% and the limit of detection was found to be 1 Colony-forming Unit (CFU)/mL for *C. tropicalis* and *C. krusei*, 2 CFU/mL for *C. albicans* and *C. glabrata*, and 3 CFU/mL for *C. parapsilosis* in blood within 3 to 5 hours (Mylonakis *et al.*, 2015). The median time of detection is 4.2 hours compared to 129 hours in blood culture-based diagnostic. In addition to the *Candida* panel, T2Biosystem also released their product for the detection of multidrug-

resistant *C. auris*, T2*C. auris* panel. The panel is currently for research use only and yet to be validated for clinical utility. The T2*C. auris* assay can detect all four known clades of *C. auris* and demonstrates a consistent limit of detection at 5 CFU/mL (Sexton *et al.*, 2018).

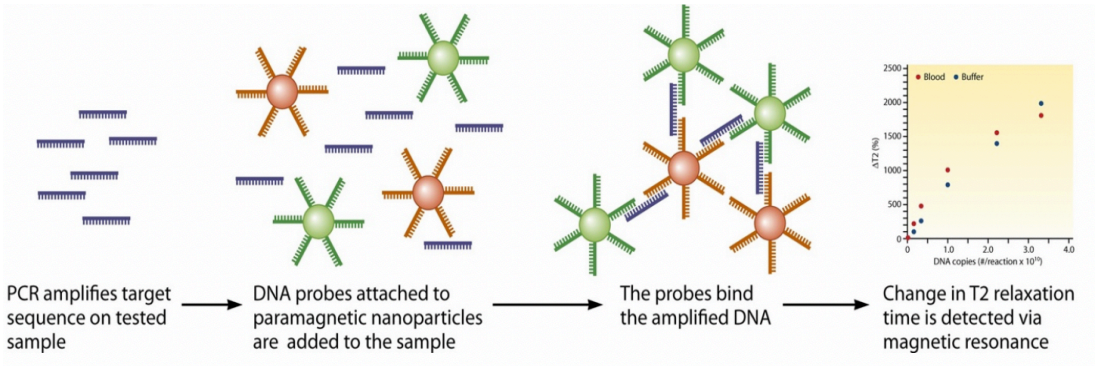

Figure 1. 2 A simplified process of T2MR. Amplification of the target sequence found in the blood sample. The DNA probes coupled with paramagnetic nanoparticles are added to the amplicon and are allowed to hybridise with the amplified sequence. As a result, the signal changes the nanoparticle T2 relaxation time, and the change is detected via magnetic resonance imaging, thus identifying the target. The diagram is adapted from Arvanitis *et al.*, (2014).

1.5.2 Peptide Nucleic Acid-Fluorescent *In situ* Hybridisation (PNA-FISH)

FISH is a technique that uses fluorescent probes to identify target areas on the genomes of microbial pathogens in human samples, which can then be detected by fluorescence microscopy (Figure 1.3). Recently, several studies have evaluated the use of PNA probes in FISH assays. PNAs are synthetic nucleic acid sequences with a neutral polyamide backbone that exhibits more consistent and robust hybridisation characteristics than traditional nucleic acid probes. Yeast Traffic Light PNA-FISH (AdvanDx, USA), a FDA-cleared rapid diagnostic test, can identify five pathogenic *Candida* species within 90 minutes from positive blood cultures. The three-probe

colours coded in the assay represent the general susceptibility of the *Candida* species to the fluconazole with the green indicator for likely susceptible (*C. albicans*/*C. parapsilosis*), red for likely resistance (*C. glabrata*/*C. krusei*) and yellow for inducible resistance (*C. tropicalis*). In multiple studies, PNA-FISH-based assays have been shown to have 99% and 100% sensitivity and specificity respectively (Hall et al. 2012, Shepard et al. 2008). The Yeast Traffic Light PNA-FISH can save between 24 to 48 hours of identification compared to conventional laboratory methods. This approach shows no fluorescence to bacteria and a limited spectrum of detection to only five *Candida* species. The PNA-FISH test successfully showed cost savings at approximately equivalent to £1,300 per patient as a result of the correct choice of antifungal in the patient with candidaemia due to *C. albicans* (Forest et al. 2006). In the same study on the patient group, fluconazole substituted caspofungin, after results of the PNA FISH-testing, has led to a significant decrease in antifungal costs and importantly, allow effective treatment to the patients.

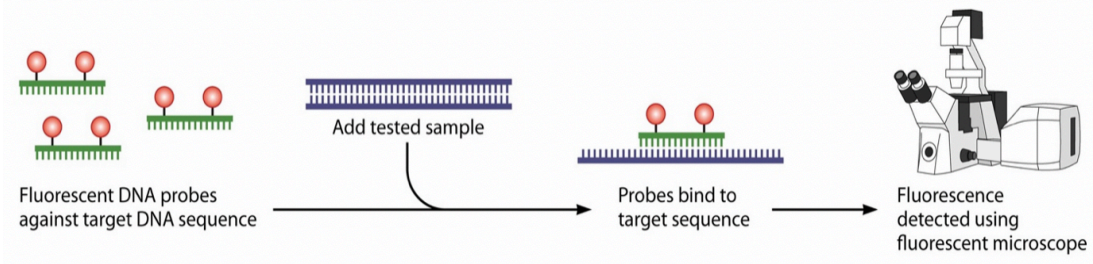

Figure 1. 3 FISH technique. Fluorescent probes against a specific target sequence are mixed with the tested sample and allowed to bind to the complementary DNA sequence, if present in the sample. The excess probes are then washed off, while the bound probes are detected via fluorescence microscopy. The diagram is adapted from Arvanitis *et al*., (2014).

1.5.3 Matrix-Assisted Laser Desorption-Ionisation Time of Flight Mass Spectrometry (MALDI-TOF MS)

MALDI-TOF MS analysis identifies protein fingerprints of an unknown fungus through direct comparison of its spectral pattern with the known patterns of different organisms in databases (Figure 1.4). It can identify pathogenic fungi at the genus, species and even to strain level. FDA-approved MALDI-TOF systems, from the Bruker Maldi Biotyper (Bruker Daltonic, Germany) are able to identify yeasts and moulds in the clinical diagnostic environment (Sanguinetti & Posteraro, 2017; Aslani *et al.*, 2018). Proteomic analysis by MALDI-TOF MS can accelerate species-level identification of yeasts directly from blood cultures, with a sensitivity of 95.9% for *C. albicans* and 86.5% for non-*albicans Candida* species, *C. guilliermondii* being the species most frequently missed (Spanu *et al.*, 2012). This species is also found to be misidentified in other studies including the one tested in the Vitek MS system (Cheng *et al.*, 2016; Dhiman *et al.*, 2011). The *C. guilliermondii* complex is a phenotypically indistinguishable yeast species (Cheng *et al.*, 2016). Updated mass spectral profiles are crucial to improving the identification accuracy of emerging species. Misidentification of multidrug-resistant *C. auris* as *C. haemulonii* was previously reported using an outdated database (Wattal *et al.*, 2017). Currently, Bruker Biotyper with Version Claim 4 System and Vitek with Saramis Version 4.14, are updated databases that should be able to accurately identify *C. auris*, though misidentifications of strains from a few clades have been reported (Centers for Disease Control and Prevention, 2018). Despite advances and acceptance into routine testing in microbiology laboratories, this method does not identify polymycosis, and sample preparation requires time and expertise (Spanu *et al.*, 2012).

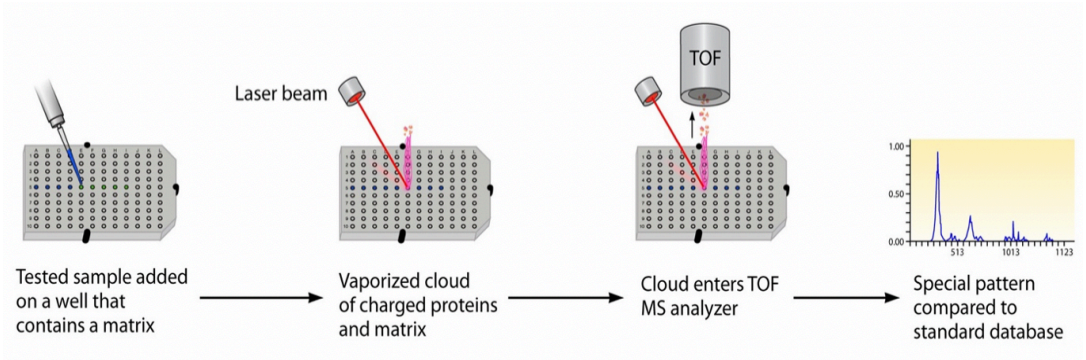

Figure 1. 4 General principles of MALDI-TOF MS. Firstly, the sample is added into a well that contains matrix material which has the ability to absorb ultraviolet (UV) light and transform it into heat. Secondly, a laser beam is targeted to the mix and absorbed by the matrix, and part of the analyte-matrix mix is vaporised and ionised, creating a cloud of ionised protein and matrix. Next, this cloud is subjected to an electric field, which leads the particles to accelerate towards a detector. The mass and charge of each particle determine the time needed to reach the detector. This allows the mass spectrometer to determine the characteristics of the particles within the tested sample. Finally, the produced spectral pattern can be compared against a standard database which allows for the identification of the microorganisms in the samples. The diagram is adapted from Arvanitis *et al*., (2014).

1.5.4 Novel nucleic acid detections platforms

1.5.4.1 Multiplex Probe Amplification (MPA)

MPA is a novel method of detecting multiple targets in the real-time PCR platform. Up to six probes with a unique melting temperature labelled with the same fluorescence dye can be detected in a single channel. Each probe for every target was designed with two oligonucleotides; a dual-labelled target-hybridising oligonucleotide (THO) and partially-complementary oligonucleotide (PCO) (Figure 1.5, panel A). The technology allows utilisation of the unbound THO after amplification to hybridise to its PCO. The PCO is composed of 17% to 23% of nucleotide mismatch against the THO sequence and has a slightly lower annealing temperature compared to the full complementary

target sequence. In the presence of the DNA target sequence, the dual-labelled oligonucleotide preferentially anneals to the fully complementary target sequence at a higher temperature and is hydrolysed during the extension steps in the PCR. In the absence of the target DNA, the intact THO is bound to its PCO and dissociates during the melt curve analysis. The probe fluoresces the most when the THO is hybridised to the PCO and reduces as the temperature is raised (Figure 1.5, panel B). The highest rate of fluorescence change is seen in the melting curve analysis when 50% of the THO dissociated from the PCO at the specific melting temperature (Figure 1.5, panel C) (Fu, Miles & Alphey, 2012).

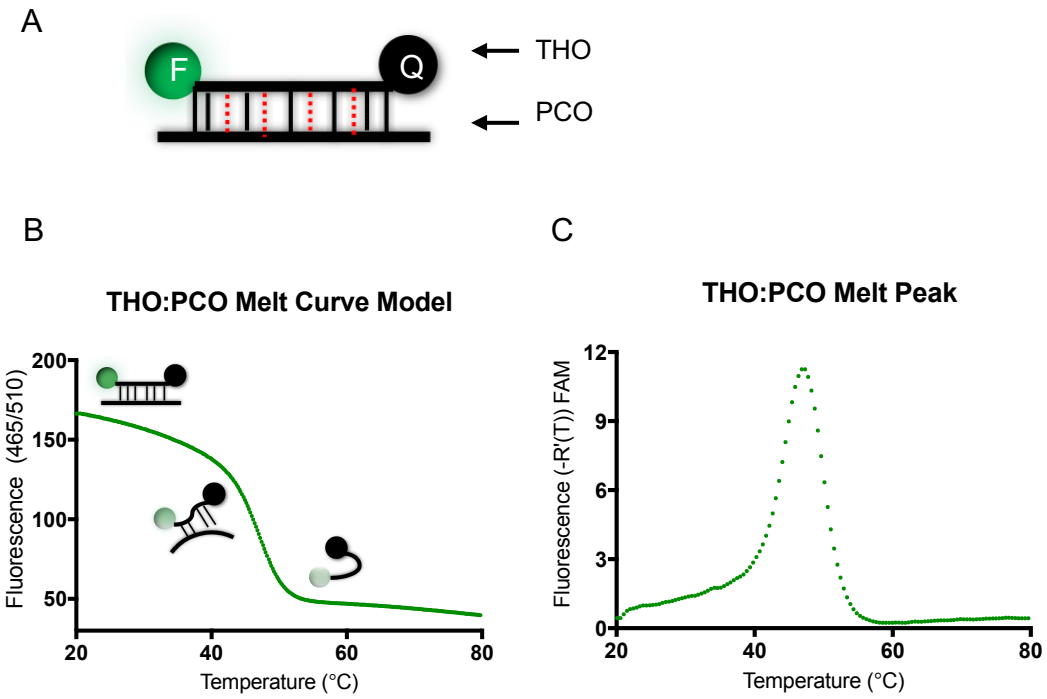

Figure 1. 5 The MPA nucleic acid probe and its melting profile. Panel A) The probe consists of a THO labelled with a fluorophore (F) at the 5'end and quencher (Q) at the 3'end, and attached with a PCO. **Panel B**) The melting curve shows decreased fluorescence emission with increasing temperature. **Panel C**) the negative derivative plot of the emission reading versus temperature reveals a positive value of the melting peak.

1.5.4.2 Multi-component Nucleic Acid Enzymes (MNAzymes)

Ribozymes (ribonucleic acid or RNA enzymes) are catalytic molecules found in nature which are hypothesised to be fossil molecules in a prebiotic 'RNA world' (Silverman, 2008). Representative ribozymes that exist in nature such as hammerhead and hairpin are capable of catalysing the phosphodiester cleavage of RNA sequences (Feldman & Sen, 2001). Conversely, Deoxyribozymes or DNAzymes are artificial molecules and not found in nature (Zhou, Ding & Liu, 2017). The development of catalytic DNA molecules through *in vitro* selection and evolution procedures has introduced a new versatile platform for the design of a variety of therapeutic tools (Fiammengo & Jäschke, 2005). Sharing the advantages of biocompatibility and simplicity of structural prediction and modification with ribozymes, DNAzymes are much more stable and cost-effective than RNA counterparts (Gerasimova & Kolpashchikov, 2010). DNAzymes have an excellent potential for sensing a variety of analytes mainly due to the possibility of catalytic signal amplification. RNA-cleaving DNAzymes are particularly useful because DNAzymes interact with their RNA substrates through Watson–Crick base pairing, and it can be tailored to recognise any RNA sequence (Feldman & Sen, 2001). Two general RNA-cleaving DNAzymes that have been extensively studied are the 10–23 and 8–17 DNAzymes (Santoro & Joyce, 1997) illustrated in Figure 1.6.

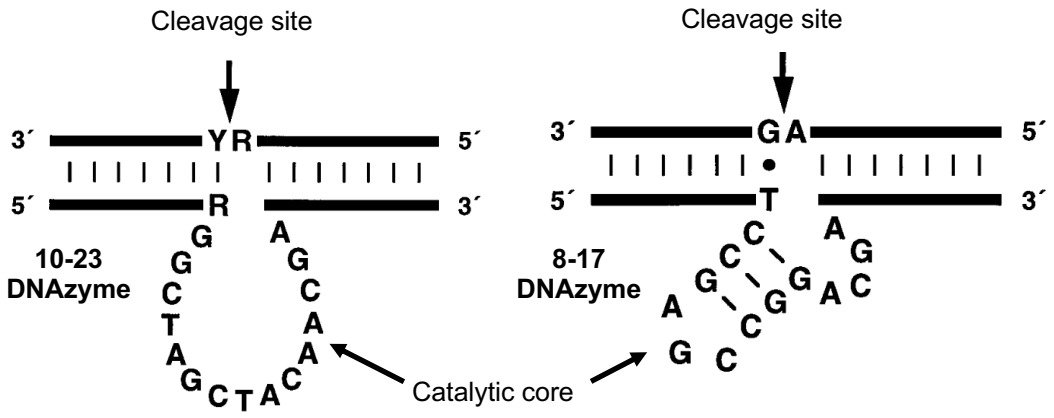

Figure 1. 6 Composition of the 10–23 and 8–17 Deoxyribozymes or DNAzymes. The DNAzyme (bottom strand) is capable of cleaving single-stranded RNA (top strand) at the specific site and forms a product with 2',3'-cyclic phosphate and 5' hydroxyl RNA termini. R = Adenine or Guanine; Y = Uracil or Cytosine. This figure is adapted from Santoro & Joyce, (1997).

Taking advantage of deoxyribozymes, Mokany *et al*., 2010 split the conserved catalytic core domains of 10–23 and 8–17 to form MNAzymes. MNAzymes provide tremendous flexibility in terms of tailoring the nucleic acid input to work with developed universal partial enzymes to produce readout fluorescence signals (output). The partial enzymes (Partzymes) are composed of a target-binding domain, a partial catalytic core derived from DNAzymes and a probe-binding domain (Figure 1.7) (Mokany *et al.*, 2010). The Input sequence, also referred to as the Assembly Facilitator (AF), is a specific sequence of 40- to 44-nucleotide bases that is tailored to complement the target-binding domains. The AF sequences that bind to the target-binding domains allow partial catalytic cores to combine to form a complete catalytic core. The active core can then bind to universal reporter probes at probe-binding domains and cleave them in between the fluorophore and quencher moieties. The loss of proximity between the quencher and reporter cause the release of a fluorescent signal that can be monitored by a spectrofluorometric in real-time.

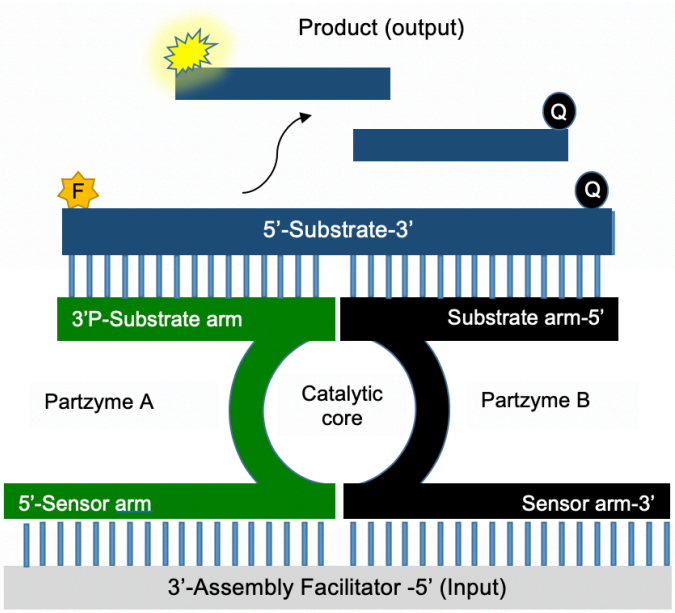

Figure 1. 7 A schematic representation of the association and subsequent cleavage activity of the MNAzyme. Partzyme A and B combine in the presence of the AF, hydrolysing the RNA substrate, separating the fluorophore (F) from the quencher (Q) to allow emissions of the fluorescence signal.

Currently, eight different universal probes have been tested with MNAzymes, and each probe could be labelled with different fluorophores to give distinctive signals (Bone *et al.*, 2014). Furthermore, two different types of MNAzymes that are derived from 10-23 and 8-17 DNAzymes indicates that this technology has the potential for multiplexing, therefore, increasing its versatility to be used in the field of molecular diagnosis. However, MNAzymes derived from the 10-23 nucleic acid enzyme have shown higher enzymatic activity and stable probe hybridisation than those derived from 8-17 nucleic acids (Mokany *et al.*, 2010).

Furthermore, to further increase the versatility of MNAzymes, the molecular switches and cascades were developed by introducing the Assembly Facilitator Components (AFc) and Assembly Inhibitor (AI) (Mokany *et al.*, 2010). This technique is capable of performing switch functions from an 'on' state (active MNAzyme) to an 'off' (inactive MNAzyme) state of the enzyme by relying on the presence of multiple

AFc and an AI. Moreover, this technique can open the possibility of incorporating up to four different substrates, with the ability to label each different substrate with different dyes for multiple detections. Therefore, the detections are performed in stages, starting from the cleavage by an 'initiating MNAzyme', to controlling the formation of the next stages of MNAzymes or also known as 'cascading MNAzymes'. Thus, the whole system will produce four different fluorescent signals indicating the stages of cleavage and cascade by the enzymes and their cleavage products (Mokany *et al.*, 2010). An MNAzyme cascade is a promising technique offering greater sensitivity through the application of a fluorescent dye, which could combine and amplify the detection signals in an isothermal temperature.

1.6 Molecular diagnostic tools for fungal infections

1.6.1 PCR-based diagnostic assays

The purpose of this sub-section is to provide the reader with an overview on the evolution of PCR-based methods in human fungal pathogens diagnostic assays. PCR is a method used for the enzymatic exponential amplification of a specific target region using short primers, leading to detectable amounts of amplified DNA from one or a few original sequences. PCR-based methods are the most common molecular-based approaches in many fields and the core method in fungal molecular diagnostics (Wickes & Wiederhold, 2018). Various methods of PCR exist for qualitative and/or quantitative detection and identification of fungi. Conventional PCR can include nested and multiplex PCR which are very simple to design, but their sensitivity is directly related to the ability to visualise the fragments and their specificity depends on the recognition of the amplicon size for a target species as the final readout

(Kauffman *et al.*, 2011). In contrast to conventional PCR, real-time PCR has shown promising results. The major advantages of real-time PCR include a rapid time to results for some targets and the flexibility of the platform (Bustin, 2005). This approach employs a closed system that provides simultaneous amplification and detection, and limits the risk of assay contamination. Real-time PCR is often fluorescence-based and allows for quantification.

Conventional PCR is not quantitative but is qualitative and has been used to detect, monitor and identify fungi either permitting species-specific, genus-specific, or broad-range (pan-fungal) detection. It relies on specific primer sequences to generate a DNA product that is visualised on an agarose gel or after capillary electrophoresis. The amplified products of the *Candida* species from conventional PCR techniques can be further discriminatory to the species-level by using restriction enzymes to digest the PCR products, which are resolved on a gel and visualised as the final step in the assay (Vijayakumar, Giri & Kindo, 2012). The Restriction Fragment Length Polymorphism (RFLP) method has been used extensively as markers on genetic maps and fungal epidemiology (Alam *et al.*, 2014). The presence or absence of a fragment and their various sizes and patterns can be used as a mean of identification.

Associated technologies include methods that increase sensitivity and are more discriminative such as nested and multiplex PCR. Two-step nested PCR in which a second round of PCR using a separate primer set internal to the first-round increases amplification of a specific region in the first PCR amplified target gene. This is not only more specific but is also much more sensitive allowing the detection of the target DNA several fold lower than conventional PCR (Ahmad *et al.*, 2002). Another robust PCR method used in molecular fungal diagnostics is multiplex PCR. Multiplex PCR can detect multiple targets sequences within the genome of the fungi and also can be used to identify several fungal genera at once in the same sample. The technique is

fairly simple and is based on the use of primers specifically designed to amplify a region that is conserved among different fungal genera. Detection of several different fungal genera in the same PCR reaction can be achieved if the highly specific primers are designed to anneal at the same temperature and the PCR products are designed to be of different sizes to allow discrimination. More recently, Jainlabdin *et al.*, 2018 have described a low-cost yet reliable method in which an optimised set of primers for the simultaneous detection of pan-fungal and three major pathogenic fungal genera was applied (*Candida* spp., *Aspergillus* spp. and *Fusarium* sp.) as well as resistant pattern species through recognition of signature amplicon sizes. Nevertheless, all electrophoresis-based PCR assays have inherent disadvantages. A primary factor that hinders it as an ideal fungal diagnostic test lies in the end-point detection that does not correlate with the starting amount of the targets that have been amplified (Nurmi *et al.*, 2000; Mackay, 2004). Therefore, the finding may be biased and not able to quantify the fungal burden within the human body.

The solution to the above problem is given by the development of real-time PCR methods. Real-time PCR assays are able to quantify the amount of amplified DNA as it occurs (Walsh *et al.*, 2011). As a result, real-time PCR techniques have largely replaced conventional PCR methods in clinical laboratories (Mackay, 2004). Real-time PCR uses fluorescent dyes to enhance specificity through either a non-specific double-stranded DNA binding dye or a specific fluorescently labelled probe directed to a target sequence lying within the amplicon. A commonly used fluorescent DNA binding dye, SYBR Green dye chemistry, binds to all double-stranded DNA by intercalating between the bases (Fraga, Meulia & Fenster, 2014). There are various chemistries for probe labelling and fluorescent detection available such as TaqMan® hydrolysis probe (also known as fluorogenic 5′ nuclease chemistry), hybridisation probe and Molecular Beacons, as well as numerous thermocycler platforms, from the

high performing, LightCycler 480 (Roche Diagnostics) to the simpler instruments such as 2-Plex HRM Rotor-Gene Q (Qiagen, Germany), which, depend on the levels of throughput and combination of the detection channel (Froehlich, Sagner & Tellmann, 2009). The TaqMan probe consists of a 5' end reporter dye coupled with a 3' end quencher dye on the sequence-specific oligonucleotide probe that hybridises to the complementary sequence within the target PCR amplicon. The probe is cleaved by the 5' endonuclease activity of *Taq* polymerase during the extension stages, thus releasing the fluorescent emission only when the probe sequence is hybridised to a complementary target. The hybridisation probe assays rely on the interaction of the two probes (known as donor and acceptor) hybridised adjacently to the target sequence and emits fluorescence signal when the donor (dye labelled at 3' end) and acceptor (dye labelled at 5' end) probes are in the close proximity. The instrument's fluorescence detector measures the emission from the excited acceptor probe. Finally, the Molecular Beacons are single-stranded hairpin-shaped oligonucleotide probes, which unfold and release fluorescence when bound to the complementary target.

The identification methods of the real-time PCR assay can be more complex and far more useful than conventional PCR assay. The higher the initial copy number of target DNA molecules in the reaction, the faster an exponential increase of fluorescence is observed during the PCR cycles. A significant fluorescence signal increase can be determined at the threshold cycle (C_t), at which the amplification plot crosses the threshold line. In contrast, an endpoint PCR assay measures the amount of accumulated PCR product from the plateau phase (level-off) in the fixed PCR cycles. Target DNA can then be quantified by construction of a calibration curve that corelates C_t to a known number of DNA copies. Secondly, numbers of fungal detection tests are based on the melting curve analysis of an amplified product or through

evaluation of the design of probes that bind to amplified fragments and have different melting temperatures, so they can be detected by melting curve analysis.

1.6.2 Use of DNA biomarkers in the taxonomic identification of fungi

The advancement of phylogeny research in fungi provides access to fungal genome sequences on the reference sequence databases. In general, the DNA biomarkers demand two essential characteristics which are high taxonomic coverage and specificity to the target group (Hebert *et al.*, 2003). Studies have analysed numerous fungal biomarkers including single copy genes, such as translation elongation factor (*TEF-1*α) and β-tubulin genes and a gene encoding mini-chromosome maintenance protein (*MCM7*), but scientific consensus has recognised the sequences within the multicopy rDNA gene complex as the most useful fungal biomarkers (Schoch *et al.*, 2012; Xu, 2016). The rDNA genes are organised in repeats of 50 to 100 copies in a haploid genome, and these multicopy genes are amplified with better sensitivity than a single-copy gene (Wickes & Wiederhold, 2018). The fungal rDNA gene complex that consists of the 18S, 28S and 5.8S and the intervening internal transcribed spacers (ITS) is illustrated in Figure 1.8.

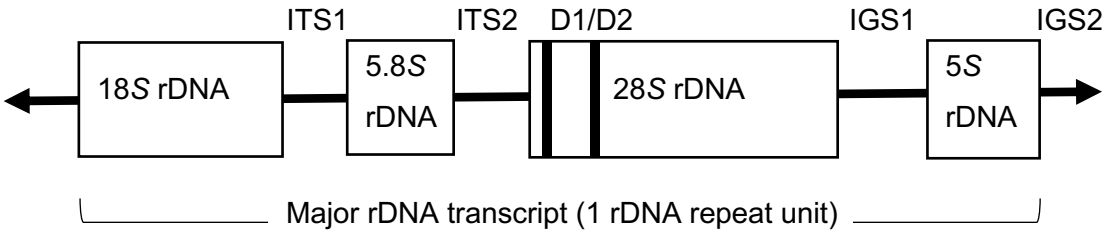

Figure 1. 8 Structural organisation of the fungal rDNA gene complex. The 18S, 5.8S and 28S rDNA genes are flanked by the ITS1 and ITS2. The 28S and 5S rDNA genes are flanked by the intergenic spacer (IGS1) meanwhile, IGS2 separates the repeat units. The conserved regions exist at the beginning and at the end (marked with

two bands) within the D1/D2 region (~600 base pair) of the 28S (large ribosomal subunit) gene.

Several loci within the rDNA genes and ITS regions have been employed as an ideal target sequence in various molecular detection assays (Arvanitis *et al.*, 2014). The ITS regions are good molecular targets for species level identification (Landlinger *et al.*, 2009) and extensively used as a universal DNA barcode in fungal taxonomy studies (Sulaiman *et al.*, 2014). Both, the rDNA and ITS regions contain the aforementioned criteria for the DNA biomarkers; highly conserved and variable regions, facilitating the design of the PCR primers within the conserved genes to amplify DNA from a large number of fungal species and identification of the target probe within the hypervariable sequence to define a particular genus or species. Although most of the universal primers used to amplify fungal ITS biomarkers are ITS1, ITS2, ITS3 and ITS4, primers SR6R, V9D, V9G, LS266, LR1, IT2 and ITS1F on the large subunit (LSU) rDNA are also recommended to avoid cross reactivity with human DNA, especially when amplification takes place directly from clinical specimens (Irinyi *et al.*, 2016; Leslie *et al.*, 2012). Within the ITS, the ITS2 region has become the genetic marker in fungal identification and molecular taxonomy because of the availability of universal primers to amplify the region in most of the fungal taxa, and the high discrimination power to distinguish even closely related fungal species (Irinyi *et al.*, 2016; Valero *et al.*, 2016; Zeller *et al.*, 2017). In addition, other useful multicopy genes include cytochrome P450 lanosterol C-14α-demethylase, alkaline proteinase and, mitochondrial cytochrome (*mtCytB*). Non-exhaustive PCR-based assays with the choice of target genes for *Candida* species as well as other targets species are listed in Table 1.2.

Table 1. 2 PCR assays and target genes for fungal species detection.

PCR assay/kit	Target gene(s) and species	Detection analysis
SeptiFast (Roche Diagnostics), FDA-approved	ITS1 for *C. albicans*, *C. tropicalis*, *C. glabrata*, *C. krusei*, *C. parapsilosis* and *A. fumigatus*	Amplification and melting curve analysis
MycoReal *Candida* (Ingenetix), RuO	ITS2 for *C. albicans*, *C. glabrata*, *C. dubliniensis*, *C. krusei*, *C. tropicalis*, *C. parapsilosis*, *C. lusitaniae*	Amplification and melting curve analysis
Genesig *Candida* kits (PrimerDesign), RuO	ITS2 for *C. albicans*, *C. glabrata*, *C. dubliniensis*, *C. tropicalis*, *C. parapsilosis*, *C. auris*	Amplification curve
FilmArray (BioFire), FDA-approved	*C. albicans*, *C. glabrata*, *C. krusei*, *C. tropicalis*, *C. parapsilosis*	Amplification curve
ViPrimePLUS *C. albicans* (Vivantis), RuO	*RPR1* gene for *C. albicans*	Amplification curve
Fungiplex *Candida*, (Bruker), IVD	*Candida* species (*C. albicans, C. tropicalis*, *C. dubliniensis*, *C. parapsilosis*, *C. krusei*, *C. glabrata*	Amplification curve
xTAG Fungal, Luminex	*RPR1* gene for *Candida* species; *Hwp1* gene for *C. albicans*; M antigen for *Histoplasma capsulatum*; *TEF1α* for *Cryptococcus neoformans*; *WI-1* adhesion gene for *Blastomyces dermatitidis*	Multiplex PCR coupled with bead probe fluid array
Seeplex STI Master Panel 3 PCR system (Seegene)	*C. albicans*, *C. glabrata*, *C. dubliniensis*, *C. krusei*, *C. tropicalis*, *C. parapsilosis*	PCR and electrophoresis
Lau *et al.*, 2010	ITS1, IT2, *TEF-1α* and β-tubulin genes for *Candida* species	Amplification curve
Tirodker *et al.*, 2003	ITS1 for *C. albicans, C. glabrata, C. tropicalis*, *C. parapsilosis*	PCR and gel electrophoresis

Moreira-Oliveira *et al.*, 2005	5.8S for *Candida* species	PCR and sequencing
Trovato *et al.*, 2012	ITS1, 18S and 28S rDNA for *Candida* species	PCR and gel electrophoresis
Ahmad *et al*., 2002	ITS2 for *C. albicans, C. glabrata*, *C. tropicalis*, *C. parapsilosis*	PCR and gel electrophoresis
Jainlabdin *et al*., 2018	ITS1 and ITS2 for pan-fungal, ITS2 for pan-*Candida* species, *C. krusei*, *C. glabrata* and *Aspergillus terreus*	PCR and gel electrophoresis

ITS, Internal Transcribed Spacer; rDNA, ribosomal deoxyribonucleic acid; LSU, large subunit; FDA, Food and Drug Administration; IVD, *in vitro* diagnostic device; RuO, Research Use Only; *Hwp1*, hyphal wall protein 1; *RPR1*, ribonuclease P RNA

1.7 Clinical specimens and source of the fungal nucleic acid

One of the considerations in designing a PCR assay is the choice of the starting clinical specimen. The methodological standardisation for an optimal sample for *Candida* PCR testing is still to be determined, for the testing on whole blood or serum/plasma (Wickes & Wiederhold, 2018). The specimen type and the effectiveness of the nucleic acid extraction procedure will affect the sensitivity of the target DNA amplification from the inhibitor-free DNA sample (Hsu *et al.*, 2011; Safavieh *et al.*, 2017). The choice of blood fraction; serum/plasma determines free circulating DNA is targeted during extraction and, the use of whole blood should target the cell-associated DNA (Halliday *et al.*, 2015). The overview of fungal DNA extraction from clinical samples for detection in PCR assays, is illustrated in Figure 1.9. However, with the presence of the complex structure of the fungal cell and the need for a rigorous cell lysis steps, the method of fungal DNA extraction is complicated when associated with the use of whole blood (Arvanitis *et al.*, 2014). Moreover, the extraction method must

consistently remove the PCR inhibitors and separate the relatively abundant human DNA from blood samples (Wickes & Wiederhold, 2018).

The serum is a specimen of choice because it requires less complicated DNA extraction and, contains fewer inhibitors than whole blood; therefore, amenable to standardisation (Alanio & Bretagne, 2014). A systematic comparison between the PCR detection of the *Candida* DNA isolated from plasma (75%) and serum (71%) are more sensitive than whole blood (54%) (Lau *et al.*, 2010). Ideally, an automatic process of DNA isolation and purification is the best approach towards standardisation of the method and shortening the test turnaround time as well as reducing the workload (Sexton *et al.*, 2018). Humans are prone to introduce processing errors by cross-contamination between the handled samples, and manual extraction may be not ideal for parallel sample processing.

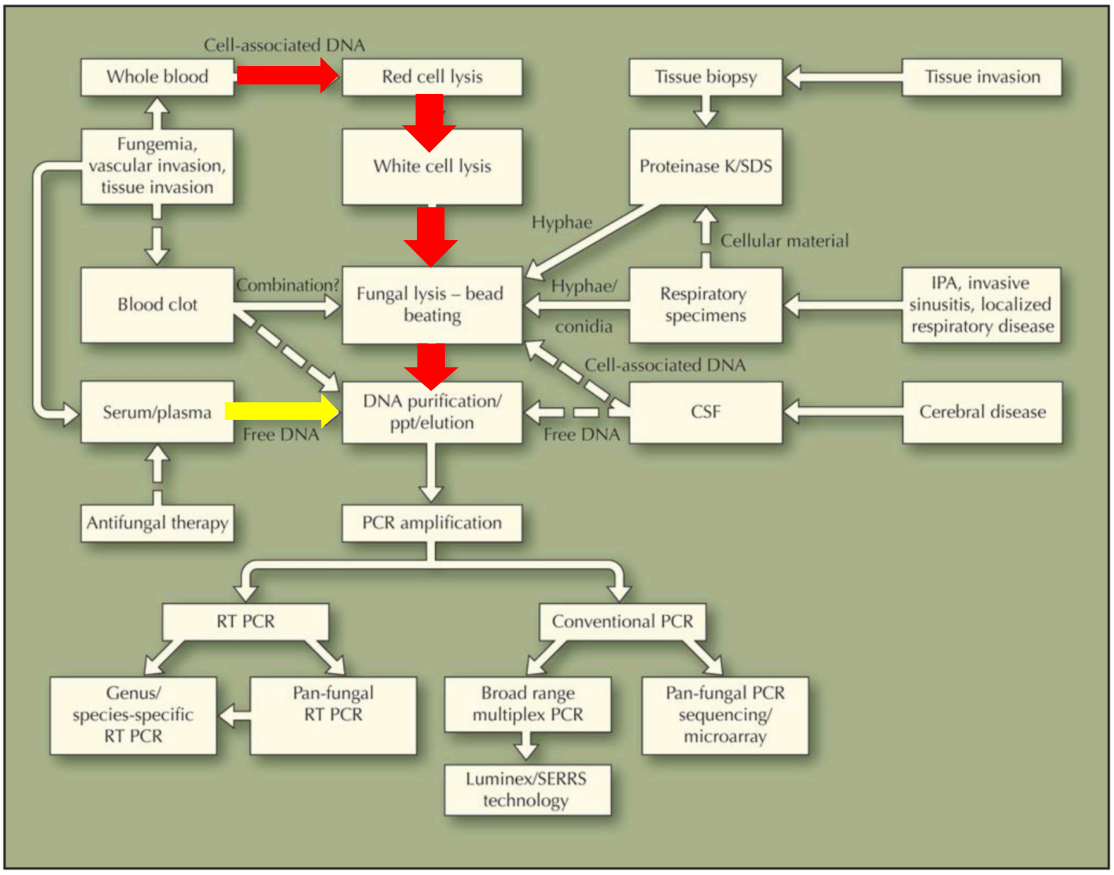

Figure 1. 9 The principles of the molecular detection of fungi and DNA extraction from clinical samples. The sources of fungal DNA from the whole blood are highlighted as red arrows and serum/plasma as a yellow arrow. Broken lines indicate limited evidence. CSF, cerebrospinal fluid; IPA, invasive pulmonary aspergillosis; ppt, precipitation; RT, real-time; SDS, sodium dodecyl sulphate; SERRS, surface-enhanced resonance Raman spectroscopy. The diagram is adapted from White, Perry & Barnes, (2009).

1.8 Research aims and objectives

This thesis aims to explore the potential of the MPA and MNAzyme biomarker detection platforms as simple nucleic acid biosensors for the diagnosis of invasive candidiasis. The research has the following work packages:

i) Identification through bioinformatic sequence analysis of nucleic acid biomarkers with a range of specificities, including pan-fungal (detection of any fungi), pan-*Candida* (detection of all *Candida* species) and species-specific biomarkers for the identification of multidrug-resistant *C. auris*, *C. glabrata*, and *C. krusei*.

ii) Engineering and *in vitro* characterisation of a single-tube, dual channel pentaplex MPA-*Candida* assay.

iii) Optimisation of the pentaplex MPA-*Candida* assay to incorporate a pan-fungal biomarker and further develop it into a single-tube, single channel reaction.

iv) Evaluation of three different *Candida* DNA isolation protocols from blood and serum samples for downstream processing with the MPA-*Candida* assays.

v) Engineering and *in vitro* characterisation of an MNAzyme test for the isothermal detection of fungi.

This thesis is organised in seven chapters:

Chapter 1 introduces the current understanding of invasive fungal infections and some critical issues related to *Candida* infections. A brief section on the biology of the yeast intended to discuss the characteristics of the relevant species and their relationship at

the genus level. This chapter also elaborates the traditional diagnostic methods for the fungal infections as well as cutting-edge technologies to provide an insight into the molecular tools used to improve the diagnosis of invasive candidiasis. The principles of novel nucleic acid detection platforms, the MPA and MNAzymes, are discussed to provide the reader with some understanding of the potential use of the platforms in achieving the research objectives. The prior knowledge of the fungal DNA biomarkers serves as a cornerstone in the development of reliable nucleic acid biosensors for the diagnosis of invasive candidiasis. The possible sources of fungal DNA from human specimens are also reviewed with considerations of the methods of fungal DNA isolation that may be involved in testing biomarker detection platforms. The research objectives are outlined in the form of work packages to provide a systematic approach to achieve the research aims. Chapter 2 describes the methods used to conduct the research as well as the laboratory instruments and equipment. The standard analysis procedures and overall numerical operations employed are also detailed in Chapter 2. Chapter 3 provides the main findings of the thesis on the development of the MPA-*Candida* assay for reliable detection of nucleic acid biomarkers of clinically relevant *Candida* species. A comprehensive description of the probe and *in vitro* characterisation of the assay are reported in this chapter. The assay's analytical specificity and sensitivity are tested against a range of *Candida* species that are frequently associated with candidiasis. This chapter also discusses the validation and evaluation tests of the assay with a standard *Candida* species Evaluation Panel and a commercial *C. auris* qPCR diagnostic kit. The potential use of the MPA-*Candida* assay is highlighted here as a novel qPCR assay for the early diagnosis of invasive candidiasis and to assist patients and doctors to make informed decisions on outlook and treatment options. Chapter 4 describes experimental exploration to improve the state of the MPA-*Candida* assay, possibly from a two-tubes system into a single tube

assay. This chapter is presented in two sections; assay design 2 for the reaction optimisations in two fluorescence detection channels, and assay design 3 for the hexa-plexing assay in three real-time PCR detection channels. Chapter 5 presents the effectiveness of independent DNA isolation protocols for the recovery of *Candida* DNA from mammalian blood and serum samples. Three commercial DNA isolation kits with a slight modification for the mechanical cell lysis step are assessed for the DNA yield by a real-time PCR assay and spectrophotometer. The optimum protocol established here is employed to process spiked serum samples of the *Candida* Evaluation Panel, of which the findings are reported in Chapter 3. Chapter 6 provides another main finding in the development of an isothermal MNAzymes assay for the detection of fungal DNA biomarkers. The results are presented from the identification of the pan-fungal DNA biomarker as a target sequence, reagents optimisation as well as specificity and sensitivity tests. The Pan-Fungal assay kinetic activity is also assessed to broaden the understanding of the kinetics of MNAzyme catalysis and compare the assay activity against the previously reported assays. Finally, Chapter 7 summarises the main findings through an overarching discussion within the context of clinical diagnosis of invasive candidiasis. The strengths and limitations of the study as well as the implications of the main findings are also acknowledged here.

CHAPTER 2: Materials and Methods

2.1 Fungal and bacterial isolates

Strains of the *Candida* species, *C. albicans, C. glabrata, C. tropicalis, C. dubliniensis, C. krusei, C. guilliermondii* and *C. parapsilosis* were a kind gift from Professor Julian Naglik (King's College London). *C. auris* (NCPF 8971) and *C. haemulonii* (NCPF 8402) strains were purchased from Public Health England, Bristol, UK. Filamentous fungi species strains of *Aspergillus fumigatus*, *Aspergillus flavus*, *Fusarium solani*, *Penicillium rubens* and, *Mucor circinelloides* as well as bacterial species strains of *Staphylococcus epidermidis*, *Staphylococcus aureus*, *Proteus mirabilis* and *Escherichia coli* were obtained from the Centre for Biomedical Sciences, Royal Holloway University of London. All isolates were handled under Biosafety Level 2 (BSL2) conditions.

2.2 Microbial growth media preparation

2.2.1 Yeast extract Peptone-Dextrose (YPD) broth

The YPD broth was prepared according to Bergman, 2001. The broth was prepared with the bacteriological Peptone, 20 grams; Yeast extract, 10 grams; Glucose, 20 grams. The ingredients were dissolved completely in 1,000 mL distilled water. The mixture was sterilised by autoclaving at 121°C for 15 minutes. Single yeast colonies were inoculated in the YPD broth and incubated at 37°C in a rotary shaker (SciQuip, UK) for 24 hours.

2.2.2 Sabouraud Dextrose Agar (SDA)

A selective medium SDA (Sigma-Aldrich, UK) for yeast, filamentous fungi and aciduric bacteria was prepared according to the manufacturer's instructions. Briefly, 65 grams medium powder, composition of mycological peptone, dextrose and agar, was suspended in 1,000 mL of distilled water. The medium was dissolved completely by heating and stirring for 5 minutes on the magnetic stirrer followed by sterilisation by autoclaving at 121°C for 15 minutes. The prepared medium was poured aseptically onto a general plastic petri dish (100 mm × 15 mm) and stored at 4°C. Fungal isolates were sub-cultured onto the SDA and incubated at 37°C for yeast and 25°C for moulds in the incubator for 15 to 24 hours.

2.2.3 Luria-Bertani (LB) medium

The LB nutrient-rich broth (Merck, Germany) for *Escherichia coli* cultivation contains peptone, yeast extract, sodium chloride and water-soluble vitamins. The medium powder (25 grams) was dissolved in 1,000 mL of distilled water. The autoclaved broth is clear and yellowish-brown. Bacterial isolates were cultured in LB broth at 37°C in a rotary shaker (SciQuip, UK) for 24 hours. The LB agar was supplemented with the Ampicillin 50 μg/mL (Merck, Germany) for cultivation of transformed *E. coli* in the DNA cloning experiment.

2.3 Nucleic acid extractions

The basic principle of nucleic acid extractions involves three common steps; cell lysis, removal of the cell components, contaminants and nucleic acid precipitation and the elution of the nucleic acids. These steps are normally applied by the commercial DNA extraction kits. The procedure, buffers, as well as the kit contents are summarised in Table 2.1.

Table 2. 1 The principle of the nucleic acid extraction kits and the equipped buffers.

Procedure/kit	**Wizard® Genomic DNA Purification Kit**	**RTP® Pathogen Kit**	**ZymoBiomics™ DNA Miniprep Kit**
Cell disruption	Cell Lysis solution	Extraction Tube with lysis components[1]	ZR Bashing Bead Lysis tube
	Nuclei Lysis solution	Resuspension buffer	ZB Lysis solution
Removal of cell membrane, lipid, protein	Protein Precipitation solution	Binding Solution (Isopropanol) & RTA Spin Filter	Zymo-Spin HRC Filter
Nucleic acid purification/binding from bulk	Isopropanol		DNA Binding Buffer
	70% ethanol	Wash buffers 1 & 2	Zymo Spin Filter-Z
			Wash buffers 1 & 2
Nucleic acid concentration	DNA Rehydration solution	Elution buffer	Zymo Spin Filter-F & Nuclease-free water
	RNase A solution		Zymo-HRC solution

[1] Extraction Tube is prefilled with lyophilised lysis components (lysis buffer, Lysozyme, Proteinase K, Carrier RNA).

2.3.1 Wizard® Genomic DNA Purification Kit (Promega Corp.)

2.3.1.1 Fungal DNA isolation

One millilitre (mL) aliquots of a culture grown was centrifuged at 13,000–16,000 × g for 2 minutes to pellet the cells. The pelleted cells were homogenised in the mini-pestle BioMasher® (Nippi Inc., Japan) (Figure 2.1) to lyse the cell wall and cell membrane. Following an additional 300 µL of lysis buffer, the homogenised cell was gently mixed by pipetting.

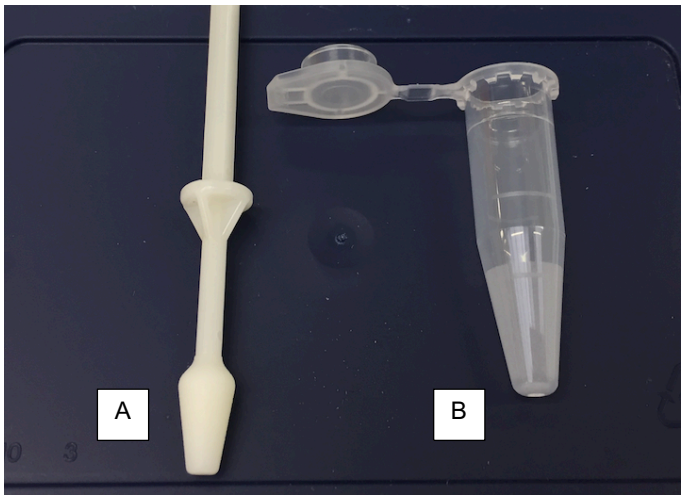

Figure 2. 1 A set of mini-pestle BioMasher®-II by Nippi Inc. Japan. Coarse-grained surfaces on the pestle tip (A) and inner tube area (B) ensure efficient grinding of samples.

The bead-beating technique is another mechanical cell wall lysis method used in this study. The technique applied after the cell pellet was resuspended in 300 µL of lysis buffer from the Wizard® Genomic DNA Purification kit (Promega, USA). Following the addition of 200 mg of 500-micron glass beads (BioSpec Products, USA) yeast cells were homogenised with a FastPrep-24™ instrument (MP Biomedicals, USA) using five pulses with 60 seconds cooling intervals at 6.5 m/s speed setting. The

same technique was also performed in the vortex-based instrument, the Disruptor Genie® (Scientific Industry, USA) for 20 minutes and can be operated in 4°C cold room.

Next, the cellular proteins were removed by a salt precipitation step and, the DNA was concentrated and desalted by isopropanol precipitation. Briefly, 100 µL of Protein Precipitation Solution was added and mixed by vortex at high speed for 20 seconds. The samples were kept on ice for 5 minutes then, further with centrifugation at 13,000–16,000 × g (bench microcentrifuge Heraeus, Germany) for 2 minutes to remove the cell debris. The supernatant containing the DNA was transferred to a clean 1.5 mL micro-centrifuge tube that has been filled with 300 µL of room temperature isopropanol. At this stage, some supernatant on top of the precipitated protein was left to avoid contaminating the DNA solution with protein. Samples were mixed by inversion until the thread-like strands of DNA form a visible mass. Then, the tubes were centrifuged at 13,000–16,000 × g for 2 minutes. The supernatant was thrown, and the tube was drained on clean absorbent paper.

The DNA pellet formed was washed by gently inverting the tube several times with 300 µL of room temperature 70% ethanol. The samples were proceeded to centrifuge at 13,000–16,000 × g for 2 minutes. Then, ethanol was carefully removed from the tubes. Again, the tubes were drained on clean absorbent paper and allowed the pellet to air-dry for 10–15 minutes. 50 µL of DNA Rehydration Solution was added into the tubes containing DNA pellet. The DNA was resuspended in 50 µL of DNA nuclease-free water, a process optimised by incubating at 65°C for 1 hour. Throughout the period, the solution was gently mixed in the tube. The extracted genomic DNA were stored at 4°C after concentration measurement.

2.3.1.2 Bacterial DNA isolation

One mL aliquots of a culture grown was centrifuged at 13,000–16,000 × g for 2 minutes to pellet the cells. The supernatant was discarded, and the bacterial cell pellet was resuspended in 60 µL of 10 mg/mL lysozyme and incubated at 37°C for 30 minutes to ensure efficient cells lysis. The cell pellet was resuspended in 300 µL of Nucleic Lysis buffer followed by the protein precipitation and nucleic acid pellet purification steps as described in sub-Section 2.3.1.1.

2.3.2 RTP® Pathogen Kit (Stratec Molecular GmbH)

A total amount of 10^7 yeast cells suspension was processed for DNA extraction using RTP® Pathogen Kit (Stratec Molecular, Germany) with slight protocol modifications for mechanical yeast cells lysis. The sample was mixed with Resuspension buffer and subjected to the Extraction tube pre-filled with lyophilised lysis components (lysis buffer, Lysozyme, Proteinase K, Carrier Nucleic acids) to lyse the samples, stabilise the nucleic acids and inactivate RNases and DNases. The sample in the extraction tube was incubated at 65°C under continuous shaking for 20 minutes in the thermomixer (Grant-bio, UK). An essential step of vigorous mechanical yeast cells lysis was performed by 400 mg of 500-micron glass beads (BioSpec Products, USA) in the Disruptor Genie® (Scientific Industry, USA) for 20 minutes operated in 4°C cold room. Subsequently, the lysed cells were loaded into the RTA Spin filter and centrifuged to remove the contaminants from the filter membrane. The nucleic acids bound to the filter membrane were washed with 100% ethanol in two steps, 500 µL and 700 µL before drying the filter with maximum speed of centrifugation for 4 minutes. The final volume of 50 µL of nuclease-free water or supplied elution buffer was used to elute the purified nucleic acids. In all cases, the Carrier RNA will account for most of the

eluted nucleic acids therefore, quantitative real-time PCR is recommended to quantify the extracted nucleic acids.

2.3.3 ZymoBiomics™ DNA Miniprep Kit (Zymo Research Corp.)

The yeast DNA isolation of 10^8 cells was performed according to the ZymoBIOMICS™ DNA kit (Zymo Research, USA) standard protocol for bead beating cell lysis steps. The sample was added to ZR Bashing Bead lysis tube containing 100-micron and 500-micron beads and mixed with the ZB lysis solution. The cell lysis steps were performed in a FastPrep-24™ instrument (MP Biomedicals, USA) using five pulses with 60 seconds cooling intervals at 6.5 m/s speed setting. The ZR Bashing Bead lysis tube containing cell extracts was subjected to centrifugation at the maximum speed for 1 minute. The supernatant was carefully transferred with no cell debris into the Zymo Spin Filter-F fitted in a collection tube. After a minute of the centrifugation step, the spin filter was discarded and the filtrate was mixed with 1,200 µL DNA Binding Buffer. The total mixture volume was loaded to the filter membrane in the Zymo Spin Filter-Z followed by centrifugation in two repeated steps. Filter bound-nucleic acids were washed with Buffer 1 and subsequently twice washing steps with Buffer 2 before placed the Zymo Spin Filter-Z into a clean 1.5 mL tube. The filter membrane was incubated for one minute in the 50 µL nuclease-free water followed by centrifugation at the maximum speed for 3 minutes. The filtered nucleic acids were added into Zymo-Spin HRC Filter containing 600 µL Zymo-HRC Solution and centrifuged at the maximum speed for 3 minutes. The purified nucleic acids are now ready for downstream applications.

2.3.4 Recombinant plasmid DNA isolation

Cloned plasmid DNA was purified from bacterial cells using a QIAprep Miniprep Kit (Qiagen, Germany) according to the manufacturer instructions. Briefly, samples were subjected to alkaline lysis in buffer PB and neutralised. Cleared lysates were applied to QIAprep purification columns under high-salt concentration affinity binding conditions and eluted in 30 µL of elution buffer. In all cases, the concentration of purified DNA was measured using a NanoDrop™ 1000 spectrophotometer (Thermo Scientific, USA) and stored at 4°C until use.

2.4 DNA purification

Extracted or amplified DNA products may require purification to remove primers, nucleotides, salts, agarose and other impurities from the DNA sample. The volume of 20 µL of the PCR product was subjected to QIAquick® PCR Purification Kit (Qiagen, Germany). Buffer PB was mixed with PCR product and observed for yellow colour indicating the correct pH condition. The QIAquick column was placed in the provided collection tube, and the sample was applied to the QIAquick column and centrifuged for 1 minute. The flow-through was discarded and the QIAquick column was returned to the same collection tubes. The buffer PE was added and centrifuged for 1 minute to wash the sample. Centrifugation was repeated for one minute to remove residual wash buffer. Next, the QIAquick column was placed in a clean 1.5 mL micro-centrifuge tube and 50 µL of elution buffer was added to centre of the QIAquick membrane. The QIAquick column in micro-centrifuge tube was spun for one minute and the flowed-through solution was collected and measure for DNA yield and purity.

2.5 Determination of nucleic acid concentration and purity

The concentration and purification of the genomic or purified DNA was determined by using a Nanodrop™ 1000 Spectrophotometer (Thermo Scientific, USA). Absorbance measured at 260 nm and 280 nm. As A_{260} of 1.0 is equal to 50 µg/mL pure DNA, DNA concentration can be estimated by measuring the absorbance at 260 nm, multiplying by the dilution factor and 50 µg/mL. The DNA purity can be estimated from the $A_{260}/_{280}$ ratio. A ratio of $A_{260/280}$ in between 1.8 and 2.0 generally represents a high-quality DNA sample with minimal protein contamination.

2.6 Calculation of DNA copy number

The number of double-stranded DNA copies can be determined from the amount of the DNA obtained in nanogram (ng) and the length of the DNA in base pair (bp). The number of molecules was calculated with this information using the following formula:

$$\text{Number of copies (molecules)} = \frac{(\text{DNA amount in ng}) \times 6.0221 \times 10^{23}\ \text{molecules/mole}}{(\text{length in bp}) \times 660\ \text{g/mole} \times 1 \times 10^{9}\ \text{ng/g}}$$

2.7 Haemocytometer cell counting

Cell counts were performed using a microscope (Leica DM500, Germany) and haemocytometer, an improved Neubauer ruling and its coverslip. Cell suspensions were diluted 1:10 and mixed in normal saline solution for a uniform distribution of the cells in the chamber represents a random sample from the total volume. Briefly, 10 µL of cell suspensions were loaded in between of the coverslip and haemocytometer and were allowed to cover the entire grid. The cells were counted systematically under an optical microscope at 40× magnification. The averages were counted from the 5 corners of the 25-square within 1-mm^2 grid area. The density of the cells/mL was

calculated from the averages multiplied by the dilution factor and divided by 0.000004 mL account for the volume of the small square counted.

2.8 Serial dilution preparation

Serial dilution of the sample was prepared to create a sequence of dilutions with the same dilution factor in each successive step. To make a 1:10 dilution of 1,000 µL sample volume, the stock was mixed well and transferred 100 µL to another tube containing 900 µL of buffer, media or nuclease-free water. Each dilution was mixed well before transferring the volume to be brought up to a predetermined volume.

2.9 Colony-Forming Unit (CFU)

CFU is a term which refers to the number of cells which grow into a colony determined from a preparation of cell dilutions. The cells from each dilution were spread on the plates in duplicate. Following an overnight incubation, the averages colonies growth on the plates were counted. The numbers CFU per millimetre was determined following the calculation:

$$\text{CFU/mL} = \frac{(\text{number of colonies present on the plate}) \times (\text{dilution factor})}{\text{volume of culture plate}}$$

2.10 DNA cloning

In order to prepare cloned plasmid DNAs, first-round PCR amplicons were cloned into the pCR® 2.1-TOPO® vector using the TOPO® TA Cloning® system (Invitrogen, USA). The reaction mixture was prepared as in Table 2.2. The mixture was mixed and incubated for 5 minutes at room temperature. The enzyme *Taq*-polymerase from the amplification reaction has terminal transferase activity that adds a single deoxyadenosine (A) to the 3' ends of PCR products (Figure 2.2). The linearised vector, pCR® 2.1-TOPO® has single, overhanging deoxythymidine (T) residues at the 3' ends

adjoining the sequence 5'-CCCT-3'. This allows hybridisation of the (A) and (T) residues between vector and the PCR product. As a result, the PCR product and the vector can efficiently ligate by the enzyme Topoisomerase I from *Vaccina* virus. The Topoisomerase I covalently attaches to the phosphate groups at the 3' end of the vector, as the vector and the PCR product are mixed, the enzyme transfers the phosphate linkages to the 5' ends of the DNA fragment, thus joining the insert and the vector. The recombinant vector was subsequently transformed into competent TOP10 *E. coli* supplied in the cloning kit. Briefly, 2 µL of the cloning reaction into chemically competent *E. coli* cells by heat shock. One mL of S.O.C (Super Optimal broth with Catabolite repression) medium was added to the cells and incubated at 37°C for 1 hour in a rotary shaker (SciQuip, UK). Each transformation sample was spread onto a LB plate containing 40 µg/mL Ampicillin (Merck, Germany). The plates were prepared in duplicate and incubated overnight at 37°C to grow colonies. Each colony grown was picked and, inoculated in 5 mL LB broth containing 40 µg/mL Ampicillin. Next, plasmid DNA was isolated using a QIAprep Miniprep Kit (Qiagen, Germany) as described in Section 2.3. The resulting plasmid with insert was quantified and sequenced to confirm the identity of the cloned DNA.

Table 2. 2 The preparation of TOPO® cloning reaction.

Reagent	**Volume**
Fresh PCR product	3 µL
Salt solution (NaCl, 1.2 M)	1 (final concentration, 0.2 M)
Water	1
TOPO® vector	1
Final volume	6

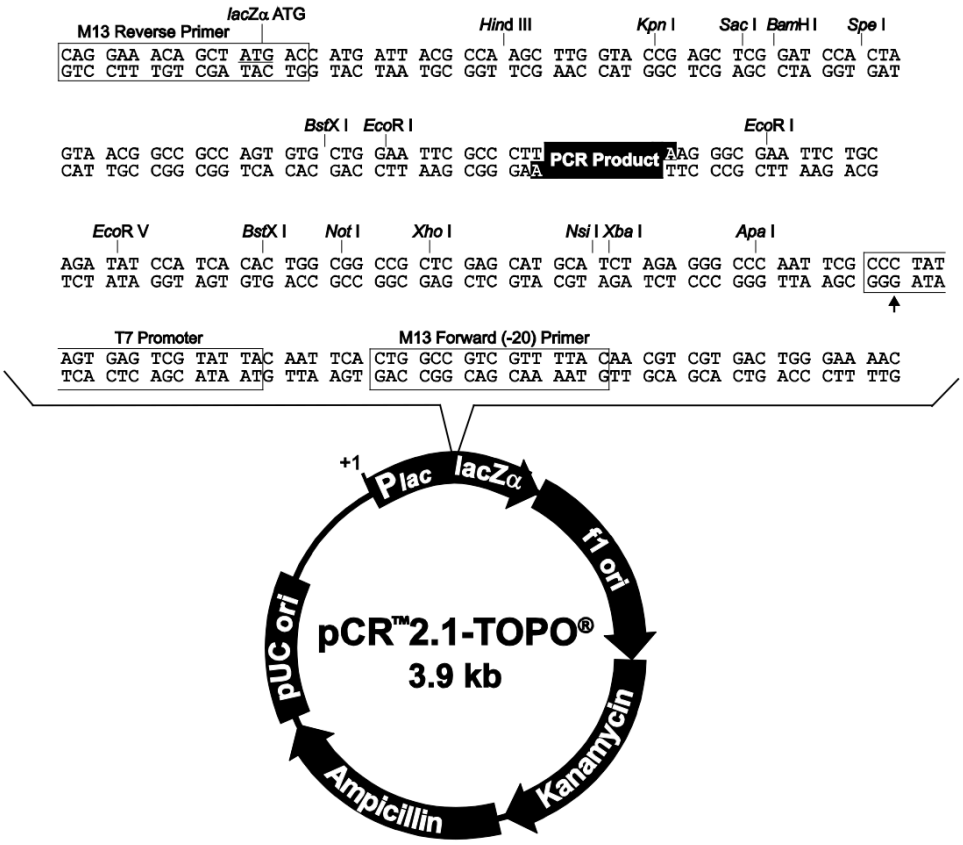

Figure 2. 2 The map of the pCR® 2.1-TOPO® vector as described in the manufacturer's instruction manual.

2.11 End-point PCR mixture preparation

The master mix for end-point PCR preparation, 2 × GoTaq® Green Master Mix (Promega, USA) composed of GoTaq® DNA Polymerase, 400 µM deoxyribonucleotide triphosphate (dNTP) and 3mM Magnesium Chloride ($MgCl_2$). The reaction mixture was prepared for amplification of DNA as showed in Table 2.3. A standard amplification condition was set in a PCR thermocycler (Techne TC-512, UK). The reaction started with 5 minutes of 94°C initial denaturation step, followed by 34 cycles at 94°C for 1.5 minutes, 55°C for 2 minutes and 72°C for 3 minutes and a final extension step at 72°C for 10 minutes. In a case of the annealing temperature optimisation, the temperature gradient performed in a range of 10°C for 2 minutes.

Table 2. 3 The preparation of the PCR mixtures for end-point analysis.

Component	Volume (µL) for 1 × reaction	Final Concentration in 20 µL reaction
2 × GoTaq® Green Master Mix, Promega	10.0	1×
Forward Primer	1.0	0.5 µM
Reverse Primer	1.0	0.5 µM
DNA	4.0	10 ng - 40 ng
Nuclease-Free Water to	4.0	-

2.12 Agarose gel electrophoresis for DNA band analysis

The preparation of 1.2% agarose gel was started with mixture of 360 mg agarose powder (Merck, Germany) into 30 mL of electrophoresis buffer, Tris-borate-EDTA (TBE) (Merck, Germany). The agarose suspension was boiled in a conventional microwave oven (Stirflow, UK) for 1 minute at the high temperature setting and swirled for the homogenous agarose solution. The molten agar was let to cool before mixed with 3 µL SYBR™ Safe Nucleic Acid Stain (Invitrogen, UK). The molten agar was poured onto the gel caster with the comb positioned at the end of the plate for the sample wells in the gel. The gel slab was let solidify for 20 minutes before removing the comb and mounting the gel in the electrophoresis tank. The electrophoresis buffer was added enough to cover agarose gel and the comb was removed. Next, 5 µL of 100 bp DNA marker (Promega, USA) was loaded in a well and continued with the 2 µL to 5 µL of PCR product mixed with 1 µL of Loading dye (Promega, USA) in each well. The gel tank lid was closed, and the electrical leads were attached for DNA migration toward the positive anode (red lead). The electrophoresis was run at 80 Volts for 60

minutes. Then, agarose gel was observed under UV trans-illuminator for the analysis of fluorescently stained DNA bands.

2.13 Bioinformatic analysis

Fungal rDNA sequences were retrieved from GenBank (https://www.ncbi.nlm.nih.gov/genbank/) and the International Society for Human and Animal Mycoses (ISHAM) ITS database (http://its.mycologylab.org/) and aligned using CLUSTALW2 or CLUSTAL Omega (EMBL-EBI; https://www.ebi.ac.uk/Tools/msa/clustalo). Sequences were manipulated and analysed using the BioEdit© Sequence Alignment Editor Version 7.2.3 (Hall, 1999).

2.14 MPA-*Candida* Assay

2.14.1 Primers and hydrolysis probe design

Primers and probes were designed within the rDNA region. Primers used in the MPA-*Candida* assay were the universal forward primer, LR0 and specifically designed reverse primer, GSCand. A universal pan-fungal primer set ITS3 and LR1 was selected to amplify the region containing pan-fungal probe. Four dual-labelled *Candida* probes were designed to specifically target the D1/D2 of the LSU rDNA region from at least 15 different *Candida* species. The pan-fungal probe was designed based on the ITS sequences. The MPA internal control (IC) probe consists of a unique nucleotide sequence cloned into the pCR™ 2.1-TOPO® vector that has no significant homology to any entry in the non-redundant nucleotide databases at NCBI. MPA probes were designed using the nucleic acid folding and hybridisation prediction software UNAFold (http://unafold.rna.albany.edu). All primers and probes were subjected to reverse Basic Local Alignment Search Tool (BLAST) in GenBank

(http://blast.ncbi.nlm.nih.gov) to test for cross-homology with other microorganisms. The MPA *Candida* and TaqMan® pan-fungal reaction sets are shown in Table 2.4.

Universal 16S primer set, 516: 5'-TGCCAGCAGCCGCGGTAA-3' and 806R: 5'-GGACTACCAGGGTATCTAAT-3' (Fredricks & Relman, 1998) was adapted for amplification of the bacterial genomic DNA tested in the cross-reactivity experiments.

Table 2. 4 The layout design for MPA-*Candida* assay and a complementary TaqMan® Pan-Fungal assay.

Reaction type	Probe target	Detection channel	Primer set
MPA	*C. krusei* (CK)	FAM	Forward: LR0 (Cubeta, 1991) & Reverse: GSCand (designed in this study)
	Pan-*Candida* (PC)		
	C. glabrata (CG)		
	C. auris (CA)	HEX	
	Internal Control (IC)		Forward: M13 (-20) & Reverse: M13 (-29)
TaqMan®	Pan-fungal (PF)	FAM	Forwards: ITS3 (White *et al.*, 1990) & Reverse: LR1 (Vilgalys & Hester, 1990)
	IC	HEX	Forward: M13 (-20) & Reverse: M13 (-29)

FAM, 6-carboxy-fluorescein, 465 nm/510 nm; HEX, Hexachloro-fluorescein, 538 nm/580 nm

2.14.2 Real-time PCR mixture preparation

Initially, the MPA-*Candida* PCR mixtures were prepared in 10× mix for a total volume of 180 µL as described in Table 2.5. In a 1× reaction, template DNA included 1 µL of IC plasmid DNA (10^6 copies) and 1 µL of extracted fungal DNA (1 to 10^5 copies) for 20 µL final reaction volume. Each THO was combined with the corresponding PCO at a ratio of 1:2. The Pan-Fungal reaction, both the pan-fungal and IC probes were present at a concentration of 0.4 µM (Table 2.6).

Table 2. 5 The preparation of the MPA-*Candida* PCR mixtures.

Component	Stock Concentration (µM)	Volume (µL) for 10× mix	Final Concentration (µM) in 20 µL reaction
LightCycler 480 Probes Master (Roche)	2×	100.0	1×
Pan-*Candida* (PC) THO	20	2.0	0.2
C. krusei-specific (CK) THO	20	4.0	0.4
C. glabrata specific (CG) THO	20	4.0	0.4
C. auris-specific (CA) THO	20	4.0	0.4
IC THO	20	4.0	0.4
PC PCO	40	2.0	0.4
CK PCO	40	4.0	0.8
CG PCO	40	4.0	0.8
CA PCO	40	4.0	0.8
IC PCO	40	4.0	0.8
LR-0, Forward primer (F)	40	3.0	0.6

GSCand, Reverse primer (R)	40	3.0	0.6
M13, F	40	3.0	0.6
M13, R	40	3.0	0.6
Nuclease-free water	N.A.	32.0	N.A.

Table 2. 6 The preparation of the Pan-Fungal PCR mixtures.

Component	**Stock Concentration (µM)**	**Volume (µL) for 10× mix**	**Final Concentration (µM) in 20 µL volume**
LightCycler 480 Probes Master (Roche)	2×	100.0	1×
Pan-fungal THO	20	4.0	0.4
IC THO	20	4.0	0.4
ITS3, F	40	3.0	0.6
LR1, R	40	3.0	0.6
M13, F	40	3.0	0.6
M13, R	40	3.0	0.6
Nuclease-free water	N.A.	60.0	N.A.

The specificity of the pan-fungal probe was evaluated from the amplification curve whereas those of *Candida* MPA probes were evaluated from their melt curve profiles. The amplification curve C_t value of the Pan-Fungal assay was standardised by an automatic threshold setting whereas for MPA-*Candida* reaction, the threshold line was set at 5 in Fit Points analysis method using the LightCycler 480 software version 1.5 (Roche Diagnostics, Germany). The amplification assay was carried out in

a LightCycler 480 Instrument II Real-time PCR unit (Roche Diagnostics, Germany) using a 384-well plate format. Real-time PCR conditions were as follows: an initial step of 9 minutes 30 seconds at 95°C, followed by 50 cycles at 95°C for 20 s, 62°C for 30 seconds, and 72°C for 1 minute and temperature maintained at 95°C for 10 seconds before melting curve profiling increases from 20°C to 80°C. Two detection channels, FAM (465 nm/510 nm) and HEX (533 nm/580 nm) were activated for fluorescence measurements during the read steps at 72°C for each experiment.

2.14.3 Pan-Fungal PCR assay standard curve

Standard curve functions to assess unknown target copy number was developed from TaqMan® pan-fungal PCR assay. Recombinant plasmid DNAs of *C. albicans*, *C. dubliniensis*, *C. krusei*, *C. glabrata*, *C. auris*, *C. parapsilosis*, *C. tropicalis*, *C. guilliermondii* were serially diluted for detection from 10^6 to 10^2 copies per reaction. Regression lines were obtained by plotting the logarithm of the initial plasmid copy number versus the corresponding C_t and used to determine the sensitivity and efficiency of the assay. Amplification efficiency was calculated by $E = 10^{-1/b} - 1$, where b is the gradient of the linear regression equation.

2.14.4 Determination of PCR assay reproducibility

Intra- and inter-assay reproducibility was assessed by two independent experiments of eight *Candida* species plasmid DNAs. The coefficient of variation (CV) calculated for C_t data was used as an indicator of relative precision and reproducibility. CV was determined by dividing the standard deviation (SD) by the arithmetic mean of the measured values: CV (%) = (SD/mean value) ×100.

2.14.5 Assay evaluation and validation tests

2.14.5.1 *Candida* sp. Evaluation Panel 01 (Qnostics, UK)

A commercial *Candida* sp. Evaluation Panel 01 (Qnostics, UK) was used to evaluate the overall performance from the DNA extraction phase through amplification for detection of *Candida* species DNA. The panel is for research use only and manufactured to the ISO (International Organisation for Standardisation) standard compliant systems. The panel consists of six 500 µL serum samples spiked with blastoconidia of *C. albicans* (S01 &S02), *C. glabrata* (S03 &S04) and *C. krusei* (S05 &S06) at high and medium concentrations respectively. For each species, the medium is one log lower concentration than the high sample. One serum sample (S07) has no cell as for the panel's negative control. Qnostics' *Candida* sp. The seven vials of the panel were processed as described in the nucleic acid extraction section using the RTP Pathogen Kit (Stratec, Germany). DNA recovered from each sample was tested in duplicate with 7 µL for each reaction of MPA-*Candida* and Pan-Fungal assays. The amplification cycle values obtained from both assays were cross-checked against Qnostics' reference assay provided in the instructions manual (Table 2.7).

Table 2. 7 Qnostics' *Candida* species panel components and characteristics.

Sample Code	Sample Description	C_t values*
S01	*C. albicans*	24.5
S02	*C. albicans*	27.2
S03	*C. glabrata*	30.4
S04	*C. glabrata*	31.9
S05	*C. krusei*	29.0
S06	*C. krusei*	31.3
S07	Negative	Negative

* The C_t value provided is specific to Qnostics' reference assay

2.14.5.2 *Candida auris* kit Genesig® Standard Real-time PCR kit (Primerdesign™ Ltd, UK)

The MPA-*Candida* for *Candida auris*-specific detection was validated against simplex *C. auris* Genesig® Standard Real-time PCR kit (Primerdesign™ Ltd, UK). The *C. auris* Genesig® Real-time PCR kit exploiting the TaqMan® principle for the probe targeting ITS2 region of the rDNA. Both assays were tested to determine the sensitivity of the dilution detection from the serially diluted genomic DNA from 10^5 to 10^1 copies in the nuclease-free water.

2.15 MNAzymes Pan-Fungal Assay

2.15.1 Basic components of MNAzymes assay for fungal detection

MNAzymes composed of two partial-enzymes (Partzymes A and B), which each contains i) a target binding sensor arm, ii) a partial catalytic core, and iii) a substrate-binding arm (Figure 2.3). Target binding sensor arms must have a complementary sequence with the input sequence (Assembly Facilitator) so that the target sequence can be detected. Furthermore, substrate arms had a complementary sequence with the substrate for it to hybridise and cleave due to enzyme catalytic activity. Each of partzyme was designed in 5'end to 3'end direction, with Partzyme A starting with sensor binding arm at 5'end and substrate binding arm at 3'end. Conversely, Partzyme B started with substrate arm at 5'end and sensor arm at 3'end. Both Partzymes' oligonucleotide was phosphorylated to prevent the sequence from being consumed during PCR extension process.

Catalytic activity of MNAzymes were monitored by cleavage of substrate that hybridised with the enzyme on the substrate arms. Substrate used in this study was Substrate 3 (Sub3) that was labelled with JOE, (2,7- dimethoxy-4,5-dichloro-6-carboxyfluorescein) at 5'end and the quencher Black Hole Quencher1 (BHQ-1) at 3'end. The sequence of substrate composed of deoxyribonucleotides and at least two ribonucleotides (Guanine and Uracil) were present in the middle of the sequence of the substrate's cleavage site. The list of substrates (Mokany *et al.*, 2010, 2013) that could be utilised for different detection of nucleic acids are described in Table 2.8.

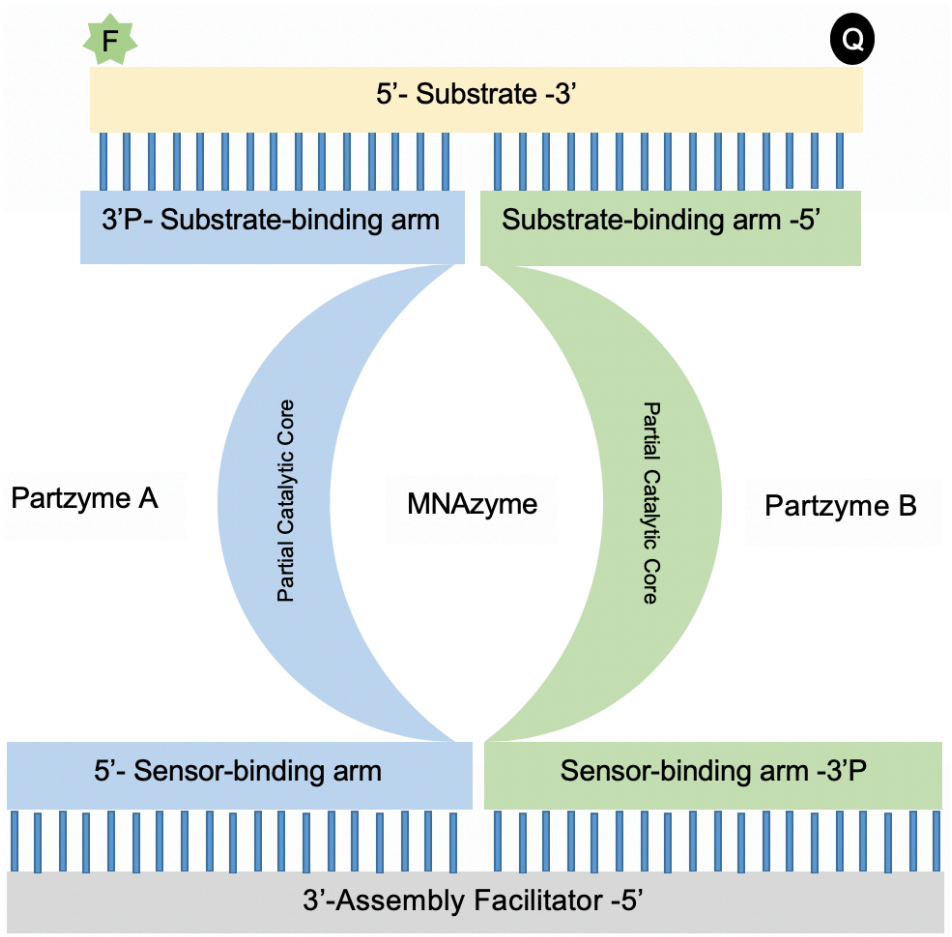

Figure 2. 3 Illustration of the MNAzyme components. Partzyme A is marked with blue colour and Partzyme B is marked with green colour. Both Partzymes bind adjacently to the AF sequence at their respective sensor-binding arms and hybridise with the substrate at substrate binding-arms. The Partzymes A and B are phosphorylated (P) at 3'end. The nucleic acid substrate is labelled with fluorophore (F) at 5'end and quencher (Q) at 3'end.

Table 2. 8 List of optimised nucleic acids substrate sequences (probe). Each substrate sequence can be labelled with fluorophore and quencher for detection in a real-time PCR instrument.

Substrate name	Sequence (5'→3')
Sub2	AAGGTTTCCTCguCCCTGGGCA
Sub3	CAGCACAACCguCACCAACCG
Sub4	CATGGCGCACguTGGGAGAAGTA
Sub6	ATCACGCCTCguTCCTCCCAG
Sub7	TTAACATGGCACguTGGCTGTGATA
Sub71	ACACTCCCCguCCCCAGCTC
Sub72	ATCACGCCTCguCTCCTCCCAG
Sub77	CTCCTCCCTCguCCCCAGCTC

2.15.2 Optimisations of the MNAzyme Pan-Fungal assay for isothermal detection

Each tube of MNAzyme reaction contained Partzyme A, Partzyme B, Substrate, AF, GeneAmp® PCR Buffer II (100 mM Tris hydrochloride, Tris-HCl; pH 8.3; 500 mM Potassium Chloride, KCl) (Applied Biosystems, USA) and 50 mM $MgCl_2$ (Invitrogen, USA) otherwise stated with the final concentration prepared as in Table 2.9. Oligonucleotide sequences for Partzymes, and synthetic AF were purified in a standard desalting and, High Performance Liquid Chromatography (HPLC) purifications for nucleic acids substrate synthesised Sigma-Aldrich, UK.

Table 2. 9 Composition of the reaction mixtures for isothermal detection method of the MNAzyme reaction.

Component	Final Concentration in 25 µL Reaction
Partzyme A	0.05 µM
Partzyme B	0.05 µM
Universal MNAzyme substrate	0.2 µM
AF	0.2 µM
GeneAmp® 10× PCR Buffer II	1 ×
$MgCl_2$, 1 M solution	10 mM / 50 mM
Nuclease-Free water (Promega, USA)	-

Designing the MNAzyme for fungal detection was performed by designing the sensor-binding sequences for each Partzyme to be complementary to a specific fungal DNA biomarker. The rate of catalytic activity of MNAzymes was subjected to the temperature, length of the substrate binding arms, the constituents and concentration of buffer (Mokany *et al.*, 2010). Therefore, in this study several parameters have been recognised for optimisations to achieve optimum and significant enzyme activity.

Firstly, the isothermal temperature at which the MNAzyme worked optimally was determined. A range of isothermal temperatures (30°C, 35°C, 40°C, 45°C, 50°C, 52°C, 55°C, 57°C, 59°C and 64°C) were tested in standard MNAzyme reactions. MNAzyme temperature optimisation reactions were prepared with the synthetic AF for fungal biomarker (AF ITS4LR1) included and each temperature was performed in triplicate as described in Table 2.9. The analyser used in this study was 2-Plex Rotor-Q Gene (Qiagen, Germany), and this instrument was used throughout the study. The data for the change in fluorescence over time, indicative of cleavage of the substrate over time, obtained was subjected to Prism 7 Software (GraphPad Software Inc.) to

measure Observed rate constant (K_{obs}) of the substrate Sub3-JB in MNAzyme Pan-Fungal assay.

Secondly, the concentrations of Partzymes in MNAzyme Pan-Fungal assay were optimised to reduce the signal obtained from 0.2 μM of Partzymes, as this concentration was used in the previous report. Partzyme A and Partzyme B concentrations were reduced from 0.2 μM to 0.1 μM, 0.05 μM, 0.01 μM and 0.005 μM.

Finally, co-factor $MgCl_2$ concentration was optimised for the highest and the most stable signal for hybridisation and cleavage of substrate that subjected to the complementary substrate-binding arms. Stock solution of 25 mM $MgCl_2$ (Applied Biosystems, USA) was used to test the final concentrations at 6 mM, 8 mM, 10 mM and 12 mM whereas, 1M stock solution of $MgCl_2$ (Invitrogen, USA) was used to test for higher final concentrations at 25 mM and 50 mM $MgCl_2$. Reactions without $MgCl_2$ and AF were also prepared as negative controls.

2.15.3 Specificity tests of MNAzyme Assay for fungal detection.

Specificity tests are important to determine the assay's capability to accurately detect AF sequences in the study. The AF used to test for specificity of the pan-fungal assay was named as AF-ITS4LR1. The tests were performed in three independent experiments and was prepared in triplicate. Fluorescence signals were detected and recorded in a real-time PCR instrument, Rotor-Q-gene (Qiagen, Germany).

Experiments were performed in 0.2 μM of substrate (Sub3-JB) and 1× buffer solution with or without AF for fungal target sequence (AF-ITS4LR1) for positive and negative controls. The experiments were performed to test six different controls with mutated sequence of the Partzymes, mutated sequence of the AF (AF-ITS4LR1mut) and a different AF (AF-RO5) in the MNAzyme Pan-Fungal assay. The assay also was

tested in the reaction without one of the Partzymes. Nuclease-free water was added in every tube to make up a final reaction volume of 25 µL. Experiments were monitored in the real-time PCR machine at 72-second intervals for 120 minutes and signals observed were compared with the positive and negative controls. The set of the sequences used in this experiment and each sequence was synthesised by Sigma-Aldrich, UK (Table 2.10).

Table 2. 10 List of sequences used in the specificity test of the MNAzyme assay for fungal detection.

Type	Name	Sequence (5'→3') *
Partzyme A	ITS4LR1A/3-P	GCTGAACTTAAGCATATCAAT ACAACGA *GGTTGTGCTG -P*
Partzyme B	ITS4LR1B/3-P	*CGGTTGGTGA* GGCTAGCT AAGCGGAGGAAAAGAAACCAAC-P
Substrate	Sub3-JB	JOE™-CAGCACAACCguCACCAACCG-BHQ1
AF	AF-ITS4LR1	GTTGGTTTCTTTTCCTCCGCTTATTGATATGC TTAAGTTCAGC
Mutated Partzyme A	ITS4LR1A/3 mut	GCTGAACTTAAGCATATCAATACA***G***CGA*GG TTGTGCT*-P
Mutated Partzyme B	ITS4LR1B/3 mut	*CGGTTGGTGA* GGC***C***AGCT AAGCGGAGGAAAAGAAACCAAC
Mutated AF	AF-ITS4LR1mut	GTTGGTTTCT***G***TTCCTCCGCTTATTGATATGC TTAAGTTCAGC
Different AF	AF-RO5	GAAGGTGTAATCCGTCTCCACACAGACAAG GCCAGGACTCGTTTG

***** Nucleotides underlined are partial catalytic core sequences; those outlined in italic are the substrate-binding arm. RNA nucleotides (-g and -u) represents Guanine and Uracil in substrate sequence. The "-P" at the end of partzyme sequence indicates that the oligonucleotide was 3' phosphorylated. JOE™ and BHQ1 indicate the dye and quencher labelled on the sequence at the 5' and 3' end. Italics and

bold nucleotide in sequences show location of point mutation made in the sequence; AF, Assembly Facilitator

2.15.4 Limit of detection of an Assembly Facilitator

MNAzyme sensitivity tests was performed to determine the assay's limit of detection. The test was performed in three independent experiments in triplicate. The assay's limit of detection was evaluated by reducing the concentration of the synthetic target sequence AF-ITS4LR1 under optimum conditions of the MNAzyme. The pan-fungal AF (AF-ITS4LR1) was diluted in MNAzyme assay at various concentrations (0.2 μM, 0.1 μM, 0.75 μM, 0.025 μM, 0.01 μM, 0.0075 μM, 0.0025 μM, 0.001 μM and 0.0005 μM). Each reaction tube contained 10 mM $MgCl_2$, 1× buffer solution, 0.2 μM substrate (Sub3-JB), 0.05 μM Partzyme A (ITS4LR1A/3-P) and Partzyme B (ITS4LR1B/3-P) and with or without AF (AF-ITS4LR1) in 25 μL reaction volume. Fluorescence signals were detected and recorded at 36-second intervals for an hour by real-time PCR machine, Rotor-Q-gene (Qiagen, Germany).

2.15.5 Detection of purified *C. albicans* DNA in the MNAzyme Pan-Fungal assay

In this experiment, the AF was *C. albicans* amplicon instead of the synthetic sequence, to be detected in MNAzyme assay. The experiment was performed to test the concept that MNAzymes must be able to become activated by any biological nucleic acid as well as synthetic nucleic acid sequences to produce an amplified output (Mokany *et al.*, 2013).

A primer set was designed (Table 2.11) to amplify the pan-fungal biomarker within *C. albicans* genome which contained the site for sensor arms hybridisation. Forward and reverse primers (pITS4LR1-F & pITS4LR1-R) were designed to amplify the sequence of interest (ITS4-LR1) with 84 bp amplicon size by using the strategy of

overlapping the forward primer with the 5'end of partzyme's sensor arm. A standard PCR assay was prepared as described in Table 2.3 with 0.5 μM final concentration of primers. The PCR product was purified using QIAquick® PCR Purification Kit (Qiagen, Germany) as described in Section 2.4. Before the purified *C. albicans* could be used for detection in MNAzyme assay, DNA sample was incubated in 95°C for 2 minutes to denature the double-stranded DNA. Afterwards, the sample was kept on ice until subjected into the MNAzyme reaction mixtures. In summary, the steps of the *C. albicans* amplicon detections in the MNAzyme Pan-Fungal assay is described in Figure 2.4.

Table 2. 11 The primer sequences used to amplify the sequence of interest for detection of the fungal kingdom.

Type	Name	Sequence (5'→3')
Forward primer	pITS4LR1-F	TACCCGCTGAACTTAAGC
Reverse primer	pITS4LR1-R	TTGCCGCTTCACTCGCCG

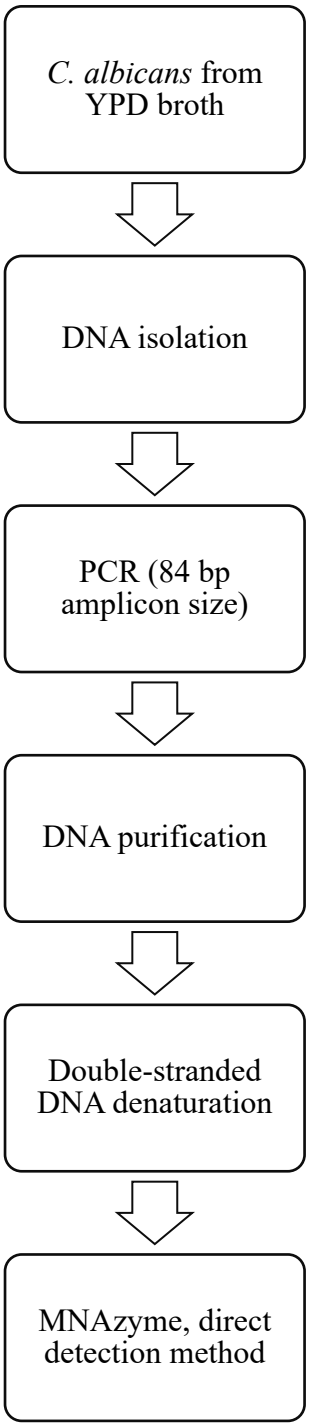

Figure 2. 4 Summarised steps for detection of *C. albicans* in the MNAzyme Pan-Fungal assay.

2.15.6 Kinetics of MNAzyme catalysis

Kinetic analysis of MNAzyme assay was initiated by converting the fluorescence data, in arbitrary units (a.u.) into reaction velocities. To do so, a standard curve of initial fluorescence signal emitted from fully cleaved substrate was established from a range of concentrations (1 μM, 0.5 μM, 0.25 μM, 0.125 μM, 0.0625 μM, 0.00311 μM). A fully cleaved or processed substrate (Sub3-JB ½) is half the sequence of the original substrate that has a fluorophore attached to the 5' end and this sequence was synthesised by Sigma-Aldrich, UK (Table 2.12). Fluorescence data obtained from a processed substrate in the buffer was subtracted from data of the substrate in water to eliminate the differences background signals. Two independent experiments were performed, with each reaction done in triplicate and monitored in real time at 36-second intervals for 30 minutes at 52°C. The value of fluorescence a.u. obtained at the initial point of every substrate's concentration was subjected to the Microsoft Excel program (Version 16) to form a linear graph with equation and R-squared properties.

Table 2. 12 Sequences of substrate used in the study to determine the kinetic activity values of developed MNAzyme assay.

Type	Name	Sequence (5'→3')
Unprocessed Substrate 3	Sub3-JB	JOE™-CAGCACAACCguCACCAACCG-BHQ1
Processed Substrate 3	Sub3-JB ½	JOE™-CAGCACAACC

To determine the enzymatic activity of MNAzymes Pan-Fungal assay, the isothermal direct detection method was used. Three independent experiments were performed, with each reaction done in triplicate with a modification of 50 mM $MgCl_2$ and various concentrations of substrate (either 1.00 μM, 0.75 μM, 0.50 μM, 0.25 μM, 0.20 μM, 0.15 μM, or 0.10 μM of Sub3-JB) in the reaction mixtures. Fluorescence

versus time data was recorded in 18 second-intervals for 30 minutes. Averages from an initial value of fluorescence (a.u.) were calculated for every substrate concentration and values were subjected to the linear equation established (Y= mX + c) as a Y value. Gradient values obtained were fitted in Michaelis-Menten equation (using Prism version 7, GraphPad Software Inc.) to derive the enzymatic parameters; maximum velocity (V_{max}) and Michaelis-Menten constant (K_m). In addition, catalytic constant (K_{cat}) was fitted by setting the concentration of enzyme sites, Et to a constant value in the model equation in Prism, GraphPad Software Inc. K_{cat} is the turnover number of substrate molecule each enzyme site converts to product per unit time. It is defined to equal V_{max}/Et. Enzymatic values for the MNAzyme Pan-Fungal assay were compared with MNAzyme assay that previously developed by Mokany, Bone, Young, *et al.*, (2010). As the substrate used in the study was different, K_{cat}/ K_m was calculated to provide direct comparison of the effectiveness of an enzyme toward different substrates. Furthermore, the observed rate constant, (K_{obs}) was determined for the catalytic rate by fitting a hyperbolic function to the fluorescence versus time data.

CHAPTER 3: Development of a Novel MPA assay for Specific and Sensitive Detection of Nucleic Acid Biomarkers of Clinically Important *Candida* Species

3.1 Introduction

Recent advances in real-time PCR are promising for the rapid and accurate detection of fungal pathogens from clinical samples. An FDA-approved multiplex qPCR kit, SeptiFast (Roche, Germany) can identify bacterial and fungal species from its unique characteristic of the hybridisation probe melting curves (Straub *et al.*, 2017; Wickes & Wiederhold, 2018). The kit detection of the fungal pathogen from blood samples is reported to have high specificity (91%), but low sensitivity (61%) (Chang *et al.*, 2013). In the case of fungal detection, the kit can only detect five *Candida* species (*C. albicans*, *C. parapsilosis*, *C. glabrata*, *C. tropicalis*, *C. krusei*) and, *A. fumigatus* and requires four detection channels in a qPCR instrument. In this study, we employed MPA nucleic acid detection platform that offers enhanced multiplexing capacity of two qPCR detection channels for detection of nine clinically relevant *Candida* species including discrimination of antifungal-resistant *C. auris*, *C. glabrata* and *C. krusei*.

MPA is an innovative and patented probe-based PCR technology of the UK biotechnology company, Genefirst Ltd. The technology relies on a novel characteristic of multiple-biomarker probe pairs that confer a unique melting temperature profile. Engineering of a PCO sequence with a few mismatches against the hydrolysis probe (THO) provide a functional melting profile in post-amplification analysis (Fu, Miles & Alphey, 2012). Here, as a proof of concept study, a dual channel, pentaplex MPA-*Candida* assay was developed to detect five target-hybridising oligonucleotide and partially-complementary oligonucleotide pairs (THO:PCO) – four *Candida* target probes and one IC probe. *Candida* DNA biomarkers were designed from the conserved

region of the D1/D2 domains of the rDNA locus. A novel IC probe was designed with non-homologous characteristics with any sequence in the GenBank database as identified using the BLAST. Pan-*Candida*, *C. krusei*-, *C. glabrata*-, *C. auris*-specific and IC target probes were paired with their PCO sequence and demonstrated an independent melting temperature across FAM and HEX detection channels. The detection of *Candida* species can also be tested in parallel with a pan-fungal reaction to provide a screening tool for fungal species and quantitative estimation of the fungal target copy present in the sample.

In this chapter, the *in vitro* characterisation of one of three alternative MPA-*Candida* assay designs is reported. The theoretical development of the two other designs is reported in Chapter 4. The work aimed to develop high throughput and easy-to-use test which is compatible with most commercial qPCR instruments. The MPA-*Candida* assay was used for the detection of the nine *Candida* species most commonly associated with candidiasis (*C. albicans*, *C. dubliniensis*, *C. tropicalis*, *C. parapsilosis*, *C. guilliermondii*, *C. haemulonii*, *C. krusei*, *C. glabrata* and *C. auris*) with high sensitivity and specificity. These species were tested over a range of genomic (10^0 to 10^5) and plasmid (10^2 to 10^6) DNA copies. The assays' analytical specificity and sensitivity were determined and evaluated against a commercial *Candida* panel (*Candida* Evaluation Panel, Qnostics Ltd) and a singleplex *C. auris* qPCR diagnostic kit (Genesig Standard Kit, Primerdesign Ltd). The *in vitro* results described here highlight the potential use of our MPA-*Candida* assay in clinical diagnosis of invasive candidiasis and suggest its applications in disease management and outbreak control.

3.2 Experimental Results

3.2.1 Target sequences identification and characterisation

Short biomarker nucleotide sequences that could reliably differentiate fungi from bacteria (pan-fungal biomarker), the genus *Candida* from any other fungi (pan-*Candida* biomarker) and discern *C. auris*, *C. glabrata* and *C. krusei* from all other *Candida* species in a highly specific manner were sought within the rDNA locus (Halliday *et al.*, 2015; Schoch *et al.*, 2012; Irinyi *et al.*, 2016), as described in Materials and Methods. The pan-fungal probe lies within the ITS2 region (Figure 3.1). A reverse BLAST search was performed to demonstrate its specificity. The probe had 100% sequence similarity with 100% query cover for all 100 fungal species tested (Table 3.1). An optimised universal primer set ITS3 and LR1 was used to amplify the pan-fungal target region (Table 3.2). Amplicon sizes ranging from 279 bp (*Candida auris*) to 451 bp (*Absidia corymbifera*) were obtained (Figure 3.2).

Genus-specific (pan-*Candida*) and species-specific *Candida* biomarkers lie within the D1/D2 region of the LSU rDNA gene (Figure 3.1). A reverse BLAST search was performed to check the specificity of these biomarkers. *C. krusei*, *C. glabrata* and *C. auris*-specific probes had 100% sequence similarity with 100% query cover to their respective *Candida* strains. The pan-*Candida* probe had 100% similarity with all *Candida* species tested. A similarity to some other yeast species rarely associated with human infection was also observed (Table 3.1). All selected biomarker sequences showed no strain-to-strain variability in the multiple sequence alignments analysis. A forward pair for pan-*Candida* target region was employed from the fungal universal primer LR0, and the reverse primer named as GSCand, was designed specifically in this study (Table 3.2). The primer set generated a 381 bp amplicon for most of the *Candida* species and has slightly smaller size (370 bp) for *C. krusei*, *C. auris* and *C.*

guilliermondii (Figure 3.3). Importantly, a single set of pan-*Candida* primers was designed to include all *Candida* probes binding sites for MPA-*Candida* assay. The list of the PCR primer sets, and the characteristics of the sequences are summarised in Table 3.2.

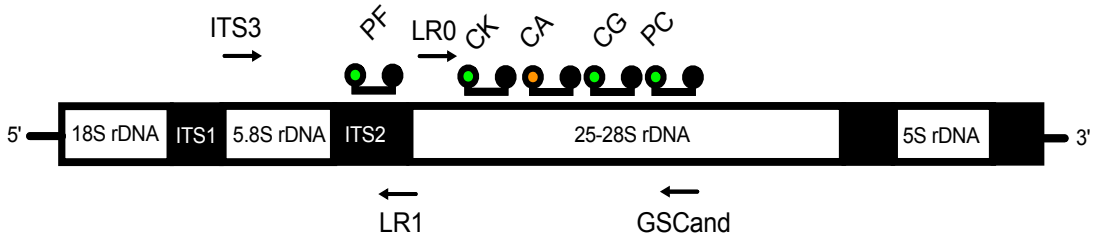

Figure 3. 1 Schematic drawing of the relative position of the primers and probes binding sites along the fungal ribosomal genes. The pan-fungal primer set (ITS3 and LR1) and pan-*Candida* primer set (LR0 and GSCand) are shown as arrows; dual-labelled probes labelled with FAM are shown as green dots for pan-fungal (PF), *C. krusei* (CK), *C. glabrata* (CG), pan-*Candida* (PC) and HEX labelled probe as orange dot for *C. auris* (CA). The quencher for the probes is shown as black dots. The figure is not drawn to scale.

Table 3. 1 The result of BLAST search of the pan-fungal and *Candida* probes.

Probe target (symbol)	**No. with 100% sequence similarity to probe/total no. in GenBank database**	**Other species with 100% sequence similarity**
Pan-fungal (PF)	100/100 fungi strains	None
Pan-*Candida* (PC)	38/38 *Candida* species strains	*Saccharomyces cerevisiae*, *Yamadazyma olivae*, *Kregervanrija pseudodelftensis*, *Zygosaccharomyces rouxii*, *Spathaspora* sp.
C. krusei-specific (CK)	100/100 *C. krusei* strains	None
C. glabrata-specific (CG)	100/100 *C. glabrata* strains	None
C. auris-specific (CA)	37/39 *C. auris* strains	None

Table 3. 2 List of primer sets for amplification of pan-fungal and pan-*Candida* target regions.

Primer set	Sequence (5'→3')	T_m (°C)	GC%
Pan-fungal:			
ITS3-F	GCATCGATGAAGAACGCA	48.0	50
LR1-R	GTTGGTTTCTTTTCCTCCG	48.9	47
Pan-*Candida*:			
LR0-F	ACCCGCTGAACTTAAGCATA	49.7	45
GSCand-R	CTGTTTCACTCTCTTTTCAAAGT	49.9	35

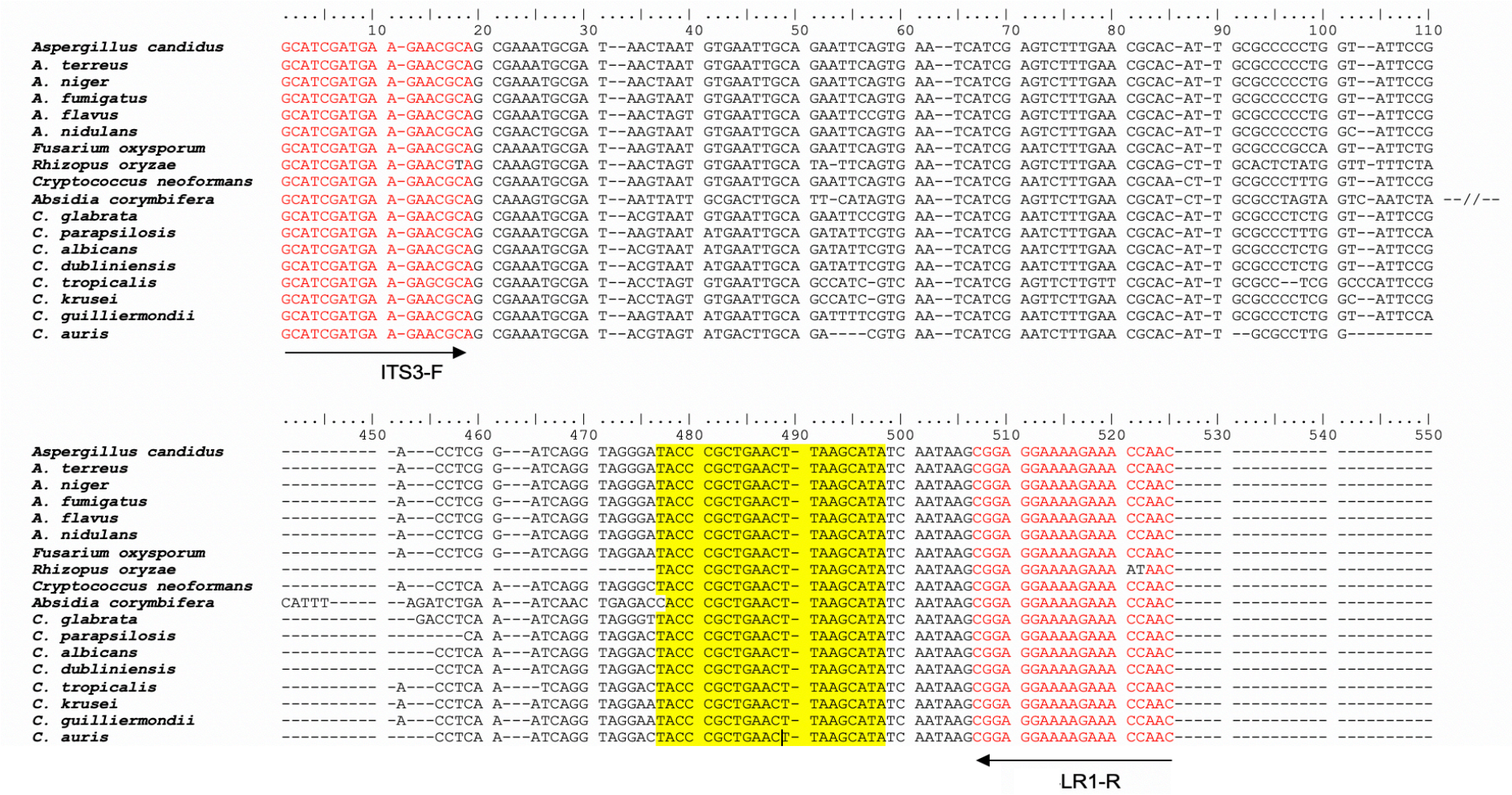

Figure 3. 2 Multiple-sequence alignment of the fungal ITS2 region. Target sequences corresponding to the pan-fungal probe are highlighted in yellow and the primer set in red.

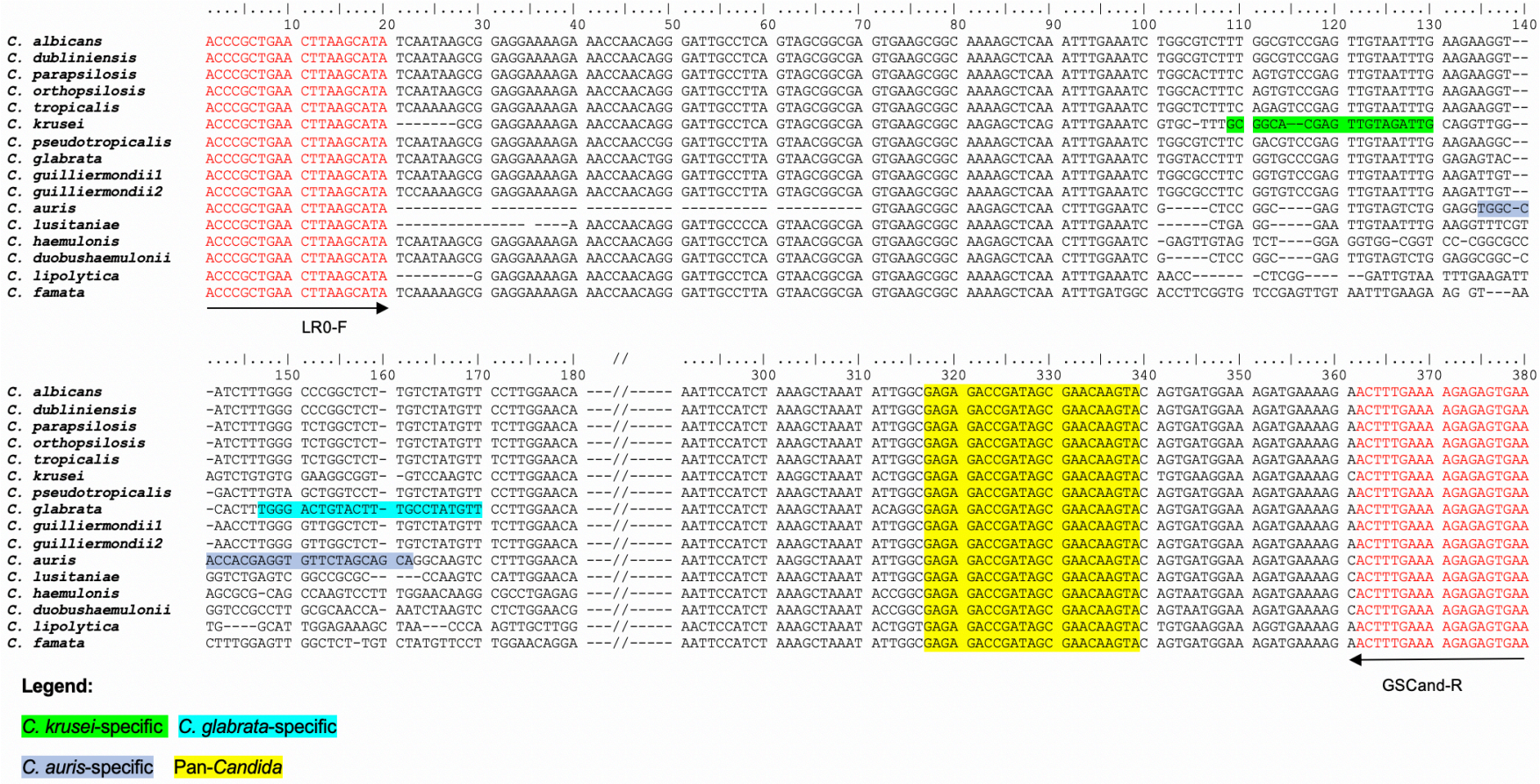

Figure 3. 3 Multiple-sequence alignment of the *Candida* species LSU rDNA gene. Target sequences corresponding to the *Candida*-specific probe is highlighted in yellow and species-specific probes are highlighted with different colours, and the primer set in red.

3.2.2 Cloning of DNA target sequences

The target sequences of *C. albicans*, *C. parapsilosis*, *C. tropicalis*, *C. glabrata*, *C. krusei*, *C. guilliermondii*, *C. dubliniensis*, *C. haemulonii* and *C. auris* were cloned into a plasmid vector pCR 2.1-TOPO. Initially, the *Candida* species DNA were amplified using the pan-fungal and pan-*Candida* primer sets in a conventional PCR method and analysed the product's band size (Figures 3.4 and 3.5). The purified pan-fungal target sequence including primer binding sites confirmed the amplicon size from the sequencing results. Moreover, the nine *Candida* species DNA with pan-*Candida* target sequences were also cloned into the pCR 2.1-TOPO vector. The target included primer sequence sites LR0 and GSCand binding site and confirmed the products through the sequencing results. The total sizes of plasmid vector pCR 2.1-TOPO with the pan-fungal and pan-*Candida* DNA fragments measured in a range of 4210 bp to 4360 bp and 4299 to 4307, respectively (Table 3.3).

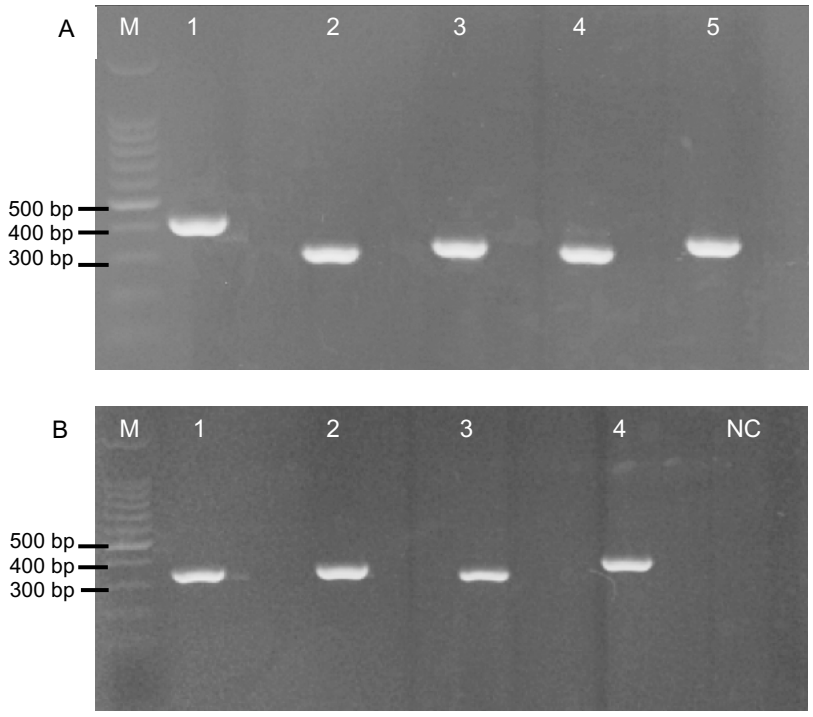

Figure 3. 4 Gel electrophoresis of PCR product using a pan-fungal primer set. Panel A) M: 100 bp marker; lane 1: *C. glabrata*; lane 2: *C. parapsilosis*; lane 3: *C.*

dubliniensis; lane 4: *C. tropicalis*; lane 5: *C. guilliermondii*. **Panel B**) M: 100 bp marker; lane 1: *C. albicans*; lane 2: *C. haemulonii*; lane 3: *C. auris*; lane 4: *C. krusei*; NC: Negative Control.

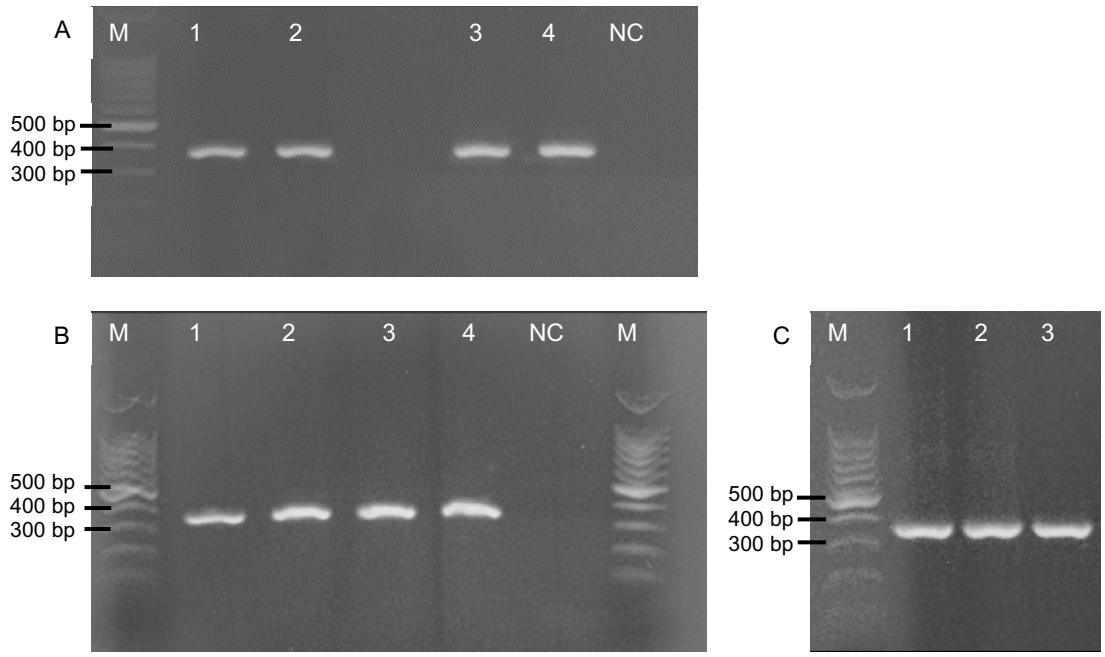

Figure 3. 5 Gel electrophoresis of PCR product using a pan-*Candida* primer set. Panel A) M: 100 bp marker; lanes 1 and 2: *C. albicans*; lanes 3 and 4: *C. krusei*; NC: Negative Control. **Panel B**) M: 100 bp marker; lane 1: *C. glabrata*; lane 2: *C. parapsilosis*; lane 3: *C. tropicalis*; lane 4: *C. dubliniensis*; NC: Negative Control; M: 100 bp marker. **Panel C)** M: 100 bp marker; lane 1: *C. auris*; lane 2: *C. haemulonii*; *C. guilliermondii*.

Table 3. 3 The pan-fungal and pan-*Candida* amplicons and cloned plasmid DNA sizes.

Target species	Amplicon size (bp)	Size (bp) from the sequencing primer set (M13F & R)	Total size plasmid DNA (amplicon + 3931 bp)
Pan-fungal			
C. albicans	350	549	4281
C. parapsilosis	323	522	4254
C. tropicalis	340	539	4271
C. dubliniensis	355	554	4286
C. haemulonii	350	549	4281
C. glabrata	429	628	4360
C. guilliermondii	391	590	4322
C. auris	279	478	4210
C. krusei	359	558	4290
Pan-*Candida*			
C. albicans	376	575	4307
C. parapsilosis	376	575	4307
C. tropicalis	376	575	4307
C. dubliniensis	376	575	4307
C. haemulonii	376	575	4307
C. glabrata	375	574	4306
C. guilliermondii	375	574	4306
C. auris	373	573	4304
C. krusei	368	567	4299

3.2.3 Engineering of a Novel IC MPA probe

A novel IC probe was obtained by recircularisation of the plasmid pCR™ 2.1-TOPO® vector which resulted in a random eight base pairs insertion. As a result, the IC dual-labelled probe was designed to contain eight nucleotide bases along with the bases already existing in the plasmid (Figure 3.6) and made up the total size of 3939 bp. A BLAST search of the IC probe sequence revealed no 100% identity to sequences on the database (Table 3.4). The universal M13 primer set was used in every reaction of the MPA-*Candida* and Pan-Fungal assays to amplify the IC plasmid DNA template.

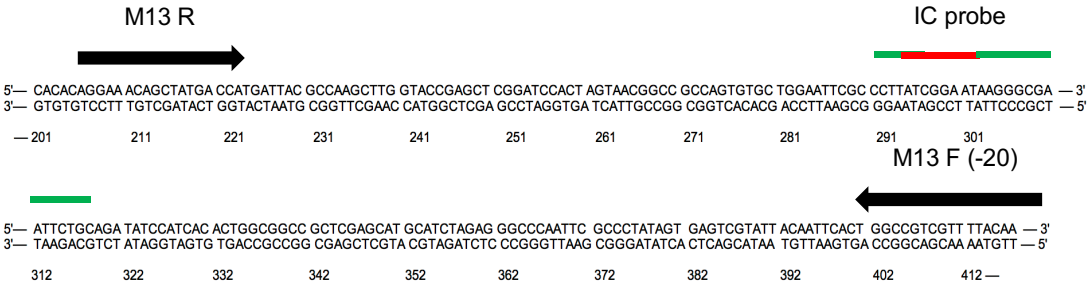

Figure 3. 6 The nucleotide sequence of the IC probe and primer set. The alignment of cloned plasmid pCR™ 2.1-TOPO® vector sequence focusing on the eight nucleotide bases insert (marked with red bar) within the IC probe sequence (marked with green bar). The total size of the DNA fragment from the primer sites (M13F and M13R) is 207 bp.

Table 3. 4 The result of BLAST search of the IC probe sequence for a non-homologous characteristic.

Description	Query cover (%)
Uncultured eukaryote clone SGSU521 18S ribosomal RNA gene, partial sequence	21/26 (80)
Acremonium sp. (in: Hypocreales) isolate	21/26 (80)
Uncultured bacterium clone 16S ribosomal RNA gene, partial sequence	20/26 (76)
Flagellophora apelti partial 28S rRNA gene, isolate 1	19/26 (73)
Lactobacillus jensenii strain SNUV360, complete genome	19/26 (73)
Salinimonas sp. HMF8227 chromosome, complete genome	19/26 (73)
Crassostrea gigas tbetaRI gene for TGF-beta Type I receptor	18/26 (69)
Uncultured bacterium clone 4-L 16S ribosomal RNA gene	18/26 (69)
Bactris pliniana phosphoribulokinase-like protein 2 gene	18/26 (69)
Spirometra erinaceieuropaei genome assembly	18/26 (69)
Xenorhabdus bovienii str. CS03 chromosome, complete genome	18/26 (69)

3.2.4 Design of MPA probes and *in silico* melting curve analysis testing

MPA probes consist of two partly complementary oligonucleotides, the dual-labelled THO and a corresponding PCO. Each THO is fully complementary to the identified biomarker target sequences meanwhile, the PCO was engineered with four to six nucleotide mismatches against the THO sequence (Table 3.5). The initial characterisation of all six MPA probes (THOs plus their corresponding PCO sequences) using UNAFold software (http://unafold.rna.albany.edu/) allowed confirmation of their theoretical melting profiles (Figure 3.7). The software predicts overlapping melting temperatures between *C. krusei*-specific and the IC probes as well as between *C. auris*- and *C. glabrata*-specific probes. However, their independent analysis is not affected under experimental conditions as each overlapping probe is labelled with a different fluorophore. For example, the pan-*Candida*, *C. krusei*-specific and *C. glabrata*-specific probes were labelled with FAM whereas the *C. auris*-specific and the IC probes were labelled with HEX. The results from the *in silico* analysis helped to assign an appropriate reporter dye to the THO probe. The probes are distinguishable based on its unique melting temperature that were detected in FAM and HEX detection channel in a real-time PCR instrument. Homodimer prediction of the THO probe melting temperatures shown five probes overlapped at 68°C; an independent *C. auris*-specific probe, CA THO:PCO at 77°C (Figure 3.8). *In silico* analysis showed that THO and its fully complementary target sequence has a higher melting temperature compared to the PCO.

Table 3. 5 Design of the MPA probe pairs. The THO and PCO sequences for pan-*Candida*, *C. krusei*-specific, *C. glabrata*-specific and *C. auris*-specific targets, pan-fungal and a non-homologous IC probe.

Probe target; (Symbol)	**Probe sequence (5'→3')**	**Fraction and percentage of mismatched**
Pan-*Candida* (PC)	THO: TACTTGTTCGCTATCGGTCTCTC	4/23 (17.4%)
	PCO1: GAGAtAtCGATAGCtAAtAAGTA-Ph	
C. krusei (CK)	THO1: CAATCTACAACTCGTGCCGC	4/20 (20.0%)
	PCO1: GCGGCAtGAaTTaTAtATTG-Ph	
C. glabrata (CG)	THO2: AACATAGGCAAAGTACAGTCCCA	4/23 (17.4%)
	PCO1: TGGGAaTGTAaTTTGaCTATaTT-Ph	
C. auris (CA)	THO2: TGGCCACCACGAGGTGTTCTAGCAGCA	5/27 (18.5%)
	PCO1: TGCTGCTAGActACtTCaTtGTGGCCA-Ph	
Pan-fungal (PF)	THO2: TATGCTTAAGTTCAGCGGGTA	4/21 (19.0%)
	PCO2: TACCCGaTtAAaTTgAGCATA-Ph	
Internal Control (IC)	THO: CTTATCGGAATAAGGGCGAATTCTGC	6/26 (23.0%)
	PCO2: GCAtAATTaGtCaTTATTaCtATAAG-Ph	

*Lower case nucleotides in PCO sequence denote nucleotide mismatches against THO sequence; -Ph, phosphorylated at the 3'end of a PCO sequence

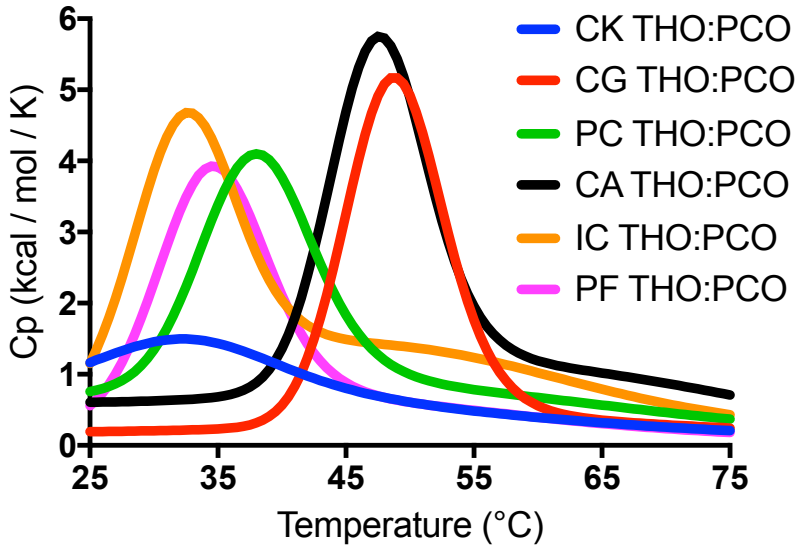

Figure 3. 7 The prediction of melting temperature of THO and PCO hybrid by UNAFold software. MPA probe pairs for *C. krusei* (CK), *C. glabrata* (CG), pan-*Candida* (PC), *C. auris* (CA), IC and pan-fungal (PF). The heat capacity (C_p) curve is the maximum amount of heat needed to change the temperature of one mole of a hybrid by one degree at constant pressure which defines the melting temperature.

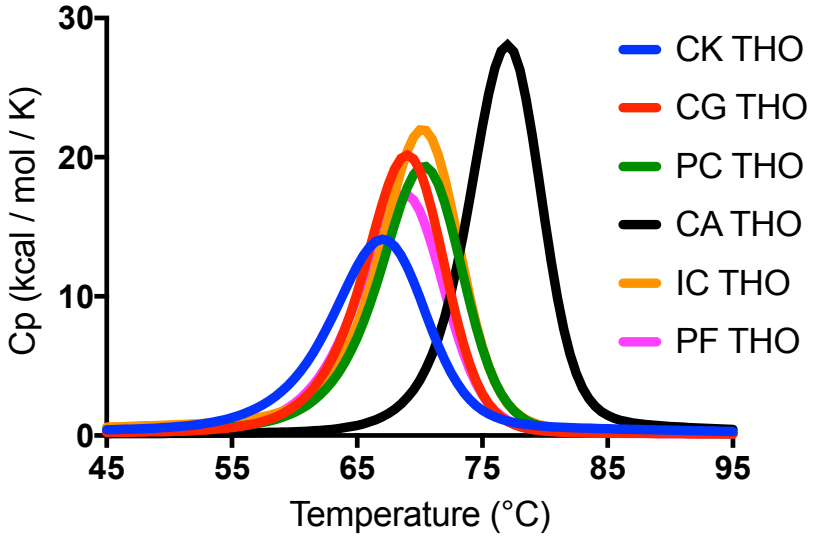

Figure 3. 8 Homodimer prediction of melting temperature of THO sequences by UNAFold software. THO melting temperature determined for *C. krusei* (CK), *C. glabrata* (CG), pan-*Candida* (PC), *C. auris* (CA), Internal Control (IC) and pan-fungal (PF). The C_p curve is the maximum amount of heat needed to change the temperature of one mole of a hybrid by one degree at constant pressure which defines the melting temperature.

3.2.5 Experimental *in vitro* testing of THO:PCO hybrid melting temperatures using the LightCycler 480 qPCR machine

The melting curve analysis was performed to determine the melting temperature between the THO and its potential PCO sequences. Each probe's THO and a PCO was tested to achieve a specific melting temperature. Initial testing of the THO:PCO hybrid melting temperature performed in an independent melting curve analysis, without the amplification step. Initial analysis of each probe melting temperature is useful for the probes multiplexing arrangement and assay design layout. The pan-*Candida* probe **(**PC THO:PCO1) and *C. krusei*-specific probes **(**CK THO:PCO1) demonstrated two distinct melting temperature peaks (Figure 3.9). The second set of *C. krusei*-specific probe hybrid (CK THO2) was also tested for its melting temperature and the probe was used in the assay design optimisations (Figure 3.10). MPA probes for *C. glabrata*-specific (CG), *C. auris*-specific (CA), pan-fungal (PF) and IC were characterised for their melting temperatures (Figure 3.11). The testing of the IC THO probe hybrids to its potential PCO1 and PCO2, produced melting temperatures at 48°C and 34°C, respectively. Some of the probe pairs overlapped and did not produce the predicted melting temperature which led to probe re-design. Two of the probes were re-designed for *C. glabrata*-specific (CG THO2:PCO1) and *C. auris*-specific (CA THO2:PCO1) and produced melting peaks at 46°C and 49°C, respectively (Figures 3.12 and 3.13). The THO of these probes were further tested for the functionality of the detection in the PCR and is reported in next sub-section. A new THO:PCO hybrid for the pan-fungal was also re-designed and generated melting temperature at 38.92°C (Figure 3.14). The summary of the probes melting temperature and the selected probe pairs for the MPA-*Candida* assay is presented in Table 3.6.

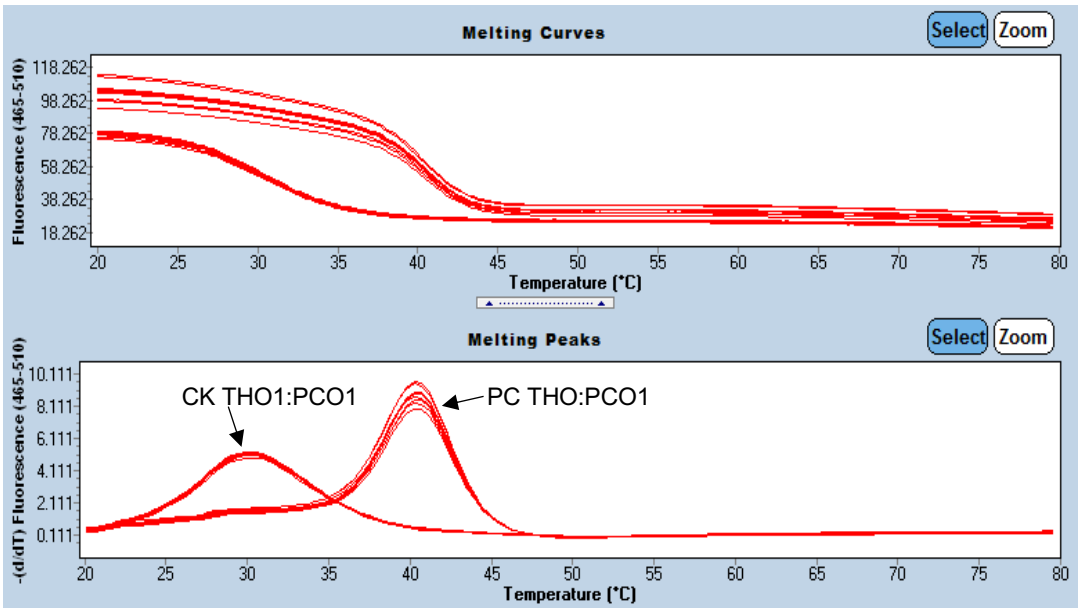

Figure 3. 9 The melt curves analysis of *C. krusei*-specific and pan-*Candida* probes. *C. krusei*-specific probe, CK THO:PCO1 at 31.7°C and pan-*Candida* probe, PC THO:PCO1 indicated at 41.04°C. Each probe was tested in a separate reaction with nine replicates.

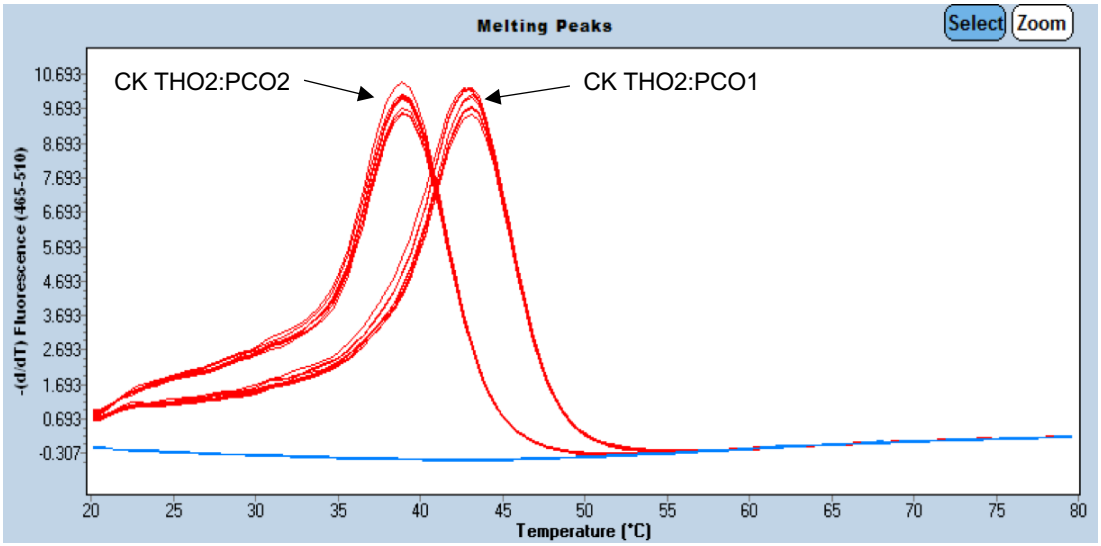

Figure 3. 10 The melting peaks generated from *C. krusei*-specific probe against its respective PCO sequences. The CK THO2 probe its melting peaks with PCO1 at 41°C and PCO2 at 39°C. CK: *C. krusei*-specific. Each THO:PCO hybrid was tested in a separate reaction with nine replicates.

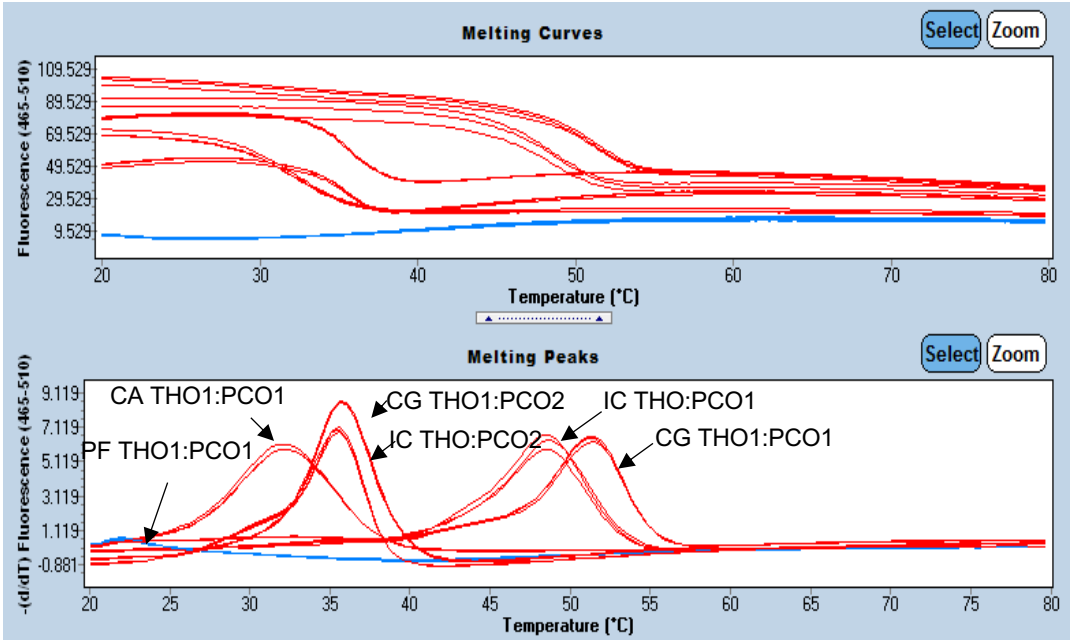

Figure 3. 11 The melt curves analysis of pan-fungal, *C. auris*, *C. glabrata* and IC probes, and each was tested in a separate reaction. *C. auris*-specific probe, CA THO1:PCO1 at 32.25°C; IC probes, IC THO1:PCO2 at 35.09°C and THO1:PCO1 at 48.80°C; *C. glabrata*-specific probes, CG THO1:PCO2 at 35.71°C and THO1:PCO1 at 51.38°C. The pan-fungal probe PF THO1:PCO1 showed no melting peak. The probe melting temperature performed in triplicates for each reaction.

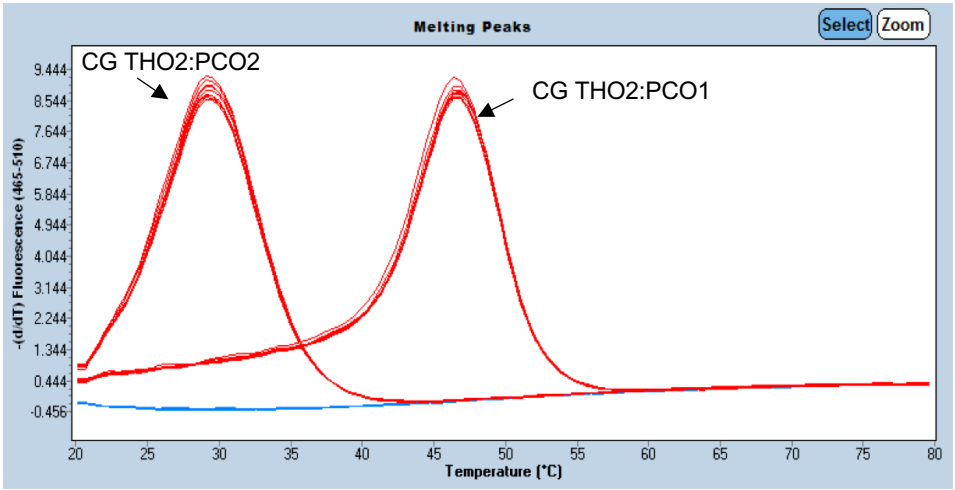

Figure 3. 12 The melt curve analysis of *C. glabrata*-specific probe with two designs of PCO sequences. Melting peaks temperature reported as means (n=9) between *C. glabrata*-specific THO (CG THO2) and PCO1 demonstrated at 46.67°C; PCO2 at 29.51°C.

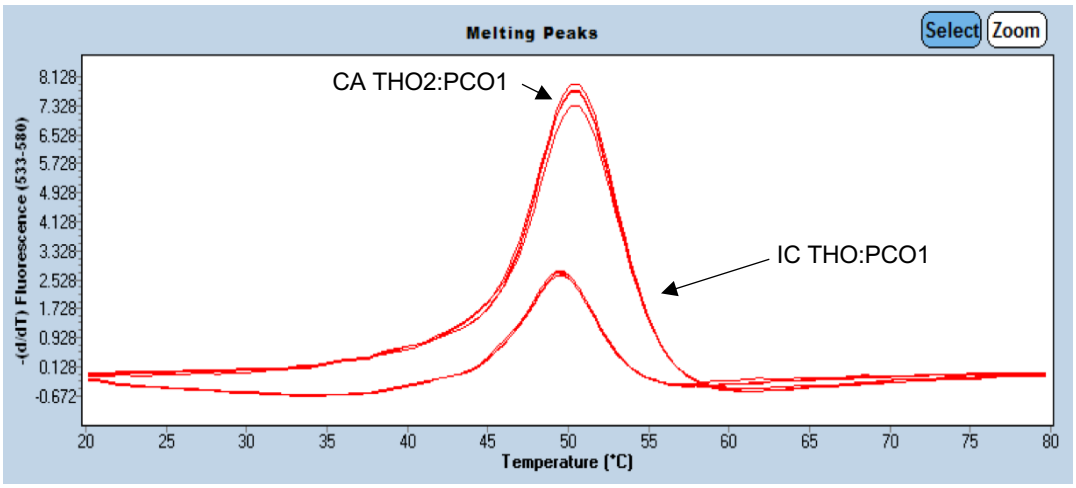

Figure 3. 13 Overlapped melting peaks at 48°C between the *C. auris*-specific probe and internal control probe. Consequently, the IC THO was paired with PCO2 in the MPA-*Candida* assay. CA: *C. auris*-specific; IC: Internal Control. Each probe melting temperature was tested in a separate reaction with replicates (n=6).

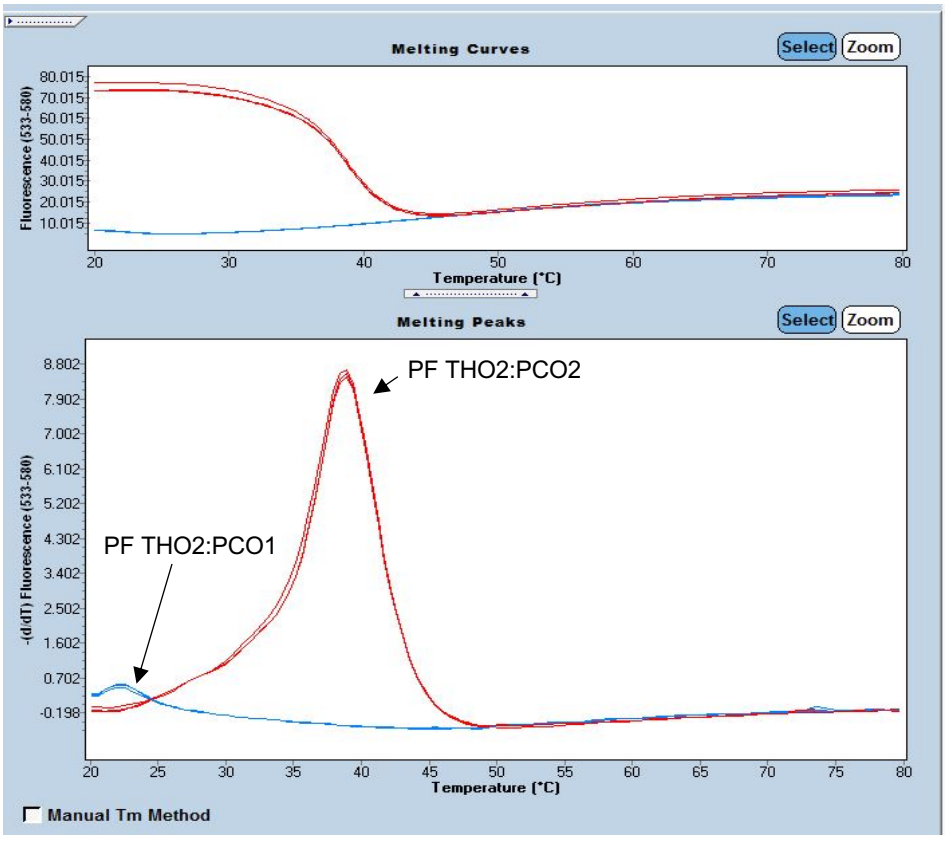

Figure 3. 14 The melt curve analysis of the pan-fungal probe with two designs of PCO sequences. Melting temperature reported as mean (n=3) between the pan-fungal (PF) THO2 and PCO2 at 38.92°C; meanwhile no temperature value detected for the PF THO2:PCO1 hybrid.

Table 3. 6 Experimental melting temperature of THO and PCO hybrid.

Probe target, (symbol)	Probe sequence (5'→3')	THO:PCO T_m (°C)
Pan-*Candida* (PC)	**THO1: TACTTGTTCGCTATCGGTCTCTC**	
	PCO1: GAGAtAtCGATAGCtAAtAAGTA-Ph	41.04
	PCO2: GAtAGAaCGATAtCGAAtAAtTA-Ph	ND
C. krusei (CK)	**THO1: CAATCTACAACTCGTGCCGC**	
	PCO1: GCGGCAtGAaTTaTAtATTG-Ph	31.70
	PCO2: GCaGCAtGAaTTaTAtATTG-Ph	ND
	THO2: TTGCGGCACGAGTTGTAGATTG	
	PCO1: CAATaTAtAAtTCaTGCCGCAA-Ph	41.00
	PCO2: CAATaTAtAACTCaTGCCtCAA-Ph	39.27
C. glabrata (CG)	THO1: CAAGGAACATAGGCAAAGTACAGTCCCA	
	PCO1: TGGGAtTGTAaTTTGaCTATaTTCCTTG-Ph	51.38
	PCO2: TGGGAaTGTAaTTTaCaTATaTTaCTTG-Ph	35.71
	THO2: AACATAGGCAAAGTACAGTCCCA	
	PCO1: TGGGAaTGTAaTTTGaCTATaTT-Ph	46.67
	PCO2: TGGtACTaTAaTTTGCaTATaTT-Ph	29.51
C. auris (CA)	THO1: CTGCTGCTAGAACACCTCGT	
	PCO1: ACGAtGTaTTaTAGtAGCAG-Ph	32.25
	PCO2: ACGAtGTaTTaTAtCATCAG-Ph	ND
	THO2: TGGCCACCACGAGGTGTTCTAGCAGCA	
	PCO1: TGCTGCTAGActACtTCaTtGTGGCCA-Ph	48.80

Pan-fungal	THO1: CTCCTTTTCTTTGGTTG	
(PF)	PCO1: CAACtAAAcAAAAGtAG-Ph	23.00
	PCO2: CAACtAAAcAAAAttAG-Ph	ND
	THO2: TATGCTTAAGTTCAGCGGGTA	
	PCO1: TACCCtaTtAAaTTAAaCATA-Ph	ND
	PCO2: TACCCGaTtAAaTTgAGCATA-Ph	38.92
Internal	**THO1: CTTATCGGAATAAGGGCGAATTCTGC**	
Control (IC)	PCO1: GCAgAATTaGCCaTTATTaCtATAAG-Ph	48.80
	PCO2: GCAtAATTaGtCaTTATTaCtATAAG-Ph	35.09

* Boldface probe sequences are the selected THO and PCO in the MPA-*Candida* and Pan-Fungal assay; the number followed after THO/PCO sequences denote version of the sequence design; lower case nucleotides within PCO are nucleotide mismatches against THO sequence; -Ph, phosphorylated at the 3'end of a PCO sequence; ND, No Detection

3.2.6 Experimental testing of the re-designed *C. glabrata*-specific and *C. auris*-specific probes for detection of targets sequence in real-time PCR.

The amplification of the *C. glabrata* plasmid DNA using the newly designed *C. glabrata*-specific probe (CG THO2) shown an amplification curve at $C_t = 19.24 \pm 0.68$ (Figure 3.15). The probe was further tested in the MPA reaction for its hybridisation with the PCO sequence. The melting temperature was determined at 46°C. Inclusion of the PCO1 of CG THO2 probe in the reaction with the *C. glabrata* plasmid DNA demonstrated an expected downwards shift of melting peak compared to the *C. glabrata*-specific probe no DNA control (NDC) melting profile (Figure 3.16).

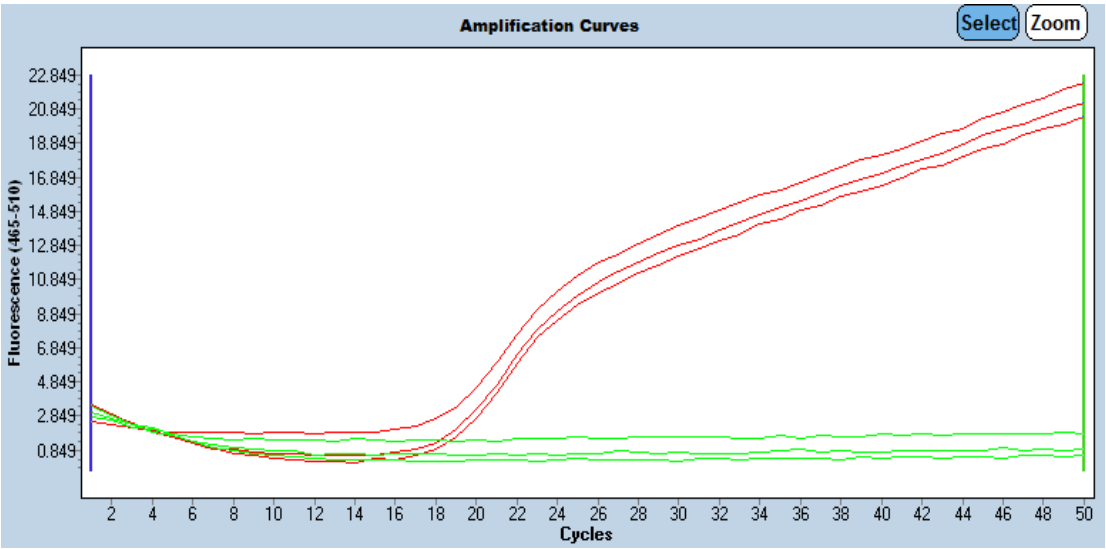

Figure 3. 15 Amplification curves detection of *C. glabrata* plasmid DNA. The C_t value at 19.24 ± SD 0.68 (n=3) using newly design *C. glabrata*-specific probe. The amplification detected by the dual-labelled probe, CG THO2 and the negative control signal (green lines) in FAM channel. Each qPCR reaction was performed in triplicate.

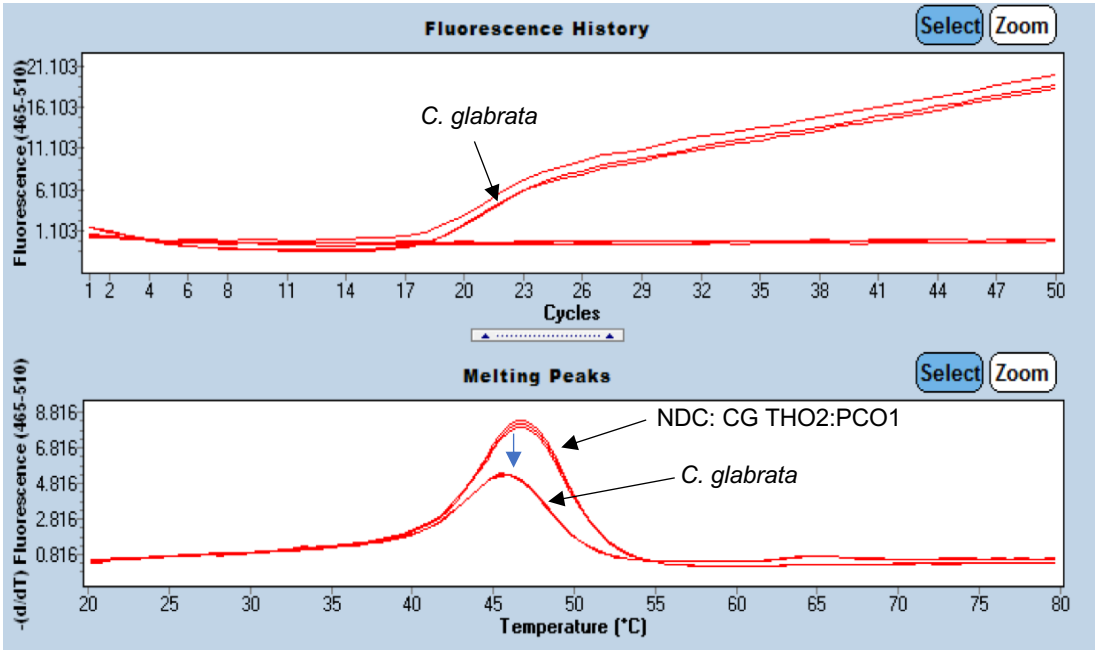

Figure 3. 16 The *C. glabrata*-specific probe amplification and melting curves analysis of the MPA reaction. *C. glabrata* plasmid DNA at 10^6 copies per reaction and MPA probe melting peaks for detection of target sequence the reaction showed lowered (with blue arrow) melting peak at CG THO2:PCO1 temperature. NDC, no DNA control; CG, *C. glabrata*-specific. The experiment was performed in triplicate and melting temperature reported at 46 ±1°C.

The *C. auris*-specific probe (CA THO1:PCO1) was tested in the reaction for the amplification of the *C. auris* plasmid DNA. As an experimental control, the pan-*Candida* probe (PC THO1:PCO1) was used to amplify the same *C. auris* DNA template. Therefore, this experiment involved two NDC profiles for pan-*Candida* (40°C) and *C. auris*-specific (32°C). The preliminary results showed that the *C. auris* target DNA is amplified by the pan-*Candida* probe (PC THO1:PCO1) but not detected by the *C. auris*-specific probe, CA THO1:PCO1 (Figure 3.17). The PCR results were supported by the melting curves analysis as only the reaction with the pan-*Candida* probe showed a decrease in melt peak against the control. The experiment also performed using the probe as a standard hydrolysis probe for detection of *C. auris*

plasmid DNA concluded there is no amplification by *C. auris*-specific probe, CA THO1 (Figure 3.18). The new design of the *C. auris*-specific MPA probe (CA THO2) successfully amplified the target DNA as expected in the hydrolysis probe reaction with the curve detected at C_t= 18 recorded for high concentration of *C. auris* plasmid DNA in the reaction (Figure 3.19). Utilisation of the *C. auris*-specific THO2 with PCO1 in a multiplex reaction of MPA-*Candida* showed specific detection of *C. auris* DNA described in the assay specificity and sensitivity sections.

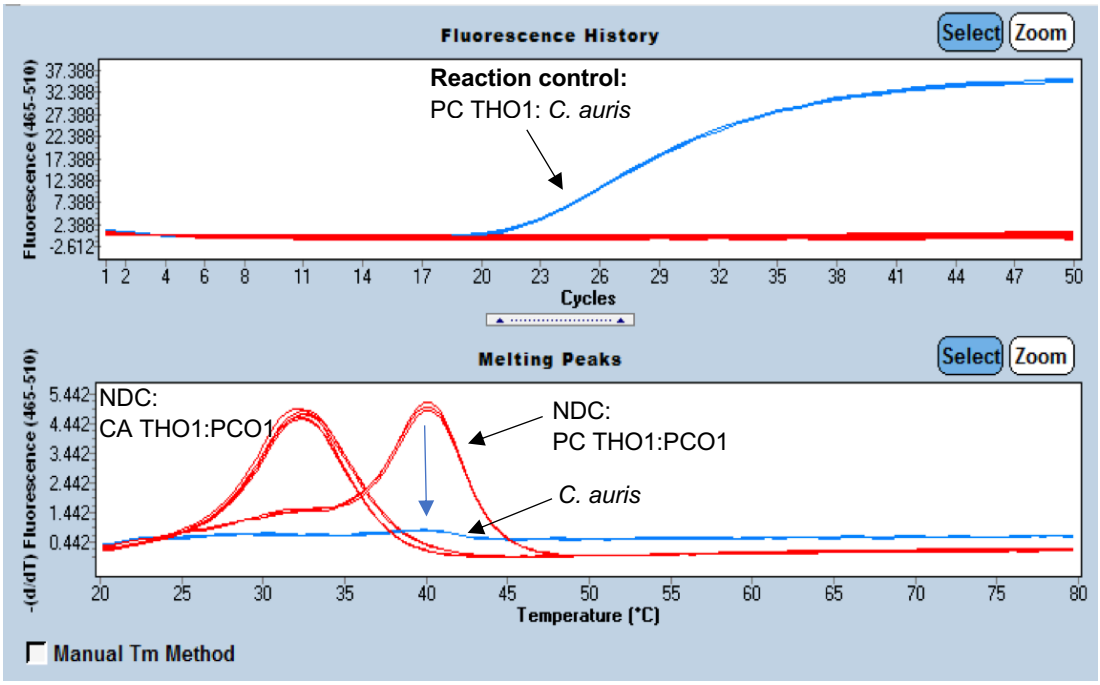

Figure 3. 17 The amplification profile and the corresponding melt curves analysis for *C. auris* plasmid DNA. The amplification signal detected in the reaction with pan-*Candida* probe (PC THO1) and melt curve showed down shift (blue arrow) of melting peak at pan-*Candida* melting peak temperature. CA: *C. auris*-specific. NDC: no DNA control. The analysis of each probe pair was performed in six replicates.

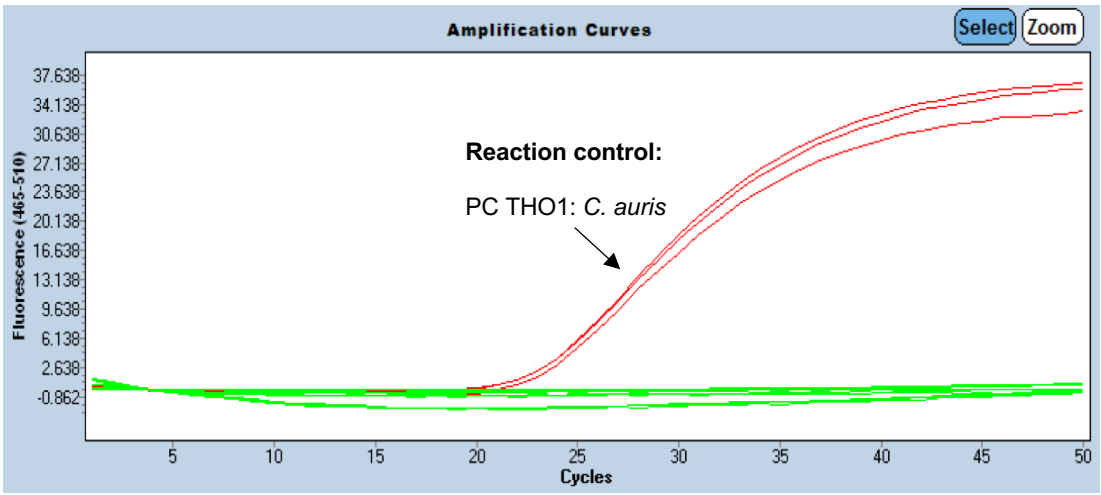

Figure 3. 18 Testing the amplification of *C. auris* plasmid DNA by the *C. auris*-specific probe. No amplification of the *C. auris* plasmid DNA in the reaction with the *C. auris*-specific probe (CA THO1) (signal in the green lines) but amplification of the DNA detected (C_t=24) in the reaction control with the pan-*Candida* probe (PC THO1). Each reaction contained 10^6 copies of *C. auris* plasmid DNA and PCR was performed in triplicate.

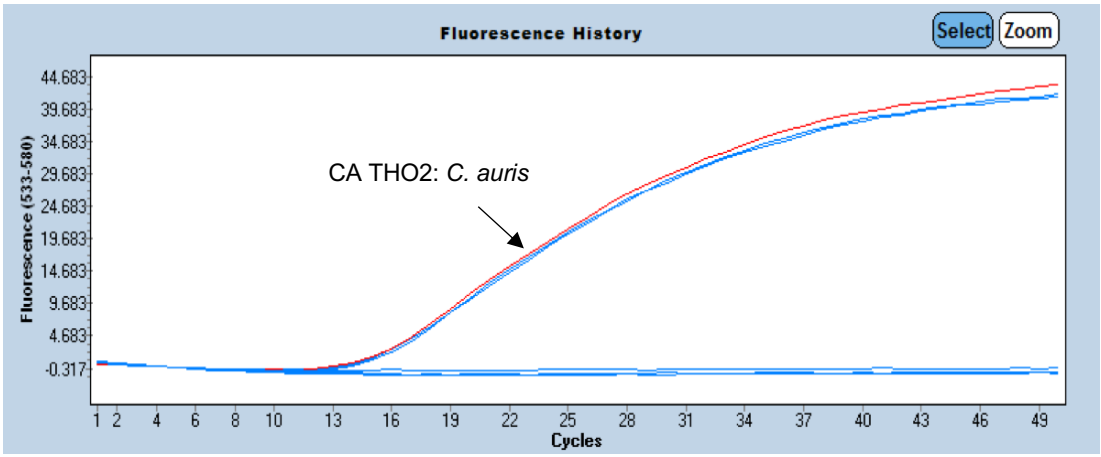

Figure 3. 19 The amplification curves detected by the *C. auris*-specific THO probe. The reaction contained 10^7 copies of the *C. auris* plasmid DNA and PCR was performed in triplicate. CA: *C. auris*-specific.

3.2.7 Characterisation of NDC melting curves profiles for MPA-*Candida* assay

MPA technology offers detection of more than one probe's melting temperature in a single real-time PCR detection channel. The MPA probe is designed in such a way that the dual-labelled THO melting temperature is based on a unique design of its PCO sequence. As a result of a specific probe's melting temperature, the THO can be labelled with the same reporter dye to maximise the multiplexing capacity of the assay. Six MPA probe pairs were optimised for their melt curve profiles and assembled into three alternative MPA-*Candida* assay designs (Table 3.7). MPA-*Candida* assay and assay designs 2 represent dual-channel 2-tube assay whereas design 3 is a triple-channel single-tube assay.

Table 3. 7 The layout of *Candida* assay designs tested either in a single- or dual-tube reaction and two- or three-channel of qPCR detection.

Detection channel/dye	**FAM**			**HEX**		**Cy5**
MPA-*Candida* assay: Tube 1						
Target (reaction probe)	CK (MPA)	PC (MPA)	CG (MPA)	IC (MPA)	CA (MPA)	
Tube 2						
Target (reaction probe)	PF (TaqMan)			IC (TaqMan)		
Design 2: Tube 1						
Target (reaction probe)	IC (MPA)	PC (MPA)	CG (MPA)	CK (MPA)	CA (MPA)	
Tube 2						
Target (reaction probe)	PF (TaqMan)			IC (TaqMan)		
Design 3						
Target (reaction probe)	CK (MPA)	PC (MPA)	CG (MPA)	PF (MPA)	CA (MPA)	IC (TaqMan)

*MPA-*Candida* and design 2 were performed in two tubes qPCR reaction with two detection channels. The *Candida* qPCR assay can be coupled with the Pan-Fungal assay for simultaneously detection in the same reaction protocol. Assay design 3 was performed in a single-tube reaction using three qPCR detection channels. FAM, 465 nm/510 nm; HEX, 533 nm/580 nm; Cy5, 618 nm/660 nm; CK, *C. krusei*-specific; PC, pan-*Candida*; CG, *C. glabrata*-specific; CA, *C. auris*-specific; IC, Internal Control-specific; PF, pan-fungal-specific.

MPA-*Candida* was fully developed and experimentally tested in this thesis work; its *in vitro* characterisation is reported below. The theoretical design and development of assay designs 2 and 3 is presented in Chapter 4.

3.2.8 Optimisations of the MPA-*Candida* probes in two detection channels

Initial testing of the two THOs were labelled with the same fluorophore, *C. krusei*-specific (CK THO1:PCO1) and pan-*Candida* (PC THO1:PCO1) in a single reaction tube have demonstrated reproducible melting curves (Figure 3.20). Initial assay design for multiple set of probes were prepared in two tubes. In tube 1 it consists of three probes of *C. krusei*-specific, pan-*Candida* and *C. glabrata*-specific, whereas in tube 2 it consists of the probes of *C. auris*-specific and IC (Figure 3.21). Multiple melting peaks from the mixture of THO and PCO sets are reproducible and specific to each probe. However, mixture of all five sets of THO and PCO in a single reaction for a single channel of detection resulted non-specific melting curves (Figure 3.22). Therefore, careful considerations of multiplexing the probes based on the melting characteristics is important for the specific melting peaks in one reaction detection channel. In the optimisation of the MPA-*Candida*, *C. glabrata*-specific (CG THO1:PCO1), *C. auris*-specific (CA THO1:PCO1) and IC probe (IC THO1:PCO1) were re-designed and the PCO sequences were modified. The IC THO was changed to pair with PCO2 to avoid an overlapping melting temperature with that of the *C. auris*-specific probe (CA THO2:PCO1) (Figure 3.23).

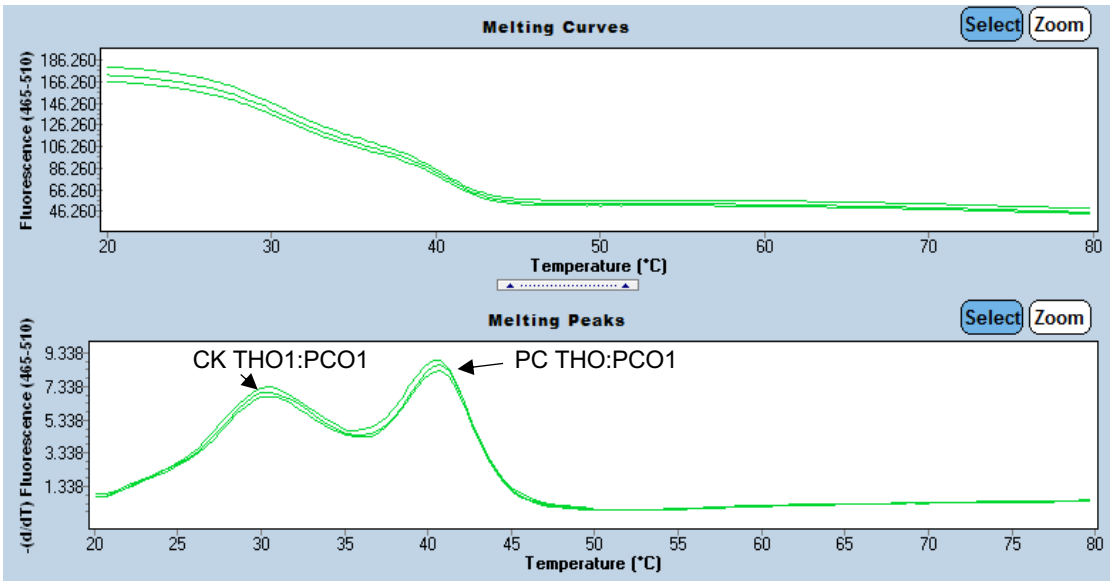

Figure 3. 20 Assembly of two MPA probes in a single reaction with a unique melting curve analysis. Two specific melting peaks were reported from triplicate reaction for *C. krusei*-specific (CK THO:PCO1) at 30.89°C and pan-*Candida* (PC THO:PCO1) at 40.52°C in a reaction without amplification step. The melt peaks are plotted as the negative derivative plot of the fluorescence emission versus temperature.

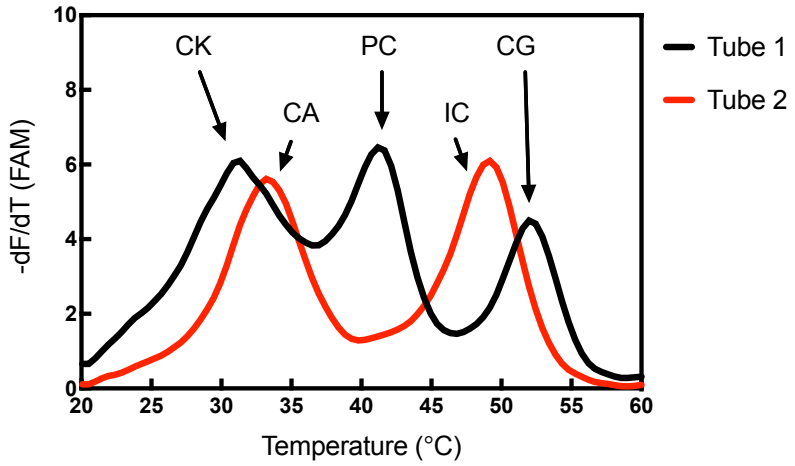

Figure 3. 21 Five target-specific melting peaks in the two reaction mixtures. In the Tube 1 is a mixture of the three probes generating melting peaks for *C. krusei*-specific (CK THO:PCO1), pan-*Candida* (PC THO:PCO1) and *C. glabrata*-specific (CG THO1:PCO1) and Tube 2 for *C. auris*-specific (CA THO1:PCO1) and internal control (IC THO:PCO1) are representative of triplicate reactions. In both tubes, melting curve analysis was performed from the FAM detection channel and the reaction contained no target sequence for the negative control profile.

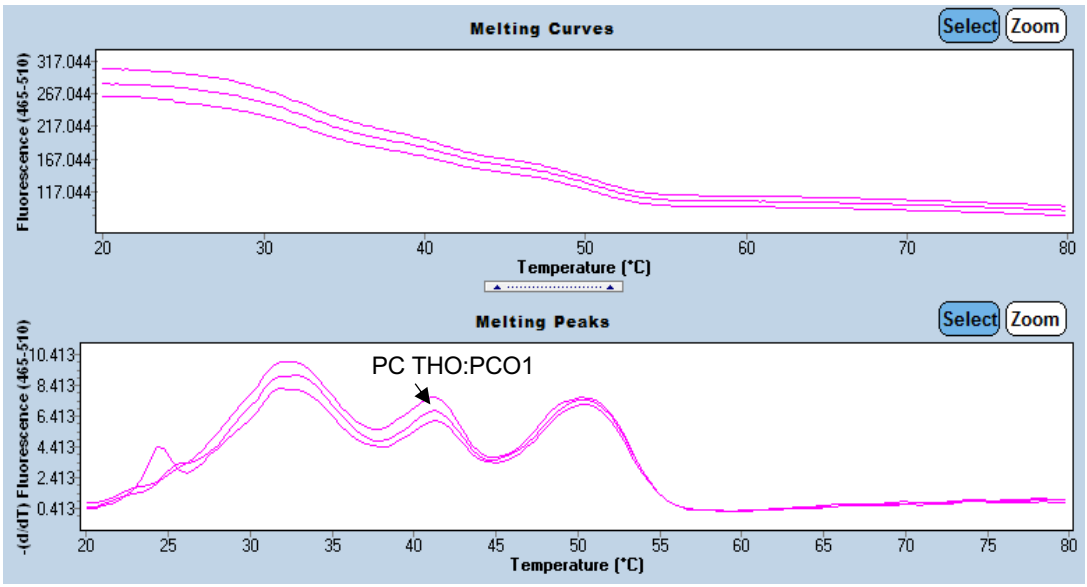

Figure 3. 22 Assembly of five MPA probes in a single reaction resulted in non-specific melting curve. The pan-*Candida* probe (PC THO:PCO1) can be detected at 41.40°C; the two other peaks approximately at 32°C and 50°C are not specific. Along with the pan-*Candida* probe, the reaction contains probes for *C. krusei*-specific (CK THO:PCO1), *C. auris*-specific (CA THO1:PCO1), internal control (IC THO:PCO1) and *C. glabrata*-specific (CG THO1:PCO1). The experiment was tested in triplicate.

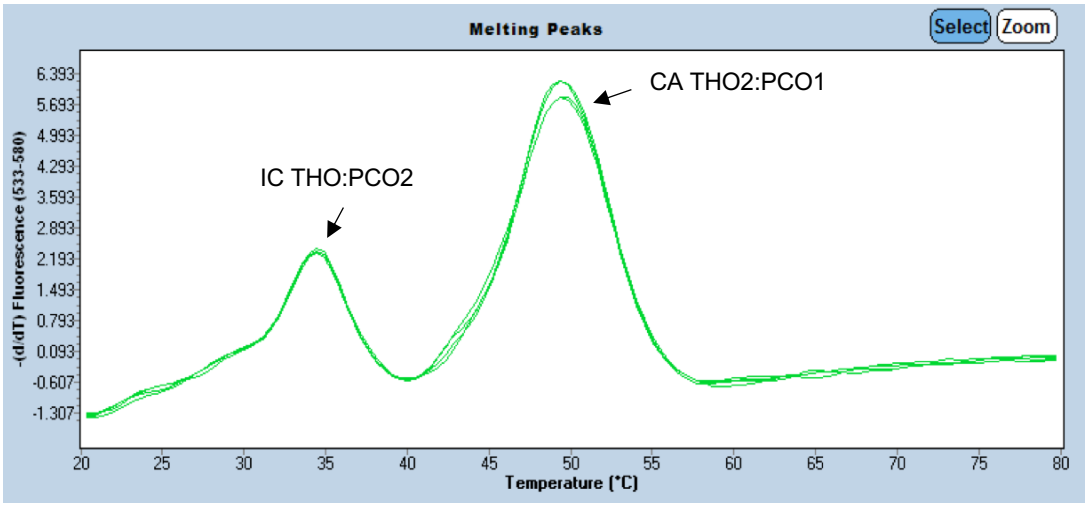

Figure 3. 23 Characterisation of the melting peaks from the mixtures *C. auris*-specific THO and IC probe in a single reaction analysis. Internal Control probe (IC THO) was paired with PCO2 produced distinguishable melting peaks (34°C) against probe CA THO2:PCO1 (48°C) within the same reaction mixture. Both probe melting peaks were detected in the HEX channel (533 nm) and analysed in triplicate.

The FAM labelled probes; *C. krusei*-specific (CK THO1:PCO1), pan-*Candida* (PC THO1:PCO1) and *C. glabrata*-specific (CG THO2:PCO1) were optimised the probes concentrations from the 0.4 µM for a sharp melting peaks in the FAM detection channel (Figures 3.24 and 3.25). The two HEX-labelled probes; *C. auris*-specific (CA THO2:PCO1) and IC (IC THO1:PCO2) probes were exclusively detected in the same tube without interfering the characteristics of melt curves of other probes. An optimised MPA-*Candida* assay with three FAM-labelled probes and two HEX-labelled probes generates a novel melt curve profiles in a single reaction mixture (Figure 3.26). For simplicity and flexibility, the MPA-*Candida* PCR assay was engineered to complement the Pan-Fungal reaction. A two-tube system that could be run simultaneously under the same experimental conditions is described in Material and Methods, Section 2.14.

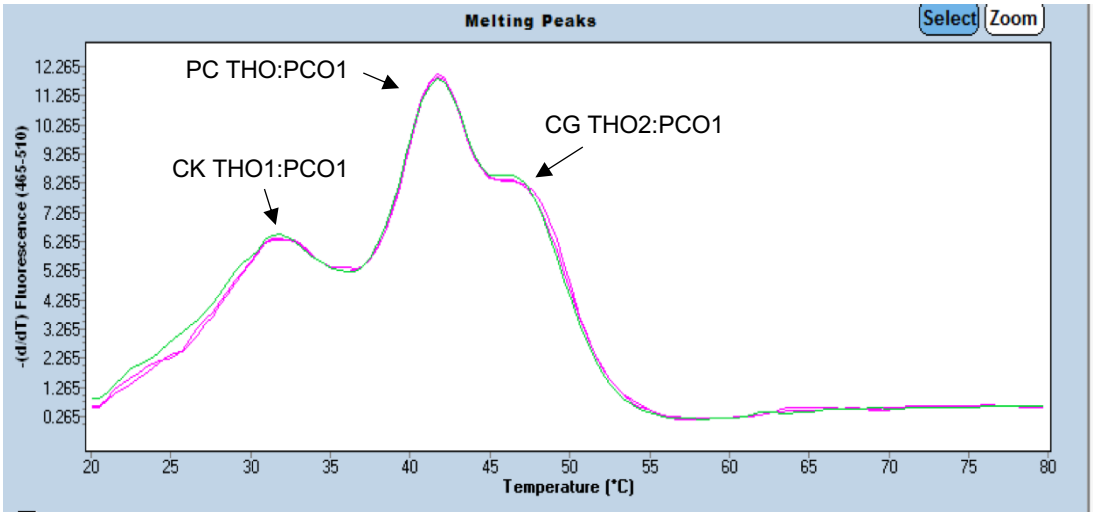

Figure 3. 24 Melt curves analysis of the FAM-labelled probes. Each probe was prepared in an equivalent final concentration, THO:PCO at 0.4:0.8 µM. MPA probes melting peaks for *C. krusei*-specific (THO1:PCO1), pan-*Candida* (PC THO:PCO1) and *C. glabrata*-specific (CG THO2:PCO1). Pan-*Candida* melting peak masked *C. glabrata*-specific probe's melting temperature. The analysis was performed in triplicate.

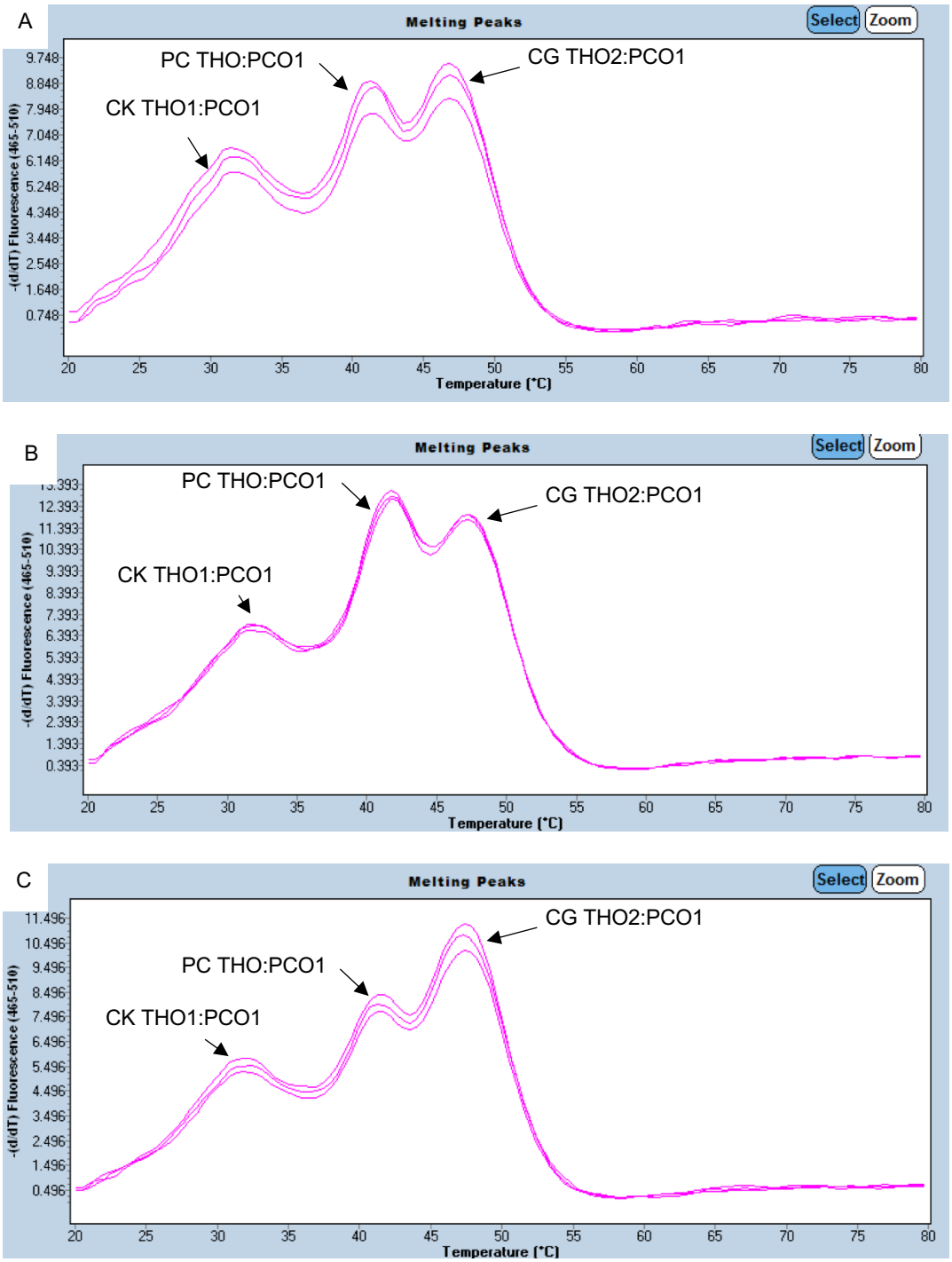

Figure 3. 25 Optimisations of the probe's concentration for comparable height of melting peaks in the FAM detection channel. Panel A) Pan-*Candida* (PC) THO reduced from 0.4 µM to 0.2 µM, *C. krusei* (CK) and *C. glabrata* (CG) THOs at 0.4 µM. **Panel B**) *C. glabrata* (CG) THO increased to 0.6 µM, *C. krusei* (CK) and pan-*Candida* (PC) THOs at 0.4 µM. **Panel C**) Pan-*Candida* (PC) THO reduced to 0.2 µM, *C. glabrata* (GC) THO increased to 0.6 and *C. krusei* (CK) THO maintained at 0.4 µM. In all cases, concentrations of the THO and PCO were prepared in 1:2 ratio. All experiments were performed in triplicate.

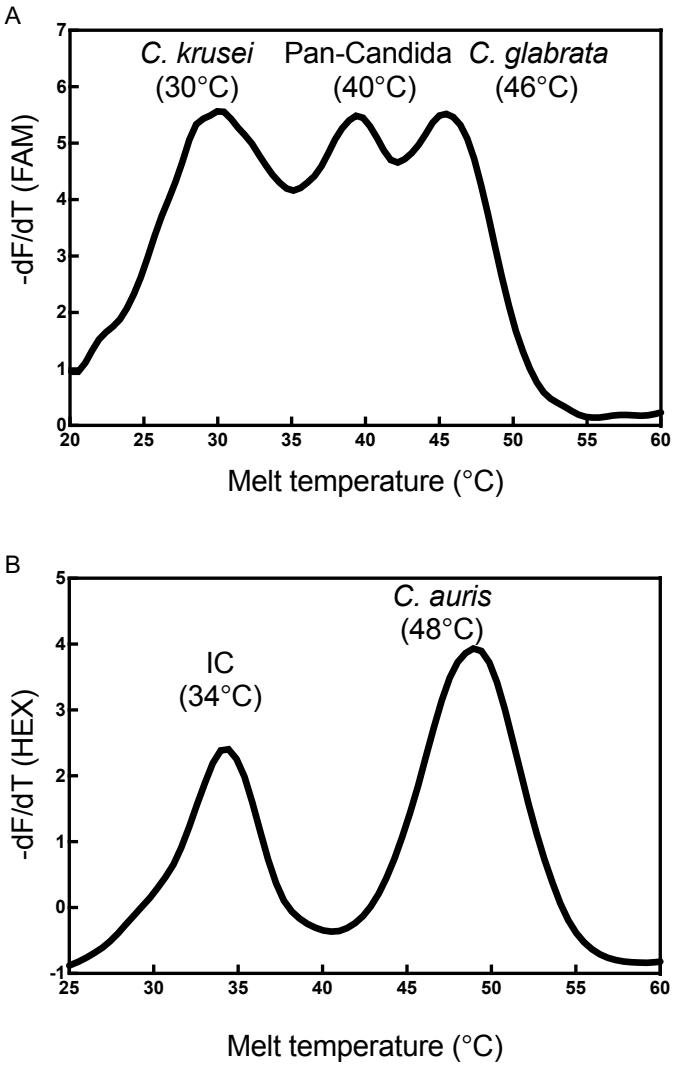

Figure 3. 26 A single tube, 2-channel MPA-*Candida* melt curve profiles. The negative fluorescence derivative (-dF/dT) melt peaks obtained from dissociation between the THO and PCO for the *C. krusei*-specific (CK THO1:PCO1), pan-*Candida* (PC THO1:PCO1) and *C. glabrata*-specific (CG THO2:PCO1) probes in the FAM channel (**Panel A**); internal control (IC THO1:PCO2) and *C. auris*-specific (CA THO2:PCO1) detection in the HEX channel (**Panel B**). All melting temperatures were determined in three independent replicates and averaged.

3.2.9 Specificity of MPA-*Candida* melting curves analysis

The specificity of each probe in the MPA-*Candida* assay was tested *in vitro* for DNA amplifications of *C. albicans*, *C. glabrata*, *C. parapsilosis*, *C. tropicalis*, *C. krusei*, *C. dubliniensis*, *C. auris*, *C. haemulonii* and *C. guilliermondii* (Table 3.8). The assay specificity was evaluated from the detection by pan-*Candida* and species-specific probes. The MPA-*Candida*, specificity experiments were reported with the probe optimisations for detection of target species. Post-amplification melting curve generated from the detection of the target species was compared against the negative control temperature profile.

Nine *Candida* species including *C. albicans*, *C. dubliniensis*, *C. krusei*, *C. glabrata*, *C. auris*, *C. parapsilosis*, *C. tropicalis*, *C. haemulonii*, *C. guilliermondii* inclusive of IC plasmid DNA in each reaction was amplified and analysed for its specificity of detection in the FAM and HEX channels. The analysis of melt curves of all the *Candida* species showed peaks which disappeared at 40°C (pan-*Candida*) as compared to the NDC melt curve (Figure 3.27, panels A to D). The detection of resistant *Candida*-species can be distinguished by an additional peak reduction in the melt curve at 30°C (*C. krusei*), 46°C (*C. glabrata*) in the FAM channel and 48°C (*C. auris*) in the HEX channel (Figure 3.27, panels B, C and D, respectively). None of the other seven *Candida* species tested showed a decrease in melt peak at *C. krusei*- or *C. glabrata*-specific melt peaks. Furthermore, none of the eight *Candida* species tested showed a decrease in the *C. auris*-specific melt peak in the HEX channel. Collectively, there was no cross-reactivity issue between the tested *Candida* species and the species-specific detections in the assay.

Table 3. 8 Nine *Candida* species DNA amplification C_t values in FAM and HEX channels. The C_t values were evaluated in parallel with the melting curve analysis for the probe(s) specificity analysis.

***Candida* species**	**FAM**	**HEX**
	Mean C_t ± SD	Mean C_t ± SD
C. albicans	26.81± 0.16	31.85± 1.57
C. dubliniensis	22.60± 0.98	30.14± 0.60
C. tropicalis	25.75± 0.62	28.44± 1.44
C. parapsilosis	25.02± 0.10	28.48± 0.50
C. guilliermondii	26.67± 0.07	30.22± 0.57
C. haemulonii	25.60± 0.44	30.90± 0.04
C. krusei	25.08± 0.13	31.83± 0.39
C. glabrata	25.83± 0.48	29.08± 2.67
C. auris	24.23± 0.65	25.97± 0.04

*The FAM channel detecting pan-*Candida*, *C. krusei*-specific, and *C. glabrata*-specific probes and the HEX channel detecting IC and *C. auris*-specific probes. The qPCR was performed in three replicates and averaged.

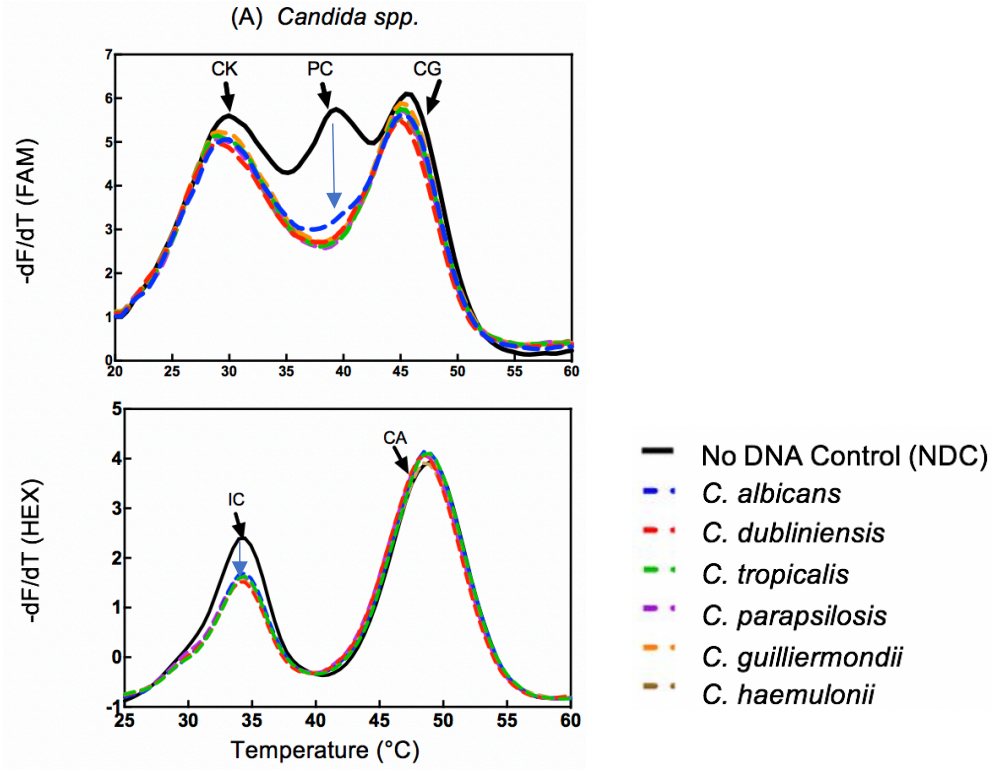
(A) Candida spp.
CK
PC
CG
-dF/dT (FAM)
IC
CA
-dF/dT (HEX)
Temperature (°C)
No DNA Control (NDC)
C. albicans
C. dubliniensis
C. tropicalis
C. parapsilosis
C. guilliermondii
C. haemulonii

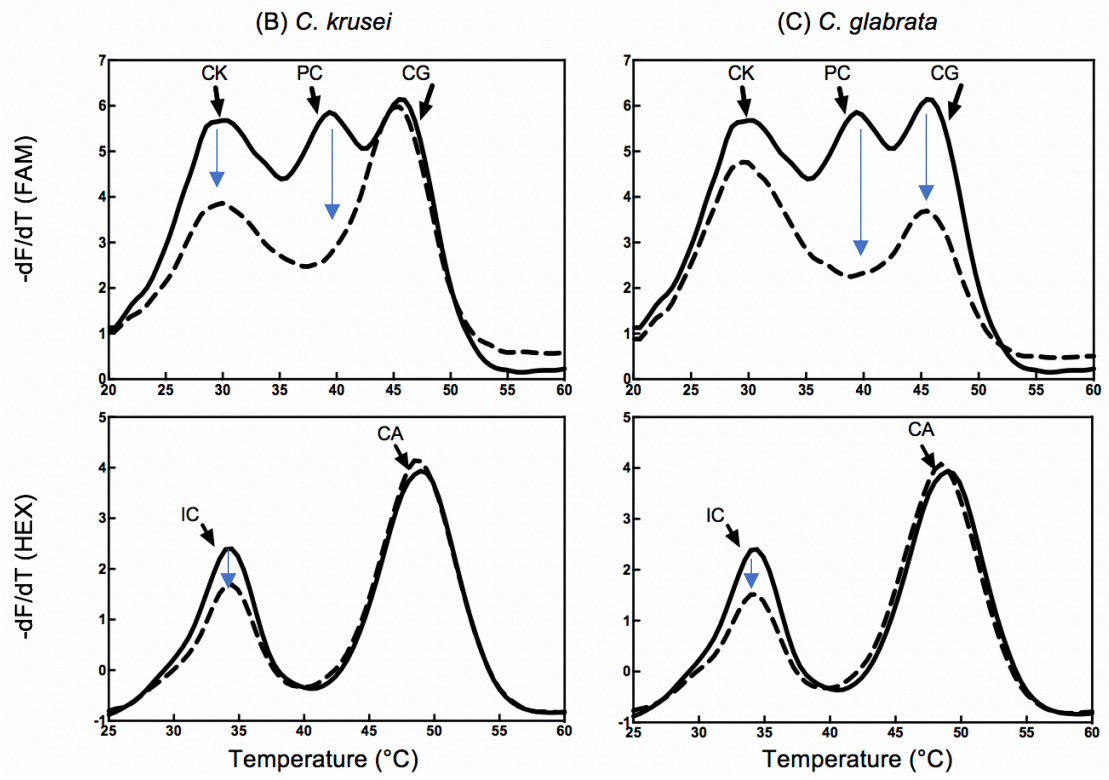
(B) C. krusei
(C) C. glabrata
CK
PC
CG
-dF/dT (FAM)
IC
CA
-dF/dT (HEX)
Temperature (°C)
Temperature (°C)

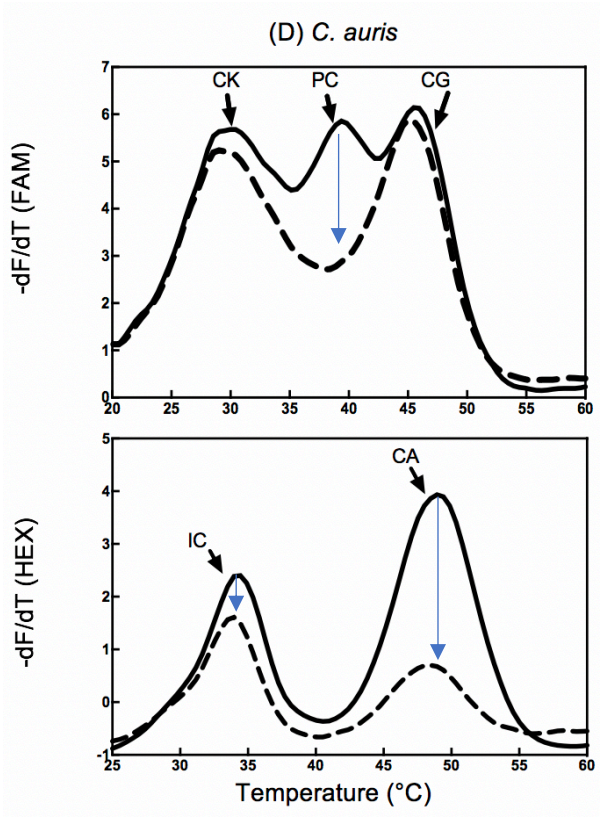

Figure 3. 27 Specific detection of *Candida* plasmid DNA in MPA-*Candida* post-amplification melt curve profiles across the FAM and HEX detection channels. Panel A) Detection of *Candida* species (dotted lines) other than *C. krusei*, *C. glabrata* and *C. auris* with reduced levels of the melt peaks only at the corresponding pan-*Candida* (PC) temperature in the FAM channel and at IC temperature for detections of IC plasmid in the HEX channel compared to NDC melting curves (solid lines) in the FAM and HEX channels. **Panels B to D**) Representative melting curves of resistant *C. krusei* and *C. glabrata* and *C. auris*, plot by the dotted lines showing lower intensity of the melt peaks at the corresponding temperature (CK: *C. krusei*, CG: *C. glabrata* or CA: *C. auris*) compared to NDC melting curves plot in solid lines in the FAM and HEX channels. In each panel, reduced level of the melt peak for pan-*Candida* temperature in the FAM channel indicates genus *Candida* biomarker detections and at IC temperature indicates IC plasmid detections in the HEX channel. In all cases diagnosis is supported by the corresponding DNA amplification curves and associated C_t values. CK: *C. krusei*-specific; PC: pan-*Candida*; CG: *C. glabrata*-specific; IC: Internal Control; CA: *C. auris*-specific. The melting curve analysis was performed in triplicate.

Comparison of the means peaks height at every melting temperature (T_m) between the detected *Candida*-species DNA and the control reaction was tested using Analysis of Variance (ANOVA) followed by Dunnett's multiple comparison test (Figures 3.28 and 3.29). Melting peaks height for detection of *C. krusei* DNA specific at 30°C of *C. krusei*-specific showed significance difference ($P<0.0001$) against the NDC. *C. dubliniensis* DNA was detected with less significance ($p<0.05$) and not significant for the rest of *Candida* species compared against the NDC (Figure 3.28, panel A). The middle T_m peak detected in the FAM channel at 39.4°C of pan-*Candida* showed significance difference values ($p<0.0001$) for all the reactions with *Candida* species against NDC melting profile (Figure 3.28, panel B). Next, the melting peaks at 45.5°C of *C. glabrata*-specific showed highly significance values ($p<0.0001$) for detection of *C. glabrata* DNA and *C. dubliniensis* was detected with less significance ($p<0.05$) and not significant for the rest of all *Candida* species (Figure 3.28, panel C). Moreover, another set of melting curves in the HEX channel for the MPA IC probe T_m at 34°C and the *C. auris*-specific probe T_m at 48.9°C were also analysed. Amplification IC templates inclusive in every *Candida* reaction was detected and showed significance difference ($p<0.0001$) in the peaks heights as compared with NDC peak (Figure 3.29, panel A). The second peak in the HEX channel detected at 48.9°C of *C. auris*-specific showed expected significance values ($p<0.0001$) for the sample with *C. auris* DNA (Figure 3.29, panel B).

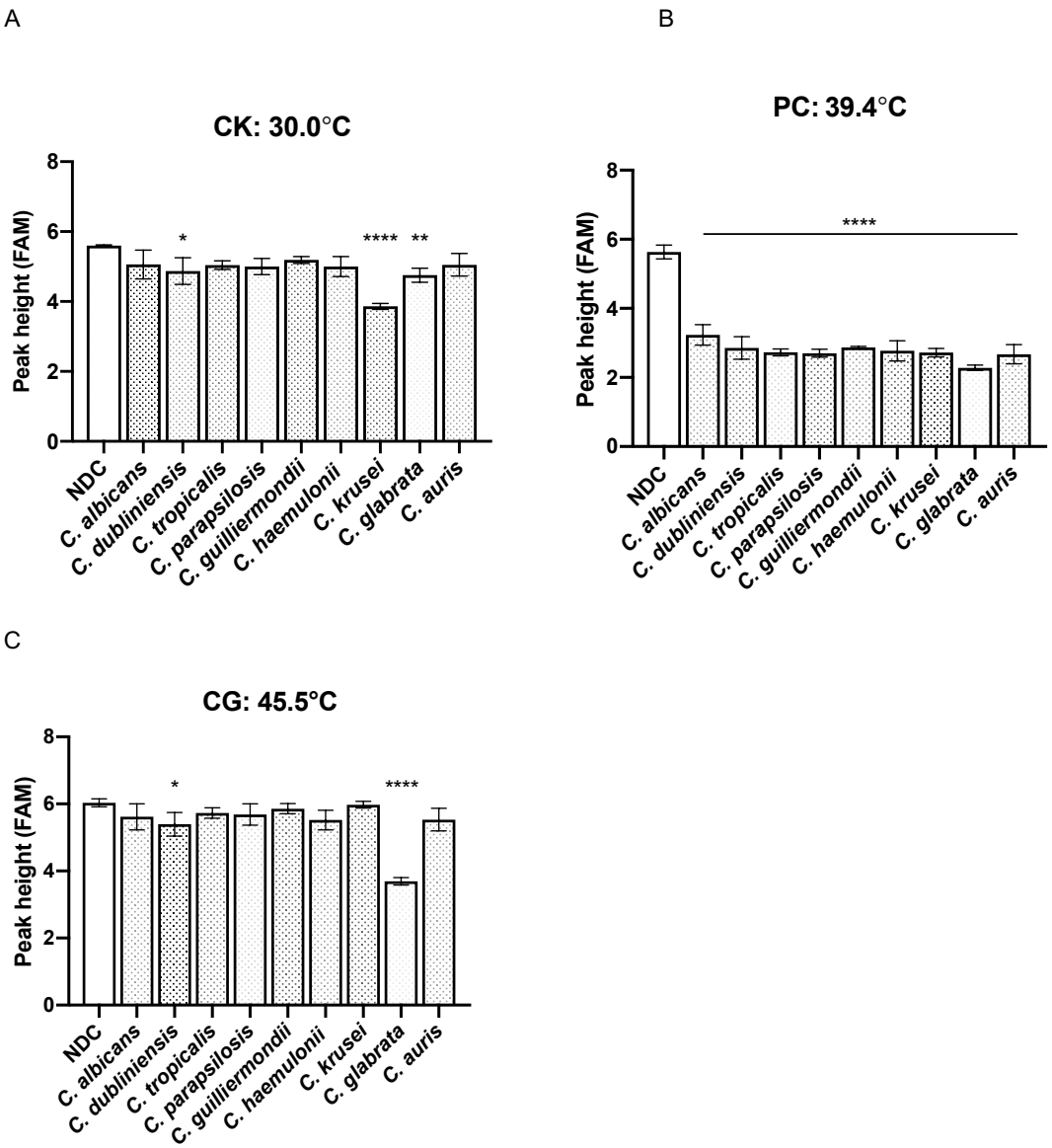

Figure 3. 28 Comparison of the melting peaks heights of the three-specific temperature in the FAM channel between the NDC and *Candida* species DNA. Panel A) A comparison between peaks height at 30°C of *C. krusei*-specific NDC and a detection of *C. krusei* DNA with highly significance p<0.0001 compared to *C. dubliniensis*, p<0.05. **Panel B**) The T_m 39.4°C of pan-*Candida* NDC peak height significantly different against all *Candida* species (p<0.0001). Next, a comparison between peaks height at 45.5°C of *C. glabrata*-specific NDC and *C. glabrata* sample DNA with highly significance p<0.0001 compared to *C. dubliniensis*, p<0.05 (**Panel C**). Each sample comparison with the NDC using Dunnett's test; ns: not significance. CK: *C. krusei*-specific; PC: pan-*Candida*; CG: *C. glabrata*-specific; NDC: no DNA control.

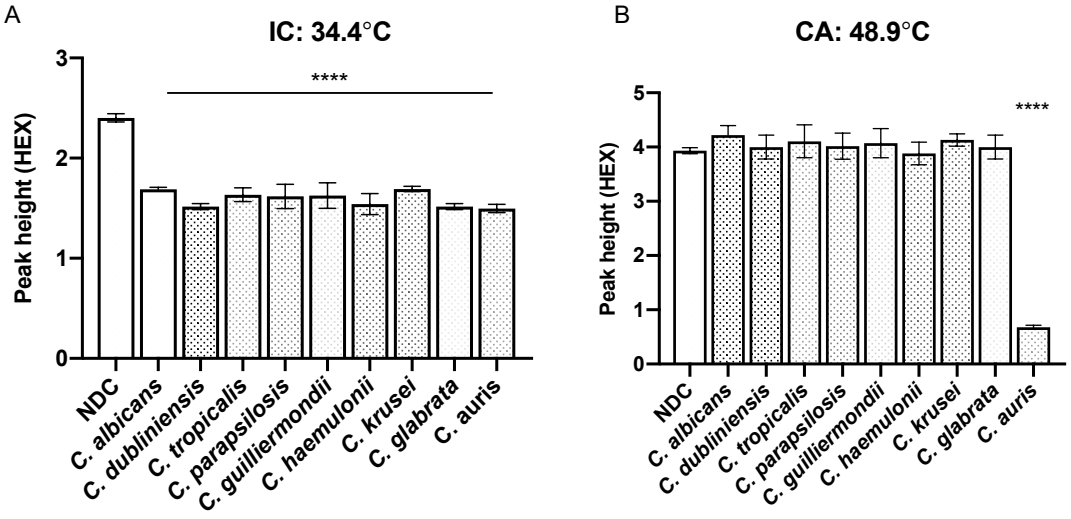

Figure 3. 29 Comparison of the melting peaks heights of the two-specific temperature in the HEX channel between the NDC and *Candida* species DNA. Panel A) A comparison between peaks height at 34.4°C of internal control NDC and detection of the IC plasmid DNA presents in all *Candida* species DNA with highly significance $p<0.0001$ values. **Panel B**) The T_m 48.9°C of *C. auris*-specific NDC peak height was significantly different ($p<0.0001$) against the reaction with *C. auris* DNA and none of the other *Candida* species has reduced melting peak height at 48.9C except *C. auris*. Each sample comparison with the NDC using Dunnett's test; ns, not significance. IC: Internal Control; CA: *C. auris*-specific; NDC: no DNA control.

The assay's specificity was further tested using heterologous fungal and bacterial DNA to rule out the possibility of cross-detection in clinical samples. None of these species were detected in the MPA-*Candida* assay (Figure 3.30). The functionality of the components in the assay with non-target fungal and bacterial DNA was monitored with the inclusion of 10^6 copies of the IC plasmid template in every sample. An amplification curve and a reduced melt peak for the detection of the amplified control template was consistently detected in the HEX detection channel. *C. albicans* genomic DNA was successfully detected with reduced melting peaks when analysed for *Candida* at 40.7°C (PC) and 34.7°C (IC) in FAM (Figure 3.31, panel A) and HEX channels (Figure 3.32, panel A), respectively. As expected, no significant reduction of peak height of reaction with *C. albicans* at 30°C (CK), 46°C (CG) and 49°C (CA). However, less significance peak reduction against NDC profile at pan-*Candida* (PC) temperature (40.7) was noted for *Staphylococcus aureus* (Figure 3.31, panel B). Meanwhile, the melting curves analysed in the HEX channel consistently with reduced height at 34.7°C (IC) for every reaction that contained IC plasmid DNA against the NDC peak (Figure 3.32, panel A). None of the species tested in this experiment with reduction of melting peaks at 49.2°C (CA) (Figure 3.32, panel B).

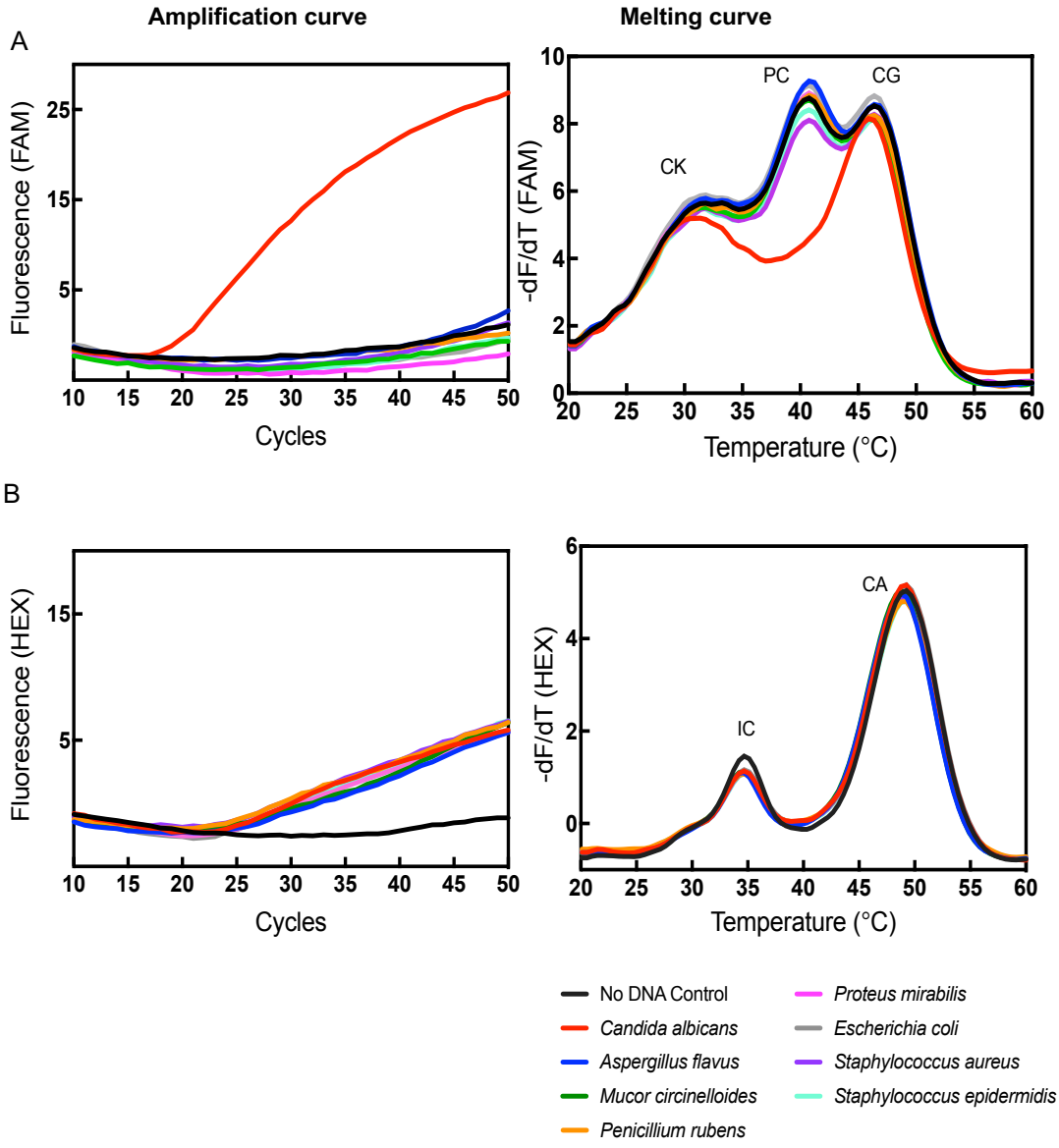

Figure 3. 30 Amplification and melt curves analysis of assay's specificity for fungal and bacterial genomic DNA detection. Panel A) Amplification curve clearly detected for *C. albicans* compared to other species with the corresponding melt curves analysis showing obvious reduction at PC peak compared to NDC in the FAM channel. **Panel B**) Amplification curves of the IC present in every fungal and bacteria samples and its melt curves analysis showing reduction at the IC temperature against NDC in the HEX channel. CK: *C. krusei*-specific; PC: pan-*Candida*; CG: *C. glabrata*-specific; IC: Internal Control; CA: *C. auris*-specific. Each sample was performed in triplicate.

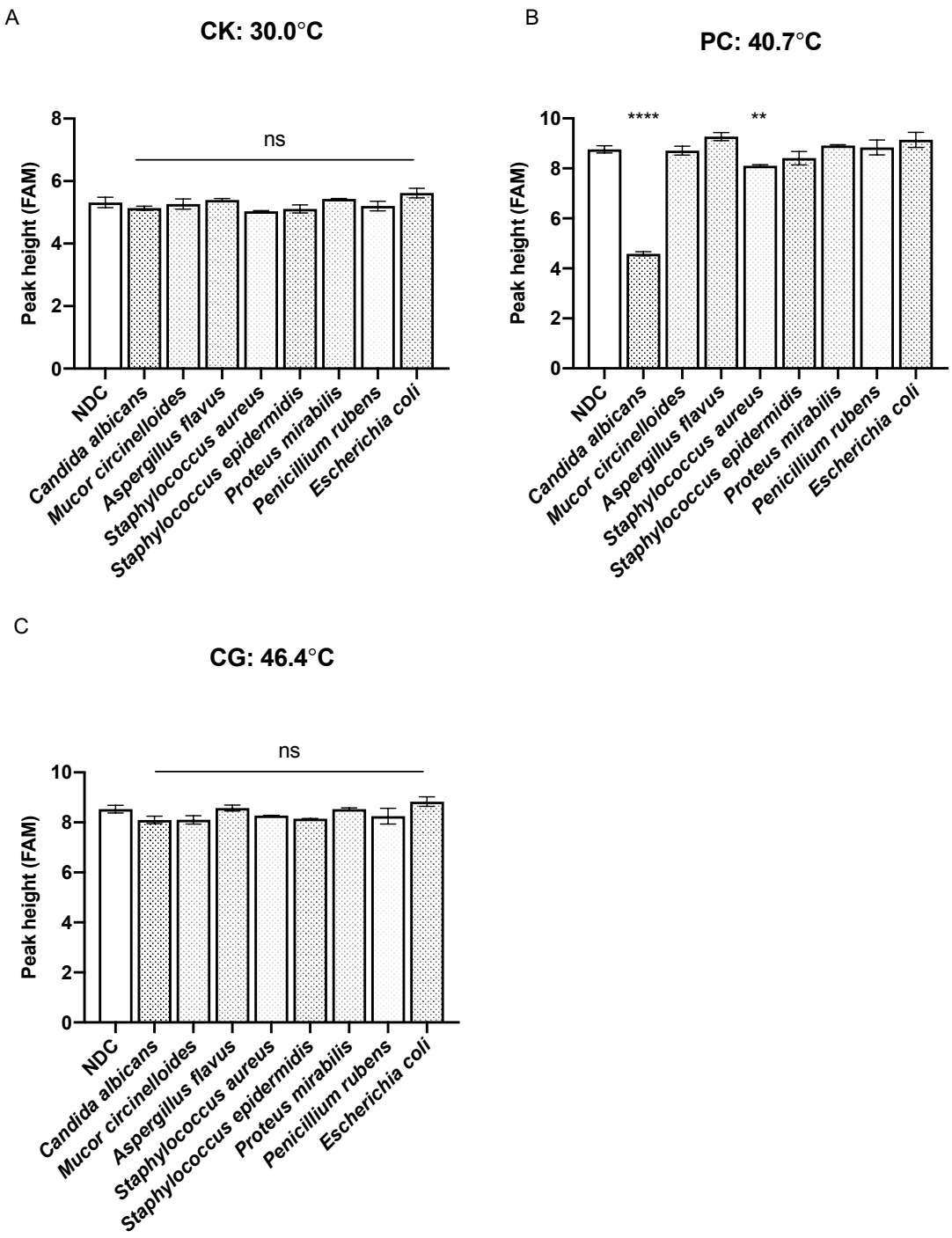

Figure 3. 31 Comparison of the melting peaks heights of the three-specific temperature in the FAM channel between the NDC and *Candida* species DNA. Panel A) A comparison between peaks height at 30°C of *C. krusei*-specific NDC and non-target fungal and bacterial species. **Panel B**) The T_m 40.7°C of pan-*Candida* NDC peak height significantly different against *C. albicans* ($p<0.0001$). **Panel C**) A comparison between peaks height at 45.5°C of *C. glabrata*-specific NDC and non-target fungal and bacterial species. Each sample comparison with the NDC using

Dunnett's test; ns, not significance. CK: *C. krusei*-specific; PC: pan-*Candida*; CG: *C. glabrata*-specific; NDC: no DNA control.

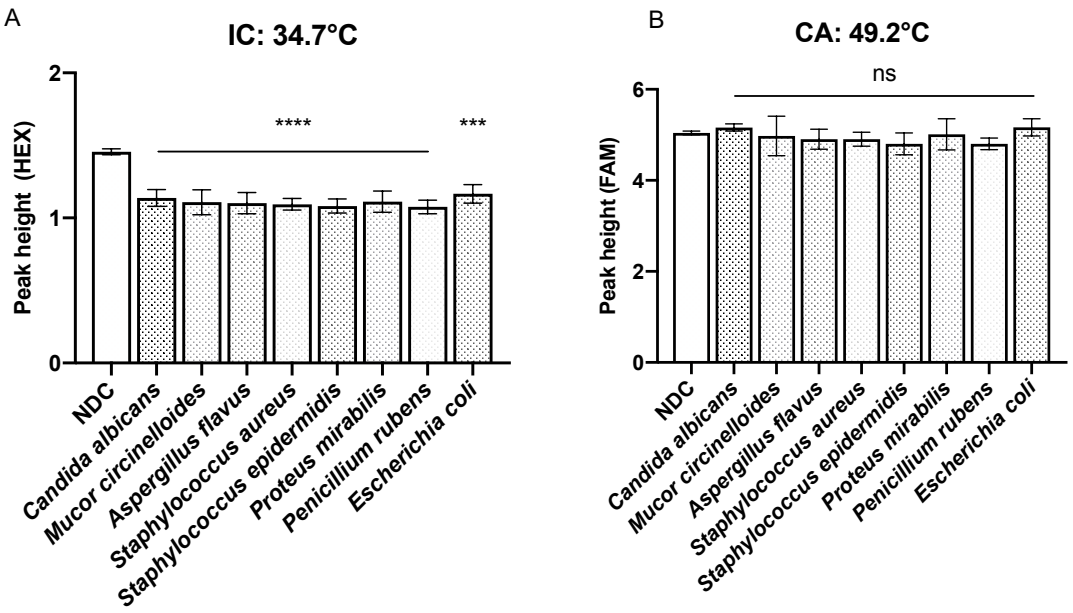

Figure 3. 32 Comparison of the melting peaks heights of the two-specific temperature in the HEX channel between the NDC and *Candida* species DNA. A comparison between peaks height at 34.7°C of internal control NDC and detection of the IC plasmid DNA presents in all *Candida* species DNA with highly significance from p = 0.0001 and p<0.0001 values (**Panel A**). The T_m 49.2°C of *C. auris*-specific NDC peak height not significantly different against non-target fungal and bacterial species (**Panel B**). Each sample comparison with the NDC using Dunnett's test; ns, not significance. IC: Internal Control; CA: *C. auris*-specific; NDC: no DNA control.

In a separate reaction tube, the Pan-Fungal assay is designed to detect a range of clinically relevant fungal pathogens that can be performed simultaneously with the MPA-*Candida* assay (Table 3.9). The TaqMan® pan-fungal reaction was designed to inherit the conditions of MPA-*Candida* PCR conditions with two channels of fluorescence detection. In this study, further to detection of *Candida* DNA in the MPA-*Candida* reaction, the pan-fungal probe was able to detect yeast from nine *Candida* species including *C. albicans*, *C. dubliniensis*, *C. krusei*, *C. glabrata*, *C. auris*, *C. parapsilosis*, *C. tropicalis*, *C. haemulonii*, *C. guilliermondii* and pathogenic filamentous fungi species including *A. fumigatus*, *A. flavus*, *F. solani*, *P. rubens* and *M. circinelloides* (Table 3.10). A specificity check of the pan-fungal probe was performed against four species of bacteria that constitute part of the normal human flora including *S. epidermidis*, *S. aureus*, *P. mirabilis* and *E. coli*. All bacterial and fungal genomic DNAs were tested at 10^5 genome equivalent copies number per reaction. None of the bacterial DNA was detected in the Pan-Fungal assay (Table 3.10). In every reaction tube, the IC plasmid DNA was included, and the amplification signal was detected in the HEX detection channel. In a separate experiment, early amplification (C_t =16) of the same *E. coli* genomic DNA samples was observed using the universal bacterial 16S primer set. The detection of the organisms' genomic DNA in the assay was summarised in Table 3.10 which includes qualitative interpretations of MPA-*Candida* and Pan-Fungal in the FAM and HEX channels of detection.

Table 3. 9 MPA-*Candida* Assay. For simplicity and flexibility, the MPA-*Candida* assay was engineered as a two-tube system, run simultaneously under the same experimental conditions. Tube 1 contains the genus-specific and species-specific *Candida* probes; tube 2 harbours the pan-fungal probe. The two fluorescent detection channels used in the multiprobe melting curve analysis are indicated.

Reaction name	**Probe target & symbol**	**Probe label & channel wavelength**
Tube 1: MPA-*Candida*	*C. krusei* (CK)	FAM (465 nm/510 nm)
	Pan-*Candida* (PC)	
	C. glabrata (CG)	
	C. auris (CA)	HEX (538 nm/580 nm)
	Internal Control (IC)	
Tube 2: TaqMan® Pan-Fungal	Pan-fungal (PF)	FAM
	IC	HEX

FAM, 6-carboxy-fluorescein; HEX, Hexachloro-fluorescein

Table 3. 10 Application of the pentaplex MPA-*Candida* and the TaqMan® Pan-Fungal assay for specific detection in only two channels of real-time PCR. Fungal and bacterial genomic DNA were tested at 10^5 genome equivalent per reaction.

	MPA-*Candida*							Pan-Fungal	
	C_t value		Melting curve analysis					C_t value	
			FAM			HEX		FAM	HEX
Target DNA	FAM	HEX	CK	PC	CG	IC	CA	PF	IC
Candida									
C. albicans	23.40	26.00	ND	+	ND	+	ND	22.00	21.00
C. krusei	22.20	26.20	+	+	ND	+	ND	22.90	25.60
C. glabrata	24.40	26.50	ND	+	+	+	ND	24.30	24.80
C. auris	23.60	29.00	ND	+	ND	+	+	23.00	26.20
C. haemulonii	24.60	27.80	ND	+	ND	+	ND	21.00	26.00
C. dubliniensis	23.60	28.00	ND	+	ND	+	ND	22.00	26.30
C. parapsilosis	23.90	26.90	ND	+	ND	+	ND	21.80	25.40
C. tropicalis	23.50	26.00	ND	+	ND	+	ND	21.00	26.00
C. guilliermondii	23.60	26.50	ND	+	ND	+	ND	22.90	26.50
Moulds									
A. fumigatus	ND	28.10	ND	ND	ND	+	ND	22.90	23.40
A. flavus	ND	28.50	ND	ND	ND	+	ND	21.10	23.20
P. rubens	ND	27.10	ND	ND	ND	+	ND	16.60	20.10

M. circinelloides	ND	28.00	ND	ND	ND	+	ND	17.00	24.10
Bacteria									
S. aureus	ND	29.70	ND	ND	ND	+	ND	ND	22.80
S. epidermidis	ND	28.90	ND	ND	ND	+	ND	ND	23.50
P. mirabilis	ND	28.40	ND	ND	ND	+	ND	ND	23.00
E. coli	ND	28.00	ND	ND	ND	+	ND	ND	23.20

C_t: Threshold Cycle, the cycle intersection with the point where the curve first clearly rises off baseline value; FAM, detection channel (465 nm/510 nm); HEX, detection channel (533 nm/580 nm); CK, *C. krusei*-specific peak (30°C); PC, Pan-*Candida* peak (40°C); CG, *C. glabrata*-specific peak (46°C); CA, *C. auris*-specific peak (48°C); IC, Internal Control-specific peak (34°C); PF, Pan-fungal; +, positive; ND, Not Detected

3.2.9.1 Optimisations of MPA-*Candida* specificity of detection

The MPA-*Candida* real-time PCR assay was tested for quantitative and qualitative efficiencies through the amplification and detection of accurate target(s) DNA sequences in the reaction. In the PCR reaction with *Candida* species DNA endonuclease activity hydrolysed the dual-labelled THO probe(s) and left minimal intact probe(s) to bind PCO sequences in the post-amplification stage. In the melting curve analysis, the hydrolysed probe was unable to hybridise to its PCO and resulted in the reduction of the specific melting peak(s) compared to the NDC melting curve profile.

An initial optimisation of the melting curve profiles was performed in the two separate reactions as described in Section 3.2.8; Figure 3.21. Amplification curves were seen for the amplification of *C. albicans*, *C. krusei*, *C. glabrata* and IC plasmid DNAs (Figure 3.33). Samples with *C. albicans*, *C. krusei* and *C. glabrata* correctly identified as *Candida* species from the melting curve analysis (Figure 3.33, panels A to C). Moreover, detection of intrinsic drug-resistant *C. krusei* can be informed from the melting curve profile with an additional reduction of melting peak at 30°C (Figure 3.33, panel B). However, the assay did not accurately identify *C. glabrata* DNA as seen from the melt curve. High copies of *C. glabrata* plasmid DNA, 10^6 and 10^5 copies per reaction, demonstrated raised melting peaks with higher than NDC signal at the *C. glabrata*-specific melting peak temperature and no reduction of peak for identification of *C. glabrata* plasmid DNA from five other dilutions (Figure 3.33, panel C). Meanwhile, in a separate reaction for tube 2, amplification and detection of IC serially diluted plasmid DNA was also tested and showed amplification curves and responsive melting curves analysis accurate to the IC temperature (Figure 3.33, panel D).

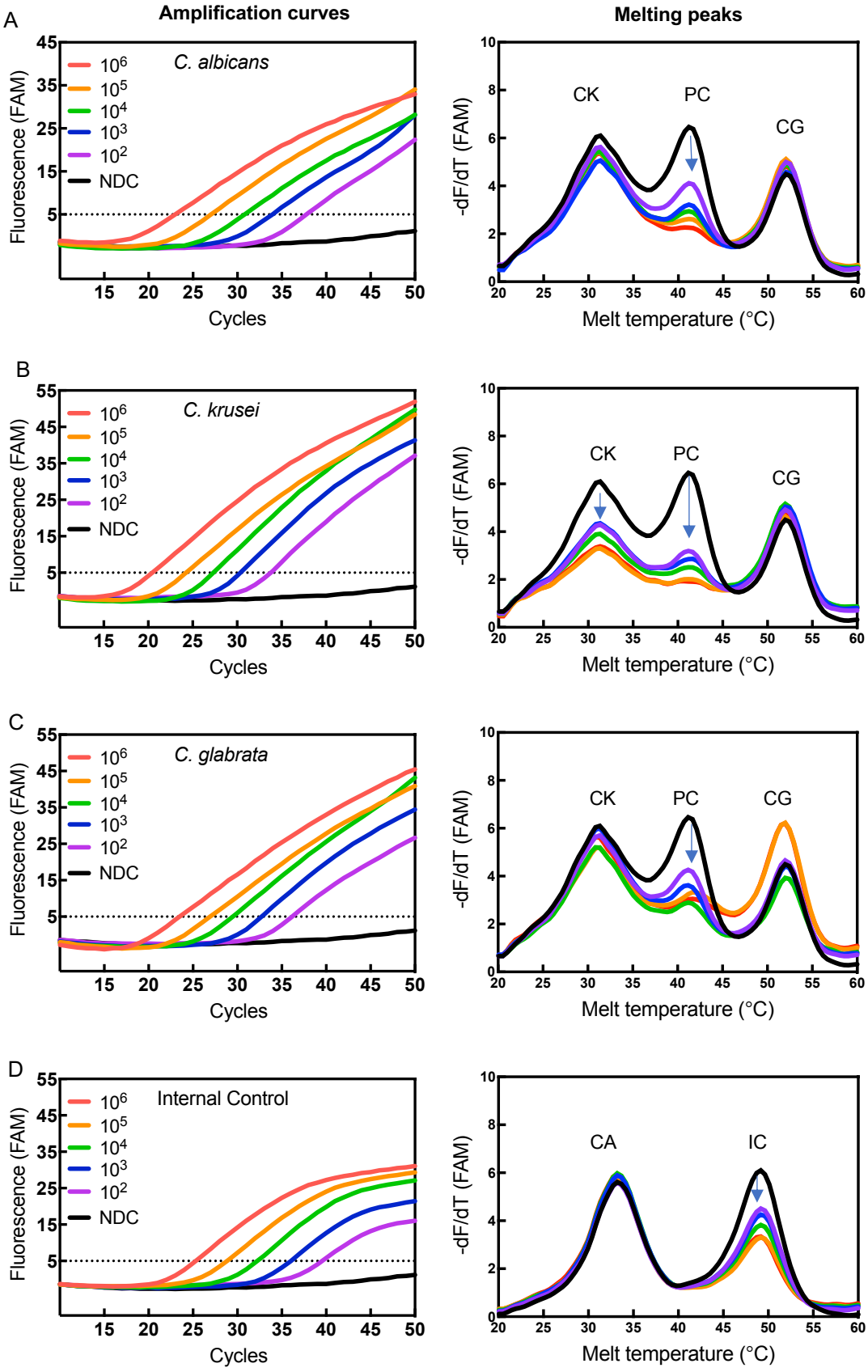

Figure 3. 33 Assessing four MPA probes arranged in two tubes for functionality in a multiplex amplification and melting curve detection reaction in the FAM channel. Tube 1 amplification curves and their respective melting curves outcome for

detection of *C. albicans* (**Panel A**), *C. krusei* (**Panel B**) and *C. glabrata* (**Panel C**) from the range of serially diluted plasmid DNA. Tube 2 amplification curves and the respective melting curves tested internal control plasmid DNA (**Panel D**) without *C. auris* DNA sample in the reaction. The melting peaks for each target was compared against NDC reaction for qualitative identification of target species. The real-time PCR was performed in triplicate and amplification and melting curves were analysed as mean values (n=3). The horizontal dotted line is fixed as the threshold value of fluorescence. CK: *C. krusei*-specific; PC: pan-*Candida*; CG: *C. glabrata*-specific; IC: Internal Control; CA: *C. auris*-specific.

As a result of the malfunctioned *C. glabrata*-specific probe, CG THO1:PCO1 probe, a second design of the probe, CG THO2:PCO1 was tested through amplification and melting curves probes analysis. The MPA-*Candida* assay with CG THO2:PCO1 along with *C. krusei*-specific probe (CK THO1:PCO1) and pan-*Candida* probe (PC THO1:PCO1) was performed for the detection of *C. glabrata* plasmid DNA for simultaneous output at the genus *Candida* and species-level. A PCR reaction of serially diluted *C. glabrata* plasmid DNA was detected from the amplification curves with the expected shifts at the pan-*Candida* (PC) and *C. glabrata* (CG) melting peaks (Figure 3.34).

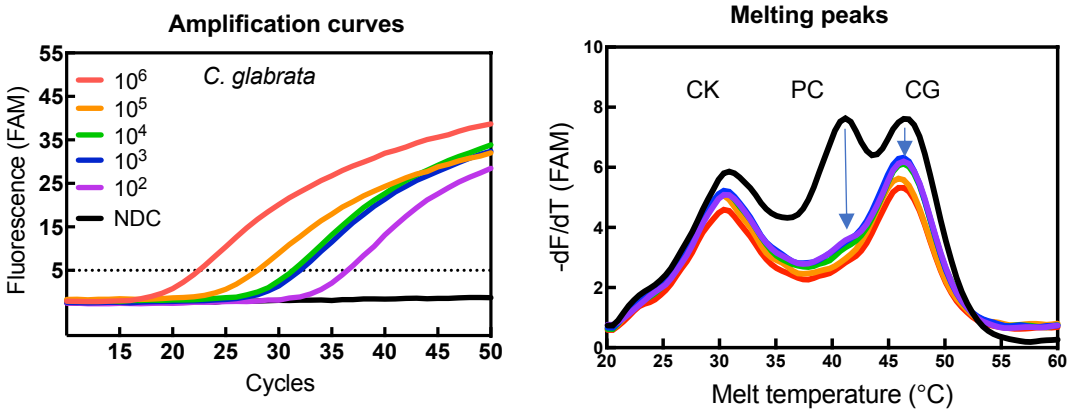

Figure 3. 34 Amplification of *C. glabrata* plasmid DNA and melting curves analysis of the samples along with NDC melt curves profile as a comparison.

Amplification curves from five ten-fold dilutions of *C. glabrata* plasmid DNA from 10^6 to 10^2 copies per PCR reaction. Post-amplification melting curve analysis of MPA probes of *C. krusei* (CK), pan-*Candida* (PC) and *C. glabrata* (CG) in a single reaction demonstrated reduction of melt peaks at pan-*Candida* (PC) and *C. glabrata* (CG). The real-time PCR was performed in triplicate and amplification and melting curves were analysed as mean values (n=3). The horizontal dotted line is fixed as the threshold value of fluorescence.

The MPA-*Candida* assay was established from the assembly of five MPA probes that generate control melting curves profile in two-channel of detection; three FAM-labelled probes and two HEX-labelled probes as depicted in Section 3.2.8; Figure 3.26. The assay is sensitive for the detection of *C. auris* plasmid DNA from the range of 10^6 to 10^2 copies of target per reaction. Amplification curves resulting from probe hydrolysis and post-amplification analysis with reduced melting peaks of pan-*Candida* (PC) temperature in the FAM channel (Figure 3.35, panel A) and identified at the species-level for *C. auris* (CA) temperature in the HEX channel (Figure 3.35, panel B). The reaction was also contained the IC plasmid DNA that was amplified and detected by the IC HEX-labelled probe to ascertain reaction functionality in the presence or absence of fungal target DNA.

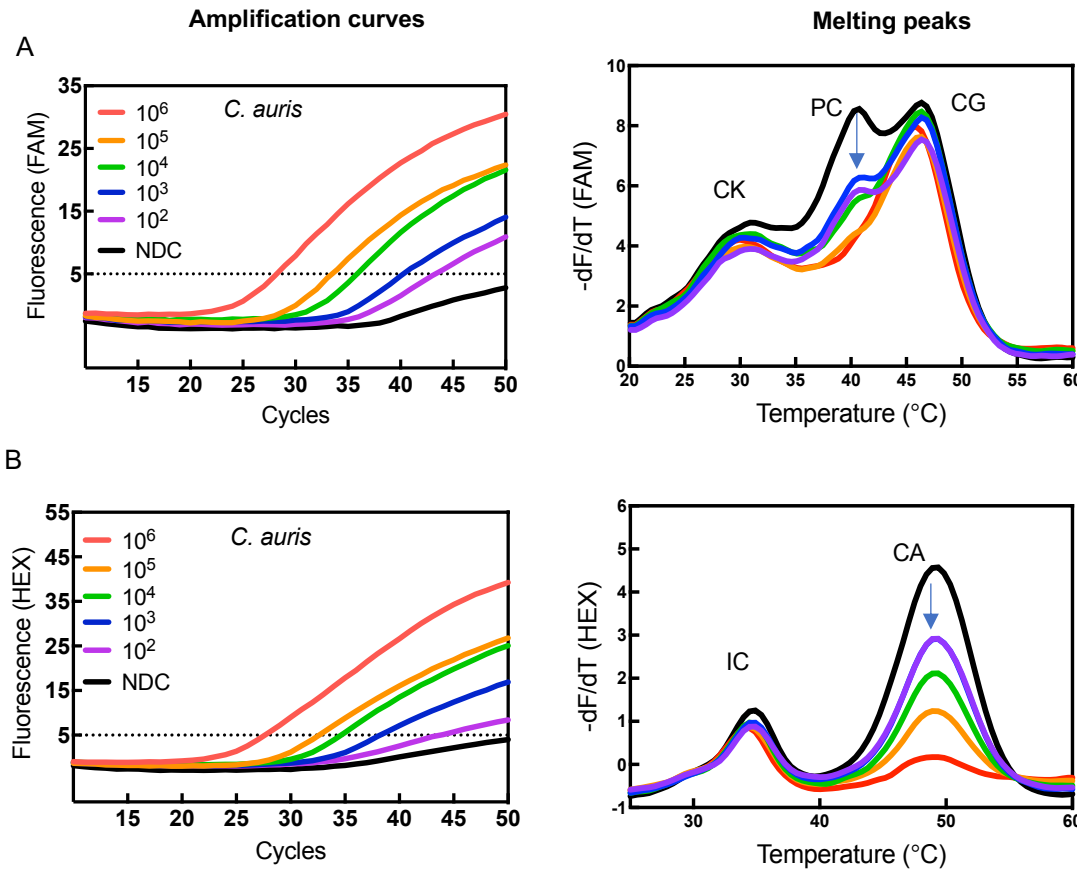

Figure 3. 35 Amplification of *C. auris* plasmid DNA and melting curves analysis of the samples along with NDC melt curves profile as a comparison in the FAM and HEX channels. Amplification curves from five ten-fold dilutions of *C. auris* plasmid DNA from 10^6 to 10^2 copies per PCR reaction. Post-amplification melting curve analysis of MPA probes of *C. krusei* (CK), pan-*Candida* (PC) and *C. glabrata* (CG) in a single reaction demonstrated reduction of melt peaks at pan-*Candida* (PC) in the FAM channel (**Panel A**) and *C. auris* (CA) in the HEX channel (**Panel B**). Internal control (IC) with reduced melting peaks ascertain assay functionality. The real-time PCR was performed in triplicate and amplification and melting curves were analysed as an average (n=3). The horizontal dotted line is fixed as the threshold value of fluorescence.

3.2.10 Determination of MPA-*Candida* sensitivity of detection

The MPA-*Candida* assay's limit of detection was determined using a genome equivalent range of 10^0 to 10^5 copies. DNA amplification profiles and the corresponding reduction of melting curve was evaluated against the NDC melt curve profiles. The amplification curve detected in both channels was used to monitor the accumulation of the pan-*Candida* and *C. krusei*, *C. glabrata* and *C. auris* DNA biomarkers. The C_t was read before 45 cycles to avoid inconclusive late amplification curve. Crucial interpretation of PCR outcomes from the MPA-*Candida* assay relied on melt curve analysis collected during post-amplification in the FAM and HEX detection channels.

The lowest copy of genomic DNA that was detected in the assay at 10-copy for *C. krusei* and *C. auris* by the pan-*Candida* probe showed from the amplification curve and a significant reduction of the pan-*Candida* peak (40°C peak in FAM channel) compared to the NDC melt curve (Figure 3.36, panel B, panel D i). *C. albicans*, *C. dubliniensis*, *C. glabrata*, *C. auris*, *C. parapsilosis*, *C. tropicalis, C. haemulonii* and *C. guilliermondii* were detected from 100 copies by the pan-*Candida* probe (Figure 3.36; Table 3.11). The *C. glabrata*-specific probe (46°C peak in the FAM channel) was able to detect *C. glabrata* genomic DNA at a 100-copy number (Figure 3.36, panel C). The *C. krusei*-specific (30°C peak in the FAM channel) and *C. auris*-specific probes and 48°C peak in HEX channel) were able to detect their respective DNA templates at a 10-fold superior in comparison to the *C. glabrata* probe. Figure 3.36, panels A to D show five different amplification and melt curves profiles that were analysed from a reduction of melt peaks in FAM and HEX detection channels.

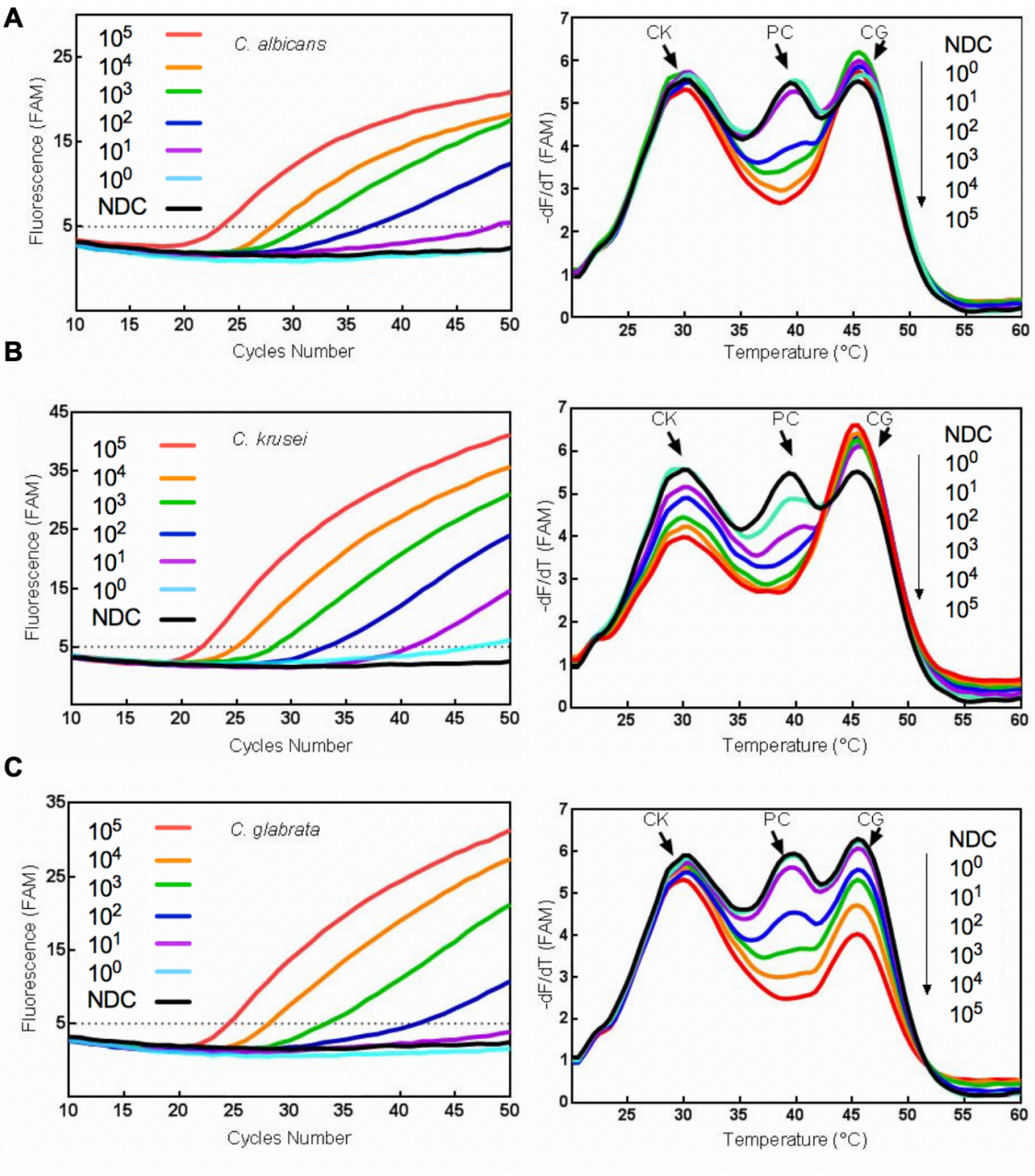
A
B
C
C. albicans
C. krusei
C. glabrata
Fluorescence (FAM)
Cycles Number
-dF/dT (FAM)
Temperature (°C)
CK
PC
CG
NDC
10^5
10^4
10^3
10^2
10^1
10^0

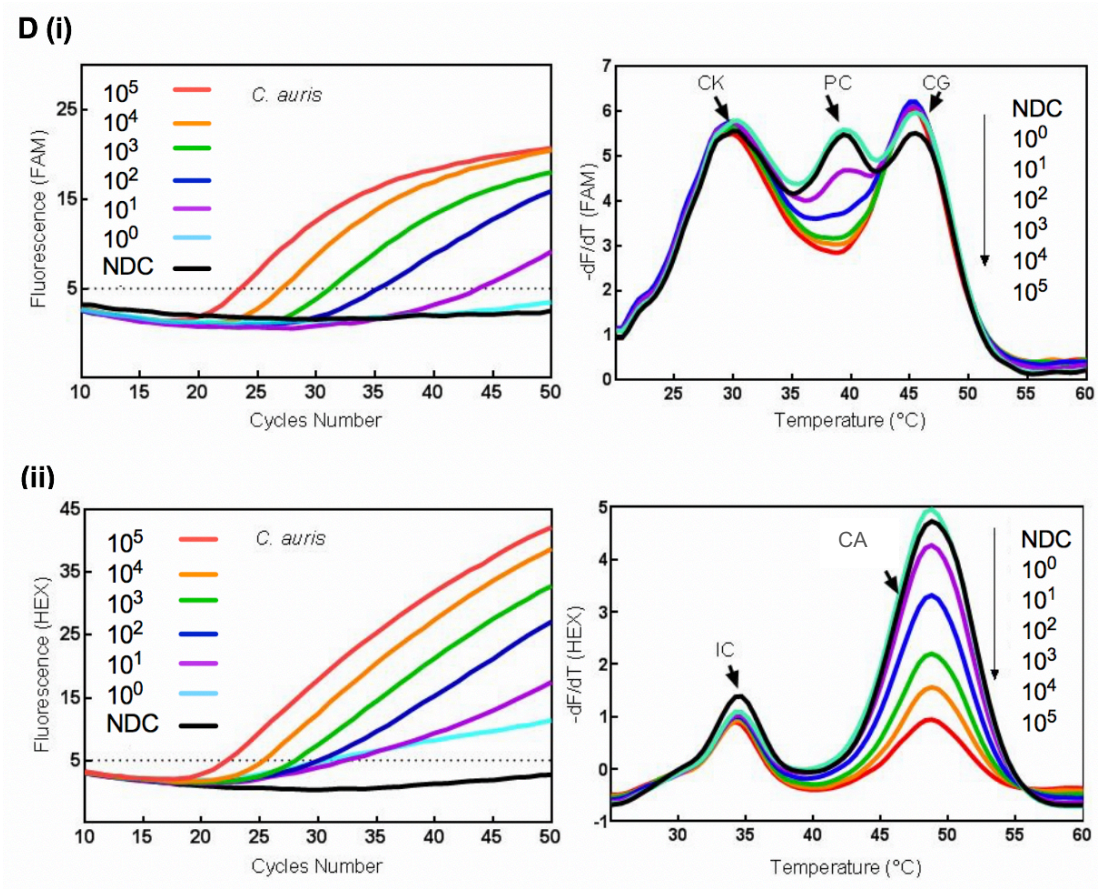

Figure 3. 36 Amplification of serially diluted *Candida* species genomic DNA and their respective melt curve analysis. Amplification reactions containing a range of 1 to 10^5 copies of target DNA per reaction were carried out. **Panel A**) Amplification plots of *C. albicans* and the corresponding melt curves analysis showing proportional to the different copies at pan *Candida* (PC) peak in the FAM channel. **Panel B**) Amplification plots of *C. krusei* and its melt curves analysis showing proportional to the different copies at pan *Candida* (PC) as well as *C. krusei* (CK) peaks in the FAM channel. **Panel C**) Amplification plots of *C. glabrata* and its melt curves analysis showing proportional to the different copies at pan *Candida* (PC) as well as *C. glabrata* (CG) peaks in the FAM channel. **Panels D**; i, ii) Amplification plots of *C. auris* and its melt curves analysis showing proportional to the different copies at pan *Candida* (PC) and *C. auris* (CA) peaks detected in the FAM and HEX channels respectively. The horizontal dotted line is fixed as the threshold value of fluorescence. NDC, no DNA control. The experiments were performed in three replicates for three times.

Table 3. 11 MPA-*Candida* assay limit of detection as analysed from amplification curve.

***Candida* species**	**Detection channel (s)**	**C_t < 45 cut-off value**	**Limit of detection (genomic DNA copies per reaction)**
C. auris	FAM, HEX	43.60, 32.40	10
C. krusei	FAM	41.00	10
C. glabrata	FAM	41.30	100
C. albicans	FAM	37.10	100
C. dubliniensis	FAM	35.60	100
C. parapsilosis	FAM	36.50	100
C. tropicalis	FAM	37.90	100
C. guilliermondii	FAM	36.50	100
C. haemulonii	FAM	37.00	100

3.2.11 The complement Pan-Fungal assay standard curve

The amplification efficiency of the Pan-Fungal quantitative assay was calculated from the gradient generated from eight *Candida* species standard curves, with three independent repeats in triplicate incorporating 360 data points. The efficiency range was 82.99 to 104.49% (Table 3.12), and the gradient between the standards were not significantly different (Analysis of Covariance, ANCOVA p value = 0.8561). A representative standard curve with an overall efficiency of 92.56% and correlation coefficient, R^2= 0.9992 (Figure 3.37). The Pan-Fungal assay exhibited an excellent reproducibility throughout the dilutions in each *Candida* species plasmid DNA with intra-assay and inter-assay CV less than 5%. Dilutions covered five orders of magnitude ranging from 10^6 to 10^2 plasmid DNA copies number per reaction.

Table 3. 12 Standard curves generated for each *Candida* species plasmid DNA in TaqMan® Pan-Fungal reaction from three independent experiments.

***Candida* species**	**Equation**	**R^2**
C. albicans	Y = -3.365*X + 46.37	0.9994
C. dubliniensis	Y = -3.393*X + 44.42	1
C. krusei	Y = -3.227*X + 45.11	0.9772
C. glabrata	Y = -3.811*X + 48.53	0.9891
C. auris	Y = -3.348*X + 41.79	0.9996
C. parapsilosis	Y = -3.633*X + 43.99	0.9957
C. guilliermondii	Y = -3.726*X + 47.61	0.9938
C. tropicalis	Y = -3.644*X + 45.89	0.9962

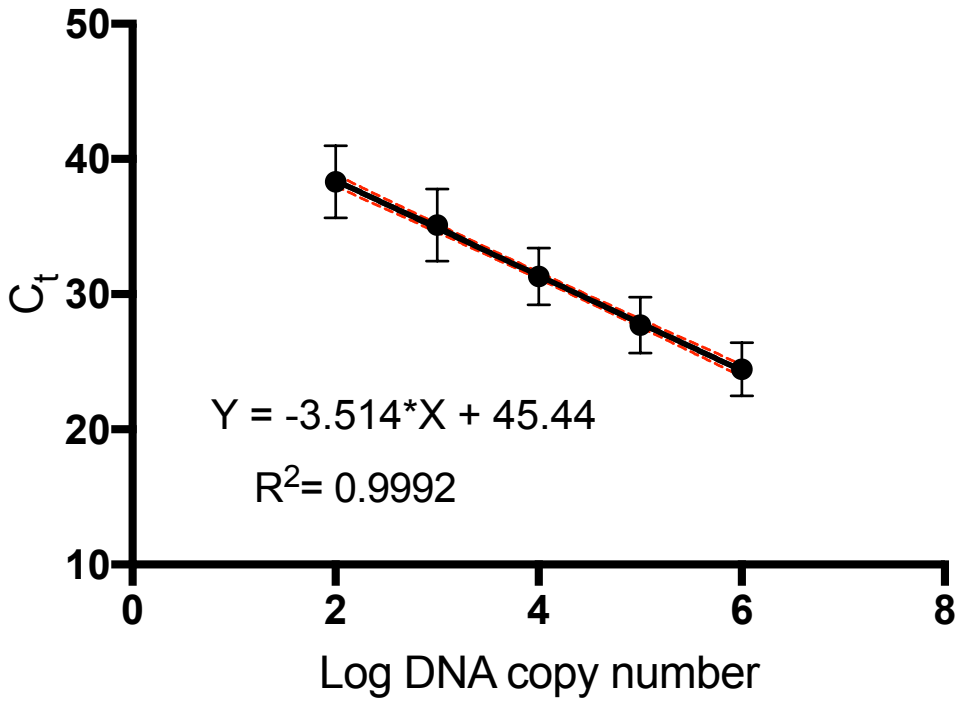

Figure 3. 37 TaqMan® Pan-Fungal assay standard curve. Standard curve generated by plotting the mean C_t values as a function of the known starting concentration of the standard dilutions. Ten-fold serial dilutions (10^6 to 10^2 copies) of the cloned *Candida* species plasmid DNA were analysed in three independent experiments with three replicate reactions per dilution step. Error bars represent SD of C_t values from replicated standards. Confidence intervals (CI) of the means of C_t values are indicated by the dashed lines.

The Pan-Fungal assay limit of detection of serially diluted fungal genomic DNA was determined from the amplification curve in the FAM channel. In general, *Candida* species can be detected from 10 genome copies except for *C. glabrata*, *C. tropicalis* and *C. guilliermondii* which 10-fold higher (Table 3.13).

Table 3. 13 TaqMan® Pan-Fungal assay limit of detection as analysed from the amplification curve.

Fungal species	C_t < 45 cut-off value in FAM detection channel	Limit of detection (genomic DNA copies per reaction)
Aspergillus flavus	40.00	10
C. auris	42.00	10
C. krusei	41.00	10
C. albicans	40.00	10
C. dubliniensis	41.30	10
C. parapsilosis	41.50	10
C. haemulonii	40.00	10
C. glabrata	43.10	100
C. tropicalis	35.00	100
C. guilliermondii	37.30	100

3.2.12 External validation and evaluation tests

All spiked serum samples (6/6) of *Candida* Evaluation Panel (Qnostics) were successfully detected in a TaqMan® Pan-Fungal assay and no detection for panel's negative sample (S07). The panel was further tested for the qualitative detection of *Candida* species in the MPA-*Candida* assay. *C. albicans* "High" positive sample (S01), *C. krusei* "High" and "Medium" (S05 & S06) positive samples were detected from the reduction of pan-*Candida* melt peak (40°C) and concomitant *C. krusei* specific-detection at 30°C melt peak (Table 3.14). No amplification was detected for the Negative sample (S07) therefore, no reduction of melt curve compared to NDC melt curve. *C. albicans* "Medium" sample (S02), *C. glabrata* "High" and "Medium" samples (S03 & S04) were not detected in MPA-*Candida* assay. However, all samples were detected positive in the Pan-Fungal assay. *C. glabrata* samples 03 & 04 were detected positive with mean C_t values of 28.55, SD ± 0.53 and 32.48, SD ± 0.75 respectively.

Multiplex *Candida* species detection assay, MPA-*Candida*, showed the comparable magnitude of detection of *C. auris* genomic DNA with a single *C. auris* detection kit (Genesig® Standard Kit, Primerdesign™ Ltd) (Figure 3.38). Linear dynamic range of detection was demonstrated for Genesig kit (correlation coefficients, R^2 = 0.997; PCR efficiency, E = 79.02%) and MPA-*Candida* in both level of detections; *C. auris*-specific (R^2 = 0.9973; E = 125.09%) and genus-*Candida* (R^2 = 0.9935; E = 73.57%). Dilutions spanned from 10^5 to 10^1 genome copies of *C. auris* per reaction. In a separate experiment, Genesig kit showed cross-reactivity with *C. auris*-related species, *C. haemulonii* (C_t = 34.43) tested at 10^5 copies of genomic DNA.

Table 3. 14 Quantitative and qualitative analysis of Qnostics *Candida* Evaluation Panel in TaqMan® Pan-Fungal and MPA-*Candida* reactions.

Sample code, description & (*reference C_t value)	Pan-fungal reaction		MPA-*Candida* melting curve qualitative analysis
	Mean C_t ± SD	Estimation of target copy number [1]	
S01: *C. albicans* (24.5)	24.19 ± 0.68	1.11×10^6	Positive Pan-*Candida*
S02: *C. albicans* (27.2)	27.70 ± 0.26	1.11×10^5	Negative
S03: *C. glabrata* (30.4)	28.55 ± 0.53	6.40×10^4	Negative
S04: *C. glabrata* (31.9)	32.48 ± 0.75	4.88×10^3	Negative
S05: *C. krusei* (29.0)	30.04 ± 0.63	2.41×10^4	Positive Pan-*Candida* & *C. krusei*
S06: *C. krusei* (31.3)	34.04 ± 0.23	1.75×10^3	Positive Pan-*Candida* & *C. krusei*
S07: Negative (Negative)	ND	ND	Negative

* Reference C_t value provided in the Qnostics *Candida* Evaluation Panel product information.

[1)] Estimation of fungal target copy number present based on the calibration curve established for the Pan-Fungal qPCR assay, y= -3.514Log (x)+ 45.44; R^2= 0.999. C_t, Threshold cycle; SD, Standard deviation; ND, No Detection

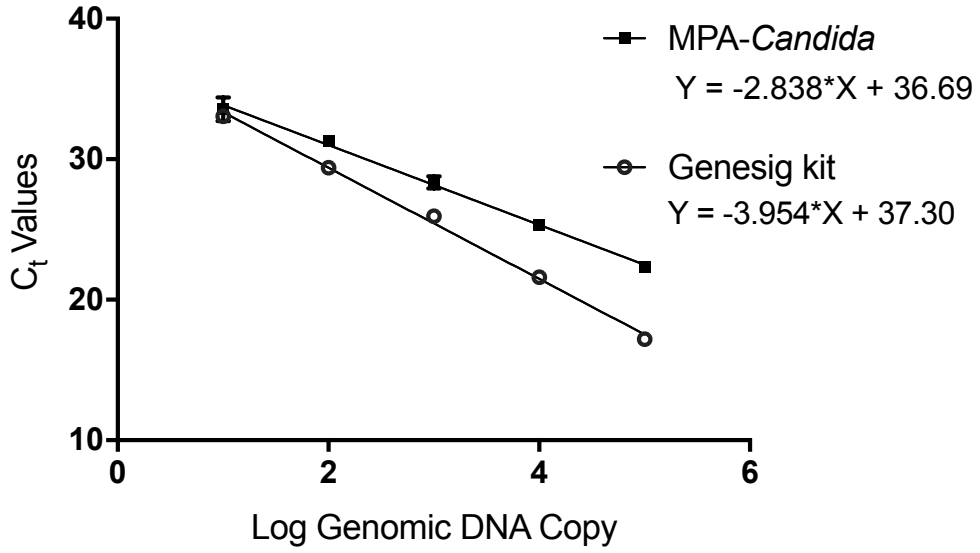

Figure 3. 38 Detection of *C. auris* genomic DNA in MPA-*Candida* and simplex *C. auris* qPCR diagnostic kit (Genesig® standard kit). *C. auris* genomic DNA was detected across five tenfold dilutions ranging from 10^5 to 10^1 genome copies per reaction. The reaction has small SD and error bar only can be seen in the latest C_t values of MPA-*Candida*. Each qPCR reaction was performed in triplicate.

3.3 Discussion

In this study, biomarkers for the detection of all fungal species (pan-fungal), all *Candida* species (pan-*Candida*) and species-specific sequences for each resistant species *C. krusei*, *C. glabrata* and *C. auris* were identified. *Candida* species biomarkers were identified and adapted as probes in the MPA-*Candida* assay from the variable domains (D1/D2) of the LSU rDNA gene. The first 381 bp from the 5' end of the LSU region showed great intraspecies sequence diversity for *Candida* species. This region has been used to analyse and identify clinically relevant *Candida* species (Makene, 2014). Availability of the D1/D2 of the LSU sequences in the database increased the sequence utility to resolve individual yeast species (Page & Kurtzman, 2005). However, a BLAST result for the pan-*Candida* probe sequence resulted in several other yeast species with 100% similarity, which could lead to cross-reactivity. Further analyses of sequence alignments of the D1/D2 of the LSU gene between *S. cerevisiae* and *C. albicans* revealed 85% sequence similarity. *S. cerevisiae* is phylogenetically related and showed a high sequence identity to other *Candida* species (Pérez-Torrado & Querol, 2016). Nevertheless, this should not be a major concern, as standard antifungal therapy with fluconazole is effective to treat *S. cerevisiae* infections (Enache-Angoulvant & Hennequin, 2005). Moreover, invasive infections caused by *S. cerevisiae* is very low compared to *Candida* species that is the predominant cause of IFIs (Miceli, Díaz & Lee, 2011).

The pan-fungal probe was selected from the ITS2 region, and the target region was amplified by the universal primer set (ITS3 and LR1). The target region was selected to ensure coverage of fungal species where most, if not all, potential pathogens can be detected in the Pan-Fungal assay. Although there is no single locus for fungal identification, consensus decided that the whole ITS region (ITS1-5.8S-ITS2) be

accepted as a universal fungal DNA barcode for fungi (Schoch *et al.*, 2012; Irinyi *et al.*, 2016). The ITS region has been long used in the fungal phylogenetic studies (Robert *et al.*, 2011), and establishment of the curated fungal sequence database such as the ISHAM (International Society for Human and Animal Mycology) Barcoding Databases (http://its.mycologylab.org/) providing a reliable identification of biomarkers at the species-level. In the present study, a unique IC probe sequence was designed and incorporated into both MPA-*Candida* and Pan-Fungal reactions. The detection of the IC plasmid DNA in the assays was independent regardless of the presence or absence of a fungal target sequence in the reaction. Through the inclusion of the IC, the functionally of the PCR mixture was monitored from inhibitors in every sample to avoid false negative results. Although the universal primers M13 was utilised in the reaction may contribute to non-specific amplification, but a novel design of the IC target probe for detection of amplified region is specific.

This novel MPA-*Candida* assay is capable of detecting nine medically important *Candida* species most frequently associated with candidiasis. The genus-level biomarker for *Candida* (pan-*Candida*) probe detects *C. albicans*, *C. dubliniensis*, *C. parapsilosis*, *C. tropicalis*, *C. guilliermondii*, *C. haemulonii*, *C. krusei*, *C. glabrata* and *C. auris*. Species-level discrimination of the drug-resistant *C. krusei*, *C. glabrata* and *C. auris* could also be correctly identified simultaneously in the assay by their corresponding specific probes. Collectively, the MPA-*Candida* assay consisted of five different probes labelled with only two different fluorophores. MPA technology provides a great advantage over the standard hydrolysis probe real-time PCR diagnostic tests which is limited to one channel for one biomarker (Fu, Miles & Alphey, 2012). In the MPA-*Candida*, the pan-*Candida*, *C. krusei*-specific and *C. glabrata*-specific probes were labelled with the FAM reporter dye. Meanwhile, the *C. auris*-specific and IC probes were labelled with the HEX reporter dye. The probes

melting temperatures can be distinguished by providing the variability of the probe constituents and composition of the probe complementarity to the target sequence (Huang *et al.*, 2011). In the MPA-*Candida* assay, the IC and *C. auris*-specific probes were labelled with HEX to avoid overlapping melting peaks from a single detection channel. The THO and PCO hybrid of the *C. auris*-specific had a melting temperature almost identical to that of the *C. glabrata*-specific probe, and the IC probe had a melting temperature less than 5°C to the *C. krusei*-specific probe. Ideally, the melting temperature between the probes labelled with the same fluorophore should differ by 5 to 7°C. Characterisation of the MPA-*Candida* assay with an assembly of the pan-*Candida* and *C. glabrata*-specific probes labelled with FAM at the equivalent concentration (0.4 μM) had masked the *C. glabrata* fluorescence signal in the melt curve. Therefore, the pan-*Candida* probe final concentration in the assay was reduced to 0.2 μM to regain the specific melting peak signal for *C. glabrata*-specific probe.

The pan-fungal probe was engineered as a separate reaction to complement the MPA-*Candida* assay diagnostic to detect and quantify other fungal species that may be present in the clinical sample. The Pan-Fungal assay was based on standard hydrolysis probe real-time PCR therefore, amplification curve analysis for the C_t was used to monitor detection of the fungal biomarker. The ITS2 region has been utilised for detection of fungal pathogens in many PCR assays (Hasseine *et al.*, 2015; Zeller *et al.*, 2017). Detection channels and the reaction protocol of the Pan-Fungal assay were consistent with the MPA-*Candida* assay, which enabled simultaneous reaction and results analysis in a single run of PCR. A separate assay designed for the Pan-Fungal reaction could assist the clinicians ruling out non-fungal infections before proceeding the diagnosis for candidiasis in the MPA-*Candida* assay. High NPV in some of the molecular tests such as LightCycler SeptiFast (Roche) and T2 *Candida* (T2 Biosystems) are useful to rule out the diseases in the population of the prevalence of

fungal infections is low (Chang *et al.*, 2013; Pfaller & Castanheira, 2016). A test with a high NPV (88-100%) could give justification to stop unnecessary antifungal treatment to the patients and would reduce development of antifungal resistance and indirectly save the cost of patient care (Halliday *et al.*, 2015). Positive and Negative Predictive Values measure the performance of diagnostic test and reflect the probability of a test result predicting whether a disease is present or absent in the specific population (Khot & Fredricks, 2009). It is also worth noting that the Pan-Fungal assay is more straightforward to analyse and could save the precious DNA material and cut the cost for unnecessary diagnosis processes. However, future approach to combine this current *Candida* and Pan-Fungal reactions into a single tube and single detection channel reaction could be promising.

The MPA-*Candida* assay demonstrated specific melt peaks for detections of *Candida* species and resistant species of *C. krusei*, *C. glabrata* and *C. auris*. The post-amplification melting curve analysis provides a qualitative value of specificity. In the presence of the target(s), the corresponding melting peak(s) either reduced or disappeared when compared with the NDC melt curves. All nine *Candida* species were detected by the pan-*Candida* probe, and each resistant species was detected by the corresponding species-specific probe. However, a slight reduction of the *C. krusei* melting peak was noticed in the presence of non- *krusei Candida* species DNA in the assay throughout this study. This phenomenon has been described as "shrunk neighbouring peaks" in the original research article reporting the MPA technology and does not affect the diagnostic specificity and accuracy of the assay (Fu, Miles & Alphey, 2012). The melting peak for *C. krusei* detection could be differentiated with a significant reduction of signal compared to a small reduction as in the presence of non-*krusei Candida* species. The probes melting temperature are widely distributed across

the two channels. One could easily tell whether single or double target sequence was detected from the melting curve pattern as compared to the control melting curve.

It was demonstrated that the MPA-*Candida* and Pan-Fungal PCR reactions were able to detect 100 copies of genomic DNA and could confidently detect 10 copies of *C. krusei* and *C. auris* genomic DNA. This range of detection is approximately equivalent to the clinical range of candidaemia of 5 to 100 CFU/mL (Loeffler *et al.*, 2000). Its detection sensitivity for fungal rDNA is comparable with other commercially available kits. For example, SeptiFast (Roche) could detect fungal DNA in a range of 30 to 100 CFU/mL blood (Chang *et al.*, 2013), and MycoReal *Candida* kit (Ingenetix) could detect from 5 to 10 CFU/mL blood (Schabereiter-Gurtner *et al.*, 2007). The amplification curve from the MPA-*Candida* reaction was evaluated in parallel with the melt curve analysis. A threshold cycle was set based on the cycle at which fluorescence from amplification exceeded the background noise. Although the exponential amplification curve was detected at early cycle, it has no mean to discern the source of the probe detected for species-specific identification. Therefore, the melt curve analysis in the MPA-*Candida* reaction is essential for the qualitative identification of the *Candida* species with reduced susceptibility or resistant to antifungals. Interestingly, although the quantification cycle value could be detected (C_t = 45.25 ± 2.07) for samples with a single copy *C. krusei* genomic DNA, the corresponding melting peak was not reduced significantly compared to the NDC peak. Thus, the interpretation of results should be carried out with caution, especially when low concentrations of DNA sample are used.

The external evaluation panel was employed in this study to assess the performance of the MPA-*Candida* and Pan-Fungal assays from the spiked serum samples. The Qnostics' *Candida* spp. Evaluation Panel was processed according to the standard technique to release the DNA from the cell wall using a vigorous mechanical

lysis method (Preuner & Lion, 2013). The spiked samples were detected positive in the TaqMan® Pan-Fungal assay confirming the presence of fungal DNA in the extraction products. The panel's negative sample was detected negative in both reactions, Pan-Fungal and MPA-*Candida*; thus, eliminating the possibility of samples cross-contamination throughout the processes. The MPA-*Candida* reaction successfully detected *C. albicans* "High" and *C. krusei* "High" and "Medium" samples from the genus-level of pan-*Candida* melt peak and with an additional reduction of melt peak to speciate *C. krusei*. Cross-reference of C_t value was comparable to the Qnostics's reference assay (Table 3.14). However, the MPA-*Candida* assay was less sensitive for *C. glabrata* and *C. albicans* "Medium" samples hence, no qualitative analysis can be evaluated to confirm these samples. The *in vitro* limit of detection testing showed 100 copies of *C. glabrata* genomic DNA was detected late (C_t = 41.30 ± 0.45) relatively to the other *Candida* species by 3 to 6 cycles (Table 3.11). This variability of the C_t values suggests the assay is less sensitive towards detection of *C. glabrata* DNA, thus limiting the detection of the panel's *C. glabrata* spiked samples.

Finally, we tested the MPA-*Candida* assay performance specifically for detection of emerging *C. auris*. The assay was sensitive up to 10 genome copies per reaction and efficient throughout the genus- and species-level of detections. Commercially available biochemically based yeast identification systems, such as Vitek 2 (bioMérieux) and BD Phoenix (BD Diagnostics) has misidentified *C. auris* as *C. haemulonii* (Centers for Disease Control and Prevention, 2018). Our multiplex *Candida* PCR assay consist of a highly specific DNA biomarker for *C. auris* and manifest an excellent specificity with no cross-reactivity with one of the closely related species, *C. haemulonii*.

In summary, the MPA technology allows the development of a real-time PCR assay for the detection of five different targets including of the IC in just two channels

of detection. The antifungal resistant *C. krusei*, *C. glabrata* and *C. auris* can be accurately discriminated from the other *Candida* species from a straightforward melt curve analysis. Robust and simple features of the MPA-*Candida* assay would allow practical adaptation in the less sophisticated qPCR instruments (Qiagen's Rotor-Gene Q 2-Plex HRM, Applied Biosystems™ 7500), with seamless integration in the laboratories that operate in the conditions of limited resources. The MPA-*Candida* assay range of species detection as well as its high specificity and sensitivity could help clinicians for a prompt initiation of accurate therapeutic drugs to the patients and effective disease management. As the results of this *in vitro* study have been highly successful, validation of this novel fungal diagnostic assay using clinical samples is warranted.

CHAPTER 4: Exploring Alternative Single-tube Designs for the MPA-*Candida* assay

4.1 Introduction

MPA technology has been used previously for the diagnosis of Human Papilloma virus (HPV) infection. Genefirst's Papilloplex® High-Risk HPV kit can multiplex 14 probes using four channels for the detection of HPV in a single closed-tube PCR test (Bhatia *et al.*, 2017). This chapter describes experiments aimed at re-designing the MPA-*Candida* assay for use as a single closed-tube diagnostic test capable of fungal biomarker detection employing either two (assay design 2) or three (assay design 3) fluorescence detection channels. Assay design 2 incorporates the pan-fungal probe into the MPA-*Candida* assay and was optimised for its melting curve profiles. A slight modification to the original MPA-*Candida*, the assay design 2 without the pan-fungal probe, was initially tested for its diagnostic specificity and sensitivity. As an alternative strategy, the inclusion of the pan-fungal probe for three detection channels was pursued. Assay design 3 incorporates the pan-fungal probe and aimed to monitor the biomarkers amplification by 3-channel hexa-plexing.

4.2 Experimental Results

4.2.1 Assay design 2: testing of MPA-*Candida* melting curve profile to incorporate pan-fungal target

Various MPA probes labelled with FAM and HEX were tested for their melting curves within the two channels of detection. The *C. krusei*-specific probe and IC probe were exchanged their fluorophore dye to avoid the overlapping melting temperatures with the pan-fungal HEX-labelled probe (PF THO2: PCO2). A modified MPA-*Candida* assay, the FAM-labelled probes; IC, pan-*Candida* and *C. glabrata*-specific and, the

HEX-labelled probes; *C. krusei*-specific probe and *C. auris*-specific were assembled in a single tube reaction for their melting curves prior to inclusion of the pan-fungal probe pair (Figure 4.1). The HEX-labelled *C. krusei*-specific probe (CK THO1:PCO1) unexpectedly showed a higher melting temperature at 34°C in multiple probes detection, than in single probe detection (Figure 4.2). As anticipated, the assembly of the HEX-labelled pan-fungal probe (PF THO2:PCO2) in a multiplex reaction had concealed the *C. krusei*-specific melting peak. Although three HEX-labelled probes were present in the reaction, only two melting peaks were appeared at 36°C and 48°C which latter was for *C. auris*-specific probe (Figure 4.3). Optimisation of probes concentration attempted to obtain three melting peaks from the HEX-labelled probes (Figures 4.4 and 4.5). Throughout the optimisations, a small and non-specific peak at low temperature can be observed in both channels of the melt curve analysis and is an unexpected melting temperature for any of the probes in the reaction. At this point, the inclusion of the pan-fungal probe for detection in the HEX channel was unsuccessful.

A second attempt was performed to accommodate the pan-fungal probe in the MPA-*Candida* assay. The *C. krusei*-specific probe was re-designed and to have a higher melting temperature detected at 41°C. The HEX-labelled THO probes, *C. krusei*-specific (CK THO2:PCO1) was assembled with the pan-fungal and *C. auris*-specific probes (Figure 4.6). However, the melting temperature profile was not reproducible in the post-amplification analysis. Three melting peaks of *C. glabrata*-specific, pan-fungal as well as *C. krusei*-specific probes disappeared in the FAM and HEX detection channels (negative data not shown).

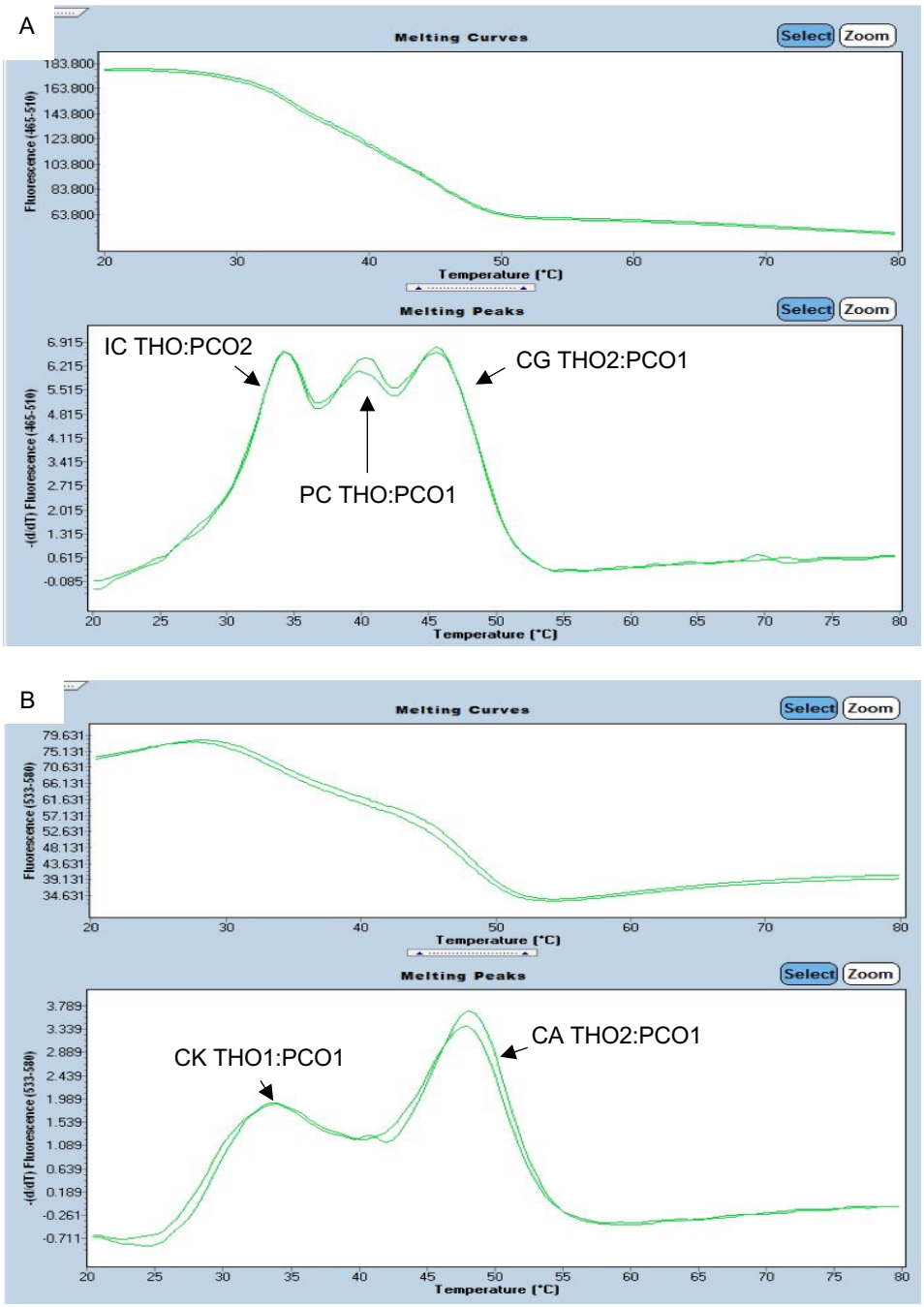

Figure 4. 1 An alternative combination of MPA probes pairs in a single reaction for five melting peaks of the control profile. Panel A shows melting peaks for IC, 34°C; pan-*Candida* (PC), 39°C; *C. glabrata* (CG), 46°C in the FAM channel and **panel B** shows melting peaks for *C. krusei*-specific (CK), 34°C and *C. auris*-specific (CA), 48°C detected in the HEX channel. The test was analysed in duplicate.

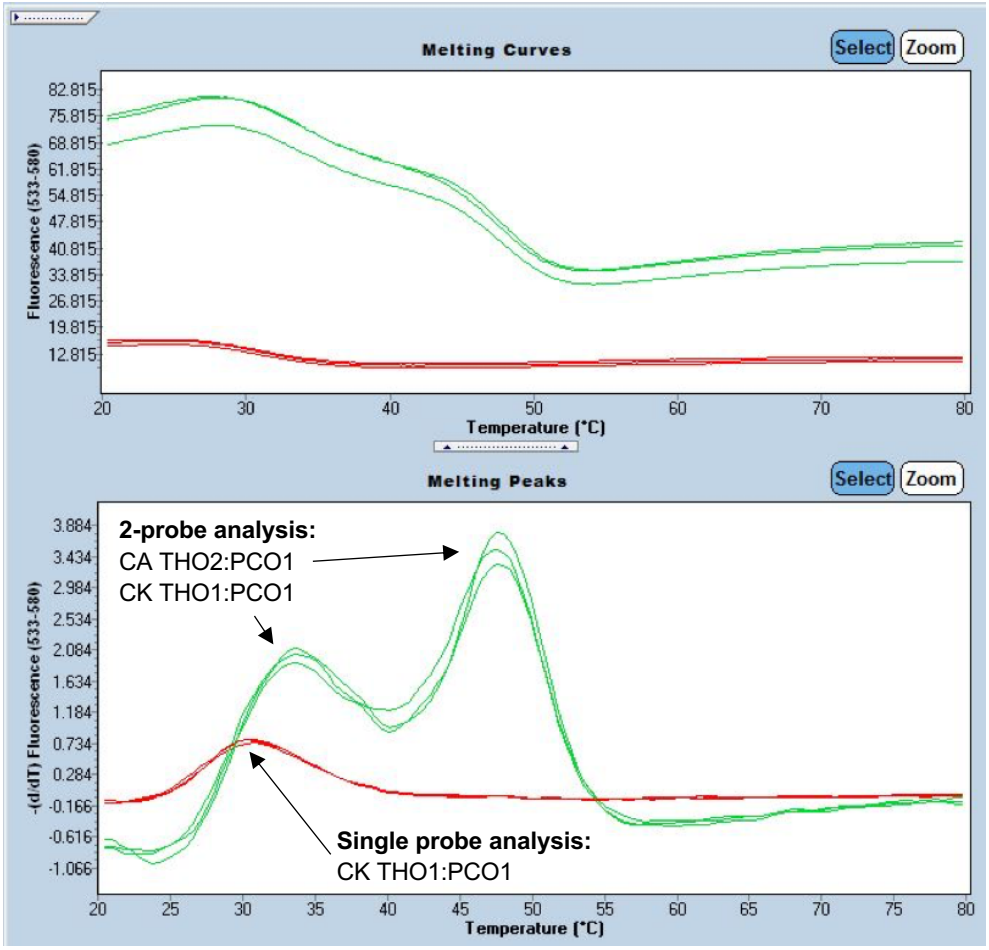

Figure 4. 2 The *C. krusei*-specific probe melting temperature was compromised in a multiplex reaction. The *C. krusei*-specific probe, CK THO1:PCO1 melting peak detected at 34°C as in 2-probe reaction (green lines) and shown at 30°C as in a single probe detection. Analysis was performed in triplicate in the HEX detection channel. CA, *C. auris*-specific probe; CK, *C. krusei*-specific probe.

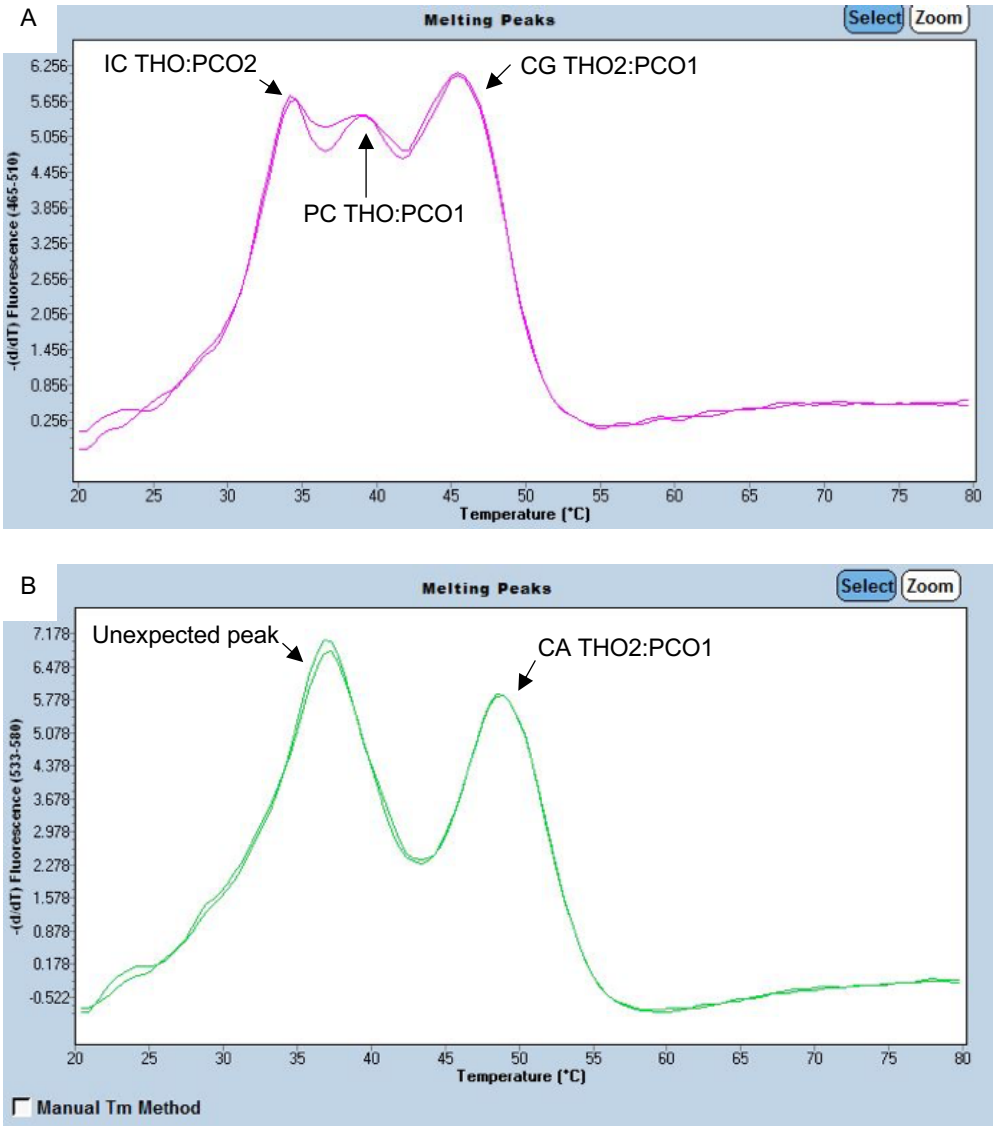

Figure 4. 3 Optimisation of six MPA probes in a single reaction. Three melting peaks detected in the FAM channel (**Panel A**), but only two melting peaks appeared in the HEX channel (**Panel B**). The melting peak which appeared at 36°C in the HEX channel is not specific for either the *C. krusei*-specific probe (CK THO1:PCO1) or the pan-fungal (PF THO2:PCO2). The concentration of the probes was tested at 0.2 µM for the IC: Internal Control, 0.2 µM for the PC: pan-*Candida*; 0.4 µM for the CG: *C. glabrata*-specific; 0.4 µM for the CK: *C. krusei*-specific; 0.4 µM for the PF: pan-fungal and; 0.4 µM for the CA: *C. auris*-specific. The test was analysed in duplicate.

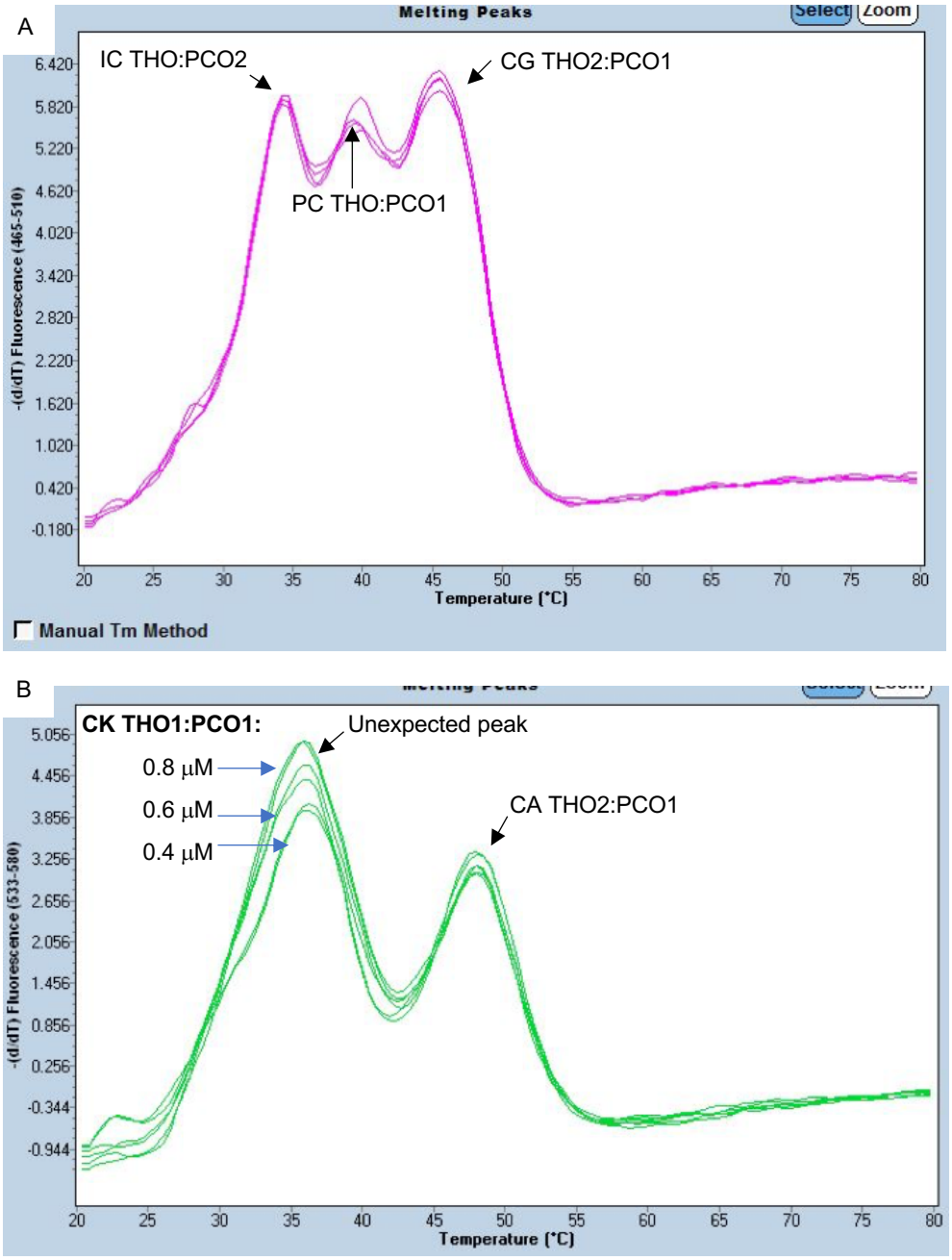

Figure 4. 4 Optimisation of *C. krusei*-specific probe (CK THO1:PCO1) concentration for a visible melt peak in the HEX channel. The reaction consists of six MPA probes in a single tube reaction. **Panel A** has three probes in the FAM channel for IC, THO:PCO2; pan-*Candida*, PC THO:PCO1; *C. glabrata*-specific, CG THO2:PCO1; **Panel B** consists of three HEX-labelled probes, but only two melting peaks can be detected at 36±1°C (the peak is not specific either to *C. krusei*-specific (CK THO1:PCO1) or pan-fungal (PF THO2:PCO2) and at 48°C for *C. auris*-specific (CA THO2:PCO1) in the HEX detection channel. Each reaction was performed in duplicate.

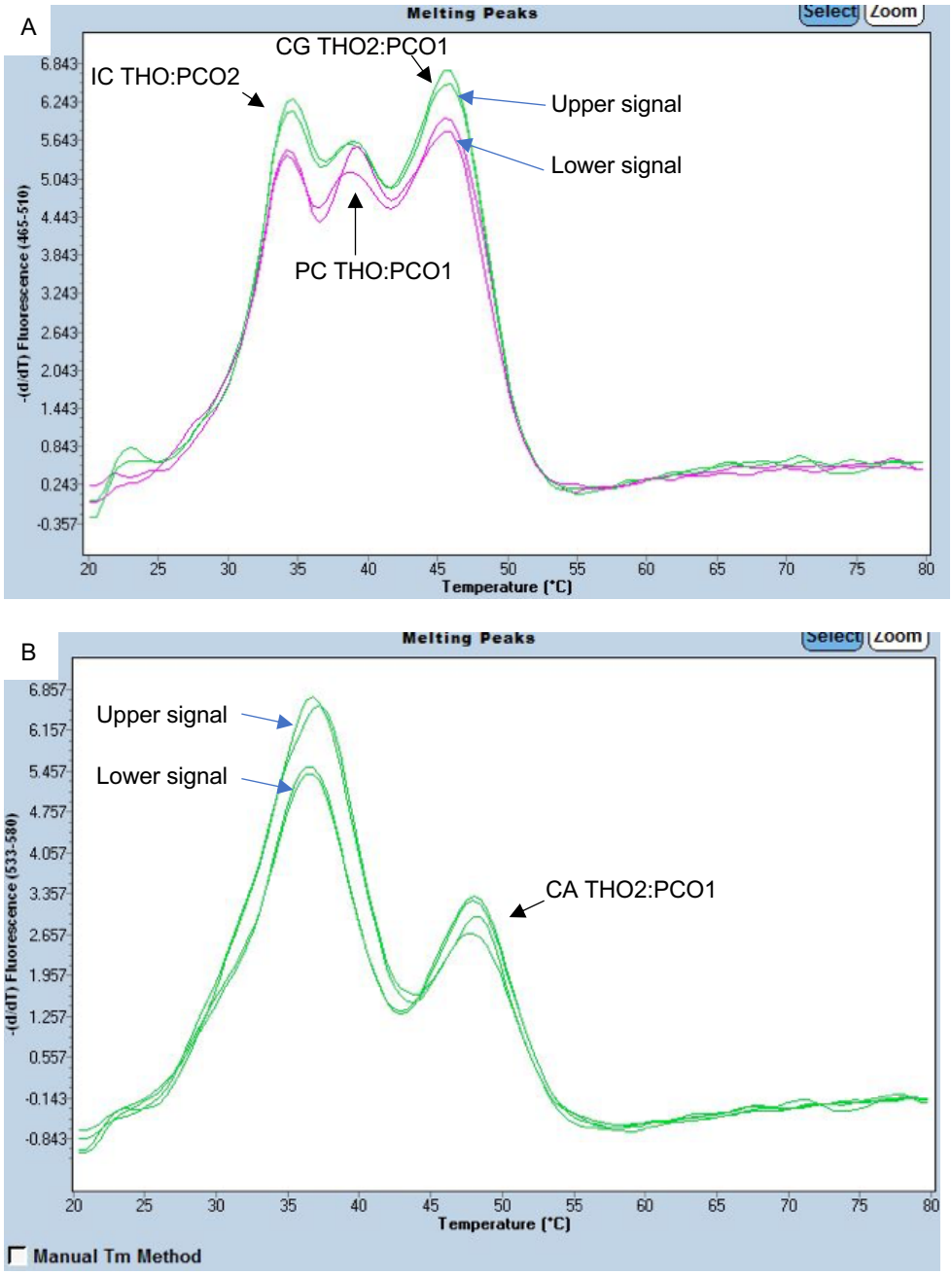

Figure 4. 5 Optimisation of the HEX-labelled probes concentration. The upper signal in Panel B (HEX channel) is a reaction with the *C. krusei*-specific probe (CK THO1:PCO1) at 0.6 µM and the pan-fungal probe (PF THO2:PCO2) at 0.4 µM and; the lower signal is a reaction with the CK THO1:PCO1 probe at 0.4 µM and; PF THO2:PCO2 probe at 0.3 µM. The experiments were unable to produce specific melt peaks for both probes in the HEX channel. The upper and lower signals in Panel A (FAM channel) consist of the probes at constant concentrations; 0.2 µM for the IC: Internal Control, 0.2 µM for the PC: pan-*Candida*; 0.4 µM for the CG: *C. glabrata*-specific. Each reaction was analysed in duplicate.

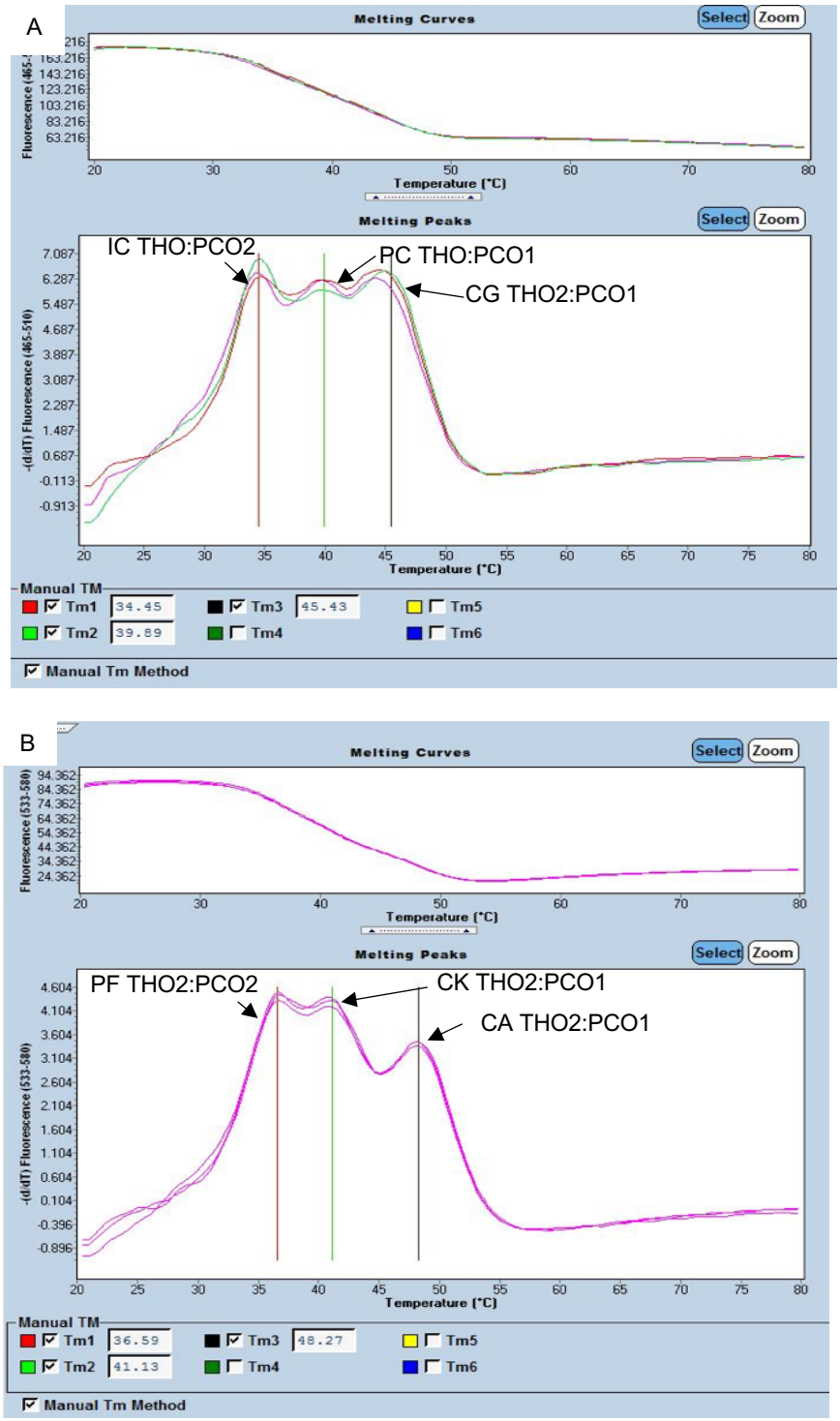

Figure 4. 6 Optimisation of six MPA probes in a single reaction for a specific melting temperature for each target probe in the FAM and HEX detection channels. Panel A consists of three probes of internal control (IC), 34°C; pan-*Candida* (PC), 39°C and *C. glabrata*-specific (CG), 45°C melting peaks detected in the FAM channel. **Panel B** consists of three probes of pan-fungal (PF), 36°C; new designed *C. krusei*-specific probe (CK), 41°C and *C. auris*-specific (CA), 48°C. The experiment was performed in triplicate.

4.2.2 Testing the specificity of the melting curve analysis

The assay design 2 as described in Figure 4.1 was evaluated for its specificity of the detection in FAM and HEX channels. Amplification of the IC plasmid template without fungal DNA showed accurate downshift of melting peak against NDC at the IC temperature (Figure 4.7). The experiment was further tested with the inclusion of *Candida* genomic DNA in every reaction. Specificity of detection of *C. albicans*, *C. glabrata*, *C. krusei* and *C. auris* in the present of IC plasmid DNA was determined with two or three peaks change their height against the NDC (from Figures 4.8 to 4.11). The qualitative outcomes including of *C. haemulonii*, *C. dubliniensis*, *C. parapsilosis*, *C. tropicalis*, *C. guilliermondii* and the filamentous fungi species as well as bacterial species tested are summarised in Table 4.1.

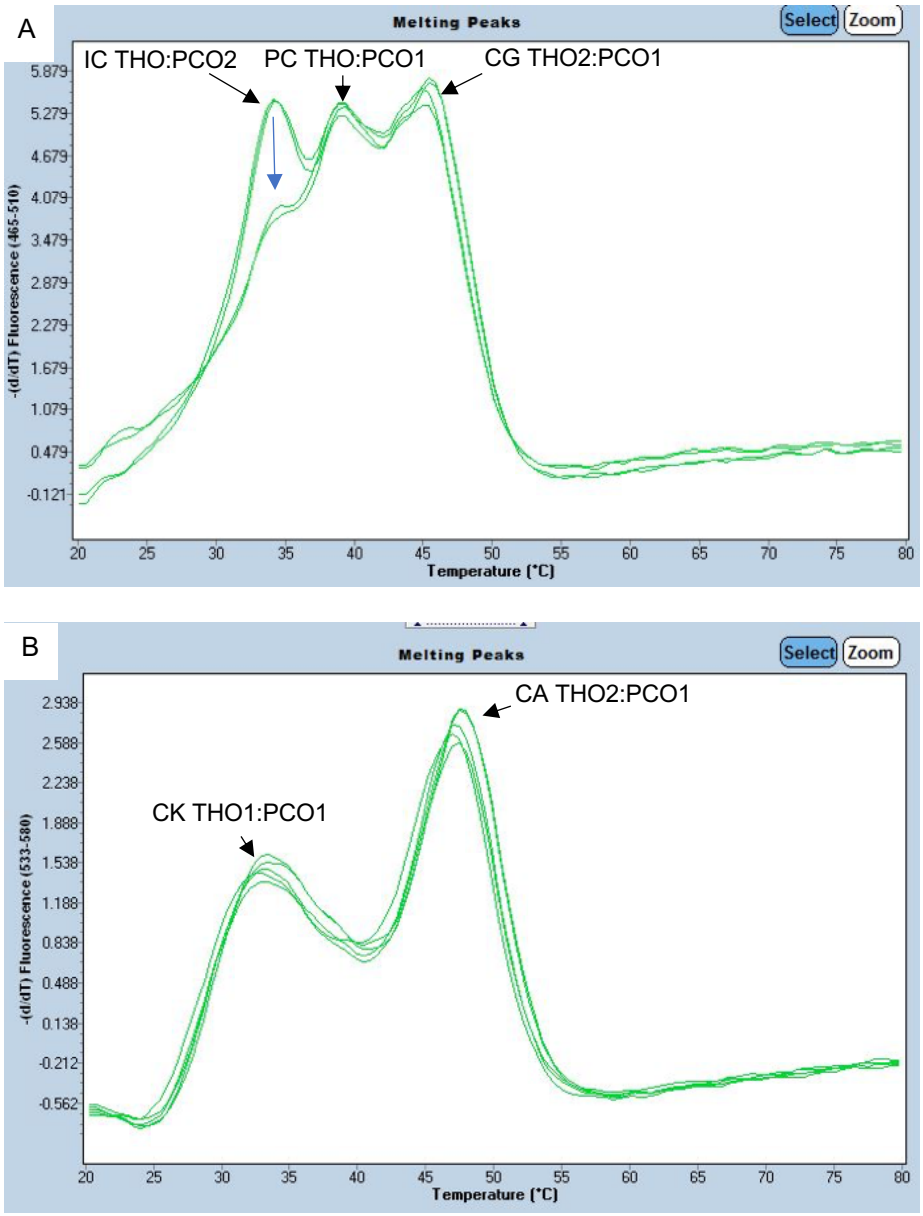

Figure 4. 7 Post-amplification melting curve analysis of the IC. The reaction contained no *Candida* genomic DNA with a specific melting peak reduction (blue arrow) at 34°C compared to NDC reaction. Melting curves analysis in the FAM channel (**Panel A**); internal control (IC) probe hybrid of THO and PCO2, pan-*Candida* (PC) probe hybrid of THO and PCO1 and *C. glabrata*-specific (CG) probe hybrid of THO2 and PCO1. Melting curves analysis in the HEX channel (**Panel B**); *C. krusei*-specific (CK) probe hybrid of THO1 and PCO1 and *C. auris*-specific (CA) probe hybrid of THO2 and PCO1. The qPCR was performed in triplicate.

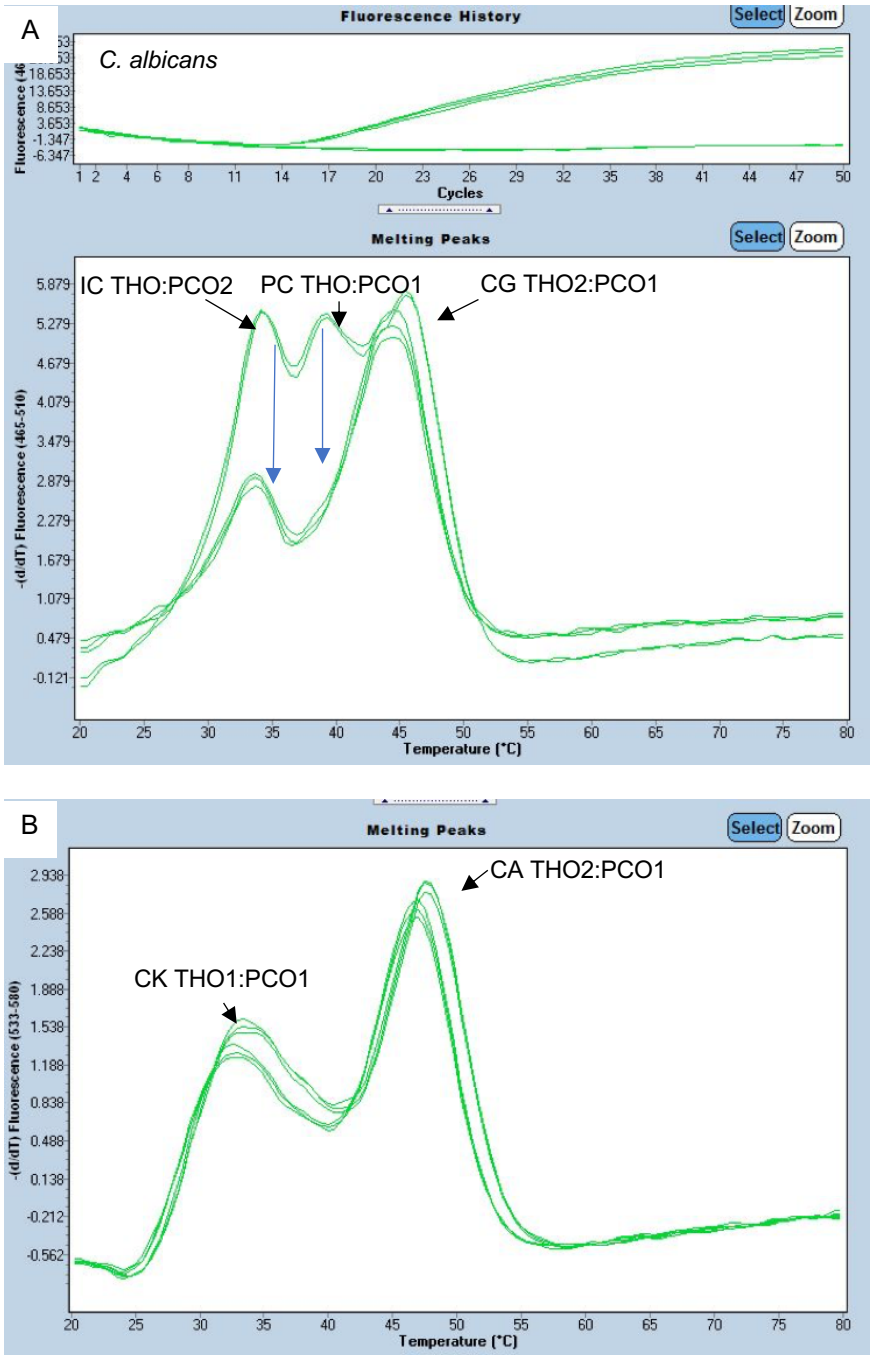

Figure 4. 8 Amplification and melting curve analysis of the IC and *C. albicans* DNA. The reaction showed two melting peaks reduction (blue arrows) at 34°C and 40°C compared to NDC profile. Melting curves analysis in the FAM channel (**Panel A**); internal control (IC) probe hybrid of THO and PCO2, pan-*Candida* (PC) probe hybrid of THO and PCO1 and *C. glabrata*-specific (CG) probe hybrid of THO2 and PCO1. Melting curves analysis in the HEX channel (**Panel B**); *C. krusei*-specific (CK) probe hybrid of THO1 and PCO1 and *C. auris*-specific (CA) probe hybrid of THO2 and PCO1. The qPCR was performed in triplicate.

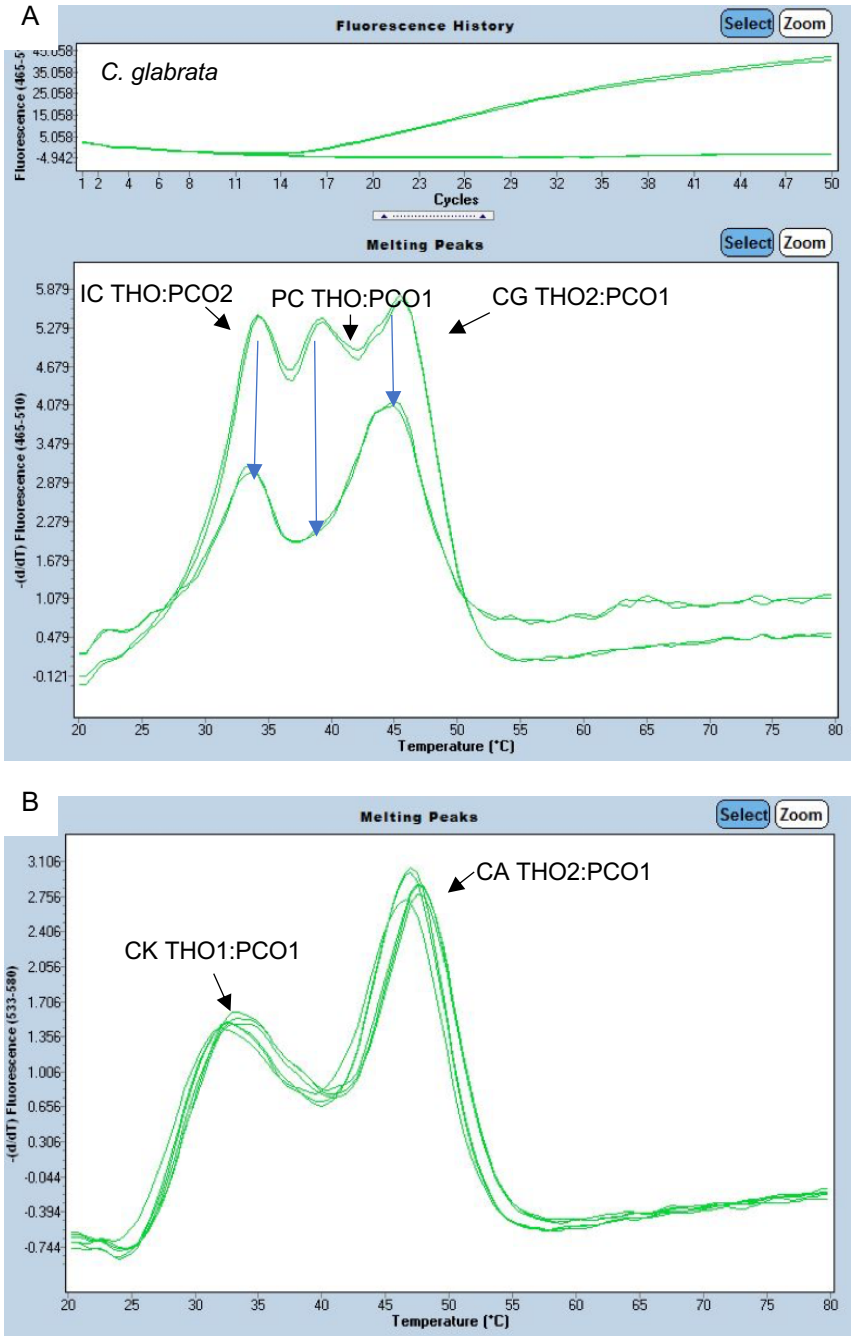

Figure 4. 9 Amplification and melting curve analysis of the IC and *C. glabrata* DNA. The reaction showed three melting peaks reduction (blue arrows) at 34°C, 40°C and 46°C compared to NDC profile. **Panel A**, melting curves analysis in the FAM channel; internal control (IC) probe hybrid of THO and PCO2, pan-*Candida* (PC) probe hybrid of THO and PCO1 and *C. glabrata*-specific (CG) probe hybrid of THO2 and PCO1. **Panel B**, melting curves analysis in the HEX channel; *C. krusei*-specific (CK) probe hybrid of THO1 and PCO1 and *C. auris*-specific (CA) probe hybrid of THO2 and PCO1. The qPCR was performed in triplicate.

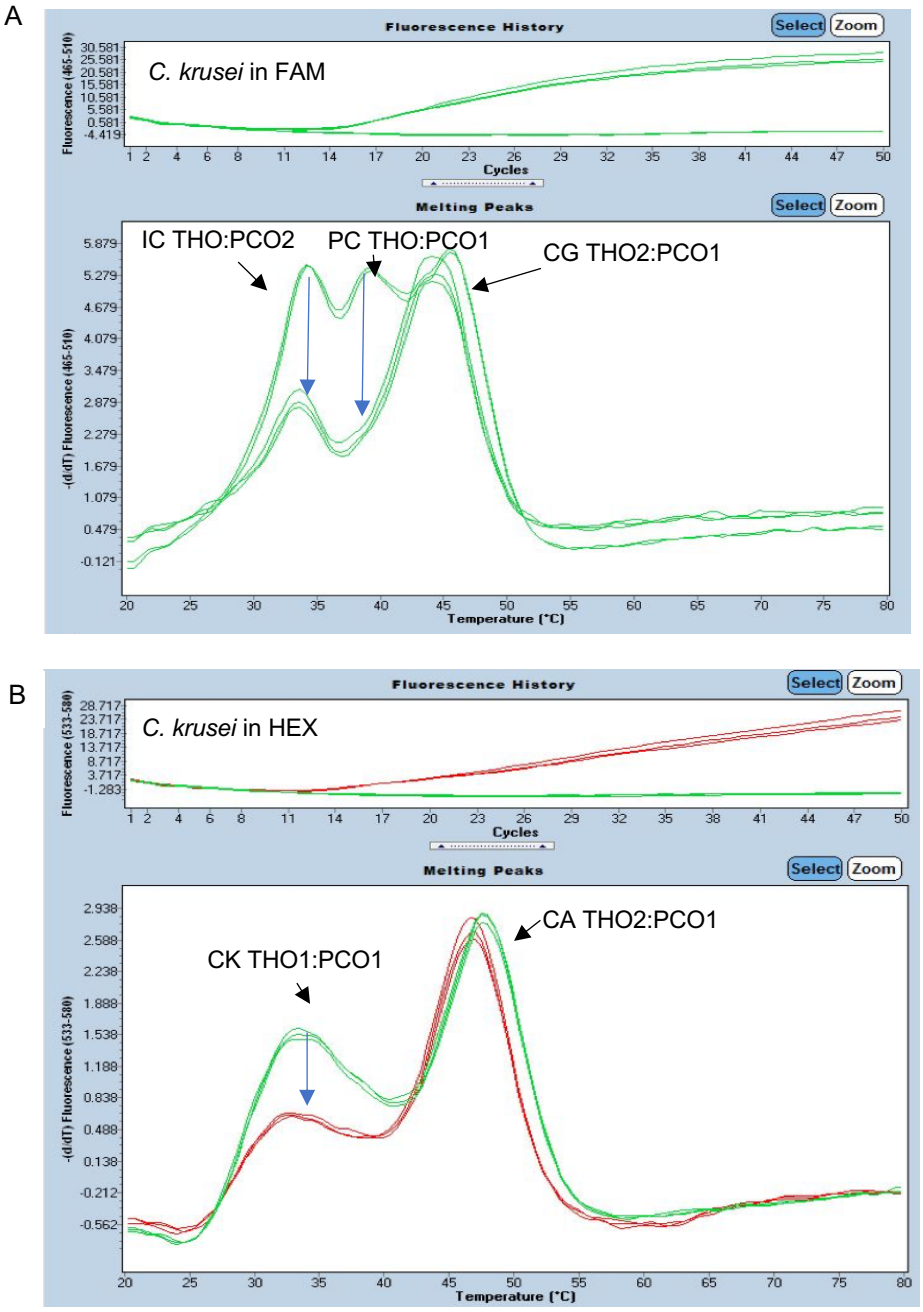

Figure 4. 10 Amplification and melting curve analysis of the IC and *C. krusei* DNA. The reaction showed three melting peaks reduction (blue arrows) across two channels; at 34°C (IC) and 40°C (PC) in the FAM detection channel and 35°C (CA) in the HEX detection channel compared to their NDC profile. **Panel A**, melting curves analysis in the FAM channel; IC probe hybrid of THO and PCO2, pan-*Candida* (PC) probe hybrid of THO and PCO1 and *C. glabrata*-specific (CG) probe hybrid of THO2 and PCO1. **Panel B**, melting curves analysis in the HEX channel; *C. krusei*-specific (CK) probe hybrid of THO1 and PCO1 and *C. auris*-specific (CA) probe hybrid of THO2 and PCO1. The qPCR was performed in triplicate.

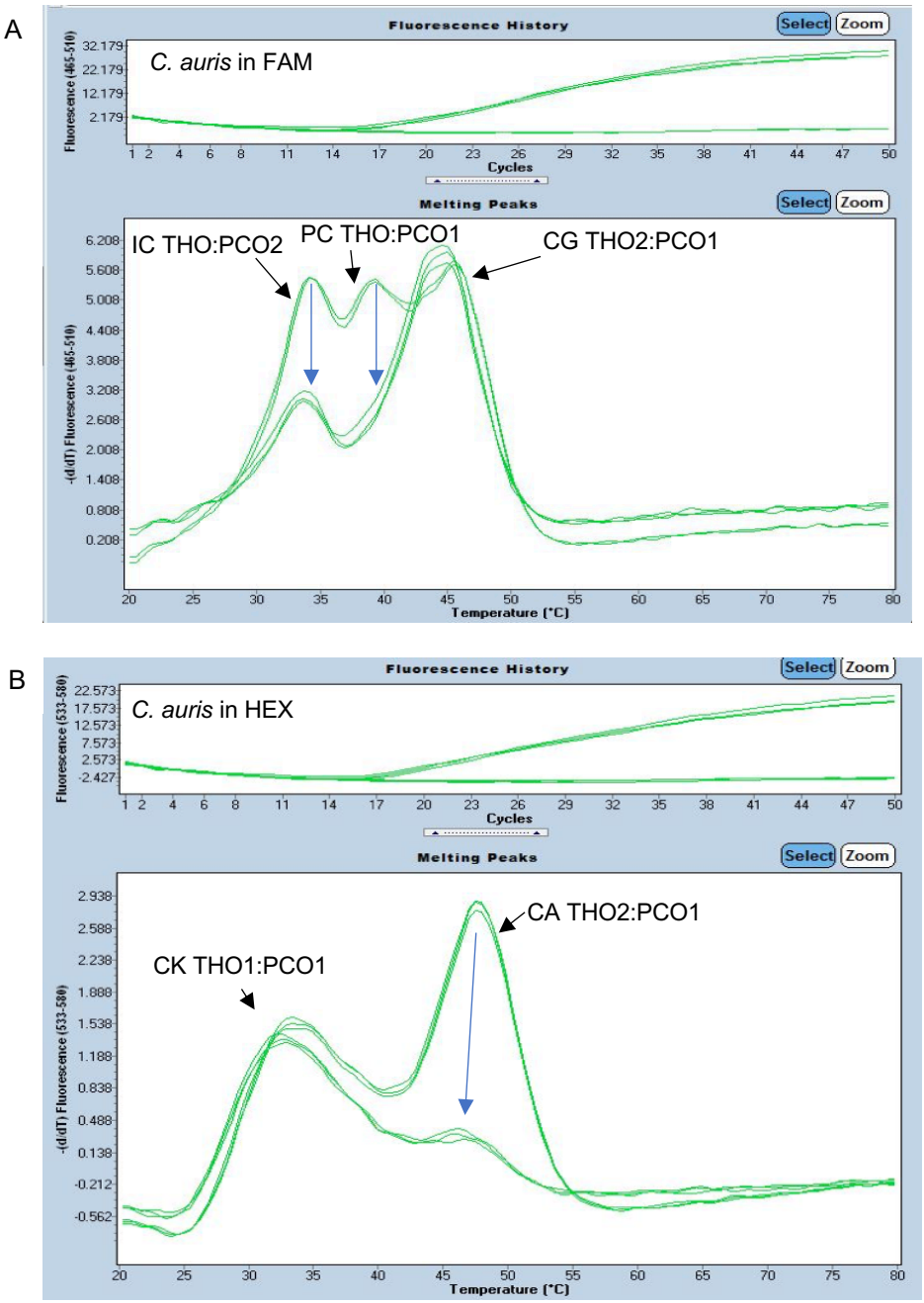

Figure 4. 11 Amplification and melting curve analysis of the IC and *C. auris* DNA. The reaction showed three melting peaks reduction (blue arrows) across two channels; at 34°C (IC) and 40°C (PC) in the FAM detection channel and 48°C (CA) in the HEX detection channel compared to their NDC profile. **Panel A**, melting curves analysis in the FAM channel; IC probe hybrid of THO and PCO2, pan-*Candida* (PC) probe hybrid of THO and PCO1 and *C. glabrata*-specific (CG) probe hybrid of THO2 and PCO1. **Panel B**, melting curves analysis in the HEX channel; *C. krusei*-specific (CK) probe hybrid of THO1 and PCO1 and *C. auris*-specific (CA) probe hybrid of THO2 and PCO1. The qPCR was performed in triplicate.

Table 4. 1 Specificity evaluation of dual-channel MPA-*Candida* assay design 2 for detections of *Candida*, moulds and bacterial species genomic DNA.

Target DNA	C_t value		Melting curve analysis				
			FAM			HEX	
	FAM	HEX	IC	PC	CG	CK	CA
Internal control	ND	ND	+	ND	ND	ND	ND
Candida							
C. albicans	19.30	ND	+	+	ND	ND	ND
C. glabrata	18.80	ND	+	+	+	ND	ND
C. krusei	20.60	19.0	+	+	ND	+	ND
C. auris	18.0	21.0	+	+	ND	ND	+
C. haemulonii	22.0	ND	+	+	ND	ND	ND
C. dubliniensis	20.5	ND	+	+	ND	ND	ND
C. parapsilosis	20.5	ND	+	+	ND	ND	ND
C. tropicalis	19.8	ND	+	+	ND	ND	ND
C. guilliermondii	19.8	ND	+	+	ND	ND	ND
Moulds							

A. fumigatus	28±1	ND	+	ND	ND	ND	ND
A. flavus	28±1	ND	+	ND	ND	ND	ND
P. rubens	28±1	ND	+	ND	ND	ND	ND
M. circinelloides	28±1	ND	+	ND	ND	ND	ND
Bacteria							
S. aureus	28±1	ND	+	ND	ND	ND	ND
S. epidermidis	28±1	ND	+	ND	ND	ND	ND
P. mirabilis	28±1	ND	+	ND	ND	ND	ND
E. coli	28±1	ND	+	ND	ND	ND	ND

***** C_t: Threshold cycle, the cycle intersection with the point where the curve first clearly rises off baseline value; FAM: Detection channel (465 nm/510 nm); HEX: Detection channel (533 nm/580 nm); IC: Internal Control-specific peak (35°C); PC: Pan-*Candida* peak (40°C); CG: *C. glabrata*-specific peak (46°C); CK: *C. krusei*-specific peak (30°C); CA: *C. auris*-specific peak (48°C); +: Positive; ND: Not Detected

4.2.3 Testing the sensitivity of detection

The melting curves analysis for the detection of five tenfold dilutions genomic DNA were tested for *C. albicans* and *C. glabrata*, *C. krusei* and *C. auris*. The signal with a significant reduction of melting peaks 40°C of pan-*Candida* (PC) generally limited up to 10^4 copies of genomic DNA per reaction in all four *Candida* species tested (Figures 4.12 and 4.13; FAM channel). Furthermore, the melting peaks 45°C of *C. glabrata*-specific (CG) shown reduced peak against the NDC only in the reaction with the highest concentration of *C. glabrata* genomic DNA (Figure 4.12, panel B). Meanwhile, the sensitivity of detections of *C. krusei* and *C. auris* were analysed across two channels of detection, FAM and HEX. *C. krusei*-specific melting peaks (CK) (Figure 4.13, panel A) showed proportionate reduction of the peaks in the HEX channel against the NDC from 10^5 to 10^1 copies genomic DNA. *C. auris*-specific melting peak (CA) (Figure 4.13, panel B) showed the assay sensitivity limited to 10^4 copies of *C. auris* genomic DNA.

In addition, the IC melting peak was also showed a significant reduction of the peak compared to its NDC at 34°C in every reaction. Nevertheless, the IC melting peaks in reaction with 10^5 or 10^4 copies of *Candida* species DNA has a greater reduced height compared to the melting peaks for the reaction with lower concentrations of *Candida* genomic DNA (from 10^3 to 10^1 copies) (Figures 4.12 and 4.13), despite of every reaction containing the same number of copies (10^5 copies) of the IC plasmid DNA. As the assay demonstrated poor sensitivity, the objective to include the pan-fungal probe into the reaction was suspended.

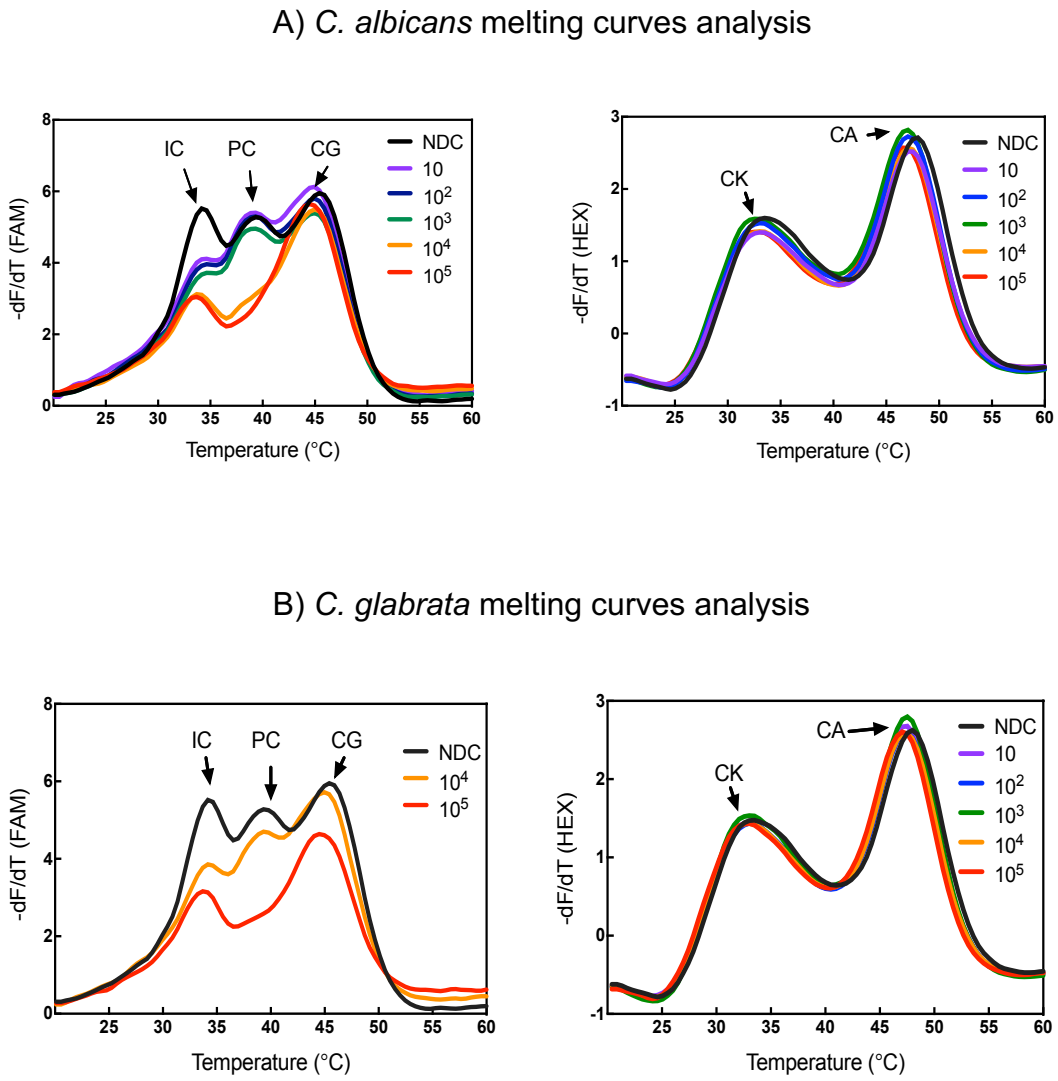

Figure 4. 12 Post-amplification melting curves analysis of the assay's sensitivity for detection of the *C. albicans and C. glabrata*. The reaction containing a range of serially diluted *C. albicans* (**Panel A**) and *C. glabrata* (**Panel B**) genomic DNAs in the present of IC plasmid DNA. The FAM channel melting curve consists of MPA probes of IC, pan-*Candida* (PC) and *C. glabrata*-specific (CG). The HEX channel melting curve consists of MPA probes for *C. krusei*-specific (CK) and *C. auris*-specific (CA). Each analysis was performed in three replicates and averaged.

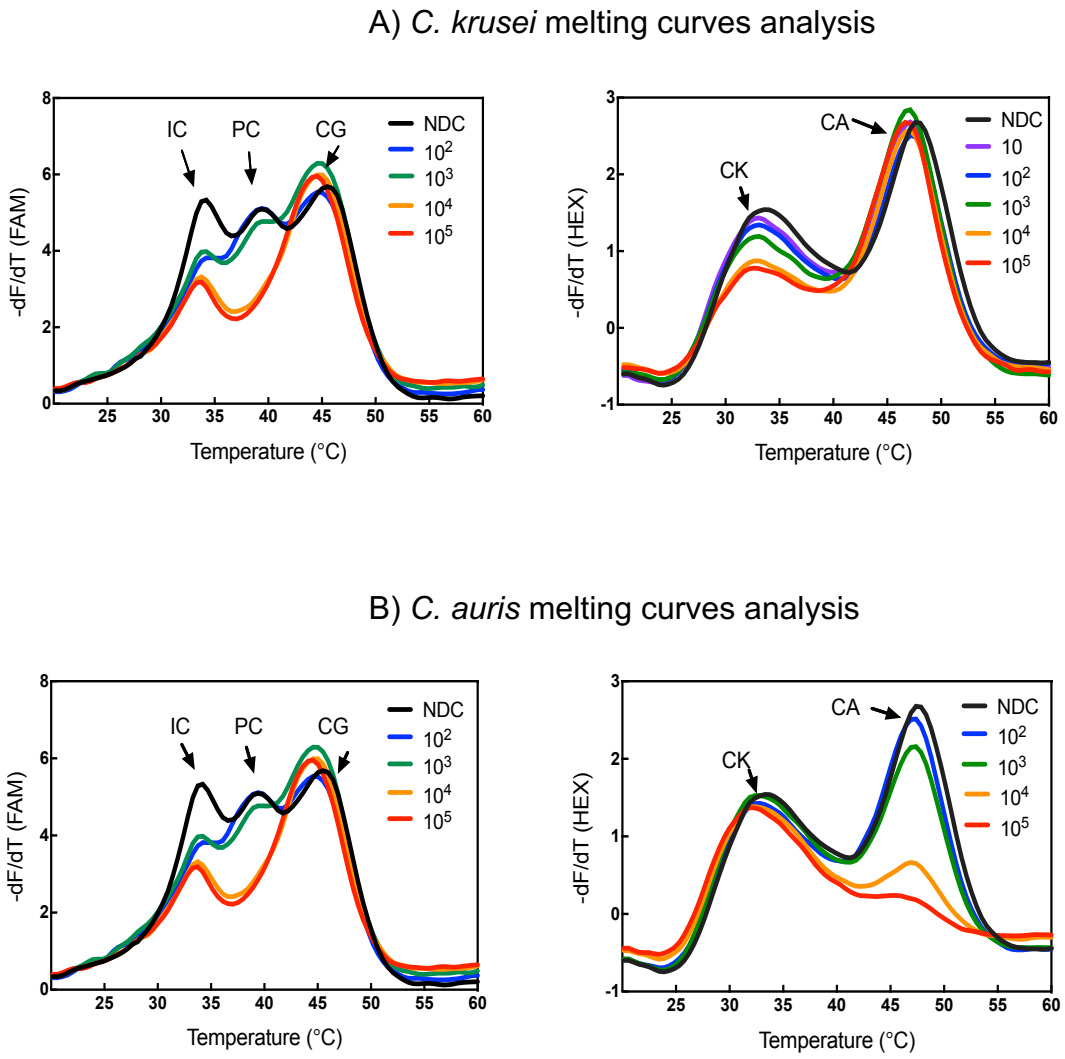

Figure 4. 13 Post-amplification melting curves analysis of the assay's sensitivity for detection of the *C. krusei and C. auris*. The reaction containing a range of serially diluted *C. krusei* (**Panel A**) and *C. auris* (**Panel B**) genomic DNAs in the present of IC plasmid DNA. The FAM channel melting curve consists of MPA probes of internal control (IC), pan-*Candida* (PC) and *C. glabrata*-specific (CG). The HEX channel melting curve consists of MPA probes for *C. krusei*-specific (CK) and *C. auris*-specific (CA). Each analysis was performed in three replicates and averaged.

4.2.4 Assay design 3: optimisation of the MPA-*Candida* melting curve and *Taq*Man internal control probe in a single reaction

Initial optimisations of the assay design 3 involved probes targeting *Candida* species with an inclusion of pan-fungal probe in a single reaction mixture. Initial experiments were performed with no IC probe in the reaction to avoid unspecific melting curves between the pan-fungal and IC probes. The pan-fungal target probe (PF THO2:PCO2) has a melt peak at 37°C (Figure 4.14, panel B). Therefore, the pan-fungal and IC probes melting temperatures differ by 3°C to 4°C.

The assay design 3 was tested for post-amplification analysis; however, the melting curves profile were unable to be reproduced (Figure 4.15). No melting peak of the pan-fungal probe from the PF THO:PCO hybrid and only *C. auris*-specific melting peak at 48°C in the HEX channel was detected (Figure 4.15; panel B, i). The reaction mixtures contained two sets of primers for the pan-fungal (ITS3-F & LR1-R) and pan-*Candida* (LR0-F & GSCand-R) which contributed to the non-specific hydrolysis of the pan-fungal THO during the PCR steps. Furthermore, the reaction was analysed for its amplification curves and recorded continuous increased of fluorescence signal over the PCR cycles that was unexpected in the negative control reaction (Figure 4.15; panel B, ii).

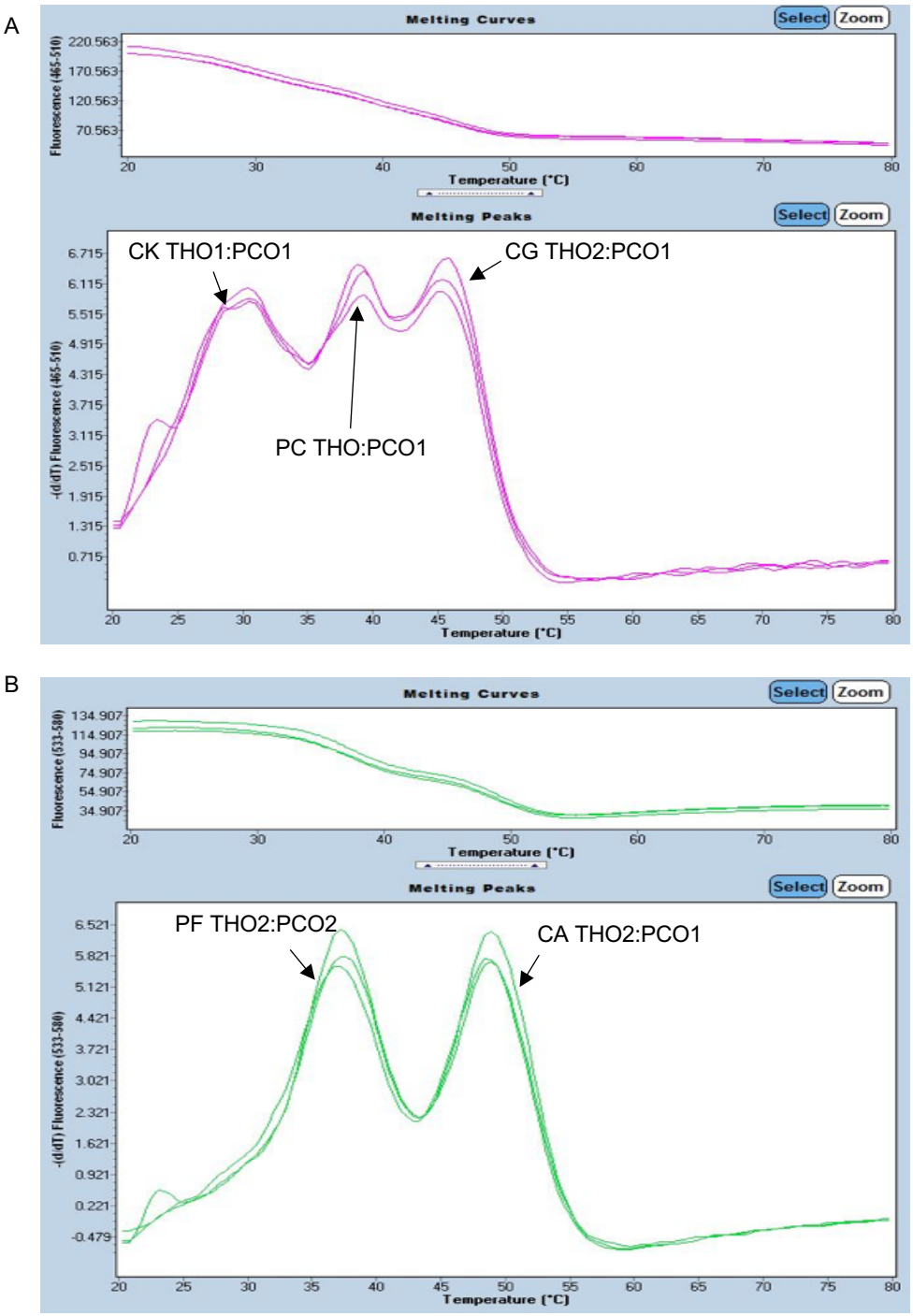

Figure 4. 14 The melt curve analysis of five MPA probes in a single reaction with dual-channel fluorescence detection. Melt curve analysis was performed independently without the amplification steps and PCR primer in the reaction. Melting peaks in the FAM channel read at 29.85°C for *C. krusei*-specific (CK), 39.29°C for pan-*Candida* (PC), 46.02°C for *C. glabrata*-specific (CG) (**Panel A**); in the HEX channel melting peaks read at 37.24°C for pan-fungal (PF) and 48.87°C for *C. auris*-specific (CA) (**Panel B**). Experiment was analysed in triplicate.

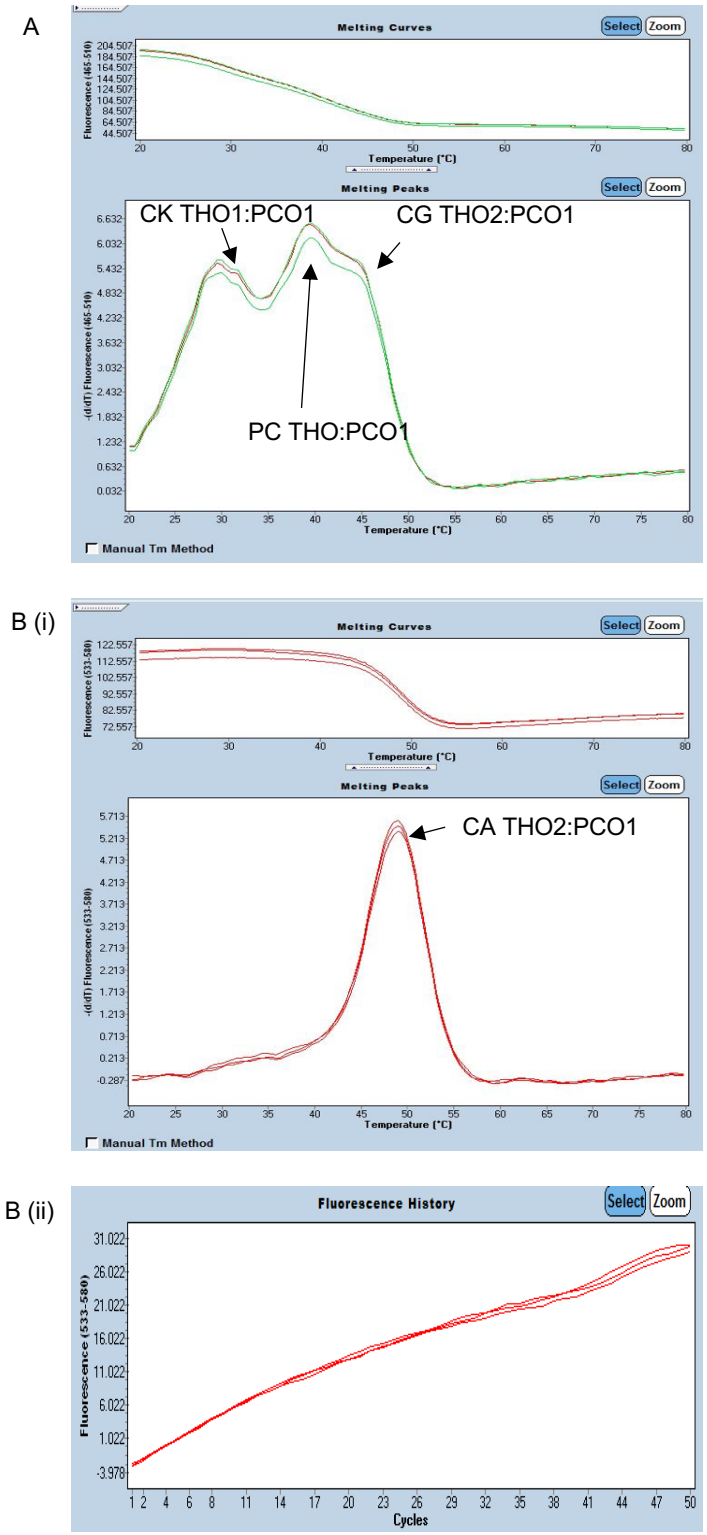

Figure 4. 15 The post-amplification melting curve analysis of the assay design 3. Panel A) Melting peaks for *C. krusei*-specific (CK), pan-*Candida* (PC); *C. glabrata*-specific (CG) in FAM channel. **Panel B, i**) Only one melting peak was detected for the *C. auris*-specific probe (CA) in the HEX channel, and the missing of a pan-fungal melting peak in the reaction is a result of the cross-reactivity between the probe and

PCR primer sets. **Panel B, ii**) An increased fluorescence signal was detected in the HEX channel. The reaction contained two primer sets. The experiment was analysed in triplicate.

Consequently, the reaction was performed only with a single set of primer, ITS3-F forward primer and GSCand-R reverse primer. The expected melting curves profile was generated from the negative control reaction (Figure 4.16). An optimised assay was tested for amplification and detection of DNA biomarkers for its specificity and sensitivity of detections. The filamentous fungi and *Candida* species genomic DNA were targeted from ITS3 to the GSCand primers binding sites eliminating the need for primer LR0 and primer LR1 in the reaction. The results of the amplification and qualitative melting curve analysis were described in Section 4.2.5.

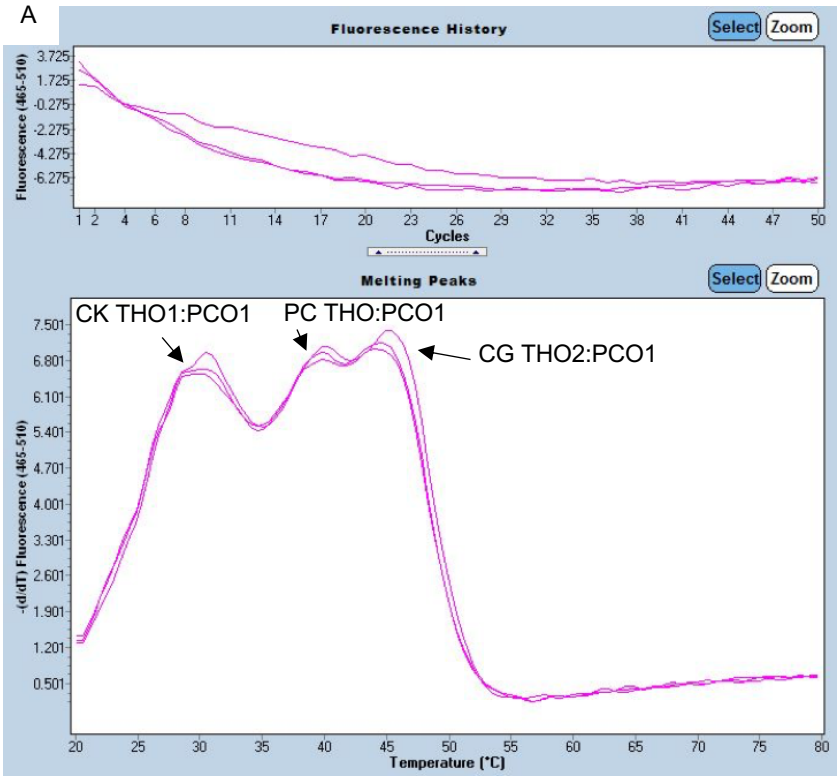

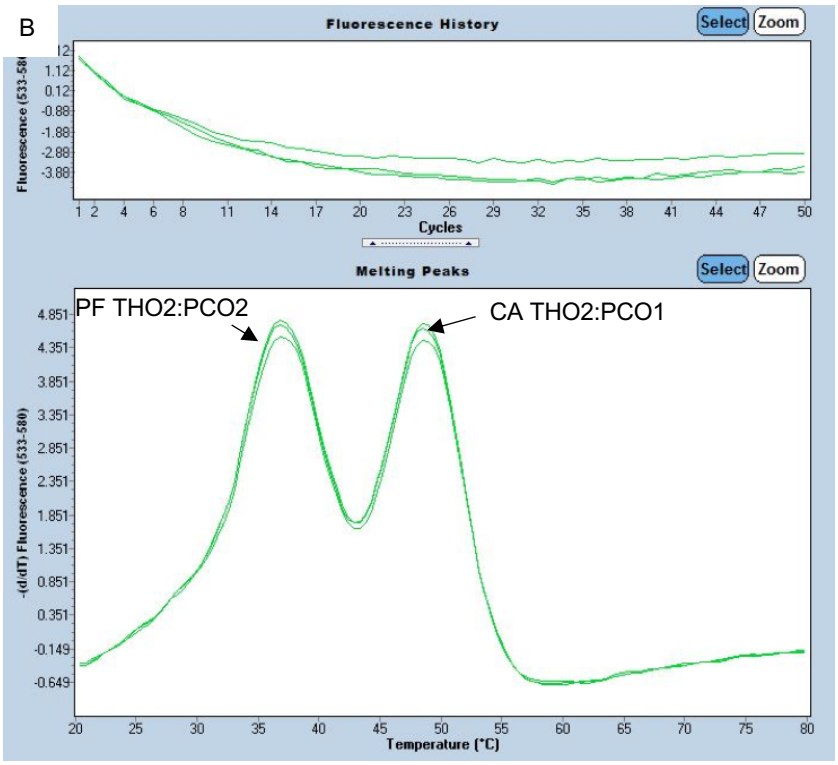

Figure 4. 16 The post-amplification melting profiles for assay design 3 in a reaction contained a single primer set. CK: *C. krusei*-specific; PC: pan-*Candida*; CG: *C. glabrata*-specific; PF: pan-fungal; CA: *C. auris*-specific. The test was performed in triplicate.

The MPA-*Candida* assay design 3 was also engineered to accommodate up to four probes per detection channel. The real-time PCR LightCycler 480 instrument principally can detect six melting peaks in a single channel of detection. The assembly of four THO:PCO probes of *C. krusei*-specific (CK THO1:PCO1), IC (IC THO:PCO2), pan-*Candida* (PC THO:PCO1) and *C. glabrata*-specific (CG THO2:PCO1) in a single reaction has successfully demonstrated four melting peaks in the FAM detection channel (Figure 4.17). The melting temperature of each probe has consistently demonstrated in the multiplex reaction as in simplex reaction. *C. krusei*-specific probe concentration was increased by 0.1 µM to the final concentration 0.5 µM of THO probe for a sharp melt peak in the reaction (Figure 4.18). An optimised

concentration for the FAM-labelled probes for the characterised melt curve profile was not reproducible with an inclusion of the HEX-labelled probes. The pan-fungal (PF THO2:PCO2) and *C. auris*-specific (CA THO2:PCO1) probes detected in the HEX channel had ablated the *C. krusei*-specific peak of 30°C in the FAM channel (Figure 4.19). Optimisation steps were performed with *C. krusei*-specific probe final concentration tested at 0.5 µM (Figure 4.20), and in a range of 0.4 to 0.8 µM (Figure 4.21) while maintaining the others concentration. The IC probe concentration was also reduced from 0.1 µM (figure 4.22) to 0.08 µM (figure 4.23) maintaining the concentration of the *C. krusei*-specific probe at 0.4 µM.

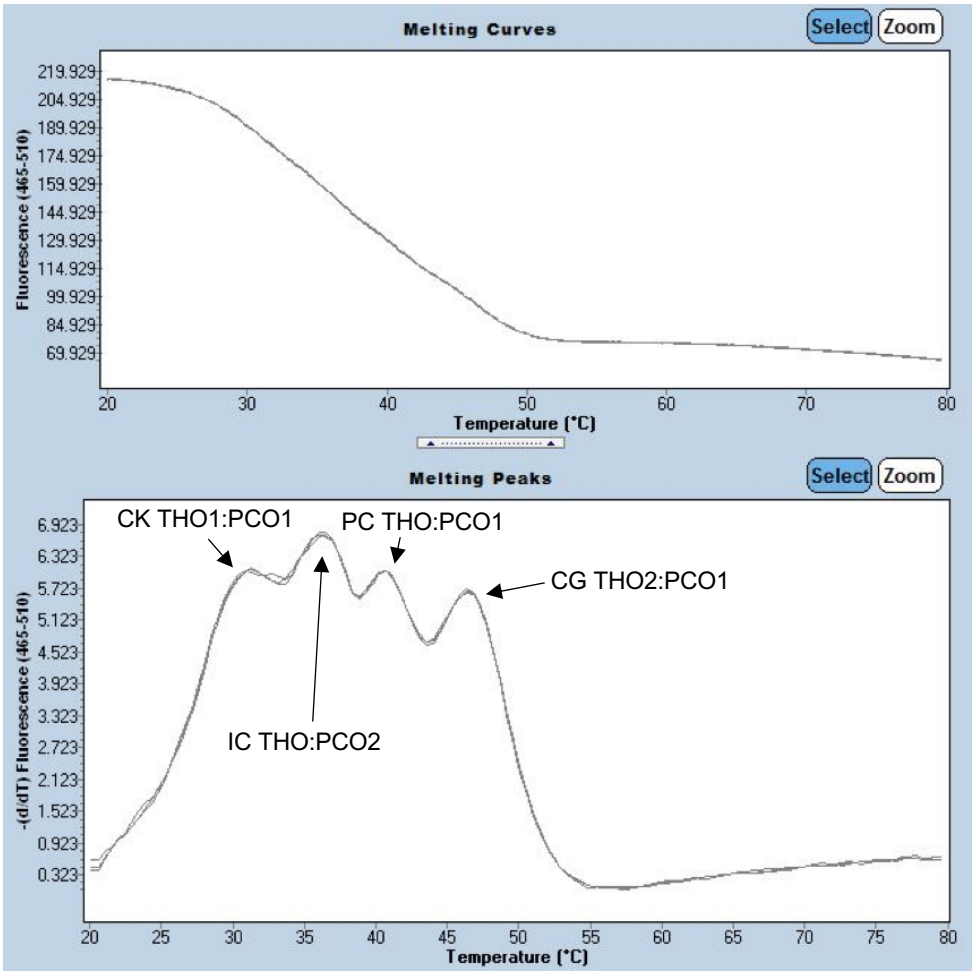

Figure 4. 17 Detection of four probes melting peaks of the negative control reaction. The probes melting peaks detected in the FAM channel for *C. krusei*-specific

(CK), 31°C; internal control-specific (IC), 35°C; pan-*Candida* (PC), 41°C and *C. glabrata*-specific (CG), 46°C. The analysis was performed in triplicate.

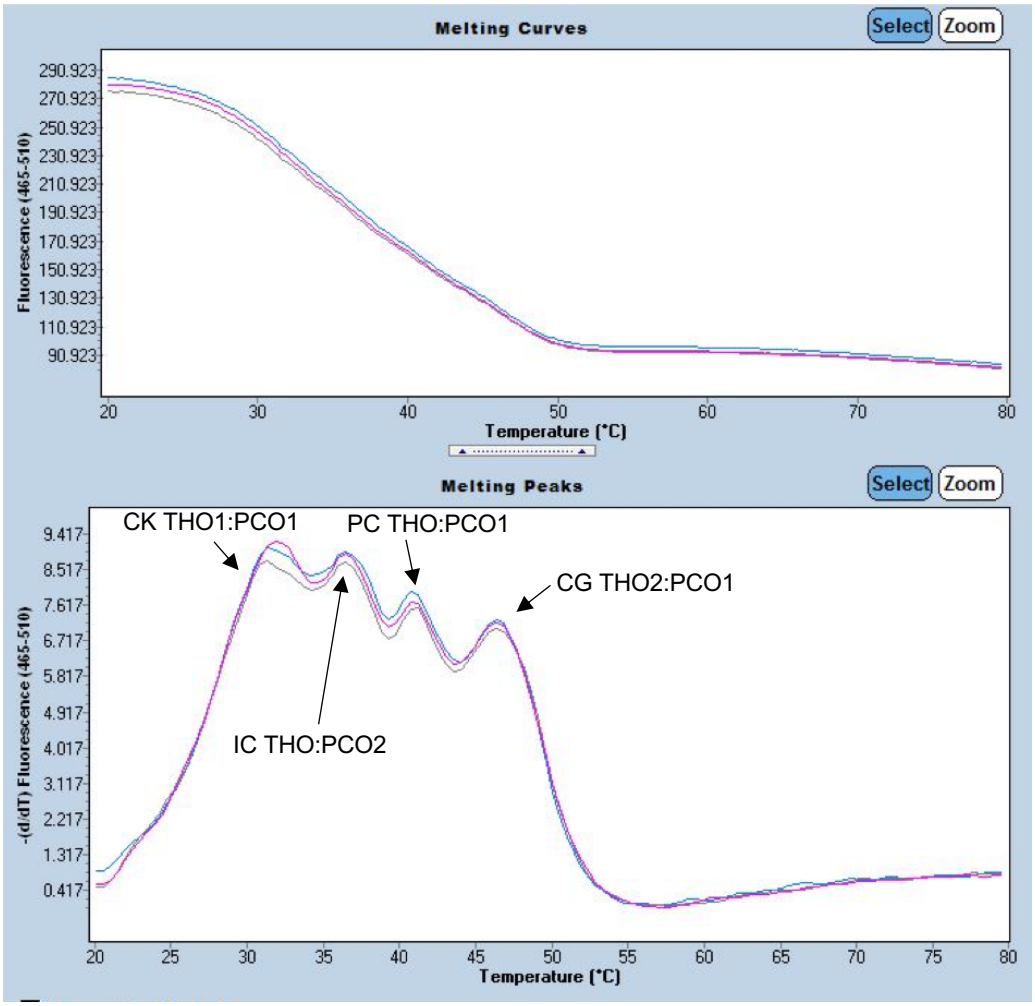

Figure 4. 18 Optimisation of *C. krusei*-specific probe concentration. The concentration was changed from 0.4 to 0.5 µM for an apparent melt peak. *C. krusei*-specific (CK), 31°C; internal control (IC), 35°C; pan-*Candida* (PC), 41°C and; *C. glabrata*-specific (CG), 46°C. The analysis was performed in triplicate.

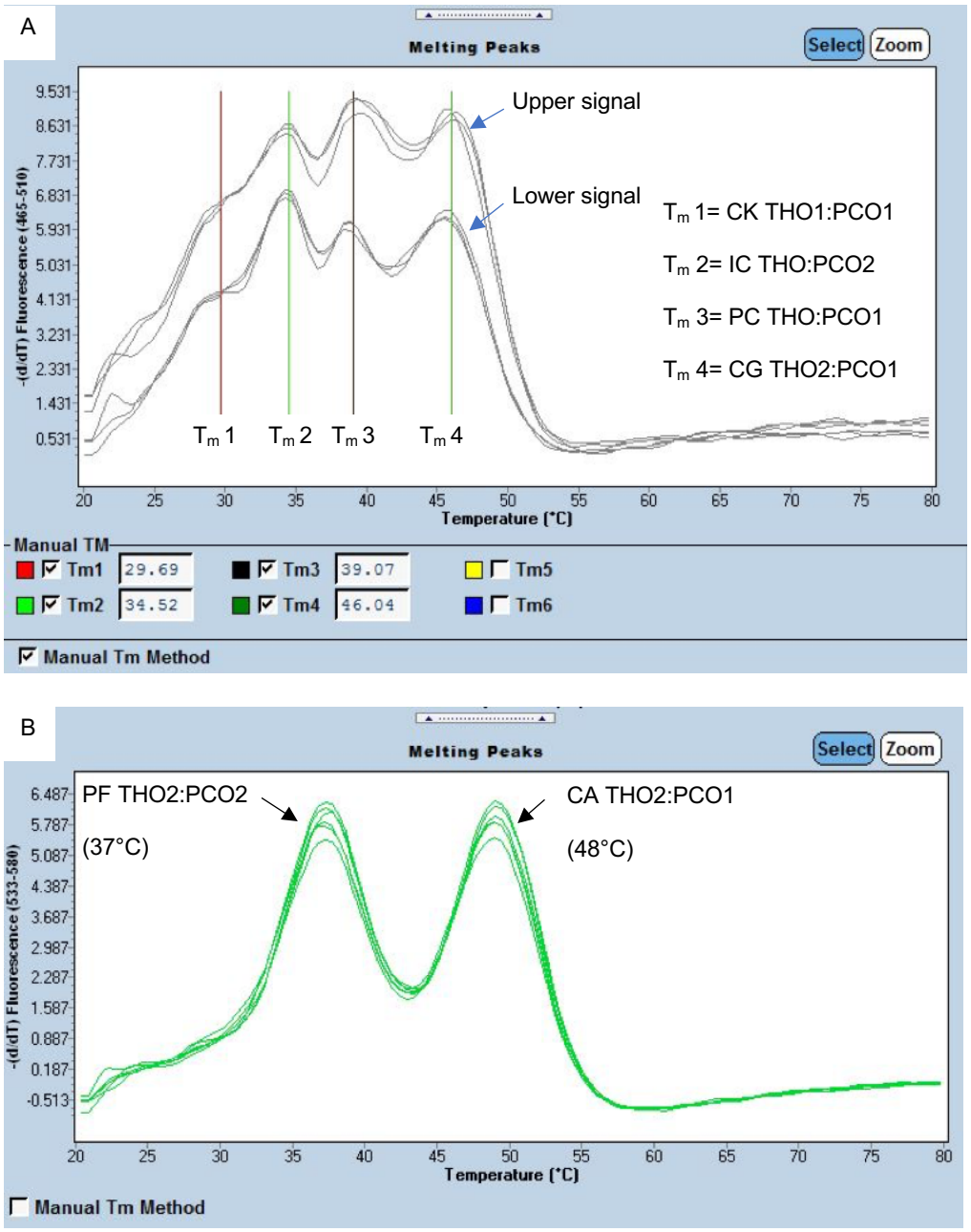

Figure 4. 19 Disappearance of *C. krusei*-specific melting peak in FAM channel. Melting curve analysis of six probes in the negative control reaction in the FAM (**Panel A**) and HEX (**Panel B**) detection channels. Upper and lower sets of peaks in the FAM channel differed by the concentration of the probes used in the reaction. The T_m of the THO and PCO hybrid in the FAM channel is specified in the boxes and in the label for the probes in the HEX detection channel. CK: *C. krusei*-specific; IC: Internal Control; PC: pan-*Candida* CG: *C. glabrata*-specific; PF: pan-fungal; CA: *C. auris*-specific. Each analysis was performed in triplicate.

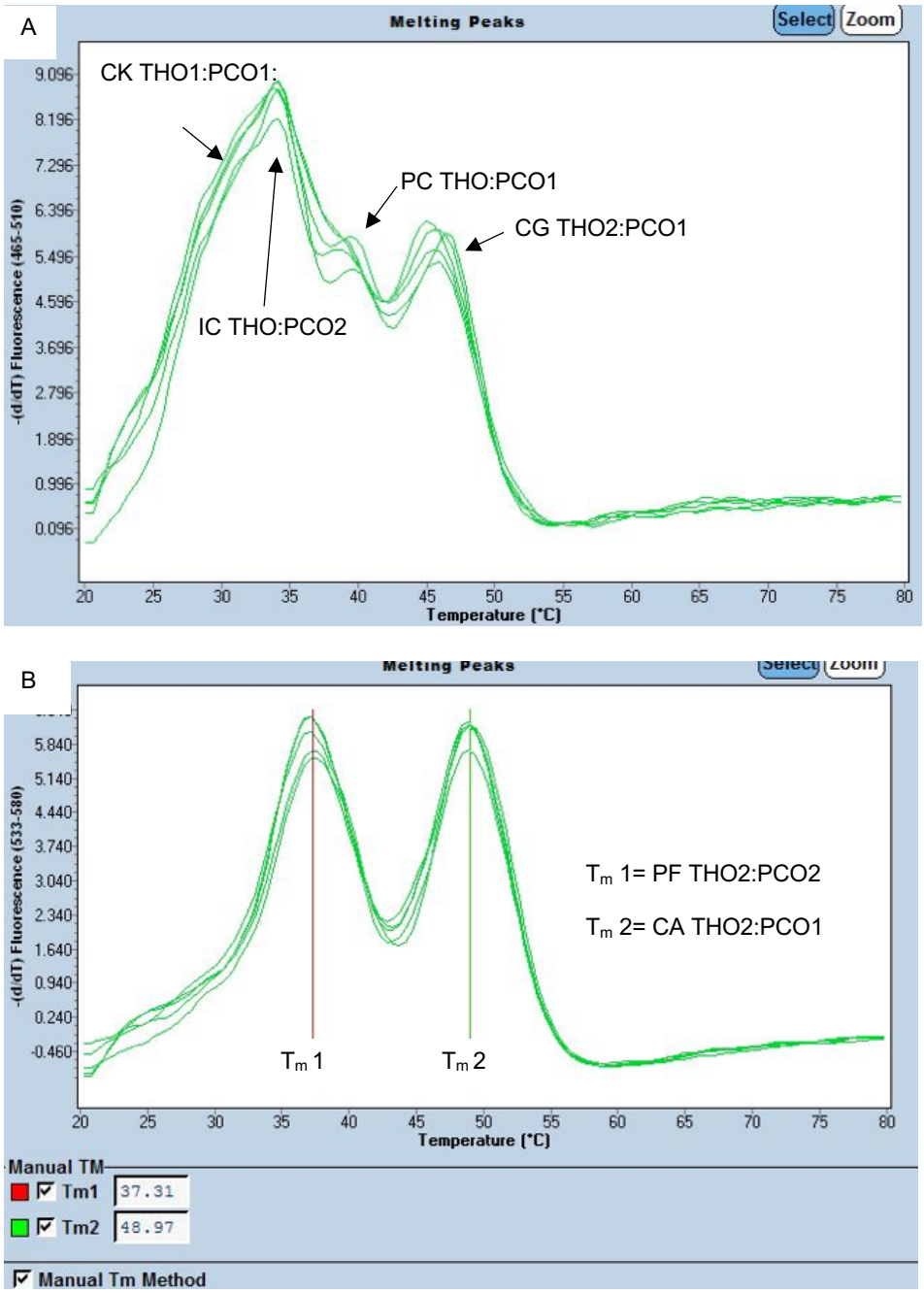

Figure 4. 20 The signal generated with an increased concentration of *C. krusei*-specific probe. No clear *C. krusei*- specific (CK) melting peak can be seen in the FAM channel (**Panel A**). The CK probe concentration was tested at 0.5 µM while other probes were kept at constant concentrations. Internal Control probe (IC), pan-*Candida* probe (PC) and *C. glabrata*-specific probe (CG), pan-fungal probe (PF) and *C. auris*-specific probe (CA). The experiment was performed with six replicates.

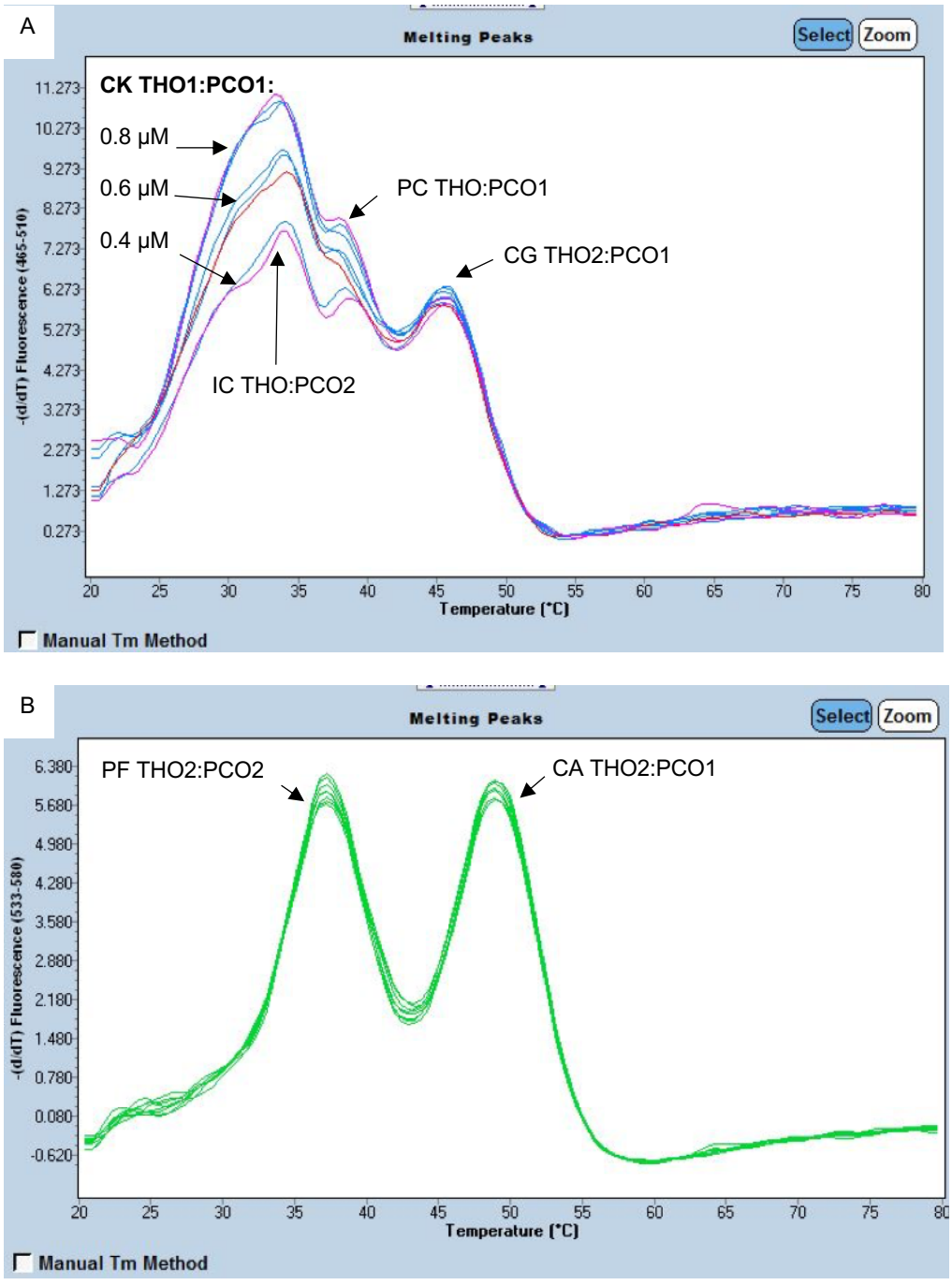

Figure 4. 21 Testing of *C. krusei*-specific probe (CK THO1:PCO1) at different concentrations in a multiplex reaction. Panel A) The reactions contained the CK probe at 0.4 µM, 0.6 µM and 0.8 µM while maintaining the other probes at constant concentration. The Internal Control probe (IC), 0.2 µM; pan-*Candida* probe (PC), 0.2 µM and *C. glabrata*-specific probe (CG), 0.4 µM. **Panel B**) The pan-fungal probe (PF), 0.4 µM; *C. auris*-specific (CA), 0.4 µM. Each reaction was performed in triplicate.

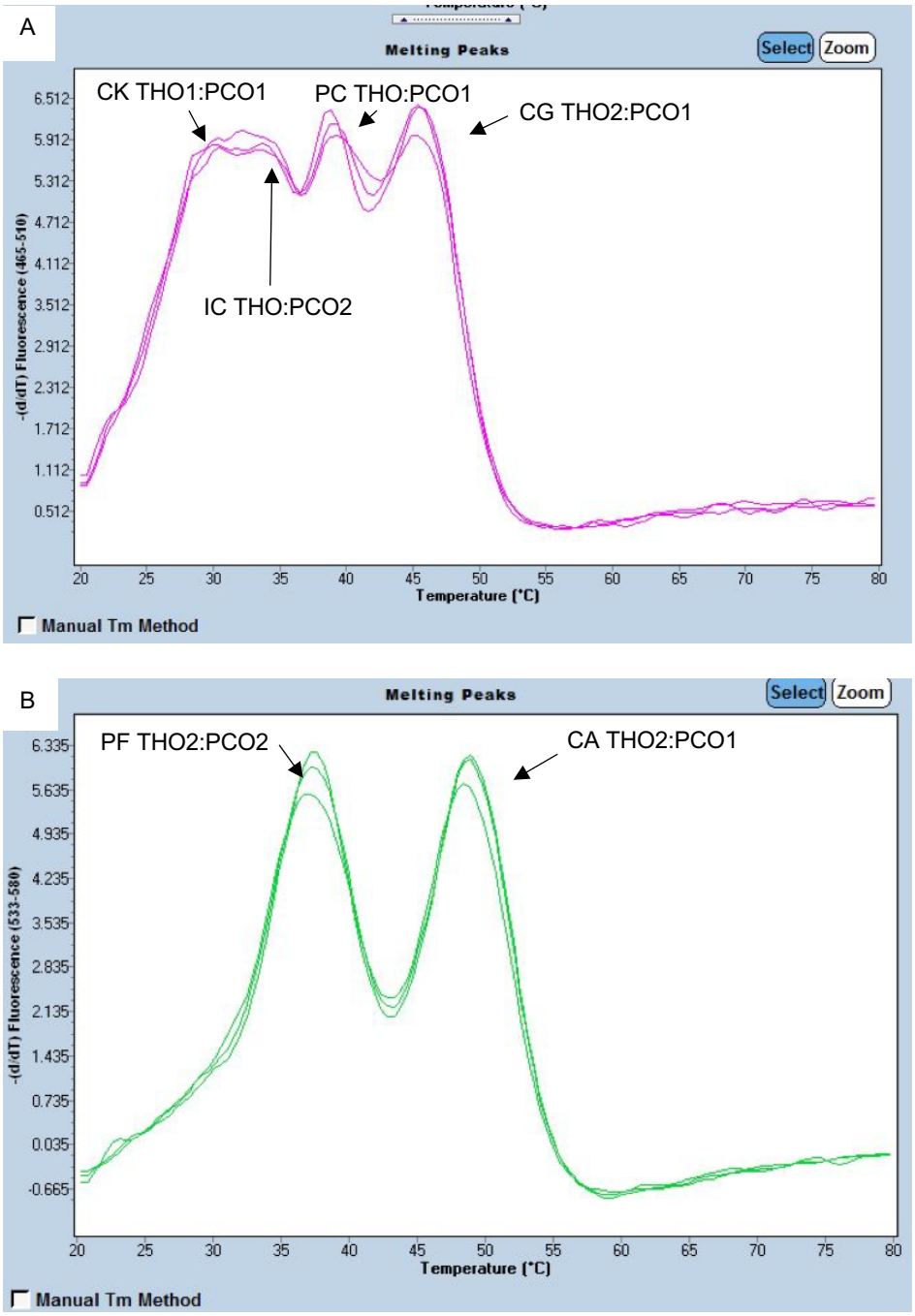

Figure 4. 22 Optimisation of the IC probe concentration for a 4-melting peak in FAM detection channel. IC probe concentration was reduced from 0.2 to 0.1 µM for a visible *C. krusei*-specific (CK) probe melting peak in the FAM channel (**Panel A**). The melting peaks in the FAM channel are the *C. krusei*-specific probe, 0.4 µM; pan-*Candida* (PC), 0.2 µM and *C. glabrata*-specific (CG), 0.4 µM. Melting peaks detected in the HEX channel (**Panel B**) are the pan-fungal probe (PF), 0.4 µM and *C. auris*-specific probe (CA), 0.4 µM. The experiment was performed in triplicate.

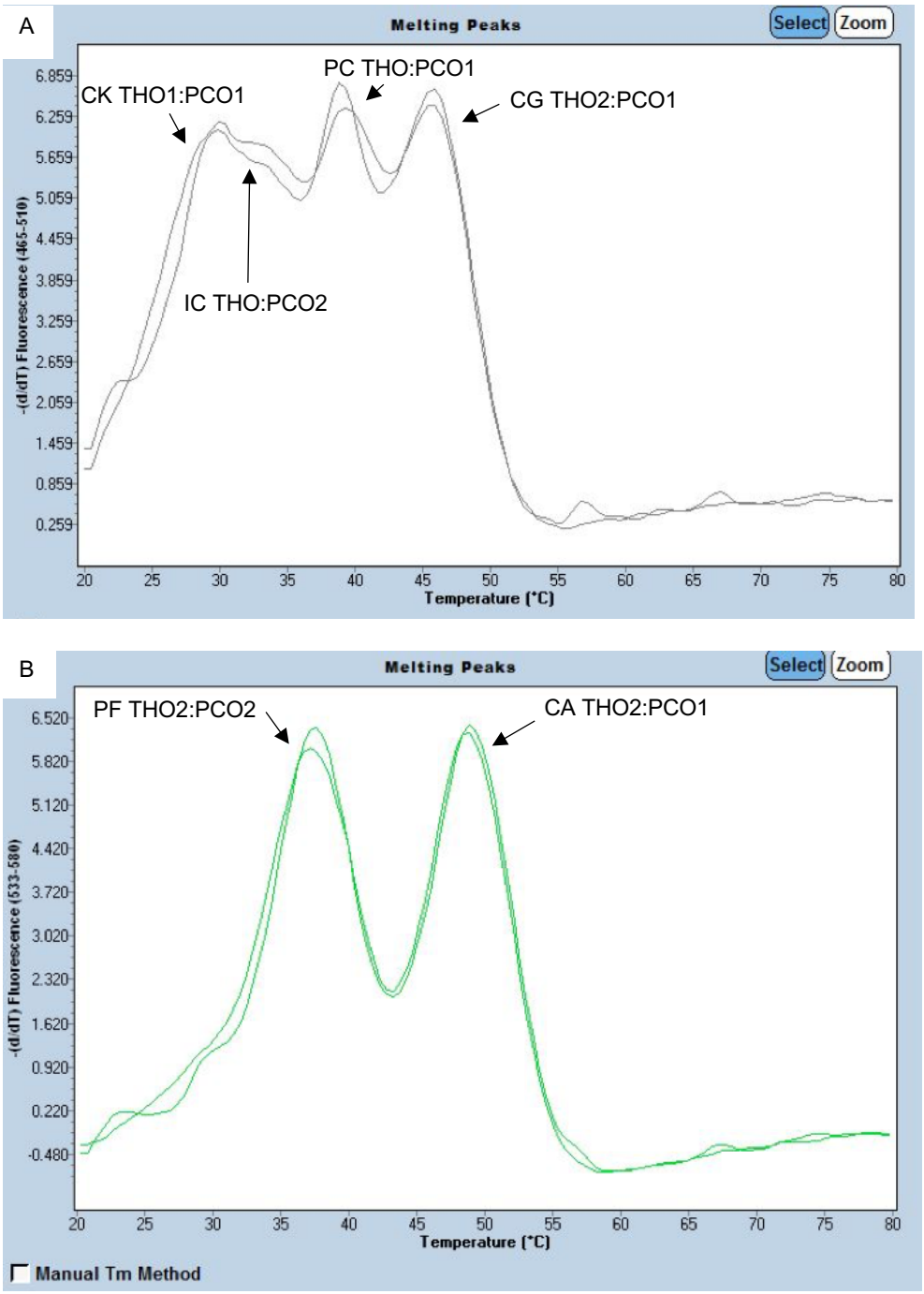

Figure 4. 23 Optimisation of the IC probe concentration. Reduction of an IC probe concentration from 0.2 µM to 0.08 µM for a visible *C. krusei*-specific (CK) probe melting peak in FAM channel (**Panel A**). Melting peaks in the FAM channel are the *C. krusei*-specific probe, 0.4 µM; pan-*Candida* (PC), 0.2 µM and *C. glabrata*-specific (CG), 0.4 µM. Melting peaks detected in the HEX channel (**Panel B**) are for the pan-fungal probe (PF), 0.4 µM and *C. auris*-specific probe (CA), 0.4 µM. The analysis was performed in duplicate.

4.2.5 Testing the specificity of the melting curve analysis

The specificity of the assay design 3 with the pan-fungal probe was determined by the amplification and detection of fungal and *Candida* genomic DNA. The melting curve analysis for *C. albicans*, *C. krusei*, *C. glabrata* and *C. auris* were specifically detected at the three levels of detections from the kingdom, genus and resistant species (Figures 4.24 to 4.27). Within a single target sequence, the different probes were detected and hydrolysed as reflected in the melting curves analysis. The amplification of non-*Candida* species was also tested with *A. fumigatus* and dramatic changes were detected in the pan-fungal melting peak only (Figure 4.28). However, late amplification curves and less significant changes of melting peaks compared to the NDC were observed in the reaction that may erroneously mislead the outcomes. No amplification and detection of the *E. coli* DNA in the reaction exhibits assay specificity (Figure 4.29).

Multiplexing the internal control in every reaction was included with the IC MPA probe THO labelled with Cyanine (Cy5) dye. The IC probe was present to ascertain the functionality of the PCR components in the reaction. The probe amplified the target plasmid DNA included in every tube and detected by the dual-labelled hydrolysis probe in the same manner of TaqMan probe reaction. The detection of *C. krusei* and *C. albicans* genomic DNA at 10^5 copies per reaction with simultaneous detection of IC in the three different detection channels were demonstrated in Figures 4.30 and 4.31. The amplification curve with the C_t value at 29 was determined in FAM and HEX channels of detection. The detection of *C. krusei* genomic DNA was detected by the pan-*Candida* and the *C. krusei*-specific probe. However, the melting peak was observed with less reduction compared to the control (NDC).

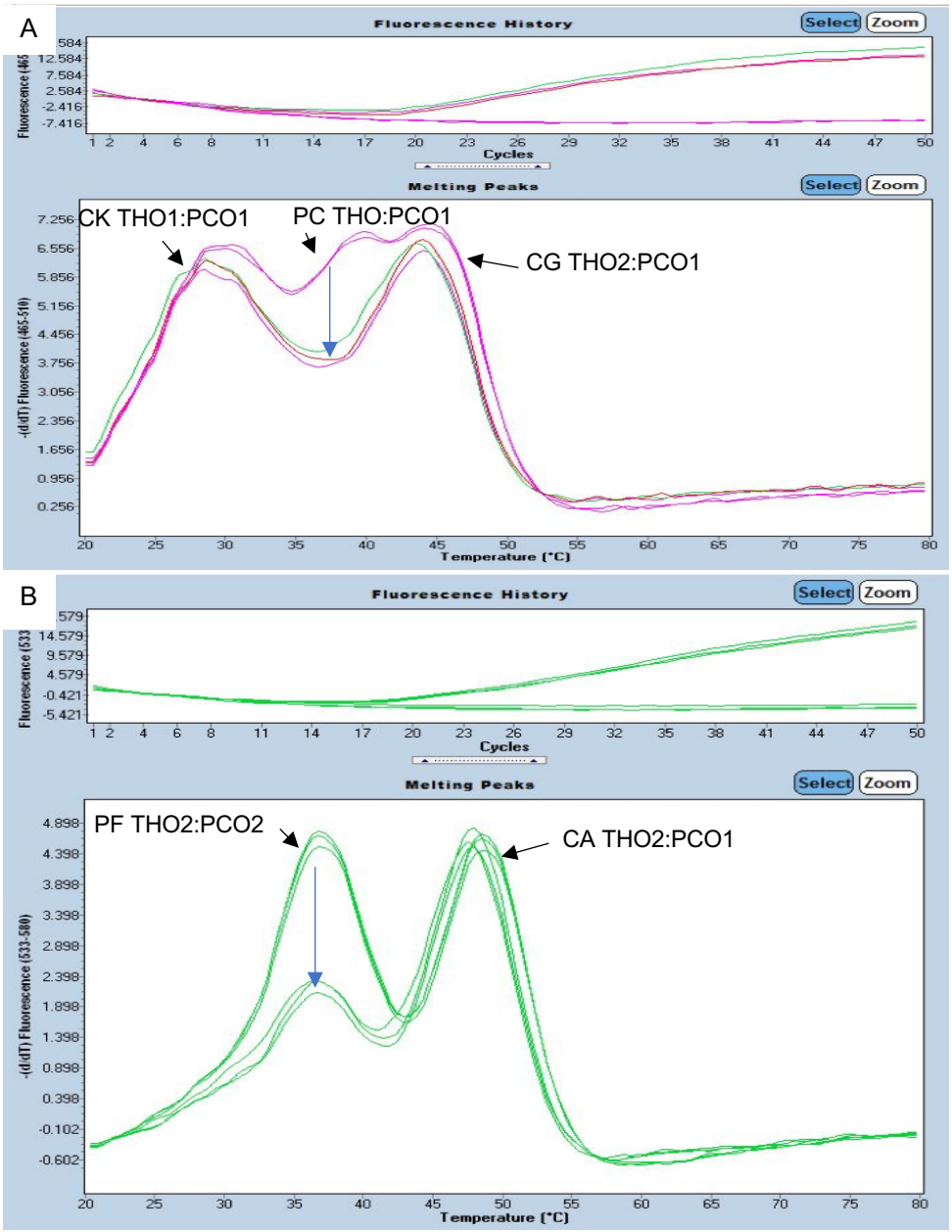

Figure 4. 24 Amplification and melt curves analysis for detection of *C. albicans* genomic DNA in dual-channel assay multiplexed with pan-fungal probe. Two melt peaks reduction (denoted by blue arrows) compared to the control melting profile across FAM and HEX detection channels. **Panel A**) *C. krusei*-specific (CK), pan-*Candida* (PC) *C. glabrata*-specific (CG) probes in the FAM channel. **Panel B**) The pan-fungal (PF) and *C. auris*-specific (CA) probes in the HEX channel. Amplification was performed with primers ITS3 and GSCand. The qPCR was performed in three replicates. The reaction contained no IC.

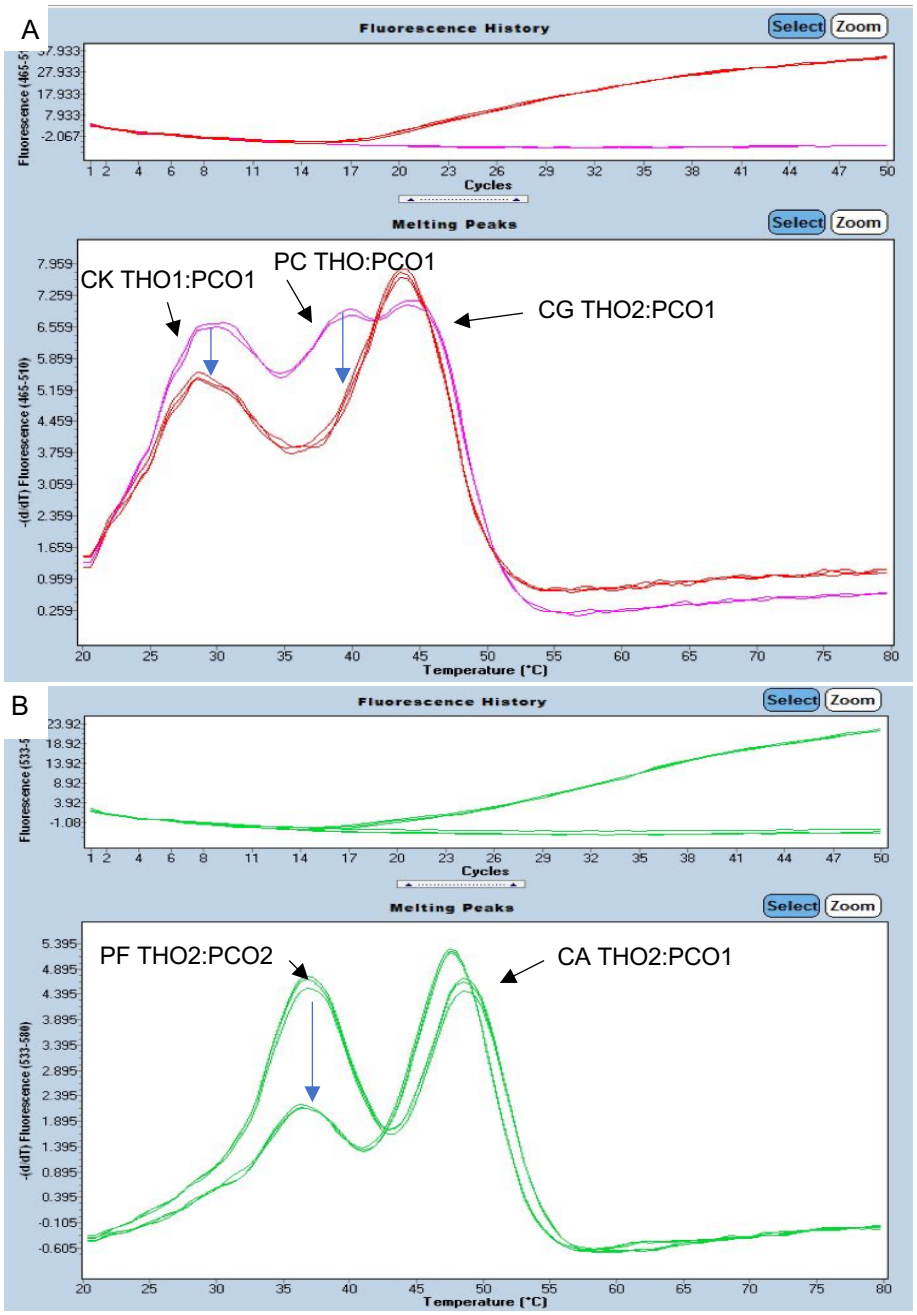

Figure 4. 25 Amplification and melt curves analysis for detection of *C. krusei* genomic DNA in dual-channel assay multiplexed with pan-fungal probe. Three melt peaks reduction (denoted by blue arrows) compared to the control melting profile across FAM and HEX detection channels. **Panel A**) *C. krusei*-specific (CK), pan-*Candida* (PC) *C. glabrata*-specific (CG) probes in the FAM channel. **Panel B**) pan-fungal (PF) and *C. auris*-specific (CA) probes in the HEX channel. Amplification was performed with primers ITS3 and GSCand. The qPCR was performed in three replicates. The reaction contained no IC.

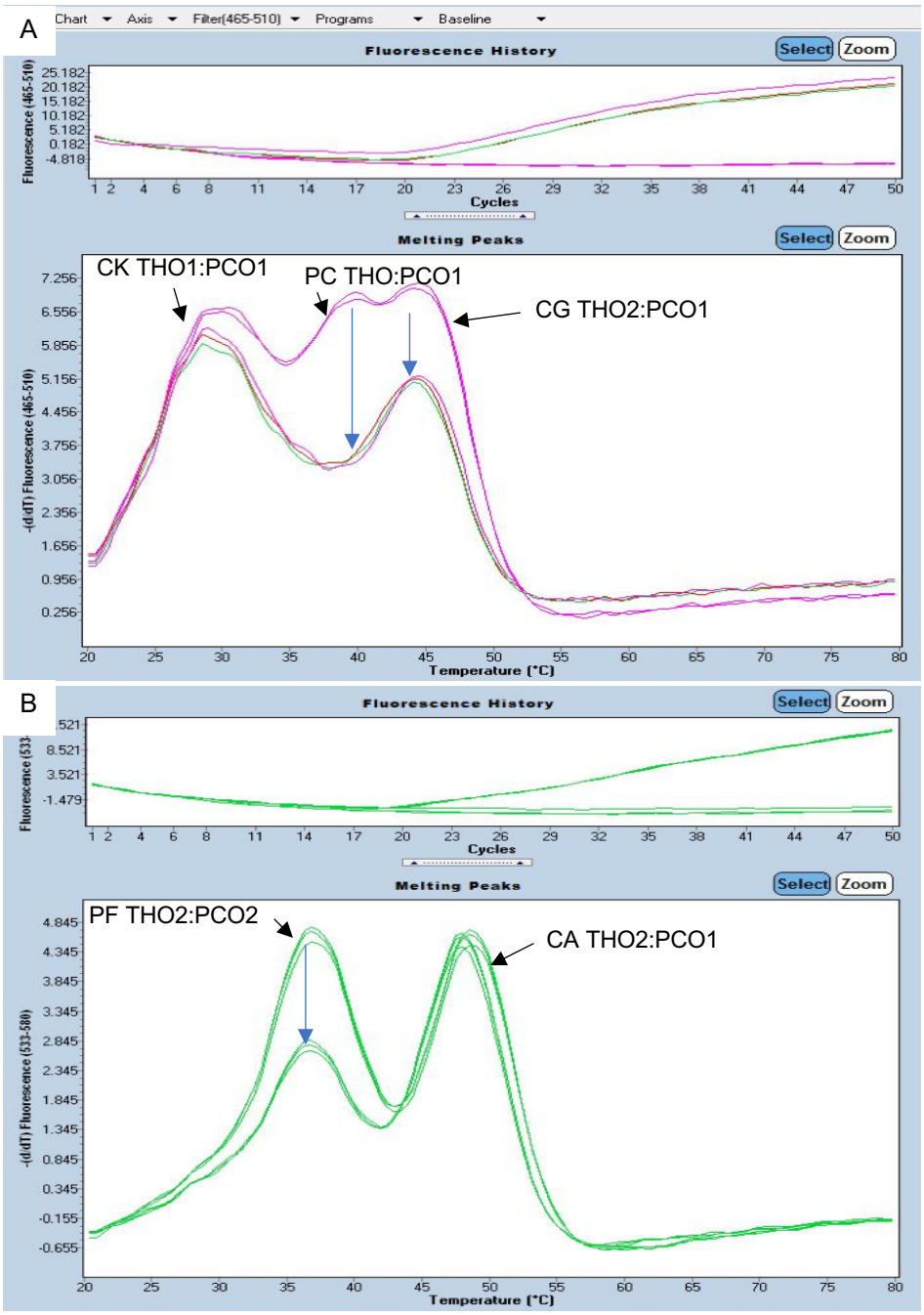

Figure 4. 26 Amplification and melt curves analysis for detection of *C. glabrata* genomic DNA in dual-channel assay multiplexed with pan-fungal probe. Three melt peaks reduction (denoted by blue arrows) compared to the control melting profile across FAM and HEX detection channels. Panel A) *C. krusei*-specific (CK), pan-*Candida* (PC) *C. glabrata*-specific (CG) probes in the FAM channel. Panel B) pan-fungal (PF) and *C. auris*-specific (CA) probes in the HEX channel. Amplification was performed with primers ITS3 and GSCand. The qPCR was performed in three replicates. The reaction contained no IC.

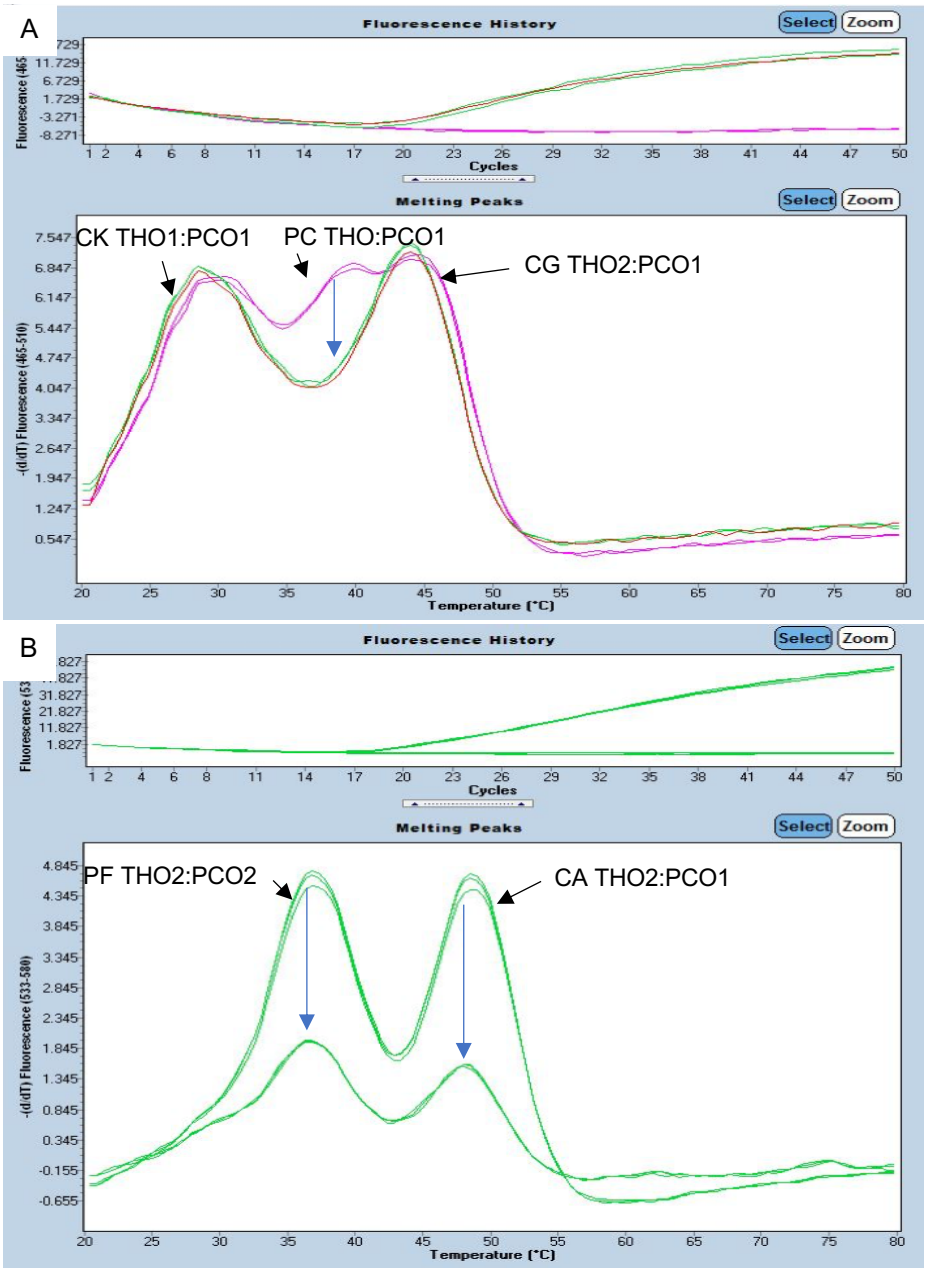

Figure 4. 27 Amplification and melt curves analysis for detection of *C. auris* genomic DNA in dual-channel assay multiplexed with pan-fungal probe. Three melt peaks reduction (denoted by blue arrows) compared to the control melting profile across FAM and HEX detection channels. **Panel A**) *C. krusei*-specific (CK), pan-*Candida* (PC) *C. glabrata*-specific (CG) probes in the FAM channel. **Panel B**) pan-fungal (PF) and *C. auris*-specific (CA) probes in the HEX channel. Amplification was performed with primers ITS3 and GSCand. The qPCR was performed in three replicates. The reaction contained no IC.

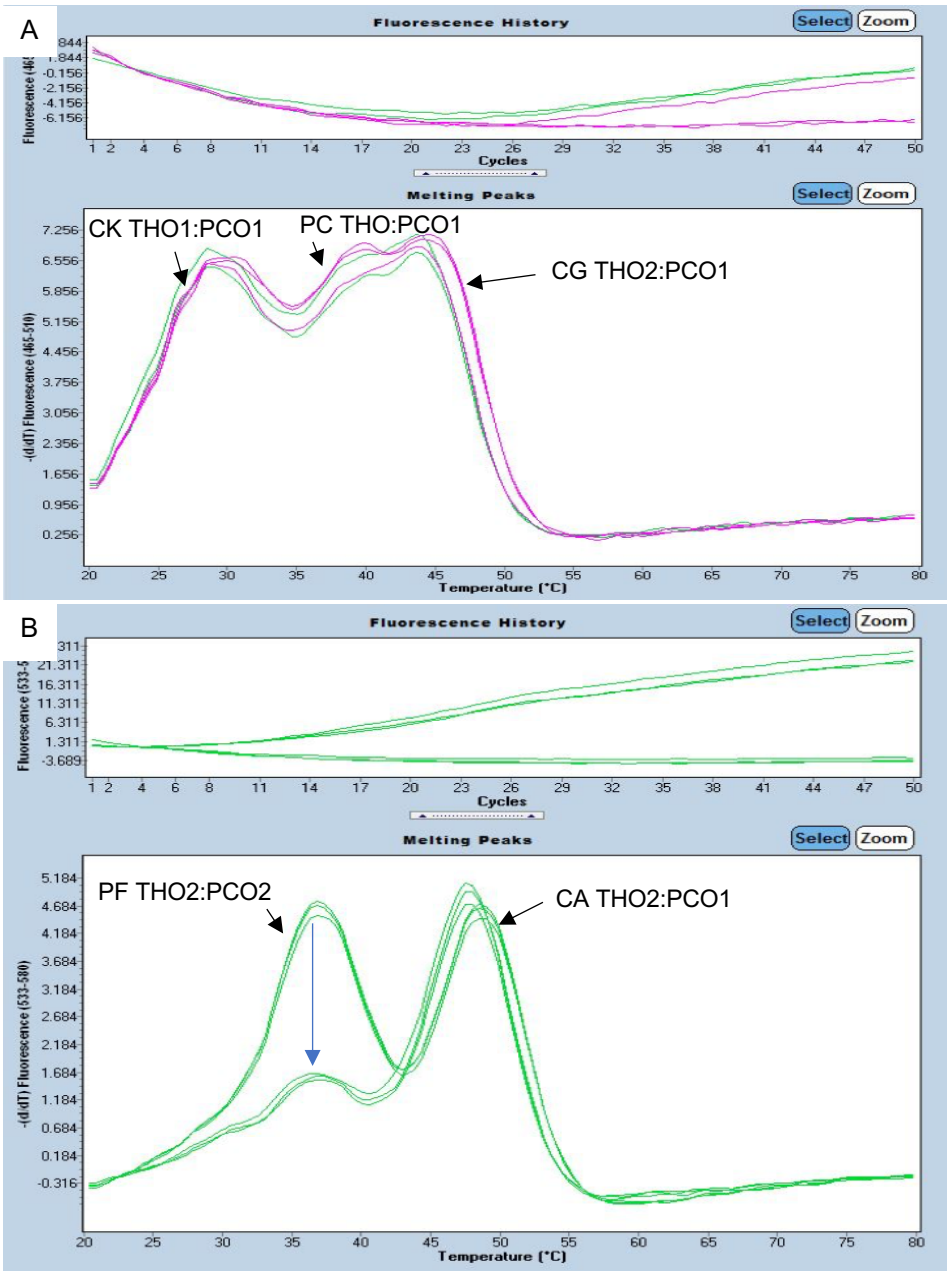

Figure 4. 28 Amplification and melt curves analysis for detection of *A. fumigatus* genomic DNA in dual-channel assay multiplexed with pan-fungal probe. One melt peak reduction (denote by blue arrow) for pan-fungal probe detection. **Panel A**) *C. krusei*-specific (CK), pan-*Candida* (PC) *C. glabrata*-specific (CG) probes in the FAM channel. **Panel B**) pan-fungal (PF) and *C. auris*-specific (CA) probes in the HEX channel. The qPCR was performed in three replicates. The reaction contained no IC.

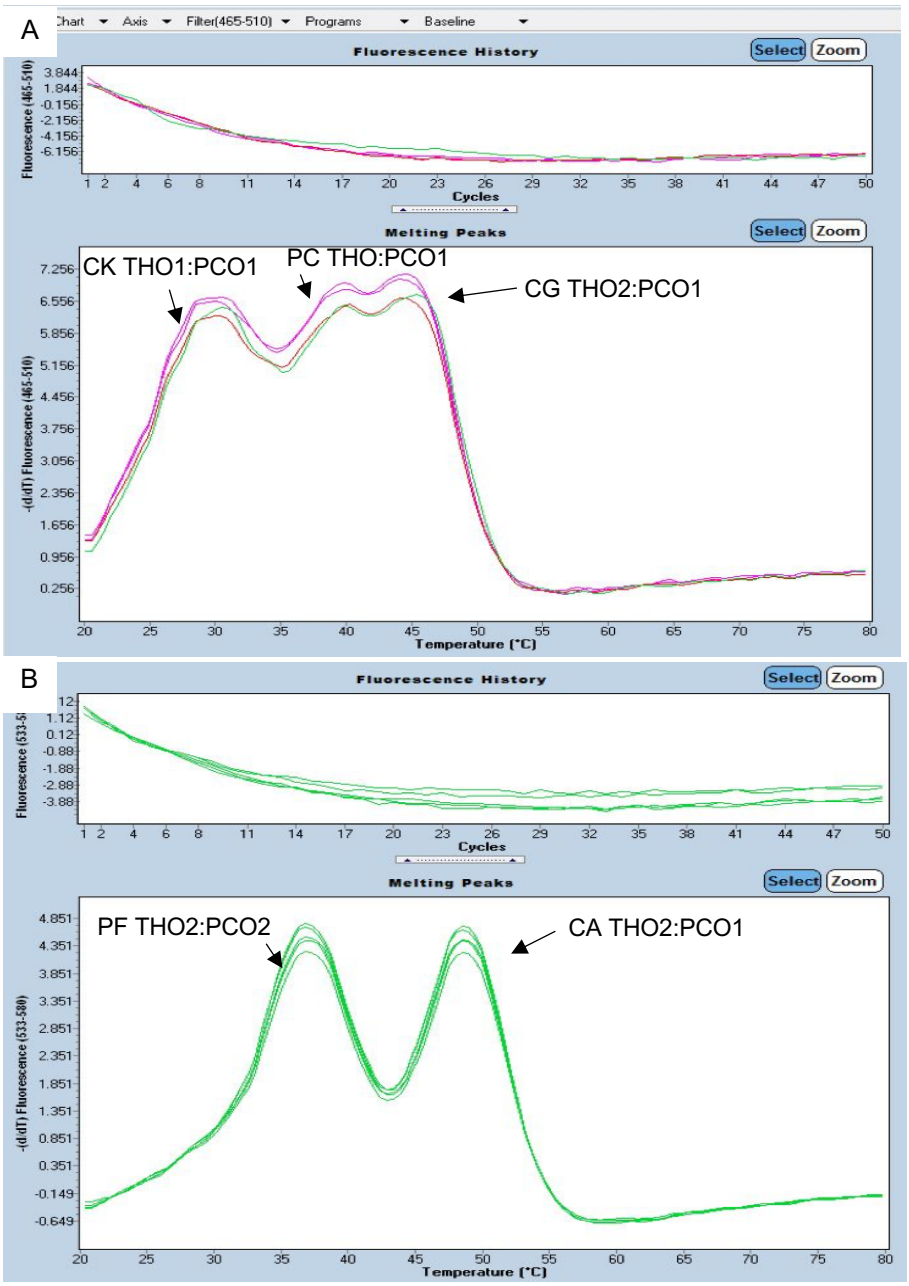

Figure 4. 29 Amplification and melt curves analysis tested for *E. coli* genomic DNA. No amplification curve can be detected in FAM (**Panel A**) and HEX (**Panel B**) channels. CK: *C. krusei*-specific; PC: pan-*Candida*; CG: *C. glabrata*-specific; PF: pan-fungal; CA: *C. auris*-specific. The qPCR was performed in three replicates.

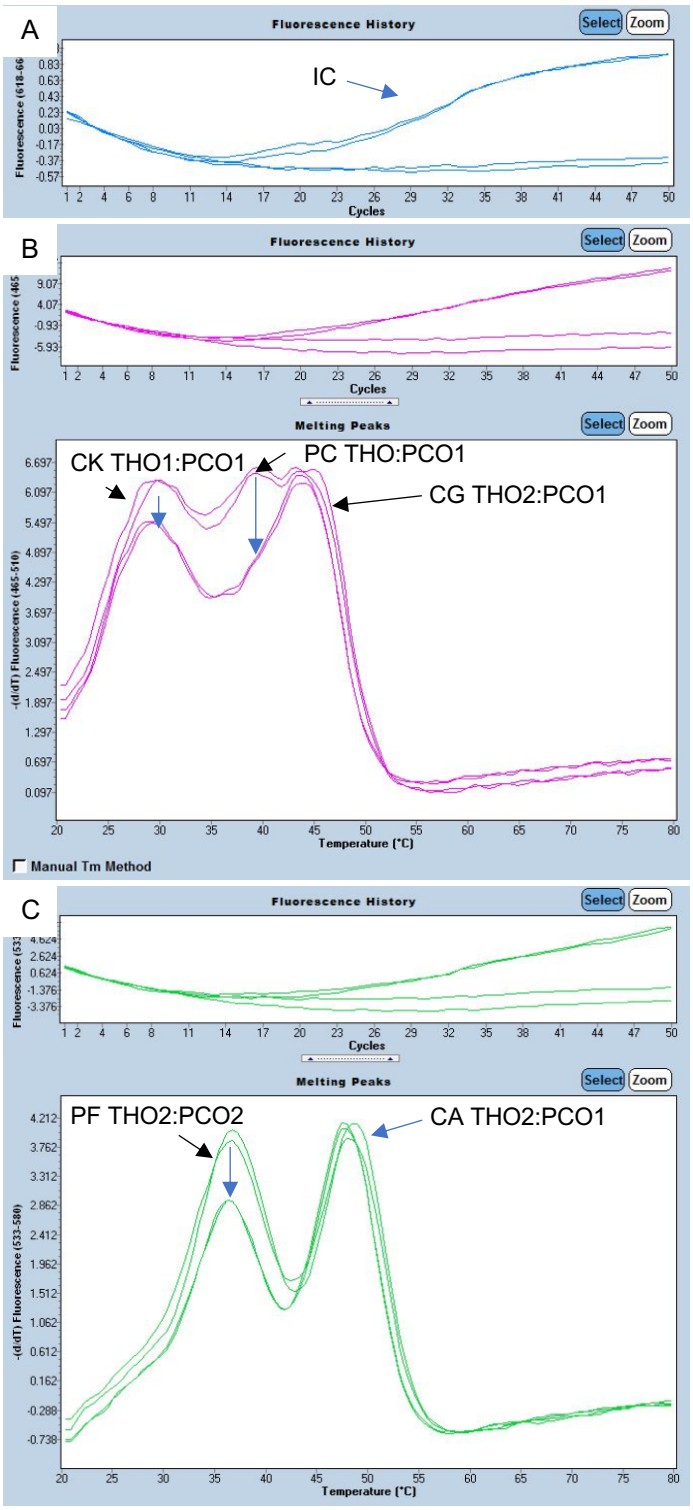

Figure 4. 30 Amplification and melt curves analysis for detection of *C. krusei* genomic DNA in three-channel assay. Panel A) IC amplification signal detected in Cy5 channel. **Panel B**) *C. krusei*-specific (CK), pan-*Candida* (PC), *C. glabrata*-specific (CG) in FAM channel. **Panel C**) PF: pan-fungal; CA: *C. auris*-specific in HEX. The qPCR was performed in three replicates.

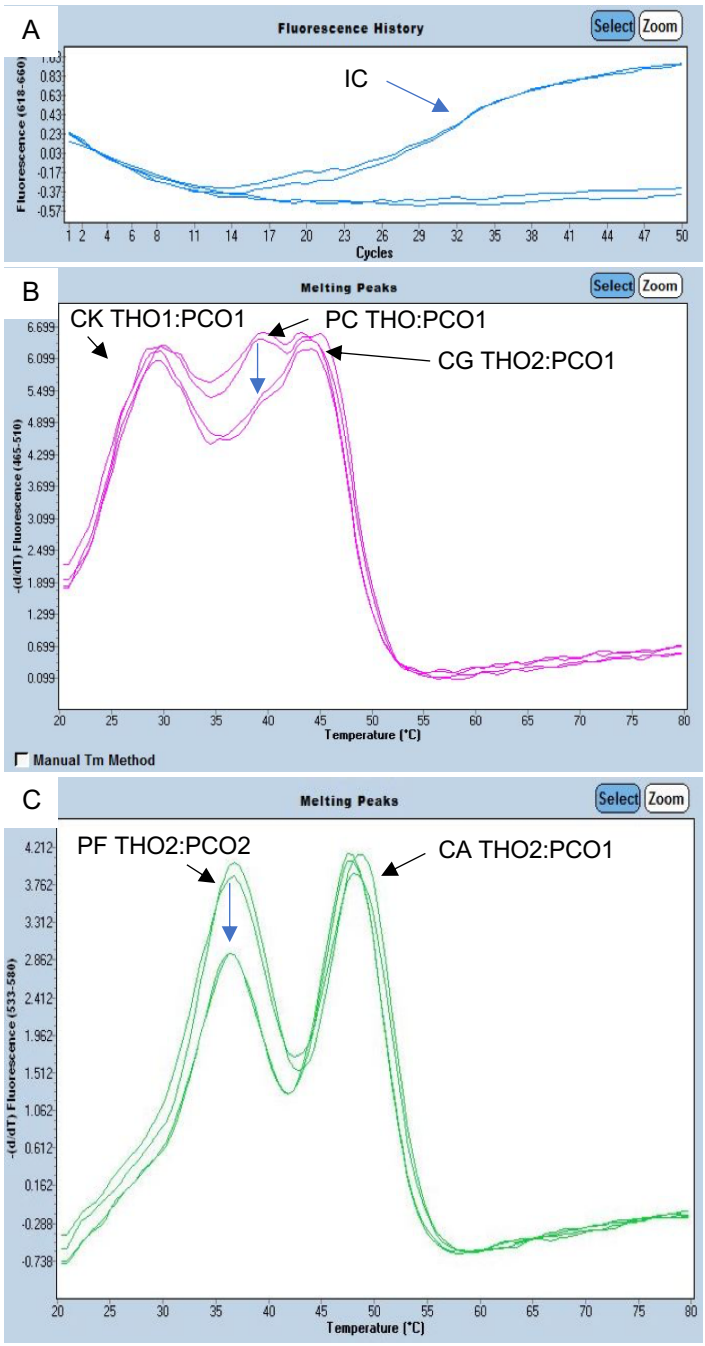

Figure 4. 31 Amplification and melt curves analysis for detection of *C. albicans* genomic DNA in three-channel assay. Panel A) IC amplification signal detected in Cy5 channel. Three melt peaks reduction (denoted by blue arrows) across FAM and HEX detection channels. **Panel B**) *C. krusei*-specific (CK), pan-*Candida* (PC), *C. glabrata*-specific (CG) in FAM channel. **Panel C**) PF: pan-fungal; CA: *C. auris*-specific in HEX. The qPCR was performed in three replicates.

4.3 Discussion

The inclusion of the pan-fungal probe into the MPA-*Candida* PCR assay offers a comprehensive diagnostic tool for the evaluation of possible fungal infections. An individual characterisation of the pan-fungal THO:PCO hybrid melting temperature was determined at 38°C as summarised in Chapter 3; Table 3.6. Ideally, the probes labelled with the same fluorophores should have the melting temperature differ by 5°C to 7°C. Therefore, addition of the pan-fungal probe into the MPA-*Candida* assay was optimised for detection in the HEX channel. However, the melting temperature of the *C. krusei*-specific probe changed from 30°C to 34°C in the HEX detection channel. The change of the probe melt peak between the channels was unexpected and has led to the ambiguity of the melting curves in the HEX channel. An alternative *C. krusei*-specific probe pair (CK THO2:PCO1) with a higher melting temperature was also tested; however, the profiles are not reproducible (Figure 4.6).

The assay design 2 without the pan-fungal probe was tested for the specificity and sensitivity of the detection. The amplification of all nine *Candida* species was detected by the pan-*Candida* probe with the reduced melting peak at 40°C compared to the no-template control. The identification of the drug-resistant *C. glabrata*, *C. krusei* and *C. auris* by their corresponding species-specific probes were detected simultaneously with the pan-*Candida* probe. In all cases, the IC was consistently recognised and ruled out the possibility of the amplification or probe failure in the reaction. The assay's limits of detection were determined using a range of 10 to 10^5 equivalent genome copies. The sensitivity of the test was poor and only can detect up to 10^4 copies of genomic DNA; however, the result showed tenfold sensitive for *C. krusei*-specific probe detection.

An attractive assay design such as incorporating the pan-fungal target probe in a single reaction with three detection channels was also attempted. Activation of three fluorescence channels in the LightCycler 480 instrument (Roche, Germany) with colour compensation setting for FAM, HEX and Cy5 can detect probes targeting for the fungal kingdom, pan-*Candida* and species-specific as well as IC plasmid DNA. Although the melting curve analysis showed the specificity for the *C. krusei* and *C. albicans* detections, the C_t values were relatively late compared to the detection of the same copy of DNA in other assay designs. For this reason, assay design 3 did not proceed with the serially diluted DNA samples for determination of the assay's limit of detection. In summary, the exploration was unable to achieve another ideal alternative for the MPA-*Candida* assay. The MPA technology allows for up to four probes detection a single detection channel (Fu, Miles & Alphey, 2012; Bhatia *et al.*, 2017). However, in this study, the detection of the three probes in one channel is more feasible to accomplish. Further improvement of the assay designs can be performed with the optimisation of the reagents and PCR master mix.

CHAPTER 5: Assessing the Effectiveness of Independent DNA Isolation Protocols for the Recovery of *Candida* DNA from Blood and Serum Samples

5.1 Introduction

Genomic DNA isolation from the fungal cell is an essential step for molecular detection techniques such as PCR to detect a specific DNA biomarker. A fungal cell including as in *Candida* species is encapsulated by a rigid cell wall that protects the cell. The structures of the cell wall are formed between the outer and inner layers of crystalline arrangements of chitin, a linear polysaccharide made of N-acetylglucosamine, forming an insoluble structure that difficult to break (Ruiz-Herrera *et al.*, 2006). Mechanical lysis process is recommended to break the fungal cell wall for optimum DNA extraction (Halliday *et al.*, 2015; White *et al.*, 2010). There are few mechanical cell lysis techniques available including a conventional method such as bead beating procedures (Lõoke, Kristjuhan & Kristjuhan, 2011), that operates in the mechanical homogeniser instrument. Meanwhile, a less conventional instrument, for example, hand-held mini-pestle that can be applied to fungal cells in a specialised extraction tube (Zhang, Chen & Lu, 2012). In this chapter, several commercial DNA isolation kits were integrated with both of the mechanical cell lysis techniques mentioned and evaluate the DNA yields. The DNA isolation protocol was also optimised to extract the DNA from the spiked samples in saline, whole blood and serum; to achieve a sensitive fungal genomic DNA extraction method from three different samples.

A range of microbial DNA isolation kits included in this study was from the RTP® Pathogen Kit (Stratec Molecular), Wizard Genomic DNA Purification Kit (Promega) and the ZymoBiomics™ DNA Miniprep Kit (Zymo Research). The kits are

intended for bacterial, yeast and viral (RTP® Pathogen Kit) DNA isolation from whole blood or blood-based samples but also can be applied to the cell cultures media or suspension. According to the manufacturer's protocol, the maximum yeast input from the overnight culture has to be in a range of 10^8 yeast cells. Therefore, a standardised starting material with the number of yeast cells from the stock culture was counted on the haemocytometer and determined the cells viability in the CFU/mL. The kit's protocol was adapted for yeast cell wall lysis technique using a standardised bead-beating instrument either in an ultra-speed beater, FastPrep-24™ (MP Biomedicals) or Disruptor Genie (Scientific Industries) cell homogeniser. Importantly, as two of the kits (RTP® Pathogen Kit and ZymoBiomics™ DNA Miniprep Kit) are using spin column, the starting amount of the sample was strictly followed as outlined in the instruction to avoid suboptimal performance of the process.

The final step of DNA dilution was standardised with 50 µL of nuclease-free water throughout the investigations. Importantly, an inhibitor-free DNA product is needed for PCR to perform efficiently. Each DNA extraction products was measured in a spectrophotometer NanoDrop™ instrument to determine the DNA concentration and purity scale.

Ultimately, *C. albicans* DNA extracted from the range of spiked and diluted samples were tested in the Pan-Fungal real-time PCR reaction. The fungal DNA biomarker targeting the detected DNA from the ITS2 region of the fungal rDNA used was quantified to evaluate the isolation methods. Quantification of DNA copy number present in the sample was also attainable through an established calibration curve to correlate the DNA extraction products. Not less important, the optimum method achieved in this study was used to process spiked serum samples of the *Candida* Evaluation Panel (Qnostic, UK) for the detection in the MPA-*Candida* assay. The detailed of the evaluation results and associated discussion are presented in Chapter 3.

5.2 Experimental Results

5.2.1 Microscopic yeast cell counting and CFU.

The yeast DNA extraction experiment was started by determining the number of cells present in the sample. For each protocol in this experiment, all the samples had almost the same concentration of cells. A stock yeast culture with a known number of cells was also serially diluted for a range of dilutions, and cell dilutions from 10^5 to 10^2 cells were plated on the SDA media for cell counting. The number of live cells in the sample suspension confirmed its viability and was expressed in terms of CFU. The *C. albicans* cells were counted using a microscope and haemocytometer, an improved Neubauer ruling and its coverslip, as described in Materials and Methods. The number of *C. albicans* cells from haemocytometer and the calculation of CFU/mL over a range of dilutions is depicted in Figure 5.1. The procedures were performed on three independent occasions on overnight cell culture.

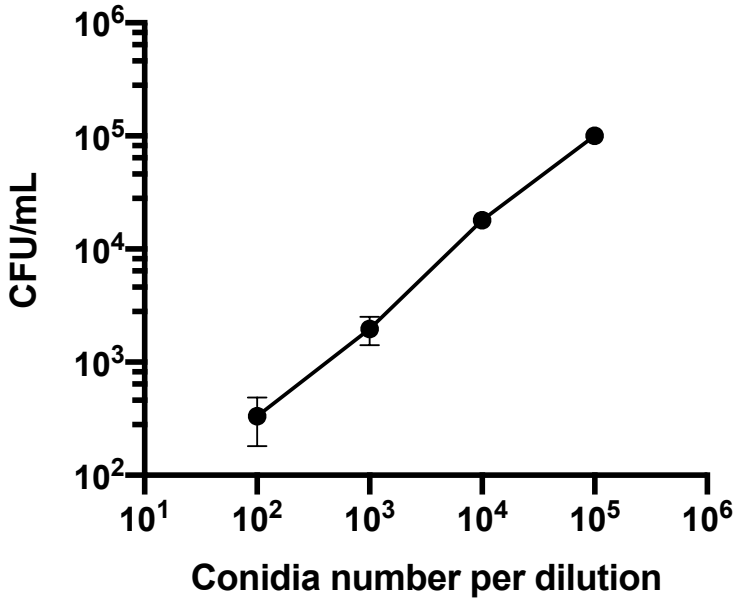

Figure 5. 1 The colony growths from the serial dilutions of the conidia. The dilutions were set up across four magnitudes of dilutions from three independent preparations.

5.2.2 DNA isolation using the RTP® Pathogen Kit (Stratec Molecular GmbH)

The isolation of *C. albicans*'s nucleic acid from a known number of cells, 1.1×10^8 cells /mL, was performed along with a control sample with the no cell spiked in the saline. A slight modification of the early steps for the cell lysis is summarised in Figure 5.2. The mechanical cell lysis steps were performed in the conditions of lysing the cells in the supplied Extraction buffer to enhance the releasing of DNA from the cells (Method 1). As a methodological comparison, a duplicate preparation of cell suspension was also processed in the absence of the Extraction buffer, which was only added in the later steps (Method 2). An experiment without the mechanical cell lysis step was tested at a high incubation temperature (95°C) to break the cell wall (Method 3). Each method was processed in duplicate along with the negative controls of no cell samples. In the case of mechanical lysis method was utilised, Method 1 and Method 2 were agitated in the bead beating tubes using the FastPrep-24™ instrument.

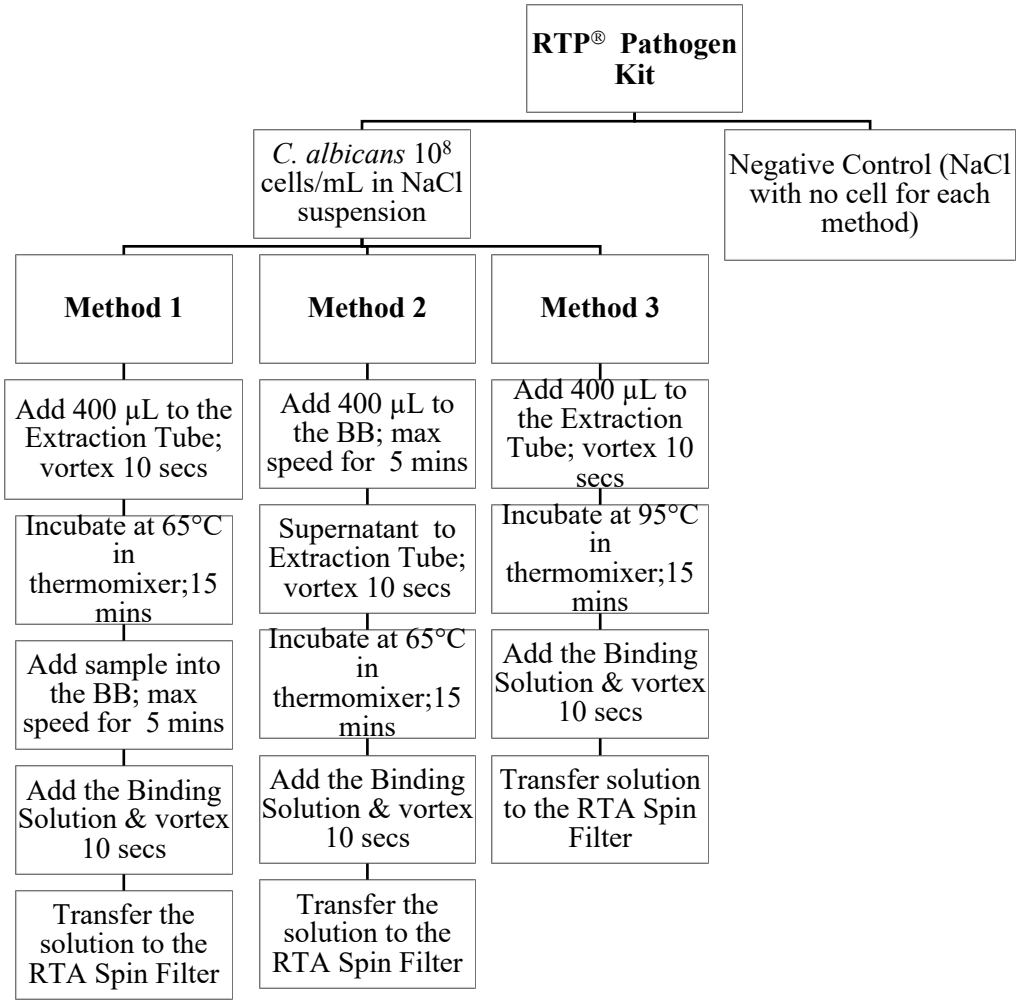

Figure 5. 2 A flow diagram of the optimisation experiments of the RTP Pathogen kit protocol for the isolation of *C. albicans* DNA/RNA.

BB, bead beating; secs, seconds; mins, minutes.

The results of the optimisations steps in this series of experiments are summarised in Table 5.1 from the spectrophotometer readings. The measurements of nucleic acid concentration for each sample was read in triplicate and reported as a mean value. The spectrophotometer readings showed that Method 1 produced the highest nucleic acid yield, at an average of 190 ng/µL followed by method 2 in an average of 175.97 ng/µL. Method 3 produces the lowest nucleic acid yield and, one of the duplicate tubes (tube 2) has lower reading than the negative control. All methods showed the purity for RNA with an absorbance 260:280 ratios of more than 2.0. The negative controls were found with a significant detection of the background DNA concentration (~64 ng/µL). According to the instruction manual, the co-purified Carrier-RNA accounted for 5 µg per 200 µL sample for most of the present DNA/RNA in the sample. This suggests for DNA concentration detected in the negative controls were from the Carrier-RNA that pre-formulated in the solid lysis reagent in the Extraction tube. The total nucleic acid concentrations measured in methods 1, 2 and 3 did not exclusively represent the DNA yields from the spiked yeast cells, therefore; spectrophotometer analysis was not helpful to gauge the concentrations of *C. albicans* DNA recovered. Ideally, the DNA extraction products from the RTP® Pathogen kit is to quantify through a calibrated qPCR assay.

Table 5. 1 The values of the *C. albicans* nucleic acid concentrations and purities using three methods of RTP Pathogen kit. Each method was performed in duplicate and the DNA readings were performed three times, and values represented as mean ± SD.

Sample	Total nucleic acid concentration (ng/µL)	Mean $A_{260/280}$ ratio	Estimation of the DNA concentration* (ng/µL)
Method 1, tube 1	185.00 ± 1.52	2.40 ± 0.01	121.98
Method 1, tube 2	196.10 ± 1.12	2.41 ± 0.02	133.08
Method 2, tube 1	193.23 ± 2.60	2.45 ± 0.01	131.23
Method 2, tube 2	158.72 ± 0.85	2.45 ± 0.02	96.72
Method 3, tube 1	71.06 ± 0.34	2.74 ± 0.57	5.19
Method 3, tube 2	62.71 ± 0.43	2.71 ± 0.04	-3.16
Method 1, NC	63.02 ± 0.37	3.24 ± 0.10	n/a
Method 2, NC	62.00 ± 0.86	3.20 ± 0.10	n/a
Method 3, NC	65.87 ± 0.67	3.32 ± 0.03	n/a

* The estimation was calculated by subtracting the background (NC, Negative Control) value from the sample mean concentration obtained for each method. n/a, not applicable

5.2.2.1 Quantification of the extracted genomic DNA using a pan-fungal PCR amplification assay.

A known number of *C. albicans* cell, 1.0×10^8 cells/mL, was spiked into 0.9% NaCl solution and was serially diluted for seven tenfold dilutions. Method 1 was followed for DNA isolation, and the final step for the DNA pellet was eluted in 50 µL elution buffer and 1 µL DNA samples subjected to the Pan-Fungal qPCR assay. The IC plasmid DNA was included in each PCR mixture to avoid false negative results. The controls reaction, which either contained the IC plasmid DNA only or no cell sample

(Negative Control), demonstrated early C_t value for IC plasmid DNA (C_t = 25.75) and no detection of the amplification curve for the negative control (Table 5.2). Moreover, each Pan-Fungal PCR reaction was considered inhibitor-free and valid with the detection of the IC plasmid DNA that present along with the extracted *C. albicans* DNA in the reaction. A consistent reading of the IC in all the reactions with a mean C_t value of 26.03 ± 0.60 detected in the HEX qPCR channel. The Pan-Fungal qPCR can detect fungal DNA from the diluted spiked sample of up to 1: 10 000 dilution ratio or equivalent to 100 cells of *C. albicans* present in the sample. However, the sample was detected at a late C_t value; therefore, under-represents the amount of extracted DNA compared to the detection of 100-copy of genomic DNA. No amplification was detected from the samples of 1: 100 000 and 1: 1 000 000 cells dilutions ratio, however, in each reaction with Pan-Fungal negative results were consistent with the detection of the IC plasmid DNA.

Table 5. 2 The Pan-Fungal PCR amplification and quantification of the extracted fungal genomic DNA from a serial dilution of saline cell suspension. The C_t values are mean (n=3) ± SD.

Number of cell (Dilution ratio of cell suspension in saline)	Pan-Fungal PCR		Estimation of fungal target copy number, y= -3.514Log (x)+ 45.44[(1)]
	IC (mean C_t ± SD)	Fungal (mean C_t ± SD)	
Negative Control	Negative (ND)	Negative (ND)	ND
IC DNA only	Positive (25.75 ± 0.41)	Negative (ND)	ND
10^7 cells (1)	Positive (25.66 ± 0.97)	Positive (18.74 ± 0.23)	3.96×10^7
10^6 cells (1:10)	Positive (26.07 ± 0.47)	Positive (20.27 ± 0.26)	1.45×10^7
10^5 cells (1:100)	Positive (25.50 ± 0.45)	Positive (22.19 ± 0.42)	4.13×10^6
10^4 cells (1:100)	Positive (25.58 ± 0.60)	Positive (23.97 ± 0.48)	1.20×10^6
10^3 cells (1:1000)	Positive (26.83 ± 0.68)	Positive (36.12 ± 0.59)	4.49×10^2
10^2 cells (1:10 000)	Positive (25.37 ± 0.76)	Positive (38.64 ± 1.10)	8.60×10^1
10 cells (1:100 000)	Positive (26.60 ± 0.23)	Negative (ND)	ND
1 cell (1:1 000 000)	Positive (26.89 ± 0.60)	Negative (ND)	ND

[1]Estimation of fungal target copy number present based on the calibration curve established for Pan-Fungal qPCR assay, R^2= 0.999. IC, Internal Control; C_t, Threshold cycle; SD, Standard deviation; ND, No detection.

5.2.2.2 Extraction and quantification of DNA from spiked blood and serum samples

To further evaluate the extraction protocol, the same number of cells were spiked into 1 mL aliquots of blood and serum. In both sample types, *C. albicans* conidia suspension was serially diluted for seven tenfold dilutions followed by DNA extraction. DNA was eluted with a standardised volume of 50 µL of elution buffer. One µL of DNA sample was subjected to PCR in triplicate, and each reaction contained the IC plasmid DNA that was monitored in the HEX channel. The multiplex qPCR assay contained pan-fungal and IC probes that are detectable in the FAM channel and HEX channel respectively.

The detection of the amplified products from the extracted whole blood spiked samples was validated by the detection of the IC in all reactions and mean of the C_t values at 26.07 ± 0.52 (Table 5.3). Briefly, the Pan-Fungal qPCR can detect fungal DNA throughout the samples from 10^7 to 10^3 cells. The limit of detection was determined at C_t value 41.76 ± 0.76 for the detection of DNA in the sample with 10^3 cells. No amplification curve was detected at the higher dilution ratio of cells, from 1: 10 000 to 1: 1 000 000 samples. All the pan-fungal negative samples were validated inhibitor-free as the IC DNA was consistently detected in the same reaction. Furthermore, the limit of detection of *C. albicans* DNA extraction performed on the spiked serum samples was also determined (Table 5.4). All samples were detected with positive for IC detection with a mean C_t value at 25.53 ± 0.46. Along with the detection of the IC, the pan-fungal C_t values spanned from 17.79 to 37.47 for detection of DNA from the extracted serum samples from 10^7 to 10^3 cells. Detection of the fungal DNA biomarkers from the extracted 10^7 cells of spiked serum was recorded early by one cycle compared to the same number of cells from the whole blood. The limit of detection of fungal DNA in the serum was demonstrated in the same magnitude as in

the whole blood sample. Each spiked sample was processed in the same way as whole blood except for the starting volume (200 µL) for the serum to load into the RTA spin column. The detection of fungal biomarkers and the magnitude of detection across the three different spiked samples (saline solution, whole blood and serum) are summarised in Figure 5.3.

Table 5. 3 The Pan-Fungal PCR amplification and quantification of the extracted fungal genomic DNA from a serial dilution of spiked whole blood samples. The C_t values are mean (n=3) ± SD.

Number of cell (Dilution ratio of cell suspension in whole blood)	Pan-Fungal PCR		Estimation of fungal target copy number, y= -3.514Log (x)+ 45.44[(1)]
	IC (mean C_t ± SD)	Fungal (mean C_t ± SD)	
Negative Control	Negative (ND)	Negative (ND)	ND
IC DNA only	Positive (25.77 ± 0.55)	Negative (ND)	ND
10^7 cells (1)	Positive (25.38 ± 0.64)	Positive (17.87 ± 0.15)	7.01×10^7
10^6 cells (1:10)	Positive (26.37 ± 0.18)	Positive (21.50 ± 0.12)	6.50×10^6
10^5 cells (1:100)	Positive (26.27 ± 0.50)	Positive (23.48 ± 0.19)	1.80×10^6
10^4 cells (1:100)	Positive (25.26 ± 1.21)	Positive (29.45 ± 0.19)	3.55×10^4
10^3 cells (1:1000)	Positive (26.64 ± 0.05)	Positive (41.76 ± 0.76)	1.10×10^1
10^2 cells (1:10 000)	Positive (26.00 ±0.78)	Negative (ND)	ND
10 cells	Positive	Negative (ND)	ND

(1:100 000)	(26.18 ± 0.36)		
1 cell (1:1 000 000)	Positive (25.78 ± 0.47)	Negative (ND)	ND

[1]Estimation of fungal target copy number present based on the calibration curve established for Pan-Fungal qPCR assay, R^2= 0.999. IC, Internal control; C_t, Threshold cycle; SD, Standard deviation; ND, No Detection

Table 5. 4 The Pan-Fungal PCR amplification and quantification of the extracted fungal genomic DNA from a serial dilution of spiked serum samples. The C_t values are mean (n=3) ± SD.

Number of cell (Dilution ratio of cell suspension in serum)	Pan-Fungal PCR		Estimation of fungal target copy number, y= -3.514Log (x)+ 45.44[(1)]
	IC (mean C_t ± SD)	Fungal (mean C_t ± SD)	
Negative Control	Negative (ND)	Negative (ND)	ND
IC DNA only	Positive (25.57 ± 0.46)	Negative (ND)	ND
10^7 cells (1:1)	Positive (24.89 ± 0.97)	Positive (17.79 ± 0.16)	7.39×10^7
10^6 cells (1:10)	Positive (25.74 ± 0.27)	Positive (21.21 ± 0.23)	7.86×10^6
10^5 cells (1:100)	Positive (24.62 ± 0.43)	Positive (23.37 ± 0.23)	1.91×10^6
10^4 cells (1:100)	Positive (25.74 ± 0.36)	Positive (33.19 ± 1.20)	3.06×10^3
10^3 cells (1:1000)	Positive (26.00 ± 0.30)	Positive (37.47 ± 0.11)	1.85×10^2
10^2 cells (1:10 000)	Positive (25.52 ± 0.54)	Negative (ND)	ND
10 cells (1:100 000)	Positive (25.76 ± 0.62)	Negative (ND)	ND

1 cell (1:1 000 000)	Positive (25.81 ± 0.56)	Negative (ND)	ND

[1]Estimation of fungal target copy number present based on the calibration curve established for Pan-Fungal qPCR assay, R^2= 0.999. IC, Internal control; C_t, Threshold cycle; SD, Standard deviation; ND, No Detection.

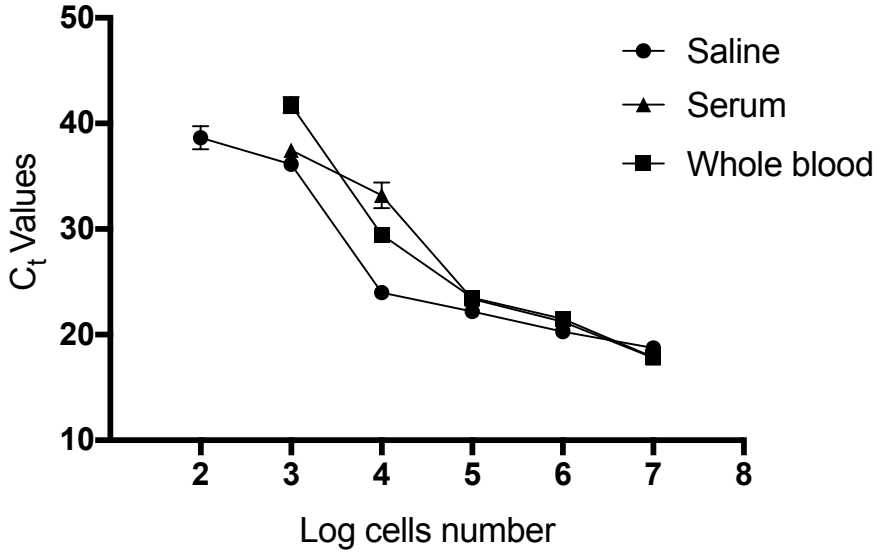

Figure 5. 3 The detection of *C. albicans* DNA in Pan-Fungal PCR assay. Variation of the C_t values and magnitude of detections of the spiked cells into three different samples. The triplicate C_t values were plotted with error bars, which represented SD. Lower C_t values indicate a higher sensitivity of the detection.

5.2.3 DNA extraction using the Wizard® Genomic DNA Isolation kit (Promega)

The isolation of *C. albicans* genomic DNA was performed using the Wizard Genomic DNA Purification kit (Promega) with a slight modification of the protocol for the cell lysis steps. The standard kit protocol was tested with two techniques of mechanical cell lysis; using a hand-held homogeniser mini-pestle (BioMasher®) and an automated bead beating instrument (FastPrep-24™). A known number of *C. albicans* cells was spiked in two different samples – saline solution and whole blood. Then, the samples were serially diluted for seven tenfold dilutions and subjected to the DNA extraction process.

The trial of instruments was performed using the mini-pestle homogeniser (BioMasher®) and bead beating (FastPrep-24™) for mechanical cell lysis. All extraction samples were processed in parallel following the modified kit's protocol (Figure 5.4). In the final step, the DNA pellet was rehydrated in 50 µL of nuclease-free water and was kept constant throughout all experiments. The average DNA concentration for each sample is summarised in Table 5.5. In the result, the highest DNA concentration measured at 48.49 ng/µL for a method using the handheld cell homogeniser but, the variation between the duplicate was noticeably high. Contrary to the bead-beating technique, although the DNA recovered was lower, it showed a consistent reading of DNA yields between the duplicates. The next experiments were followed with the mechanical cell lysis method using the bead beating technique and the standard Wizard Genomic DNA isolation protocol.

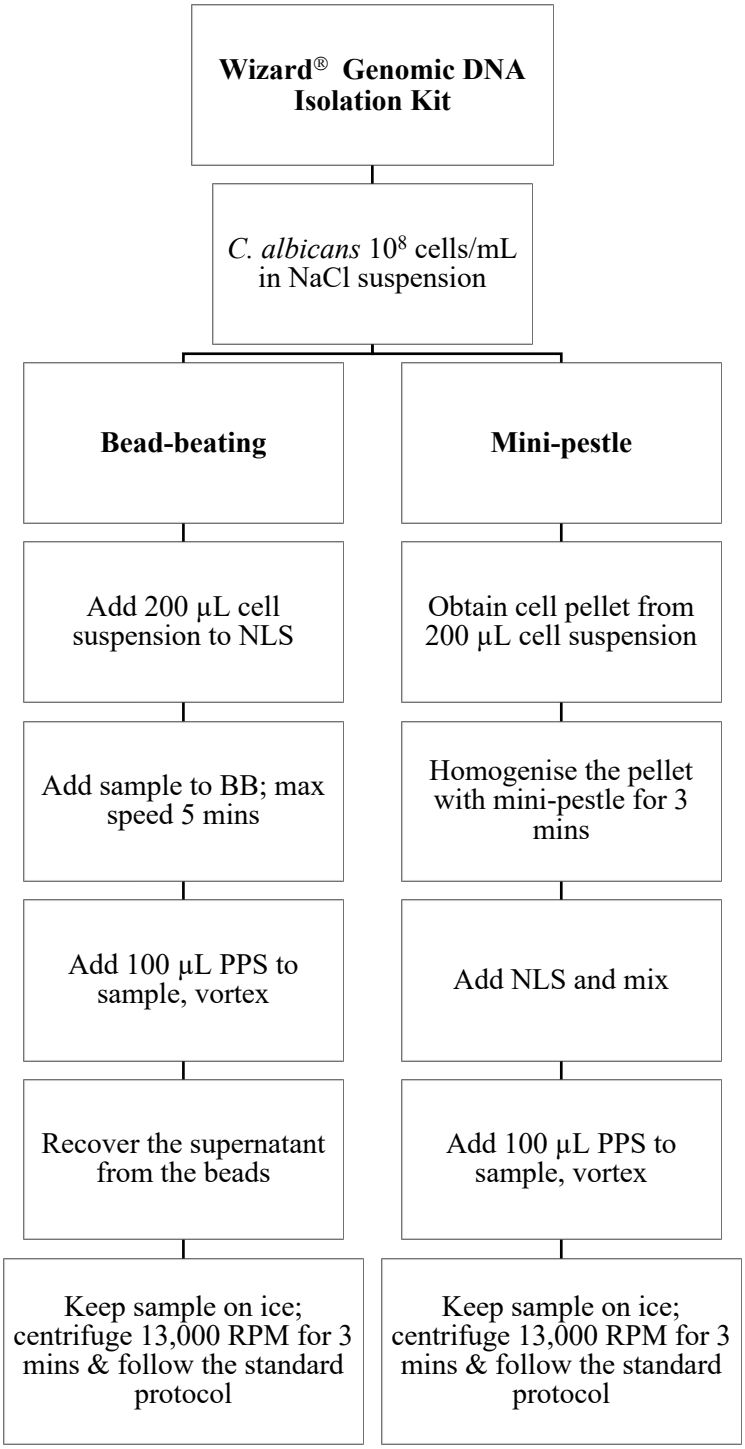

Figure 5. 4 A flow diagram of the optimisation process of the Promega Wizard Genomic DNA isolation kit protocol for *C. albicans* DNA. BB, Bead-beating tube; NLS, Nuclei Lysis Solution; PPS, Protein Precipitation Solution; RPM, Revolutions Per Minute; secs, seconds; mins, minutes.

Table 5. 5 The values of DNA concentrations and purities extracted from the 10^7 *C. albicans* cells in saline solution. The DNA extraction was performed by the Wizard Genomic DNA isolation kit tested with two different mechanical cell lysis techniques.

Mechanical cell lysis technique & Promega isolation kit	**Mean Concentration (ng/µL)**	**Mean $A_{260/280}$ ratio**
Mini-pestle + kit, tube1	48.49 ± 0.37	2.09 ± 0.015
Mini-pestle + kit, tube 2	27.57 ± 0.30	2.10 ± 0.093
Negative Control, tube 1	ND	ND
Negative Control, tube 2	ND	ND
Bead beating + kit, tube 1	36.59 ± 0.79	2.01 ± 0.093
Bead beating + kit, tube 2	35.83 ± 0.75	2.06 ± 0.11
Negative Control, tube 1	ND	ND
Negative Control, tube 2	ND	ND

* Each technique was performed in duplicate and the DNA readings were performed three times. Values represented as mean ± SD. ND, No detection.

5.2.3.1 Extraction and quantification of DNA from spiked blood and saline samples

The experiment was continued using the spiked whole blood sample using the method established from the previous experiment. Initially, the whole blood sample containing 1.0×10^7 cells was diluted 1:10 in blood sample to contain one log lower amount of *C. albicans* cells (10^6) and subjected to the extraction procedures. The same cell preparation was made in the saline solution as a control reaction. Both sample types were prepared in duplicate and were processed in parallel using the same established protocol. The total DNA concentrations reduced significantly from the cell dilution step in the whole blood sample compared to the saline solution (Table 5.6). An absorbance ratio in a range of 1.8 and 2.0 taken at 260 nm and 280 nm as an indicator of reasonable DNA purity of the samples of 10^7 cells in whole blood; however, a lower than 1.8 indicator for protein contamination measured for other samples. The DNA concentrations detected from the spiked saline samples were considerably lower than the whole blood; however, it demonstrates way far less decreased over the dilution step.

A wider dilution range of the spiked whole blood sample was prepared and processed according to the DNA isolation protocol. The results were reproducible for the whole blood samples with the reading of DNA concentration loss considerably over the first 1:10 dilution step (Table 5.7). For all samples, including a negative control, the DNA yield was read in triplicate using a spectrophotometry instrument. Next, all samples were amplified in the real-time PCR assay for detection of biomarker targeting ITS2 region of fungal rDNA (Table 5.8). Three-fold dilution samples, from 10^7 to 10^6 cells, were detected positive for detection of the pan-fungal biomarkers in the sample. The pan-fungal biomarker copy quantified in those samples did not correlate with the number of cells spiked in the samples.

Table 5. 6 The values concentrations and purities of nucleic acids isolated from the spiked whole blood and saline solution. All samples were processed in parallel using a bead-beating cell lysis technique followed by the Wizard Genomic DNA Isolation kit (Promega).

Number of cells spiked in sample:	Mean concentration (ng/µL)	Mean $A_{260/280}$ ratio
Whole blood		
10^7 cells tube 1	80.57 ± 0.98	2.03 ± 0.03
10^7 cells tube 2	76.53 ± 3.44	2.08 ± 0.04
10^6 cells tube 1	8.54 ± 0.28	1.47 ± 0.26
10^6 cells tube 2	8.30 ± 0.58	1.44 ± 0.01
0 cell (Negative Control 1)	ND	ND
0 cell (Negative Control 2)	ND	ND
NaCl saline solution		
10^7 cells tube 1	38.91	1.36
10^7 cells tube 2	37.51	1.29
10^6 cells tube 1	25.12	0.75
10^6 cells tube 2	25.20	0.68
0 cell (Negative Control 1)	ND	ND
0 cell (Negative Control 2)	ND	ND

* Each dilution was performed in duplicate, and the DNA readings were performed three times. Values represented as mean ± SD; ND, No detection.

Table 5. 7 The values of the nucleic acid concentration and purity from a range of spiked whole blood samples.

Number of cells spiked in whole blood	Mean Concentration (ng/µL)	Mean $A_{260/280}$ ratio
10^7 cells tube 1	101.10 ± 2.20	1.99 ± 0.08
10^7 cells tube 2	120.18 ± 1.24	2.04 ± 0.03
10^6 cells tube 1	11.65 ± 1.50	1.61 ± 0.05
10^6 cells tube 2	11.51 ± 1.61	1.53 ± 0.09
10^5 cells tube 1	6.64 ± 0.32	1.42 ± 0.10
10^5 cells tube 2	6.20 ± 0.05	1.25 ± 0.05
10^4 cells tube 1	6.00 ± 1.20	1.13 ± 0.05
10^4 cells tube 2	6.35 ± 0.27	1.45 ± 0.18
10^3 cells tube 1	6.55 ± 0.90	1.04 ± 0.24
10^3 cells tube 2	7.12 ± 0.21	1.34 ± 0.04
10^2 cells tube 1	6.44 ± 0.56	1.36 ± 0.20
10^2 cells tube 2	5.18 ± 0.54	1.58 ± 0.13
10 cells tube 1	6.40 ± 0.90	1.34 ± 0.03
10 cells tube 2	5.26 ± 0.84	1.22 ± 0.04
1 cell tube 1	6.23 ± 0.21	1.21 ± 0.10
1 cell tube 2	5.64 ± 0.40	1.41 ± 0.15
0 cell (Negative Control 1)	6.07 ± 0.30	1.18 ± 0.10
0 cell (Negative Control 2)	6.39 ± 0.05	1.28 ± 0.05

*Each dilution was performed in duplicate, and the DNA readings were performed three times, and values represented as mean ± SD

Table 5. 8 The Pan-Fungal PCR amplification and quantification of extracted DNA products from a serial dilution of spiked whole blood samples. Extraction of *C. albicans* genomic DNA using the bead-beating cell lysis technique and the Wizard Genomic DNA Isolation kit (Promega). The C_t values are mean (n=3) ± SD.

Number of cell (Dilution ratio of the whole blood)	Pan-Fungal reaction		Estimation of fungal target copy number, y= -3.514Log (x)+ 45.44[(1)]
	IC (mean C_t ± SD)	Fungal (mean C_t ± SD)	
Negative Control	Negative (ND)	Negative (ND)	ND
IC DNA only	Positive (30.40 ± 0.89)	Negative (ND)	ND
10^7 cells (1)	Positive (36.55 ± 1.96)	Positive (16.99 ± 0.28)	1.25×10^8
10^6 cells (1:10)	Positive (28.72 ± 0.99)	Positive (29.63 ± 0.40	3.16×10^4
10^5 cells (1:100)	Positive (29.21 ± 1.43)	Positive (30.79 ± 0.30)	1.48×10^4
10^4 cells (1:100)	Positive (30.30 ± 0.95)	Negative (ND)	ND
10^3 cells (1:1000)	Positive (29.45 ± 1.40)	Negative (ND)	ND
10^2 cells (1:10 000)	Positive (26.43 ± 2.67)	Negative (ND)	ND
10 cells (1:100 000)	Positive (30.16 ± 0.76)	Negative (ND)	ND
1 cell (1:1 000 000)	Positive (29.26 ± 0.16)	Negative (ND)	ND

[1]Estimation of fungal target copy number present based on the calibration curve established for Pan-Fungal qPCR assay, R^2= 0.999; IC, Internal control; C_t, Threshold cycle; SD, Standard deviation; ND, No Detection.

5.2.4 DNA extraction using the ZymoBIOMICS™ DNA Miniprep Kit (Zymo Research)

The DNA isolation of the yeast cell was performed in ZymoBIOMICS DNA kit. *C. albicans* cell suspension (1.1×10^8 cells/mL) was prepared in 0.9% NaCl solution. The cell suspension was processed for DNA isolation using the kit's standard instruction manual. The manufacturer's recommendation was followed using a homogeniser instrument, FastPrep-24™ bead-beating steps (Figure 5.5). The final step of DNA elution of 50 µL with nuclease-free water was kept constant for all samples. In all samples, including a negative control, the DNA yield was measured three times using a spectrophotometer NanoDrop™ instrument. The DNA concentration recovered from the 10^7 cells was very low and inconsistent amongst replicates, compared to the other two methods used (Table 5.9). For this reason, this line of investigation was not pursued further.

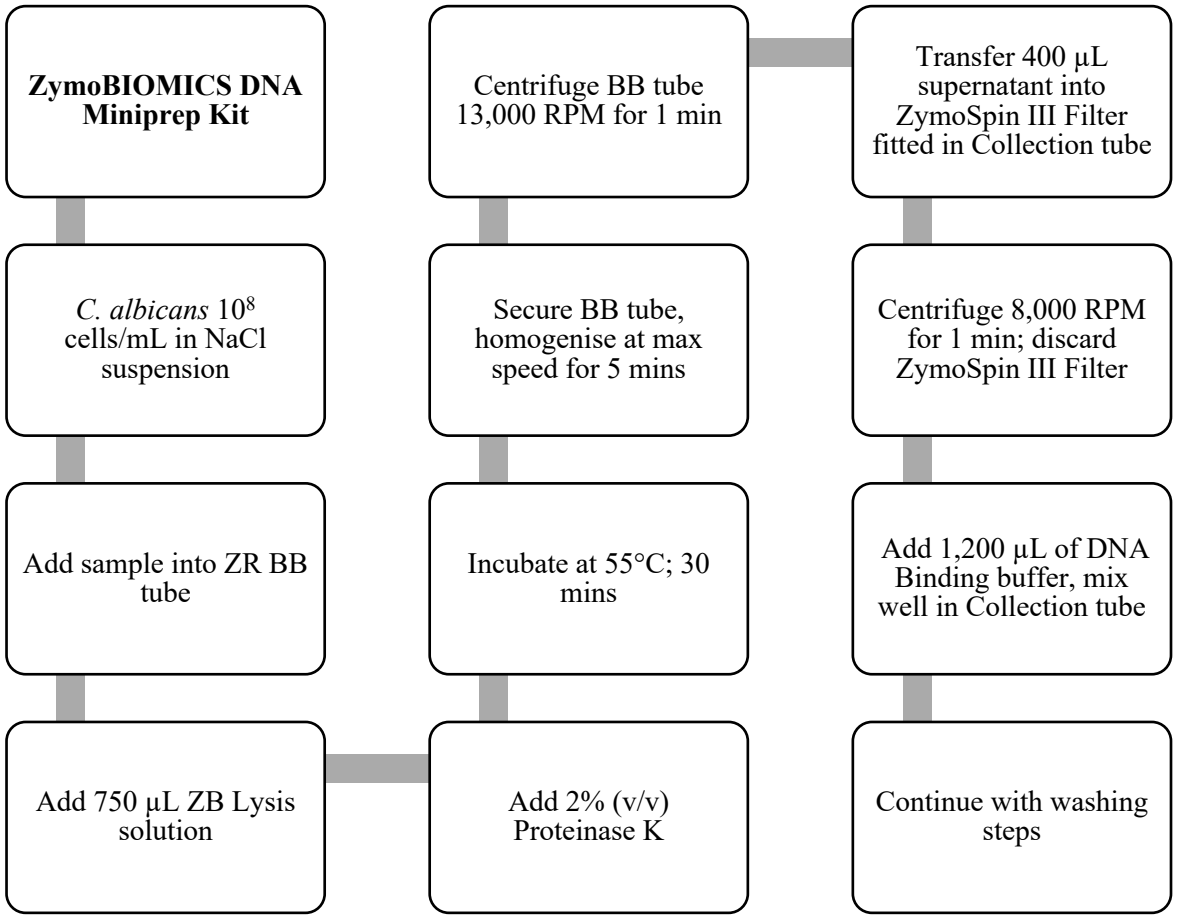

Figure 5. 5 The recommended flow of extraction steps for yeast DNA isolation using the bead beating technique and ZymoBIOMICS™ DNA kit. BB, Bead-beating; RPM, Revolutions Per Minute.

Table 5. 9 The mean values of the concentrations and purities of genomic DNA isolated using ZymoBIOMICS™ DNA Miniprep Kit. *C. albicans* cells were spiked in saline solution and processed in duplicate using the bead-beating cell lysis technique.

Number of cells spiked in saline	Mean Concentration (ng/µL)	Mean $A_{260/280}$ ratio
10^7 cells tube 1	9.96 ± 0.33	1.60 ± 0.07
10^7 cells tube 2	5.04 ± 0.21	1.96 ± 0.09
0 cell (Negative Control 1)	ND	ND
0 cell (Negative Control 2)	ND	ND

*Each dilution was performed in duplicate, and the DNA readings were performed three times, and values represented as mean ± SD; ND, No Detection.

5.3 Discussion

This investigation was driven by the need to develop an optimum *C. albicans* DNA isolation protocol using a bead-beating technique incorporated with several commercial DNA isolation kits. Generally, the RTP® Pathogen kit, Wizard Genomic DNA Purification kit and the ZymoBiomics™ DNA Miniprep kit are suitable for high protein content samples such as whole blood, serum, plasma and tissues biopsies. The RTP® Pathogen and ZymoBiomics™ DNA Miniprep kits are the specialised kits for viral and bacterial DNA extractions whereas, the Wizard Genomic DNA Purification is optimum for bacterial and yeast DNA. Ultimately, the DNA product was quantified in the Pan-Fungal PCR assay to evaluate the effectiveness of each isolation protocol. The quantification of genomic DNA is most accurately determined by the real-time PCR assay (Clements *et al.*, 2008). The reagent in the RTP Pathogen kit is prefilled

with poly A carrier RNA fragments of 100-1000 bases. This RNA accounts for 5 μg per 200 μL sample (equivalent to 25 ng/μL) and likely exceeds the amount of isolated nucleic acid from samples. The RTP Extraction tube contained preformulated solid lysis reagent, lytic enzyme, Proteinase K to mix with the buffer at a particular pH. According to the extraction kit manual, the carrier RNA helps to stabilise the nucleic acids and enhance DNA adsorption to the membrane in the RTA Spin Filter. An analytical study shows that the presented method could improve the extraction efficiency of the small amount of DNA by five times compared to the extraction without the carrier RNA (Thain *et al.*, 2009). Furthermore, the DNA extracted from spiked whole blood or serum samples may also contain a significant nucleic acid originated from the biological samples; thus, it is not a pure form of fungal genomic DNA. In these conditions, the measurement of nucleic acid concentration using a spectrophotometer does not reflect the functional quantity of genomic DNA isolation using the RTP Pathogen Kit method. Therefore, in this investigation, it was not suitable to analyse the DNA products from the optimisation experiments from the spectrophotometer results.

Real-time PCR detection of fungal DNA was evaluated for the three different types of spiked samples spanned from 10^7 cells to 1 cell (approximately from 10^9 CFU/mL to 10^2 CFU/mL equivalent). A consistent sensitivity of extraction was noted between the spiked cells in serum and whole blood samples. However, the detection limit of fungal DNA was increased by tenfold for the spiked saline sample. Although all the spiked samples used contained the recommended amount of starting material (10^7 cells), the yeast cells in the saline were the most efficient to be processed in every step. A small part of the filter membrane was noticed to clog the RTA spin column which may have led to the reduction of nucleic acid binding to the filter membrane. This suggestion for a significant accidental loss of nucleic acid particularly at the low

quantity of spiked yeast cells in the high protein containing samples. All recommendations were followed including increasing the cell lysis time and centrifugations speed and time during washing steps to remove the cellular contaminants. The necessary step was also adhered with a vigorous mixing of the cells in the buffer to ensure no cell clumps before subject the sample to the RTA spin column. The estimation of target DNA copy number from the Pan-Fungal assay calibration curve showed more than a one hundred-fold loss of genomic DNA (assuming 100% extraction efficiency) compared to the theoretical cell number, through the process of the DNA isolation by the RTP Pathogen Kit method. The target region presents in the tandem repetitive (50-100 copies per haploid genome) of the fungal rDNA gene cluster (Halliday *et al.*, 2015; White *et al.*, 2010).

The use of other commercial DNA extraction kits with differently available cell lysis instrument was advocated in this investigation in order to achieve standardised methods and reagents. However, the different DNA extraction methods demonstrated large discrepancies of the fungal DNA detection by the Pan-Fungal real-time PCR, highlighting the importance of the extraction step in nucleic acid-based fungal diagnostics. There was almost a hundred-fold difference in DNA recovery levels from the spiked whole blood between the RTP pathogen and Wizard Genomics methods. Reproducibly low sensitivity of detection for the DNA products from the Wizard Genomics suggested the protocol is not flexible to integrate the process with the mechanical cell lysis steps in this study. Mini-pestle cell homogeniser using the hand-held instrument (BioMasher) was not able to demonstrate reproducible DNA yield by almost 50% difference measured between the duplicate samples although one of the samples (Mini-pestle + kit, tube 1) produced 70% more DNA yields than another lysis method (Table 5.5). Inconsistency pressure or force from the human handling the instrument between the samples contribute to this error. The poor DNA yields were

noticed from the spiked sample with consistent loss of DNA concentration over the first sample dilution. The DNA yields from the amount of yeast (10^7 cells) spiked in whole blood and saline were not reproducible and significantly different (Table 5.6). A far less efficient method of extraction was demonstrated using ZymoBIOMICS™ kit with a minimal amount of DNA recovered from *C. albicans* 10^7 cells in saline samples. These methods are not practical for use in a clinical microbiology laboratory, where many samples must be processed for fungal DNA and where cross-contamination of samples must be avoided.

In summary, the yeast DNA isolation method using RTP pathogen kit in combination with the bead-beating cell lysis step was used as an optimum method of DNA isolation. An effective method should produce maximal fungal DNA yield and purity in the absence of carryover contaminants that can significantly inhibit PCR amplification (Ali *et al.*, 2017). Although the method is not exceptional from the inhibitor issues, it outperformed the other methods in extracting DNA of *C. albicans* from saline, whole blood and serum.

CHAPTER 6: Development of MNAzymes for the Isothermal Detection of Fungal DNA Biomarkers

6.1 Introduction

The aim of this research is to develop an isothermal fungal biomarker detection technique based on MNAzymes for detection of fungi frequently associated with human fungal infection. MNAzymes that were successfully engineered from natural DNA enzymes further increase the practically of this non-protein class of enzyme (Mokany *et al.*, 2010). Naturally, DNAzymes are capable to cleave a RNA sequence (RNA substrate) after it specifically binds to the enzymes (Santoro & Joyce, 1997). Taking advantage of deoxyribonucleic acid enzymes, Mokany *et al.*, 2010 had elegantly engineered two types of optimised MNAzyme, originally derived from 10 – 23 and 8 – 17 DNAzymes. The component of the MNAzyme is presented in the Introduction; Figure 1.7. MNAzymes are naturally inactive until they hybridize to both a specific target sequence (known as the Assembly Facilitator) and a hydrolysable oligonucleotide probe (the substrate). As illustrated in Figure 1.7 the substrate is doubly labelled with a fluorophore and a quencher molecule and, upon hydrolysis, it provides a measurable output signal that can be used to quantify the amount of target DNA present in a sample. The use of differently labelled substrates allows the development of multiplex MNAzyme-based assays. Furthermore, MNAzymes can be coupled with a qPCR approach that has proven to be useful strategy for multiplex detections and quantifications of multiples targets (Mokany *et al.*, 2013).

Current epidemiological trends suggest that IFIs claim the lives of around 1.5 million people every year and *Candida* species are recognised among the common fungal pathogens and a significant cause of nosocomial infections (Wisplinghoff *et al.*,

2014; Brown *et al.*, 2012). As a pilot study, an MNAzyme system was designed to identify a pan-fungal DNA biomarker sequence present in all pathogenic fungal species tested. The pan-fungal DNA biomarker is part of the D1/D2 domain within the rDNA locus. As yet, this technique is still laboratory based, but the aim in the future is to develop multiplex assay-based detection kits that can be taken into the field to assess IFIs.

6.2 Experimental Results

6.2.1 Selection of DNA biomarker target sequences

Loci of primers ITS4 and LR1 were assessed and found to be conserved in all the pathogenic fungi species (Figure 6.1). Primer ITS4 is a reverse primer that universally amplifies the ITS2 region in combination with a forward primer, either with ITS3 or ITS1. The conserved sequences around the 5'end and 3'end of the whole ITS4 and LR1 provide a suitable length of the target sequence up to 43 bp. The query sequence was searched in BLAST nucleotide database and resulted in 100% homology hits for the fungal species in the top 100 subject sequences.

Analysis of the pan-fungal DNA biomarker LS266 was found with sequence variation in *Fusarium solani* strains and hindered the sequence to be used as a target sequence for fungal detection in MNAzyme assay. Moreover, two points of single nucleotide changes were observed at the 5' and 3' end of LS266 sequences of the *F. solani* strains and in several *Candida* species strains. This limits the possibility of the sequence to be expanded to match an ideal length of AF sequence.

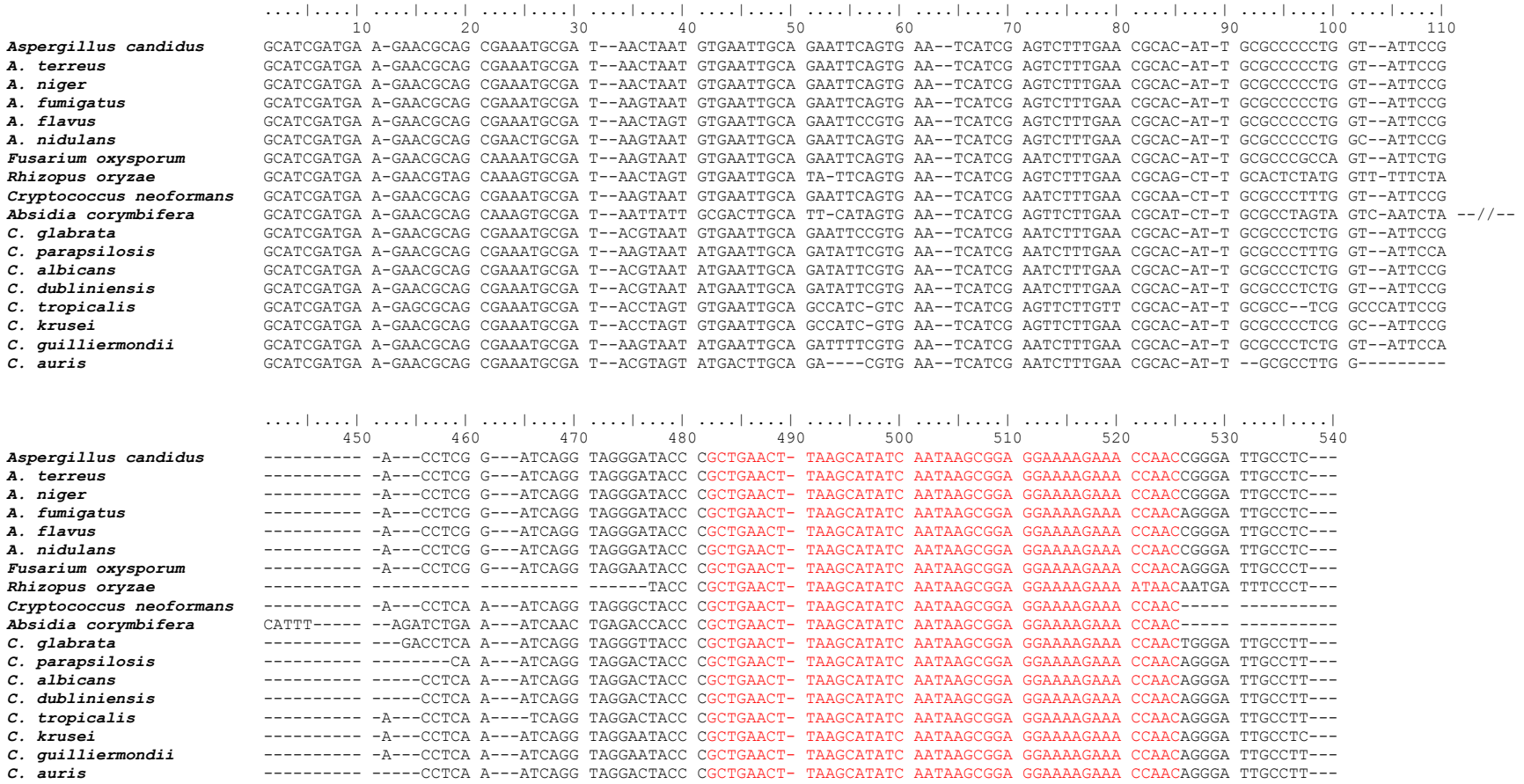

Figure 6. 1 Multiple-sequence alignment of the partial ITS and LSU regions of the fungal rDNA sequence. The conserved region around primers ITS4 and LR1 sequences (in red) for 43 nucleotides pan-fungal AF (AF-ITS4LR1).

6.2.2 Basic components of MNAzyme for fungal detection

The MNAzyme Pan-Fungal assay was designed based on the universal partial enzymes and nucleic acid substrate (probe) that were developed by Mokany, Bone, Young, *et al.*, (2010) (Figure 6.2). The Partzymes were derived from the 10 – 23 DNAzyme, which are single strands of deoxyribozymes comprising of a catalytic core of 15 deoxynucleotides, flanked by two specific substrate binding arms of seven to eight deoxynucleotides each (Santoro & Joyce, 1997). The substrate is bound through Watson-Crick base pairing against substrate binding arms and is cleaved at a specific site with RNA bases on the substrate. The substrate is a dual-labelled probe that generates a fluorescent signal upon the cleavage and can be detected and monitored in real-time.

In this study, the MNAzyme Pan-Fungal assay developed to detect fungal DNA biomarker as an AF or input sequence. The sequences of Partzymes were altered at the sensor arms to match the target sequence of interest and each constituent arrangement on the sequences has been detailed in Table 6.1. Although, the current assay would need further developing to incorporate with amplification steps, it may provide a concrete platform for the detection of fungal species in isothermal reaction. In the technical aspect, the 3'end of each Partzyme was phosphorylated to prevent it from being consumed by some 3' exonucleases and to block extension by DNA polymerases hence, to make it feasible in a qPCR approach.

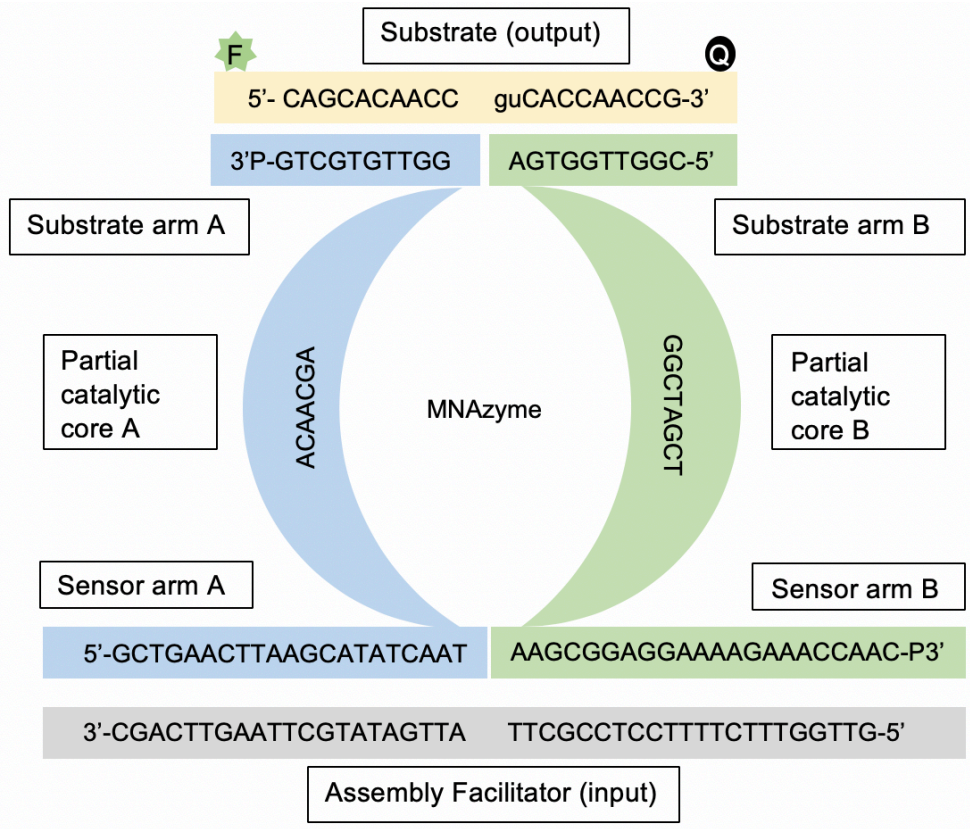

Figure 6. 2 Structural components of the MNAzyme Pan-Fungal assay. The nucleotide sequence of Partzyme A (in blue) is present in a 5' to 3' direction, composed of a sensor binding domain (sensor arm), partial catalytic core and substrate binding domain (substrate arm) to hybridise towards 5'end of substrate (in yellow). Meanwhile, the nucleotide sequence of Partzyme B (in green) is present in a 5' to 3' direction composed of a substrate binding domain (substrate arm), partial catalytic core and sensor binding domain (sensor arm) portion capable of binding to the same AF (in grey) adjacent to the Partzyme A sensor arm. The Partzymes A and B were phosphorylated (P) at 3'end. The nucleic acid substrate was labelled with fluorophore (F) at 5'end and quencher (Q) at 3'end.

Table 6. 1 List of sequences used in MNAzyme assay for fungal detection.

Component	Name	Sequence (5'→3') *
Partzyme A	ITS4LR1A/3-P	GCTGAACTTAAGCATATCAAT ACAACGA *GGTTGTGCTG* -P
Partzyme B	ITS4LR1B/3-P	*CGGTTGGTGA* GGCTAGCT AAGCGGAGGAAAAGAAACCAAC-P
Substrate	Sub3-JB	JOE- CAGCACAACCguCACCAACCG BHQ1
AF	AF-ITS4LR1 (pan-fungal)	GTTGGTTTCTTTTCCTCCGCTTATTGATA TGCTTAAGTTCAGC

*Nucleotides underlined are partial catalytic core sequences and those in italics form part of the substrate-binding arm. The "-P" at the end of the partzyme sequence indicates that the oligonucleotide was 3' phosphorylated. RNA nucleotides (-g and -u) represents Guanine and Uracil present in the substrate sequence; JOE, 6-carboxy-4',5'-dichloro-2',7'-dimethoxyfluoresceine; BHQ1, Black Hole Quencher 1

6.2.3 Optimisations of MNAzyme assay

Several paramount parameters such as temperature, concentration of Partzymes and concentration of metal ion cofactor in the reactions were optimised to produce signals for the highest enzymatic activity.

6.2.3.1 Optimisation of isothermal temperature

Catalytic activity of the MNAzyme Pan-Fungal assay was assessed at various temperatures to determine the turnover (Figure 6.3). A series of experiments tested the temperatures at 30°C, 35°C, 40°C, 45°C, 50°C, 52°C, 55°C, 57°C, 59°C and 64°C, using isothermal direct detection method. The K_{obs} values were obtained by performing

a fit a hyperbolic equation to the fluorescence versus time data using Prism Version 7.0 statistical package (GraphPad Software) The enzymatic activity measured shown increased the substrate catalytic rate dramatically by almost 10 times from 40°C to 45°C and further increased to the highest point at 50°C. The data shown the activity decreased for the assay exposed to higher than 50°C and no significant activity at 60°C.

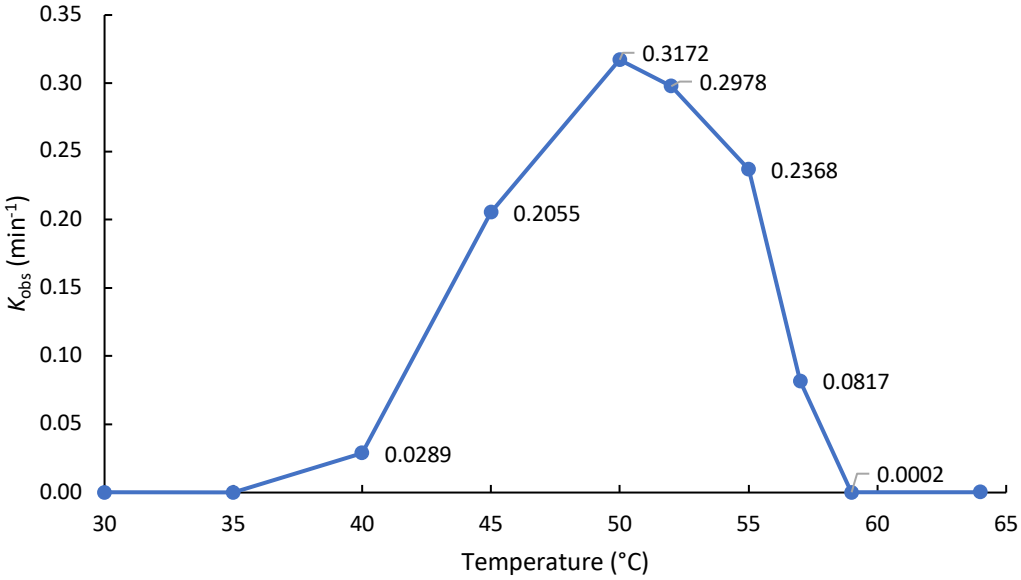

Figure 6. 3 Enzymatic activity against different isothermal temperature. The MNAzyme Pan-Fungal assay was tested at various temperature to determine the catalytic rate. The optimal temperature for cleavage of the 19 nucleotides substrate in this assay is 50°C with the cleavage rate at 3.2 x 10^{-1} min^{-1}. The reactions containing 50 mM $MgCl_2$, 0.2 µM substrate, 0.05 µM Partzyme and 0.2 µM AF sequence (AF-ITS4LR1).

6.2.3.2 Optimisation of Partzyme concentration

The purpose of this optimisation was to achieve measurable fluorescence signal from the starting time against the negative control (reaction without AF). Initially, enzyme activity was observed too high from the starting point as the concentration of Partzymes (0.2 μM) was adapted from Mokany, Bone, Young, *et al.*, (2010) into our MNAzyme assay. It could be thought that different set of nucleic acid substrate, design and constituents of Partzyme used in the MNAzyme, as well as level of sensitivity of the real-time PCR machine may contributes to this factor. In the experiment conducted, high signals readout, at approximately two fluorescence a.u., appeared at the first cycle of reaction although, both Partzyme A and B final concentrations were reduced to 0.1 μM (Figure 6.4, panel A).

The result testifies that, the reaction Partzymes concentration of 0.05 μM started the substrate hydrolysis at the same point as the negative control despite of abundance of AF (Figure 6.4, panel B). There was no increased signal over the time for the reactions with 0.01 μM and 0.005 μM. The Partzyme concentration in the Pan-Fungal assay is 0.05 μM, and this concentration was maintained throughout the study.

Optimisation of Partzyme Concentrations in MNAzyme Pan-Fungal Assay

A)

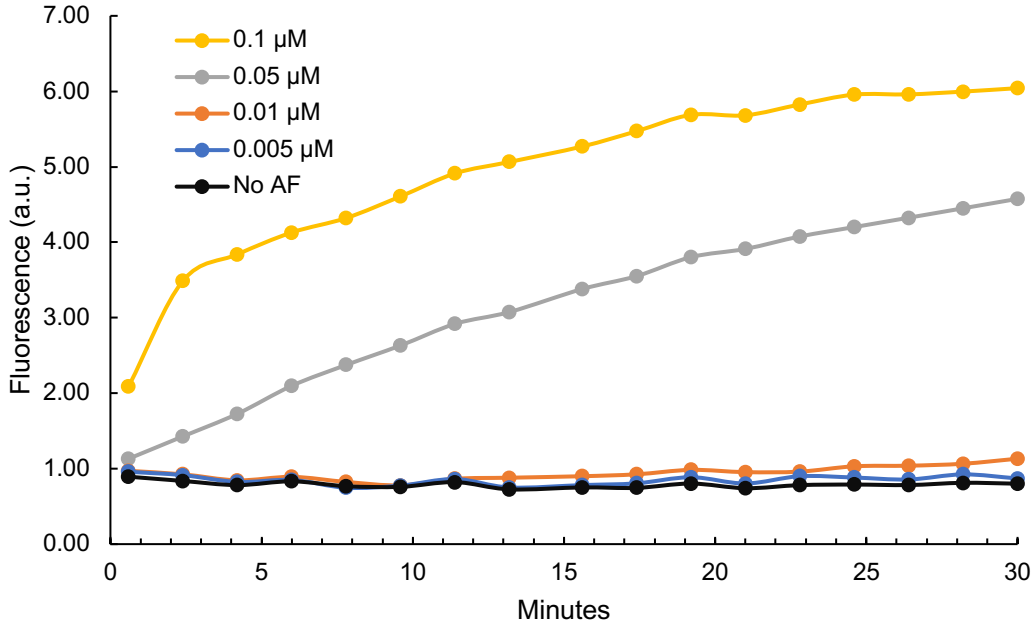

B)

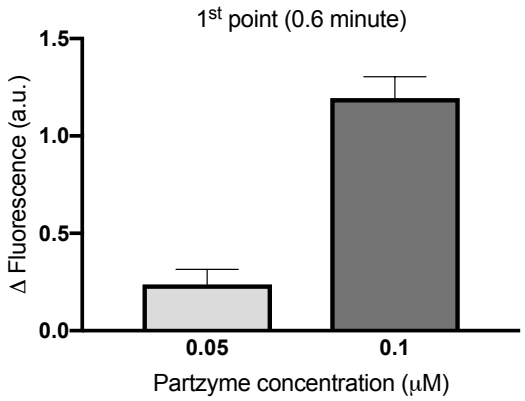

Figure 6. 4 The effect of the Partzyme concentrations towards enzyme activity determined at the first signal point. Panel A) Higher rate of substrate hydrolysis in the reaction with 0.1 µM partzyme compared to 0.05 µM partzyme in the first 2.5 minutes. No activity in the reaction with 0.01 µM and 0.005 µM Partzymes (No AF). **Panel B**) Fluorescence changes against the negative control (No AF) at the starting data collection point (0.6 minute) for the reactions with 0.05 µM and 0.1 µM Partzyme concentrations. The error bars represent the SD of the data from two independent experiments.

6.2.3.3 Optimisation of $MgCl_2$ concentration

The concentration of $MgCl_2$ was optimised for the highest and stable enzymatic activity possible in the MNAzyme Pan-Fungal assay. The concentration of $MgCl_2$ is generally higher than in other qPCR protocols since the metal ion cofactor is vital for the MNAzyme's catalytic activity. In this experiment, 8 mM and 12 mM of $MgCl_2$ shows lower catalytic activities compared to reactions with 6 mM and 10 mM $MgCl_2$ before the signals reached plateau (Figure 6.5, i). The reaction with 10 mM $MgCl_2$ exhibited the highest fluorescence signal output achieved by catalytic activity and the signal surpassing the highest concentration (12 mM $MgCl_2$) used in this experiment. It is reported that 8 mM is suitable for a single target reactions and may be increased to 10 mM for multiplex reactions detecting three or more targets (Mokany *et al.*, 2013). In any condition with absence of magnesium, there was no evidence of exponential accumulation of cleaved substrate (Figure 6.5, ii). Interestingly, constant high intensity of the fluorescence signals from the substrate (with no activity) were noted although in reactions with incomplete assay's components.

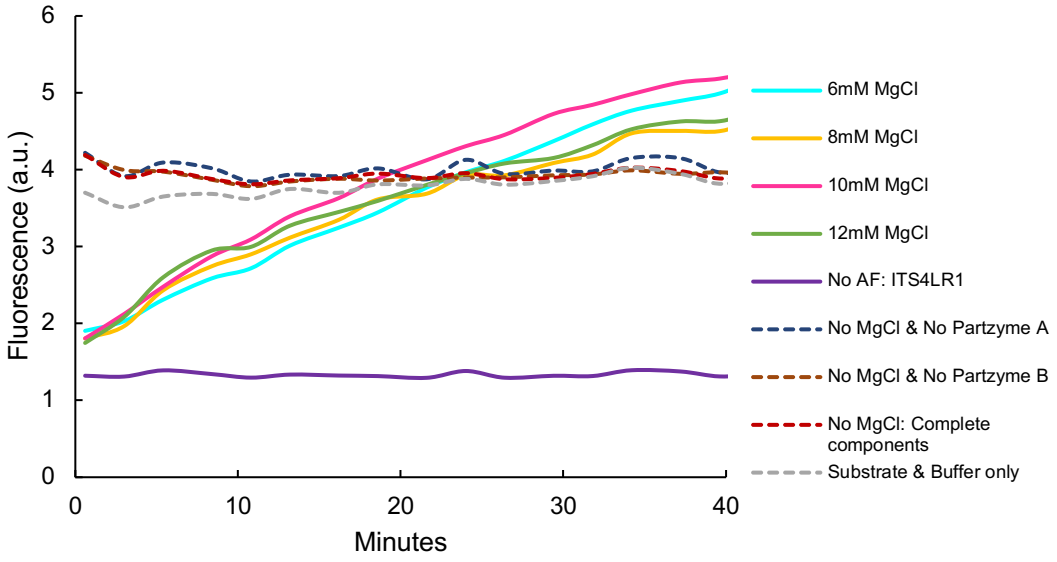

Figure 6. 5 Effect of $MgCl_2$ and different concentrations of $MgCl_2$ on MNAzyme cleavage activity. The isothermal detection of the pan-fungal AF in various concentrations of magnesium in the MNAzyme assay. The detection was performed; **i)** in different concentrations of $MgCl_2$ (6 mM, 8 mM, 10 mM and 12 mM) and negative control (no AF) represented as solid lines; **ii)** in the absence of $MgCl_2$ either in the reaction with complete parts of MNAzyme or incomplete part of MNAzyme (No Partzyme A, No Partzyme B) represented as dotted lines. In all cases, the MNAzyme reactions contained 0.2 µM of the pan-fungal AF (AF ITS4LR) except of the negative control (No AF ITS4LR1) and the background reaction which only contained dual-labelled probe in the PCR buffer.

In a separate experiment, higher concentrations of $MgCl_2$ in the reaction were tested to observe their effect towards the MNAzyme activity. In the original MNAzyme studies, various $MgCl_2$ concentrations were used and can be categorised according to the experiments performed. The concentration of $MgCl_2$ at 8 mM was used for detection in real-time PCR amplification; 25 mM for isothermal direct detection protocol and; 50 mM in the kinetics of MNAzymes catalysis experiments (Mokany *et al.*, 2013, 2010). In the isothermal direct detection method of the MNAzyme Pan-Fungal assay, the results showed that the highest fluorescence signal

output was in the reaction with 10 mM $MgCl_2$ but, it has wider error bar between its replicates (Figure 6.6). The reactions with $MgCl_2$ tested at 25 mM and 50 mM yield stable fluorescence signals between its replicates and denote from the narrow error bars.

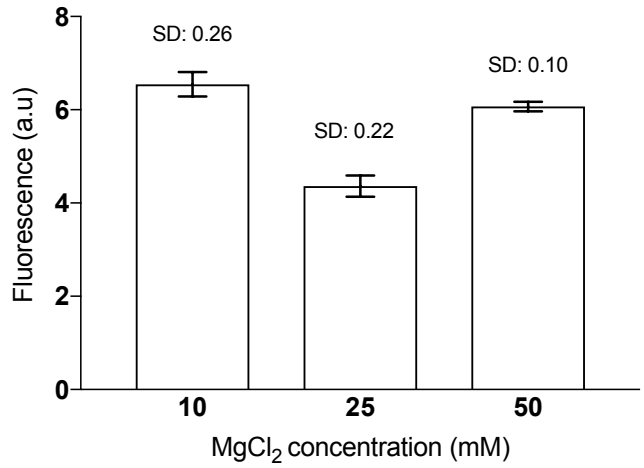

Figure 6. 6 The MNAzyme Pan-Fungal activity at high $MgCl_2$ concentrations. The mean of the fluorescence signals until the reaction plateaus with error bars depict SD between the triplicates in the MNAzyme Pan-Fungal assay with 10 mM, 25 mM and, 50 mM of MgCl2. All reactions were tested in 50°C with constant concentrations of enzyme, 0.05 μM; substrate, 0.2 μM and pan-fungal AF, 0.2 μM.

6.2.4 Specificity testing of MNAzyme assay for detection of the synthetic AF sequence

The purpose of this experiment was to assess the specificity of the MNAzyme Pan-Fungal assay towards any possible detection of inaccurate target nucleic acids. The experiment was conducted in the various reaction controls. The direct detection of the pan-fungal AF as the positive control was compared against six different control reactions. Control 1 contained an AF sequence with a single point mutation (AF-

ITS4LR1mut) and Control 2 with a totally different AF sequence (AF-RO5). The pan-fungal AF was also tested for detection in the reaction with the mutated partial catalytic core sequence of the Partzyme A (ITS4LR1A/3mut) represented as a Control 3 and mutated partial catalytic core sequence of the Partzyme B (ITS4LR1B/3mut) represented as a Control 4. The Pan-Fungal assay was also tested with incomplete components such as without one of the Partzymes; no Partzyme A for Control 5 and, no Partzyme B for Control 6. As a negative control, the reaction with no AF sequence (No AF) was included in the reaction. All controls were tested in an optimum MNAzyme reactions conditions described in the Materials and Methods chapter.

The results of which are shown in Figure 6.7, the assay performance is not compromised, even with one nucleotide change in the sequence of the AF. The assay results in an increase intensity of fluorescence signal (up to six fluorescence a.u.), demonstrating cleavage activity, when only all correct components are present in the system. In the absence of any component that prevents the formation of complete MNAzyme systems, there is no catalytic activity to cleave the substrates, and therefore no fluorescence signals can be observed. This is consistent with experiments performed by Mokany, Bone, Young, *et al.*, (2010), reported no cleavage activity by MNAzyme Mz2 in the reactions conditions without one of the Partzymes, or a different sequence of an AF or with a point mutation in one of the partial catalytic domains. This characteristic is important for specific detection of the fungal DNA biomarkers and preventing cross-reactions or misdetection with closely related fungal species.

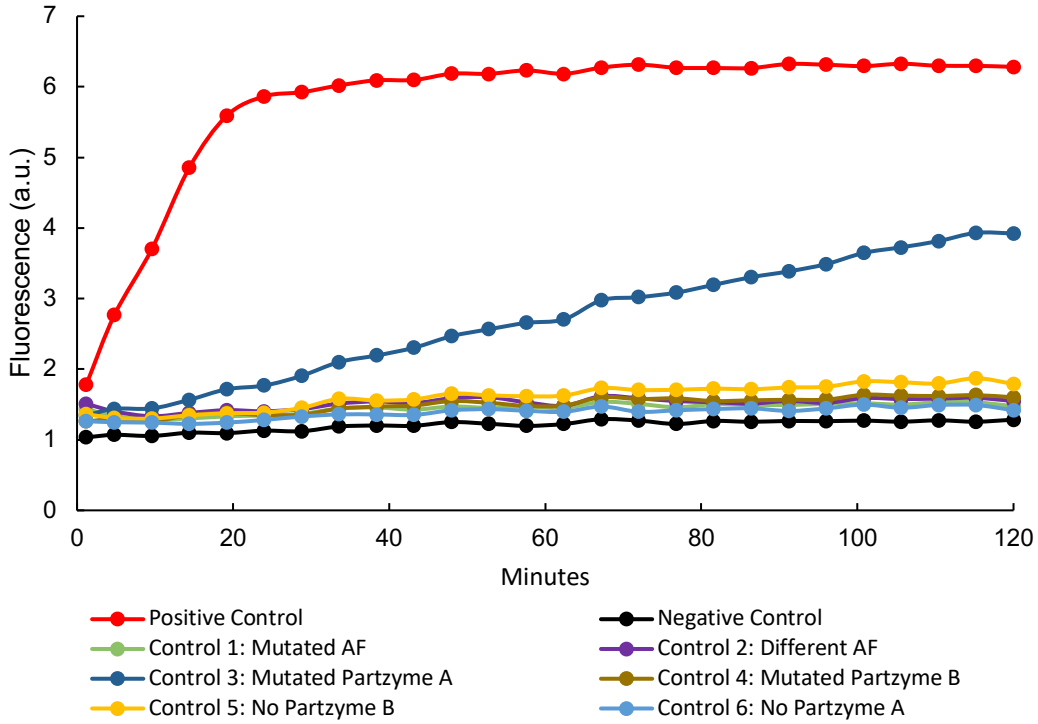

Figure 6. 7 Specificity test of MNAzyme Pan-Fungal assay in six reaction controls. The positive control contained complete and correct components of MNAzyme, Partzyme A (ITS4LR1A/3-P), Partzyme B (ITS4LR1B/3-P) and AF (AF-ITS4LR1), and a negative control contained Partzyme A (ITS4LR1A/3-P) and B (ITS4LR1B/3-P) without AF. **Control 1:** Partzyme A (ITS4LR1A/3-P), Partzyme B (ITS4LR1B/3-P) with mutated AF (AF-ITS4LR1mut); **Control 2:** A (ITS4LR1A/3-P) and Partzyme B (ITS4LR1B/3-P) with totally noncomplementary sequence of AF (AF-RO5); **Control 3:** Partzyme B (ITS4LR1B/3) and AF (AF-ITS4LR1) with mutated Partzyme A (ITS4LR1A/3mut-P); **Control 4:** Partzyme A (ITS4LR1A/3-P) and AF (AF-ITS4LR1) with mutated Partzyme B (ITS4LR1B/3mut); **Control 5:** Partzyme A (ITS4LR1A/3-P) only with AF (AF-ITS4LR1); **Control 6:** Partzyme B (ITS4LR1B/3-P) only with AF (AF-ITS4LR1).

6.2.5 Limit of Detection of an Assembly Facilitator

A limit of detection experiment was performed to determine the lowest concentration of AF detectable by the MNAzyme Pan-Fungal assay. Three independent experiments were performed, and each reaction was carried out in triplicate and monitored in real time at 36-second intervals for an hour at 52°C. Isothermal direct detection method was prepared in 25 μL total reaction under optimum conditions. Reactions contained a range of pan-fungal AF (AF-ITS4LR1) concentrations (0.2 μM, 0.1 μM, 0.75 μM, 0.025 μM, 0.01 μM, 0.0075 μM, 0.0025 μM, 0.001 μM and 0.0005 μM) and no AF (negative control). Reactions contained the optimal concentrations that were determined previously, with Partzyme A and B concentrations at 0.05 μM and $MgCl_2$ at 10 mM. The assay limit of detection was determined by reducing the concentration of the AF until no accumulation of fluorescence signal was detected. Consistent outcomes were obtained throughout the experiments, with the lowest concentration of AF detectable at 0.0025 μM (Figure 6.8). This equals to approximately 62.5 fmol or 3.76×10^{10} copies of the AF nucleic acid sequence in a reaction. Further lower concentrations from 0.001 μM and 0.0005 μM lead to the MNAzyme becoming catalytically inactive due to lack of target sequence in the assay. An increase in fluorescence, demonstrated cleavage activity, which observed and compared with the signal of the negative control reaction. Consistently in the experiments performed, 0.75 μM of pan-fungal AF showed a higher detection signal than 0.1 μM.

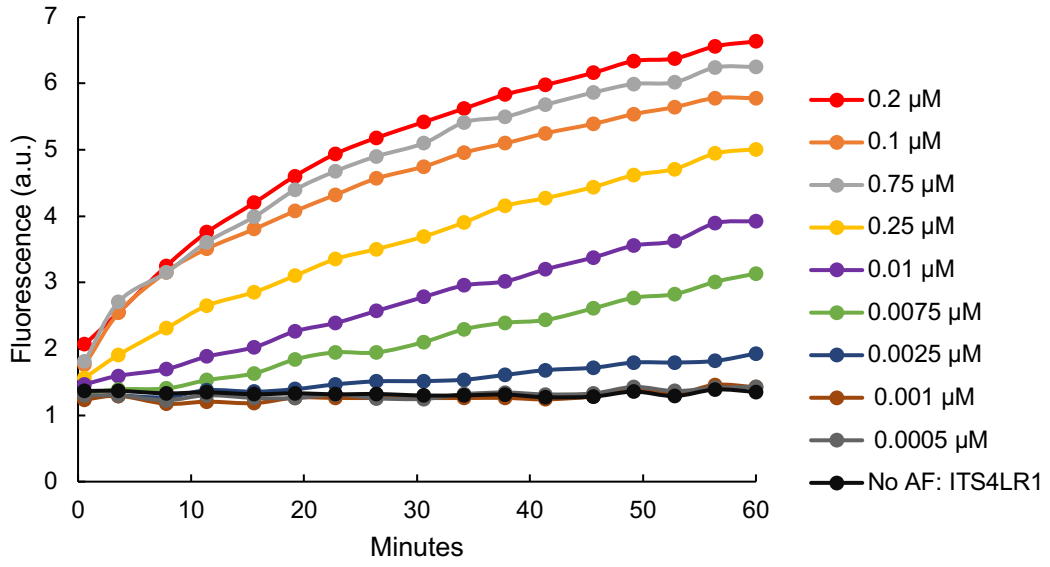

Figure 6. 8 Limit of detection of the MNAzyme Pan-Fungal assay. Test reactions contained Partzyme A (ITS4LR1/A-3), Partzyme B (ITS4LR1/B-3) and, substrate (Sub3-JB), with different concentrations of target sequence AF-ITS4LR1 (0.2 µM, 0.1 µM, 0.75 µM, 0.025 µM, 0.01 µM, 0.0075 µM, 0.0025 µM, 0.001 µM and 0.0005 µM) and the negative control with no AF (No AF-ITS4LR1).

6.2.6 *In vitro* detection of the *C. albicans* DNA in an isothermal MNAzyme Pan-Fungal assay

This experiment was performed to prove the concept that MNAzymes could produce significant catalytic activity by detection of *C. albicans* genomic DNA. In this experiment, the input was an amplified *C. albicans* double-stranded DNA containing the pan-fungal biomarker sequence. Prior to the detection in the MNAzyme reaction, the amplicon was allowed to denature to provide an access to the sensor binding domain towards the complementary target sequence. The total length of the amplicon from the primer sites was 84 bp, compared to the synthetic AF sequence which is only 43 bp that fits perfectly against the sensor binding arms. From the results obtained, an increase in fluorescence signal can be seen in the reactions with the *C. albicans* amplified DNA, until the signal levelled off approximately after 45 minutes, which

was achieved as the enzymes catalysed all substrates completely (Figure 6.9). As expected, the fluorescence signal in the positive control reaction, containing a synthetic AF sequence, rapidly levelled off within the first 10 minutes, demonstrating a quick cleavage activity.

The experimental demonstration for detection of *C. albicans* double-stranded DNA in the isothermal MNAzyme direct detection method was used the same molar concentration (0.2 μM) as to the concentration of synthetic sequence of an AF (Positive Control) in a 25 μL reaction. The *C. albicans* target DNA used was a thousand-fold higher copy number (3.43×10^{12} copies) than the AF sequence; however, the reaction rate was observed to be slower compared to the AF reaction. The assay catalytic rate, K_{obs} obtained in the reaction with the target amplicon was 3.6×10^{-2} min^{-1} meanwhile, the positive control reaction had a higher rate of 2.1×10^{-1} min^{-1}. This result suggests that the double-stranded DNA renatured conforming to the base pairing arrangement after the high temperature disrupts the hydrogen bonds between the bases. The complexity of the double-stranded DNA and the complementary of the target sequence to the Partzymes' sensor arms to hybridise could influence the enzymes catalytic activity. Further investigations could be performed to improve the experimental results by incorporating the amplification step into the MNAzyme assay for real-time detection and quantification of the DNA biomarkers.

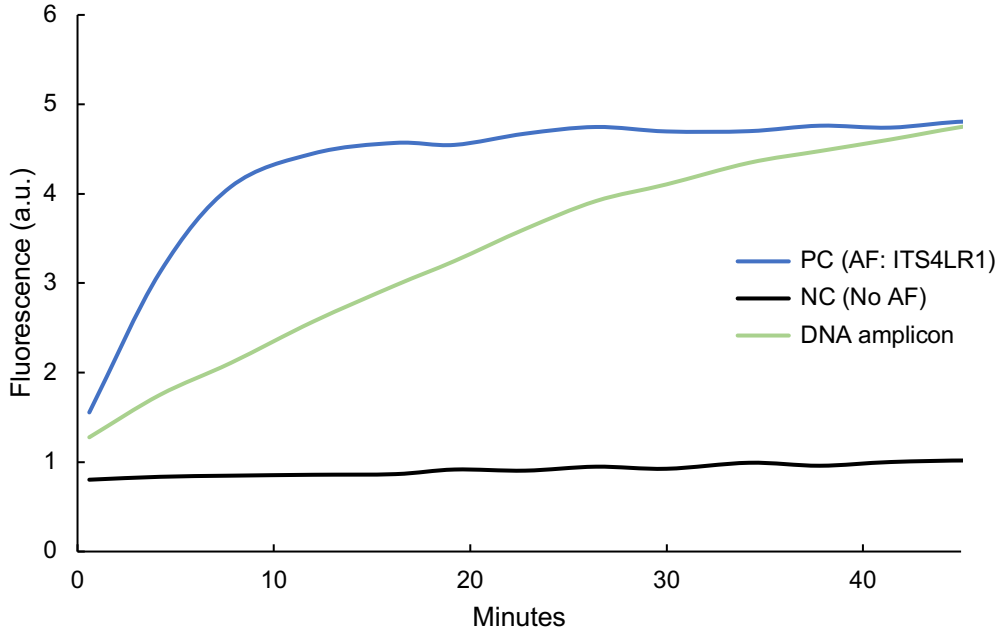

Figure 6. 9 MNAzyme isothermal detection of *C. albicans* genomic DNA. Signals of cleavage activity for detection of an amplified *C. albicans* DNA in the MNAzyme Pan-Fungal assay. The experiment contained the synthetic target AF sequence (AF-ITS4LR1) at 0.2 µM as a positive control (PC) and the reaction with no AF as a negative control (NC).

6.2.7 Assessing the MNAzyme Pan-Fungal assay Kinetic Activity

Kinetic analysis of the MNAzyme Pan-Fungal assay was initiated by converting the fluorescence data, in arbitrary units, into reaction velocities. To do so, a standard curve graph was plotted for a range of concentrations of the processed substrate (1, 0.5, 0.25, 0.125, 0.0625 and 0.00311 μM of Sub3-JB ½). The processed substrate in this study was a half probe sequence from the 5' end labelled with the JOE reporter dye (the sequence in Materials and Methods chapter). An initial fluorescence signal detected in various substrate concentrations, was subjected to linear formula generated, y = 51.067(x) – 3.0966; correlation coefficient, R^2= 0.9926 to assess the concentration of the substrate that was successfully cleaved at the first 18 seconds by the enzymes (Figure 6.10). The values obtained were used to calculate the gradient to gather enzyme activity values for different substrate concentrations used in the assay (Table 6.2).

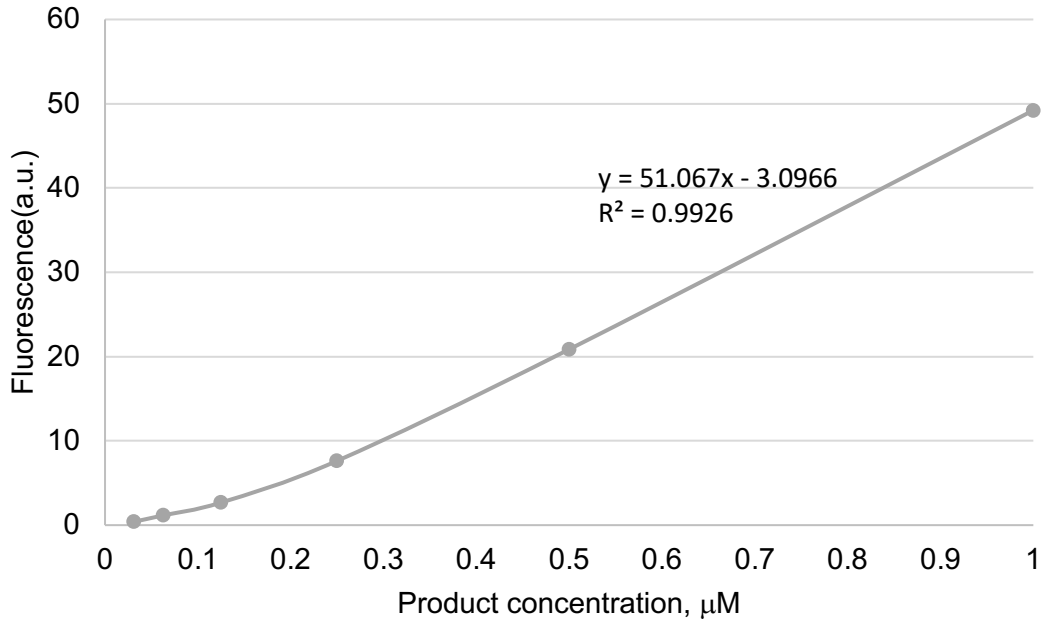

Figure 6. 10 Standard curve: total cleaved substrate. Standard curve generated from different concentrations of the cleaved substrate (Subs3-JB ½) that emitted fluorescence signal at the first 18 seconds of detections.

Table 6. 2 The calculated gradient, m (data set obtained from the standard curve).

Substrate concentration (μM)	Gradient value			
	Test 1	Test 2	Test 3	Average ± SD
1.00	43.17	43.81	43.90	43.63 ± 0.40
0.75	41.56	41.73	41.75	41.68 ± 0.10
0.50	38.30	38.69	37.75	38.25 ± 0.48
0.25	30.75	30.61	31.19	30.85 ± 0.30
0.20	28.18	27.08	27.73	27.66 ± 0.55
0.15	23.97	24.32	24.07	24.12 ± 0.18
0.10	20.25	20.37	18.88	19.83 ± 0.83

Enzyme kinetic analysis was performed to determine the enzyme's K_m and V_{max} for the MNAzyme Pan-Fungal assay (Table 6.3 and Figure 6.11). In definition, K_m is the substrate concentration needed to achieve a half-maximum enzyme velocity. Whereas V_{max} is the maximum enzyme velocity, it is the velocity of the enzyme extrapolated to very high concentrations of substrate, so its value is almost always higher than any velocity measured in the experiment. In fact, V_{max} is only approached but never attained. The V_{max} is determined by the total enzyme concentration (Et) in a reaction and the rate at which the enzyme can convert substrate to product (K_{cat}). Therefore, K_{cat} is equal to V_{max} divide by Et ($K_{cat} = V_{max}/Et$).

Table 6. 3 Michaelis-Menten analysis of V_{max} and K_m for the MNAzyme Pan-Fungal assay. It is also noted that the P value from the variation among triplicates is larger than 0.05 and suggests that the data was suitable to fit the model (values in bold). Table result obtained from Prism statistical pack version 7, GraphPad Software Inc.

	Enzyme Activity
Michaelis-Menten	
Best-fit values	
Vmax	50.62
Km	0.1615
Std. Error	
Vmax	0.3388
Km	0.003411
95% CI (profile likelihood)	
Vmax	49.91 to 51.33
Km	0.1545 to 0.1688
Goodness of Fit	
Degrees of Freedom	19
R squared	0.9971
Sum of Squares	4.274
Sy.x	0.4743
Replicates test for lack of fit	
SD replicates	0.4636
SD lack of fit	0.5030
Discrepancy (F)	1.177
P value	0.3686
Evidence of inadequate model?	No
Constraints	
Km	Km > 0
Number of points	
# of X values	21
# Y values analyzed	21

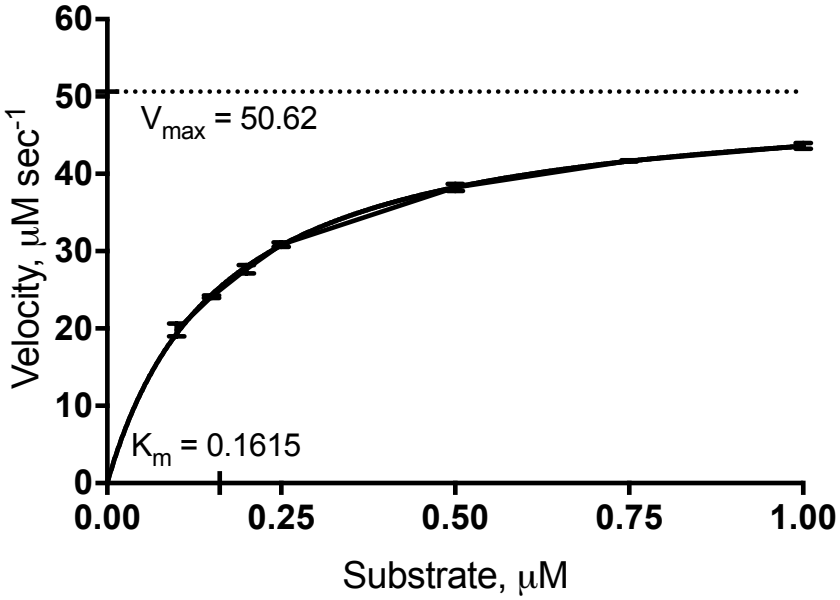

Figure 6. 11 Michaelis-Menten analysis for the MNAzyme Pan-Fungal assay. Values of the maximum enzyme velocity, V_{max} = 50.62 μM per second and the affinity of the enzyme for the substrate assessed by the Michaelis-Menten constant, K_m= 0.1615 μM. The error bars represent the SD of the data from three independent experiments.

The turnover was compared by measuring the k_{cat}. The value for the Pan-Fungal assay was determined (k_{cat} = 16.87 min^{-1}) by constraining the enzyme site present to a constant value (Et = 0.05), and graph generated was identical to the curve defined by the Michaelis-Menten model (Figure 6.11). K_{cat} and k_m values for the MNAzyme Pan-Fungal were 16.87 min^{-1} and 0.1615 μM, respectively. Therefore, the catalytic efficacy (K_{cat}/ K_m) of the MNAzyme Pan-Fungal can be determined at 1.04×10^8 min^{-1} M^{-1}.

Table 6. 4 Turnover number, K_{cat} value by specifying the concentration of total enzyme (Et) of the MNAzyme Pan-Fungal assay. Table result obtained from Prism GraphPad statistical pack.

	Enzyme Activity
kcat	
Best-fit values	
Et	= 0.05000
kcat	1012
Km	0.1615
Vmax	= 50.62
Std. Error	
kcat	6.776
Km	0.003411
95% CI (profile likelihood)	
kcat	998.2 to 1027
Km	0.1545 to 0.1688
Goodness of Fit	
Degrees of Freedom	19
R squared	0.9971
Sum of Squares	4.274
Sy.x	0.4743
Replicates test for lack of fit	
SD replicates	0.4636
SD lack of fit	0.5030
Discrepancy (F)	1.177
P value	0.3686
Evidence of inadequate model?	No
Constraints	
Et	Et = 0.05
Number of points	
# of X values	21
# Y values analyzed	21

6.3 Discussion

The screening for the target sequence in the MNAzymes assay was based on comparative sequence analysis. The engineering of the MNAzymes input AF sequence is challenging with the requirement of a long target sequence. The MNAzyme fungal DNA biomarkers were screened for the length of ~40 bp and examined for their specificity before it could be adapted as an AF. The practical analysis strategy applied for searching of a target sequence examined from the closely positioned universal fungal primers and, found the combined primers ITS4 and LR1 as a pan-fungal AF in the assay. Among other loci within the regions that were examined are PCR primer sites LS266 and NL4b, however these were not ideal to be used as an AF. In contrast, the standard PCR primers and specific probe-based detection sequence are 20-25 bp with either two or three levels of the specificity determinants derived from the recognition of two PCR primers and/or one target-specific probe hybridisation site. Meanwhile, a novel MNAzyme qPCR assay relies on the synergistic actions of amplification and detection with four levels of specificity originated from two primer sites and two Partzymes target-binding site on the AF or amplified products (Mokany *et al.*, 2013). The pan-fungal AF sequence is a specific target for fungal detection, while other components involved in the MNAzyme system contribute to its function as a probe for the specific key.

The nucleic acid sensing machineries of the MNAzymes are composed of multiple, nucleic acid oligonucleotides which are catalytically active in the presence of the target sequences. This class of enzyme has been modified from a single molecular DNAzymes to increase enzyme functionality and versatility (Mokany *et al.*, 2010). The DNAzymes split at the catalytic core (domains required for enzyme activity) into two parts and form a partial catalytic core (inactive state of enzyme).

Briefly, the MNAzymes are composed of oligonucleotide partzymes, each of which contain a partial catalytic core flanked by a substrate-binding domain (substrate arm) and sensor-binding domain (sensor arm) which can be designed to complement the specific target AF. In the events of the target detection, the sensor-arms bind to the AF sequence and align adjacently which re-unite the catalytic core. Once assembled, the catalytic core becomes active and capable of cleaving a nucleic acid substrate in between of the fluorophore and quencher labels to produce a fluorescent signal detected in the real-time PCR instrument. The difference in nucleotide positions splitting the whole core has shown a substantial impact on the enzyme activity (Mokany *et al.*, 2010). In this study, the MNAzyme Pan-Fungal assay was employed the optimum design of partial catalytic core which was divided between T^8 and A^9 of the DNAzyme 10–23 enzymatic core. MNAzyme features increase the functionality of nucleic acid enzymes enabling it to be incorporated with any specific input, which in turn simplifies the development of biosensors. The catalytic active MNAzyme modifies the hybridised substrate, thus generating an enzymatically amplified output signal.

Numerous different substrates available could be used to design multiple or different target sequences, and this has tremendously increased the practicality of MNAzyme technology. The qPCR assay that use TaqMan® hydrolysis probe and PCR primers must be designed and optimised the target probe for detection of the amplified products in each of the new assay. The development of the multiplex TaqMan-based PCR assay for the detection of two or more targets are complex and involve further optimisations which can be time-consuming. In contrast, exemplified by at least one universal substrate reporter probe for detection of a target sequence, the same probe can be engineered for the detection of different targets in the qPCR assay (Mokany *et al.*, 2013). The detection of the new target sequence requires minimal optimisation of

the sensor-binding domain and the rest are based on the universal characteristics of the MNAzyme oligonucleotides which simplifies assay design and development (Bone *et al.*, 2014). Although the substrate probe is the most expensive to manufacture with the integration of ribonucleotides and deoxyribonucleotides labelled with the fluorophore and quencher moieties, this component is completely universal and can be used for different MNAzyme assays.

Moreover, each substrate could be labelled with a different compatible fluorophore and quencher. Nevertheless, properties of each fluorophore, such as excitation and emission wavelength values and the analyser compatibility, must be carefully considered in designing a multiplex assay. Each real-time PCR instrument has a fixed spectrum to detect the fluorescence signals especially involving multiple (more than two) wavelength fluorescence readouts at the same time. Real-time PCR machines such as Roche Light Cycler® 480 have recommended combinations of dyes to use in the multiplex assay detection for up to four detections simultaneously. Issues dealing with the multiple detections in real-time PCR machines, such as "crosstalk" could result in one filter combination that may pick up signals from a dye measured by another channel due an overlap of the emission spectra of the dyes. This problem may cause result misinterpretations and a loss of sensitivity. Therefore, optimisation steps such as Colour Compensation analysis should be performed before running the real experiment (Molenkamp *et al.*, 2007).

In this study, sequences of the substrates and substrate binding arms in the MNAzyme Pan-Fungal assay were designed to be a total 19 nucleotides in length. Substrate binding arms were designed to be complementary towards the substrate sequence. The nucleic acids substrate sequence used in the MNAzyme Pan-Fungal assay is Sub 3-JB (Table 6.1) which was optimised by Mokany, Tan, Bone, *et al.*, (2013). The optimal temperature achieved in our study for the Pan-Fungal assay was

consistent with the isothermal temperature used in other studies, which is 50°C (Gao, Shimada & Maruyama, 2015; Bone, Hasick, Lima, *et al.*, 2014). Recently, re-engineering of the MNAzyme's substrate and substrate binding domains with a shorter sequence length has been demonstrated its potential to function at room temperature (Ven *et al.*, 2019). It also has been proven that the optimum isothermal temperature for MNAzyme is directly influenced by the length of the substrate binding arms (Ven *et al.*, 2019; Gao, Shimada & Maruyama, 2015). The needs for cycled and higher temperatures have limited the application of PCR-based assays in deprived resources area. Therefore, modification of MNAzyme assays with this enhancer will increase the adaptation of this technology to produce simple point-of-care diagnostic devices.

The MNAzyme Pan-Fungal assay has shown 100-fold higher catalytic activity compared to the MNAzyme assay developed by Gao, Shimada & Maruyama, (2015). Although their assay was developed using the same set of the partial catalytic core that was previously engineered by Mokany, Bone, Young, *et al.*, (2010), it shows the substrate cleavage rate, K_{obs} to be approximately 10^{-3} min^{-1}. In the same study, the reaction was optimised using an enhancer which had proved to increase the catalytic rate tremendously to the value around 10^{-1} min^{-1}. A cationic comb-type copolymer (PLL-*g*-Dex) facilitates hybridisation of the MNAzyme with the substrate. This cationic copolymer may improve the efficiency of less stable enzyme-substrate complexes, resulting in truncated substrate binding arms, which work at 37°C. Incorporation of this cationic copolymer into MNAzyme assay may increase the temperature window in which an MNAzyme is at maximum activity at a relatively lower temperature.

The Partzyme concentration in the MNAzyme Pan-Fungal assay was optimised to achieve measurable signal over time. The pan-fungal Partzyme concentration that gives closer signal starting point with the negative control was determined. Measuring

initial velocity of this enzyme activity is not possible since the initial signals were not comparable starting point either with negative control (contains no AF) or the lowest concentrations of Partzyme used in the reaction. In the study conducted by Bone et al., 0.04 μM concentrations of Partzyme A and Partzyme B were utilised in the MNAzyme developed to detect CAMP gene *Streptococcus agalactiae* (meningitis-causing bacterium) (Bone *et al.*, 2014). Multiple substrates were cleaved from the assembled MNAzyme over time and the detection signal amplified throughout the process until the substrate exhausted (plateau).

The concentration of magnesium in MNAzyme assays is generally higher (8 to 10 mM) than for the standard PCR or probe-based protocols (1 mM to 4 mM) since the magnesium is required for the catalytic activity (Mokany *et al.*, 2013). The low concentrations of magnesium ions may cause weak binding of the DNAzyme to the reporter substrate, causing no catalytic activity to occur (Yuan *et al.*, 2007). Another role of magnesium includes neutralisation of the negative charges of the DNA phosphate backbone, thus facilitating interactions between DNAzyme and the substrate (Cieslak *et al.*, 2003). The high concentrations of magnesium ions induce proper folding of the catalytic core allowing the enzyme to hydrolyse its substrate efficiently (Cieslak *et al.*, 2003). Therefore, it could be suggested that the magnesium is also responsible for maintaining the proximity of the fluorophore and quencher on the substrate. In the absence of magnesium, the fluorophore and quencher on the probe are widely separated that may cause by the disrupted random coil structure of the substrate itself (Juskowiak, 2011). Interestingly, the absence of magnesium in our experiments showed high fluorescence levels (Figure 6.5); this result was unexpected, but it could be suggested that substrate molecules disintegrated or cleaved instantaneously in the absence of magnesium, leading to an increase in the intensity of the fluorescence signal. Future investigations to test these arguments through

incubation of the substrate with and without magnesium and perform polyacrylamide gel electrophoresis (PAGE) to observe the cleaved or un-cleaved substrate bands could be performed. Overall, it seems that high concentration of the magnesium ions in a reaction is necessary to ensure active conformational of the substrate-enzyme complex and favour hydrolysis or cleavage of substrates.

The MNAzyme Pan-Fungal assay components – a substrate (Sub3-JB), Partzyme A (ITS4LR1A/3-P) and Partzyme B (ITS4LR1B/3-P), are associated with a specific target sequence designed from the fungal biomarker (AF-ITS4LR1) which then form a nucleic acid enzyme, capable to cleave the substrates and emits fluorescence which is subsequently detected and measured. It is reported that misidentification of fungal species frequently occurs in a clinical setting (Kwiatkowski *et al.*, 2012). This problem is due to many factors such as low specificity of the diagnostic assay used and the characteristic of the species itself, which may have a similar morphology to other species (Osei Sekyere, 2018). Therefore, MNAzymes, through the development of a species-specific assay could promise a more accurate identification of closely related species and rule out uncertainties.

The MNAzyme Pan-Fungal assay showed sensitivity (3.7×10^{10} molecules) one order of magnitude lower than MNAzyme assay demonstrated by Gao, Shimada & Maruyama 2015, of which the limit of detection was determined at 2.4×10^{9} molecules of an input sequence. An improved limit of an AF detection was demonstrated in the Mz1d assay at 5.0×10^{-6} μM, corresponds to 7.5×10^{7} molecules or 0.125 fmol in a 25 μL reaction (Mokany *et al.*, 2010). Several factors may affect the signal sensitivity including the difference in length of the sensor arms that significantly influenced the stability of MNAzyme complex (Gao, Shimada & Maruyama, 2015). Furthermore, it could be suggested that different substrates used in reactions may contribute to catalytic efficiency in the MNAzyme. From the higher range of AF

concentrations tested, 0.75 μM has a higher binding efficiency compared to 0.1 μM, and therefore has greater catalytic activity and cleaving more substrates.

The target sequence of *C. albicans* was amplified in a standard PCR amplification method before it was subjected for detection in the MNAzyme Pan-Fungal assay. The PCR product was purified to ensure it was not in contact with any PCR primers that could mislead the detection, as the forward primer (pITS4LR1-F) was designed in overlapping position with 5'end of the sensor arm. Ideally, the detection of the target sequence by MNAzymes is performed with amplification of the target region in a qPCR-MNAzyme assay (Mokany *et al.*, 2013). However, in this study, the reaction was included with the target sequence from *C. albicans* double-stranded genomic DNA for the direct-detection method of the MNAzyme assay. The amplicon was detected at 50°C isothermal conditions and showed consistent outcomes at the end of the reaction with the synthetic target sequence reactions (Figure 6.9). The K_{obs} values obtained (2.1×10^{-1} min^{-1}) are comparable with the values obtained from two designs of Partzymes Mz1c and Mz1e, which are 7.1×10^{-1} min^{-1} and 1.1×10^{-1} min^{-1}, respectively (Mokany *et al.*, 2010). Although the catalytic rate is lower in the reaction with the *C. albicans* DNA template, it could be improved by incorporating an amplification step into the MNAzyme direct detection method, a method established by Mokany, Tan, Bone, *et al.*, (2013).

An enzyme-catalysed reaction has a hyperbolic relationship between the rate of reaction and the concentration of substrate, as shown in Figure 6.11. At low concentrations of substrate, there is a steep increase in the rate of reaction with increasing substrate concentration. The catalytic site of the enzyme is empty, as it is not bound to a substrate, for much of the time, and the rate at which product can be formed is limited by the concentration of substrate which is available. Meanwhile, as the concentration of substrate increases (from 0.25 μM and above), the enzyme

becomes saturated with substrate. As soon as the catalytic site is empty, more substrate is available to bind and undergo reaction. The rate of formation of product now depends on the activity of the enzyme itself and adding more substrate will not affect the rate of the reaction to any significant effect.

The value of K_{cat}/ K_m was calculated for the MNAzyme Pan-Fungal assay to provide a direct comparison of the effectiveness of an enzyme toward different substrates that have been previously reported in separate assays. The parent enzyme, DNAzyme 10–23 is the most catalytically active DNA enzyme with K_{cat}/ K_m of ~ 10^9 M^{-1} min^{-1} approaching the efficiency of the most "catalytically perfect" enzymes (Gerasimova & Kolpashchikov, 2010). In this study, the catalytic efficacy of the MNAzyme Pan-Fungal was determined at 1.0×10^8 min^{-1} M^{-1}. It is comparable with the catalytic efficiency of the Mz1d assay (2.9×10^8 min^{-1} M^{-1}) and with DNAzyme 10-23 (5.6×10^8 $min^{-1}M^{-1}$) (Mokany *et al.*, 2010). It is clear, therefore, that the enzymatic activity demonstrated for the Pan-Fungal MNAzyme assay developed here would be capable of functioning efficiently in detecting pathogenic fungi DNA biomarkers.

In summary, the purpose of this study was to design and characterise a pan-fungal MNAzyme assay for the rapid and isothermal direct detection of pathogens associated with the invasive fungal diseases and may enable the diagnosis of uncommon and rare fungal infections. Although the investigation can be advanced with the incorporation of the PCR method for the amplification and quantification of the targets, current results laid the foundation for development of the multiplex qPCR-MNAzyme assay. The robust and expandable features of the MNAzyme technology as a strategy for multiplexing assay can be developed for the multiple target detection in a single tube reaction (Zhou, Ding & Liu, 2017). Development of the qPCR-MNAzyme *Candida* assay, for instance, could detect the pathogenic species from the

kingdom-level (pan-fungal), genus-level (pan-*Candida*) and further discrimination to the species-level for multi-drug sensitive species such as *C. krusei*, *C. glabrata*, *C. auris* and could facilitate diagnosis of invasive candidiasis (Casadevall, 2018; Schelenz *et al.*, 2016). Nonetheless, these ideas and techniques are still at the laboratory stage, and the future aim is to develop a multiplex assay-based detection kit that can be taken into the field to assess fungal infections.

CHAPTER 7: Discussion

7.1 Overview of the main findings

Clinical diagnosis of IFIs is challenging as there is a lack of early signs of infection and non-specific symptoms undistinguishable from those of bacterial sepsis (Pfaller & Castanheira, 2016; Brown *et al.*, 2012). Fever is the most common manifestation of disseminated fungal infection and may occur with or without localising clinical features (Martino & Girmenia, 2000). In most cases, diagnosis is complicated by the host's underlying conditions (Patterson & Donnelly, 2019). Thus, laboratory procedures are primary to investigate and confirm the diagnosis of invasive fungal and establish disease aetiology. It has been suggested that reliable and rapid diagnostic tools are important to tackle most of the problems with regards to IFIs (Brown, Denning & Levitz, 2012).

An ideal fungal detection test should exclusively differentiate organisms at the species level, as some species may respond differently to antimicrobials. The specific information is useful for the clinicians to prescribe an accurate antifungal drug to the infected patients and avoid broad-spectrum antifungals. The implications of long term broad-spectrum or wrong antifungal treatments to the patients could lead to the emergence of resistant species and no cure for such diseases (Shor & Perlin, 2015). Multidrug resistant *Candida* species are reported all over the world, and their development is of particular concern (Ben-Ami *et al.*, 2017; Jeffery-Smith *et al.*, 2018; Alexander *et al.*, 2013). Moreover, overuse of fluconazole as a prophylactic agent has been associated with the emergence of non-*albicans Candida* which selects those species that are intrinsically resistant or less susceptible to azole drugs. In this study, the detection assay can discriminate the drug-resistant *C. krusei*, *C. glabrata* and *C. auris* from other pathogenic *Candida* species. To date, there are over 5,100 cases of

life-threatening *Candida* infections in the UK (Pegorie, Denning & Welfare, 2017) associated with 40% to 50% mortality rates (Dhillon & Clark, 2011). Accurate diagnosis and therapies are important to reduce the mortality rates and reflect correct epidemiological data related to IFIs as well as successful delivery of the antimicrobial resistance (AMR) agenda (Ahmadi *et al.*, 2014; Brown *et al.*, 2012; O'Neill, 2016). However, early and accurate diagnosis and the subsequent usage of appropriate antifungal therapy are difficult to achieve (Casadevall, 2018).

The traditional microbiological methods such as organism cultivation, microscopic and histopathological evaluations are 'gold standard' and used widely in the hospital to diagnose IFIs. However, fungal cultures, for example, lack sensitivity and are time-consuming, leading to delayed treatments (Ostrosky-Zeichner, 2012; Hammond *et al.*, 2011). Conventional microbiological techniques such as blood cultures lack sensitivity, as they were shown to be positive in less than 50% of patients with chronic candidiasis and it is rare to recover fungi from patients with invasive aspergillosis (Pemán *et al.*, 2011; Bašková & Buchta, 2012). Methods of direct microscopy and histopathology require high laboratory skills to identify the species which are laborious and time-consuming. Immunological detection of the fungal cell wall polysaccharides is a routine test for screening of fungal infections and has shown limited specificity and low sensitivity to meet early-stage treatment needs (Badiee & Hashemizadeh, 2014). Therefore, it is impossible to deliver accurate treatment to the patients as these methods are not specific, and only appear positive in the late stage of IFI.

On the other hand, recent advances in the development of molecular methods have led to the significant improvement of IFI management by facilitating earlier detection of fungal pathogens (Al-Jalbout *et al.*, 2019). These methods include nucleic acid probe chemistries and PCR technology. They are rapid, highly specific and can

be used to detect low quantities of fungal nucleic acids from patient samples before the symptoms are prominent; therefore, allowing appropriate therapy. There are various probe chemistries available (hydrolysis probes – TaqMan®; dual hybridisation probes) that rely on the fluorescent signal emission during target sequence amplification. A multiplex assay can be designed for multiple target detection and discrimination in a single tube reaction. The multiple target probes in a single assay allowed the diagnostic testing for more comprehensive, rather than testing for individual pathogens in multiple tests. Furthermore, patients may be infected with more than one fungal pathogen and can be used to monitor the emergence of new fungal pathogens. However, probe-based assays often limit its potential due to the instrument's incompatibility to some fluorogenic probes. The MPA technology enhance the full benefits of the dual-labelled hydrolysis probe with multiplexing capacity in a single fluorescence channel (Fu, Miles & Alphey, 2012). This offers interesting possibilities in the development of novel molecular diagnostic tools for fungal infections. For example, the Light Cycler SeptiFast® (Roche Diagnostics) and MycoReal *Candida* (Ingenetix GmbH) qPCR kits require four fluorescence channels in detecting five to seven *Candida* target species. In this thesis, an MPA-*Candida* diagnostic assay was developed that allows the identification of up to nine of the yeast species most frequently associated with invasive candidiasis. Crucially, this enhanced range of pathogen detection is achieved using only two fluorescence detection channels. It has been further demonstrated that the dual channel penta-plexing MPA assay reported here allows the species-specific identification of three of the most problematic antifungal drug resistant *Candida* species, including *C. auris*, an emerging pathogen responsible for severe hospital outbreaks worldwide (Forsberg *et al.*, 2019; Benedict *et al.*, 2017). This assay has therefore the potential to allow clinicians to prescribe the correct chemotherapy for patients infected with drug-resistant strains, thus saving lives

and contributing to antifungal stewardship efforts worldwide (Rautemaa-Richardson *et al.*, 2018; Pfaller & Castanheira, 2016).

Limitations of PCR-based diagnostic methods, including the requirement for expensive laboratory equipment and a clean environment to prevent sample cross-contamination have driven the development of alternative molecular detection platforms based on isothermal DNA amplification methods. Isothermal amplification offers simplicity and eliminates the need for sophisticated thermal cycler machines and hence, are suitable to be developed as hand-held diagnostic devices that could be used at the patient's bedside. One such method, loop-mediated isothermal amplification (LAMP), provides real-time monitoring of the reaction as reaction mixture turbidity correlates with the amount of DNA synthesised (Parida & Sannarangaiah, 2008). Numerous LAMP-based assays have been developed to detect fungal pathogens (Niessen, 2015). However, although LAMP has high sensitivity and specificity, the method requires a complicated design of primers and is limited to the detection of a single target per reaction (Eboigbodin & Hoser, 2016). An alternative robust and cost-effective detection platform based on hydrolytic MNAzymes has simplified the development of the isothermal nucleic acid assay. The MNAzyme assay has excellent sensitivity of up to picomolar target concentration and requires no previous DNA amplification steps (Mokany *et al.*, 2010); this suggests its potential use in a limited resources area and during outbreaks controls. In this thesis a highly specific MNAzyme Pan-Fungal assay was developed. *In vitro* characterisation demonstrated its capacity to discern between two putative target sequences with a single nucleotide base pair difference. Such high level of specificity would allow differentiation between two closely related species such as multidrug-resistant *C. auris* and drug-sensitive *C. haemulonii*. In recent years, the former has sparked outbreaks in hospital settings around the world (Chowdhary, Sharma & Meis, 2017; Schelenz *et al.*, 2016).

The use of multiplex, qPCR test such as Roche SeptiFast® has enabled simultaneous and rapid detections of blood pathogens while maintaining excellent analytical sensitivity (Straub *et al.*, 2017). Despite the vast potential of qPCR detections, the sensitivity associated with the use of fungal DNA from the clinical samples negatively impacted by the technical issues related to the fungal DNA isolation. In the SeptiFast® qPCR assay, the detection sensitivity of the fungaemia is significantly low (61%) compared to 80% in bacteraemia detection (Chang *et al.*, 2013). The SeptiFast® overall sensitivity (69%) and specificity (81%) for bacterial and fungal detection from blood samples (Lehmann *et al.*, 2010). The discrepancies of the sensitivity could be suggested from the cumbersome and complex methods of the thick fungal cell wall digestion that possibly impede the quantity of the nucleic acid biomarkers for amplification. In the study conducted by Gosiewski *et al.*, (2014), comparing the detection of fungi and bacteria species from the patient's blood in the qPCR assay, resulted in no detection of fungi due to the complicated process of fungal DNA isolation. Bacterial and viral detection assays are not facing the same issue as the process of the microbial nucleic acid isolation can be accomplished from straightforward nucleic acid isolation and purification steps (Kajiura *et al.*, 2015). In this thesis, the nucleic acids isolated from spiked blood and serum samples showed a 1-log difference in sensitivity compared to the control sample (spiked saline sample) for pan-fungal DNA biomarker detection. The preferred clinical specimen to obtain for molecular-based screening is serum over whole blood mainly for its superior sensitivity (Lau *et al.*, 2010), simple nucleic acid purification process, and allows utilisation of the same sample for multiple tests (Nguyen *et al.*, 2012; Alanio & Bretagne, 2014). The complexities of the PCR assay's requirements for inhibitor-free sample and a cumbersome fungal DNA preparation process may be the factors that hindered the methodological standardisation and limit its widespread clinical utility. A

collaboration network within the Fungal PCR Initiative (FPCRI) – *Candida* group; a working group under International Society for Human and Animal Mycology (ISHAM) focusing on a concerted effort towards standardisation and clinical trials of the PCR methods may shed a brighter light on the clinical utility of this method.

7.2 Implications of research and future work

The major challenge for a diagnostic assay development is that it must be able to sensitively detect infections early, possibly before the manifestations of symptoms, for appropriate therapy to take place to stop disease progression. Simple and robust diagnostic tests that could lead to a shorter turnaround time are desirable. This is particularly important in disseminated fungal infections as the mortality rate increases due to delays in diagnosis and ultimately treatment (Farmakiotis *et al.*, 2015). The detection of antifungal drug resistance and the corresponding specific gene mutations (*FKS1* gene; *ERG11* gene mutations) enable more rapid identification of resistant *Candida* species. The DNA biomarkers identified could be utilised in other isothermal DNA amplification techniques such as Strand Invasion Based Amplification (SIBA®) and Recombinase Polymerase Amplification (RPA) for sensitive detection or further *in vitro* characterisations of the MNAzymes assay with the PCR amplification steps. Accessibility to the instruments particularly to the hospitals which have limited resources conditions should benefit from the development of the rapid molecular diagnostic tools. This research project opened up a range of potential applications of the MPA and MNAzymes platforms including to design a PCO sequence for the RNA substrate in the MNAzymes assay as a way of multiplexing the probes detection in a single fluorescence channel. However, it is also important to consider the cost of the assay relative to the economic impact it causes, including the difficult estimations of the cost of misdiagnosis, leading to over or under treatment. Finally, the prototype

assay should then pave the road towards clinical validity and clinical utility before entering extensive clinical practice.

7.3 Conclusion

The exploration of potential biomarkers detection platforms as simple nucleic acid biosensors for the diagnosis of invasive candidiasis has demonstrated a vast potential to further the prototype development and validations. The *in vitro* characterisations of the MPA-*Candida* and MNAzyme Pan-Fungal assays suggest their potential value in the clinical diagnosis and management of invasive candidiasis and outbreak control.

BIBLIOGRAPHY

Abbas, J., Bodey, G.P., Hanna, H.A., Mardani, M., et al. (2000) *Candida krusei* fungemia an escalating serious infection in immunocompromised patients. *Archives of Internal Medicine*. 160 (17), 2659–2664. Available from: doi:10.1001/archinte.160.17.2659.

Ahmad, S., Khan, Z., Mustafa, A.S. & Khan, Z.U. (2002) Seminested PCR for diagnosis of candidemia: Comparison with culture, antigen detection, and biochemical methods for species identification. *Journal of Clinical Microbiology*. 40 (7), 2483–2489. Available from: doi:10.1128/JCM.40.7.2483.

Ahmadi, A., Ardehali, S.H., Beigmohammadi, M.T., Hajiabdolbaghi, M., et al. (2014) Invasive candidiasis in intensive care unit; consensus statement from an Iranian panel of experts, July 2013. *Journal of the Royal Society of Medicine Open*. 5 (3), 1–10. Available from: doi:10.1177/2042533313517689.

Al-Jalbout, N., Rothman, R.E., Troncoso, R., Hinson, J.S., et al. (2019) Biomarkers and molecular diagnostics for early detection and targeted management of sepsis and septic shock in the emergency department. *The Journal of Applied Laboratory Medicine*. 3 (4), 724–729. Available from: doi:10.1373/jalm.2018.027425.

Alam, M.Z., Alam, Q., Jiman-Fatani, A., Kamal, M.A., et al. (2014) *Candida* identification: A journey from conventional to molecular methods in medical mycology. *World Journal of Microbiology and Biotechnology*. 30 (5), 1437–1451. Available from: doi:10.1007/s11274-013-1574-z.

Alanio, A. & Bretagne, S. (2014) Difficulties with molecular diagnostic tests for mould and yeast infections: Where do we stand?. *Clinical Microbiology and Infection*. 20 (6), 36–41. Available from: doi:10.1111/1469-0691.12617.

Alexander, B.D., Johnson, M.D., Pfeiffer, C.D., Jiménez-Ortigosa, C., et al. (2013) Increasing echinocandin resistance in *Candida glabrata*: Clinical failure correlates with presence of FKS mutations and elevated minimum inhibitory concentrations. *Clinical Infectious Diseases*. 56 (12), 1724–1732. Available from: doi:10.1093/cid/cit136.

Alhambra, A., Cuétara, M.S., Ortiz, M.C., Moreno, J.M., et al. (2007) False positive galactomannan results in adult hematological patients treated with piperacillin-tazobactam. *Revista iberoamericana de micologia*. 24 (2), 106–112.

Ali, N., Rampazzo, R., Costa, A. & Krieger, M. (2017) Current nucleic acid extraction methods and their implications to point-of-care diagnostics. *BioMed Research International*. 2017, 1–13. Available from: doi:10.1155/2017/9306564.

Arendrup, M.C., Fisher, B.T. & Zaoutis, T.E. (2009) Invasive fungal infections in the paediatric and neonatal population: Diagnostics and management issues. *Clinical Microbiology and Infection*. 15 (7), 613–624. Available from: doi:10.1111/j.1469-0691.2009.02909.x.

Arvanitis, M., Anagnostou, T., Fuchs, B.B., Caliendo, A.M., et al. (2014) Molecular and nonmolecular diagnostic methods for invasive fungal infections. *Clinical Microbiology Reviews*. 27 (3), 490–526. Available from: doi:10.1128/CMR.00091-13.

Aslani, N., Janbabaei, G., Abastabar, M., Meis, J.F., et al. (2018) Identification of uncommon oral yeasts from cancer patients by MALDI-TOF mass spectrometry. *BMC Infectious Diseases*. 18 (24), 1–11. Available from: doi:10.1186/s12879-017-2916-5.

Azoulay, E., Guigue, N., Darmon, M., Mokart, D., et al. (2016) (1, 3)-β-D-glucan assay for diagnosing invasive fungal infections in critically ill patients with hematological malignancies. *Oncotarget*. 7 (16), 21484–21495. Available from:

doi:10.18632/oncotarget.7471.

Badiee, P., Badali, H., Boekhout, T., Diba, K., et al. (2017) Antifungal susceptibility testing of *Candida* species isolated from the immunocompromised patients admitted to ten university hospitals in Iran: Comparison of colonizing and infecting isolates. *BMC Infectious Diseases*. 17 (727), 1–8. Available from: doi:10.1186/s12879-017-2825-7.

Badiee, P. & Hashemizadeh, Z. (2014) Opportunistic invasive fungal infections: Diagnosis & clinical management. *The Indian Journal of Medical Research*. 139 (2), 195–204.

Barton, R.C. (2013) Laboratory diagnosis of invasive aspergillosis: From diagnosis to prediction of outcome. *Scientifica*. 2013 (459405), 1–29. Available from: doi:10.1155/2013/459405.

Bašková, L. & Buchta, V. (2012) Laboratory diagnostics of invasive fungal infections: An overview with emphasis on molecular approach. *Folia microbiologica*. 57 (5), 421–430. Available from: doi:10.1007/s12223-012-0152-3.

Bassetti, M., Righi, E., Montravers, P. & Cornely, O.A. (2018) What has changed in the treatment of invasive candidiasis? a look at the past 10 years and ahead. *Journal of Antimicrobial Chemotherapy*. 73 (1), 14–25. Available from: doi:10.1093/jac/dkx445.

Ben-Ami, R., Berman, J., Novikov, A., Bash, E., et al. (2017) Multidrug-resistant *Candida haemulonii* and *C. auris*, Tel Aviv, Israel. *Emerging Infectious Diseases*. 23 (2). Available from: doi:10.3201/eid2302.161486.

Benedict, K., Richardson, M., Vallabhaneni, S., Jackson, B.R., et al. (2017) Emerging issues, challenges, and changing epidemiology of fungal disease outbreaks. *The Lancet Infectious Diseases*. 17 (12), 403–411. Available from: doi:10.1016/S1473-3099(17)30443-7.

Bergman, L.W. (2001) Growth and maintenance of yeast. In: *Two-Hybrid Systems*. New Jersey, Humana Press. 009–014. Available from: doi:10.1385/1-59259-210-4:009.

Bhatia, R., Cuschieri, K., Cubie, H., Boland, E., et al. (2017) Evaluation of a novel single-tube method for extended genotyping of human papillomavirus. *Journal of Clinical Microbiology*. 56 (3), 1–7. Available from: doi:10.1128/jcm.01687-17.

Blanco, J.L. & Garcia, M.E. (2008) Immune response to fungal infections. *Veterinary Immunology and Immunopathology*. 125 (1–2), 47–70. Available from: doi:10.1016/j.vetimm.2008.04.020.

Bone, S.M., Hasick, N.J., Lima, N.E., Erskine, S.M., et al. (2014) DNA-only cascade: A universal tool for signal amplification, enhancing the detection of target analytes. *Analytical Chemistry*. 86 (18), 9106–9113. Available from: doi:10.1021/ac501811r.

Bongomin, F., Gago, S., Oladele, R. & Denning, D. (2017) Global and multi-national prevalence of fungal diseases—estimate precision. *Journal of Fungi*. 3 (4), 1–29. Available from: doi:10.3390/jof3040057.

Borman, A.M. & Johnson, E.M. (2014) Interpretation of fungal culture results. *Current Fungal Infection Reports*. 8 (4), 312–321. Available from: doi:10.1007/s12281-014-0204-z.

Brooks, G.F., Carroll, K.C., Butel, J., Morse, S.A., et al. (2013) *Jawetz, Melnick, & Adelberg's Medical Microbiology*. The McGraw-Hill Companies, Inc. Available from: doi:10.1017/CBO9781107415324.004.

Brown, A.J.P., Budge, S., Kaloriti, D., Tillmann, A., et al. (2014) Stress adaptation in a pathogenic fungus. *Journal of Experimental Biology*. 217 (1), 144–155. Available from: doi:10.1242/jeb.088930.

Brown, G.D., Denning, D.W., Gow, N.A.R., Levitz, S.M., et al. (2012b) Hidden

killers: Human fungal infections. *Science Translational Medicine*. 4 (165), 1–9. Available from: doi:10.1126/scitranslmed.3004404.

Brown, G.D., Denning, D.W. & Levitz, S.M. (2012) *Tackling Human Fungal Infections*.336 (5).

Brunke, S. & Hube, B. (2013) Two unlike cousins: *Candida albicans* and *C. glabrata* infection strategies. *Cellular Microbiology*. 15 (5), 701–708. Available from: doi:10.1111/cmi.12091.

Bustin, S.A. (2005) Real-Time PCR. In: *Encyclopedia of Diagnostic Genomics and Proteomics*. 1117–1125. Available from: doi:10.1081/E-EDGP.

Casadevall, A. (2018) Fungal diseases in the 21st century: the near and far horizons. *Pathogens and Immunity*. 3 (2), 183–196. Available from: doi:10.20411/pai.v3i2.249.

Centers for Disease Control and Prevention (2018) *Recommendations for identification of Candida auris.* 2018. Available from: https://www.cdc.gov/fungal/candida-auris/recommendations.html [Accessed: 30 October 2018].

Chakrabarti, A., Sood, P., Rudramurthy, S.M., Chen, S., et al. (2015) Incidence, characteristics and outcome of ICU-acquired candidemia in India. *Intensive Care Medicine*. 41 (2), 285–295. Available from: doi:10.1007/s00134-014-3603-2.

Chang, S.S., Hsieh, W.H., Liu, T.S., Lee, S.H., et al. (2013) Multiplex PCR system for rapid detection of pathogens in patients with presumed sepsis - a systemic review and meta-analysis. *PloS ONE*. 8 (5). Available from: doi:10.1371/journal.pone.0062323.

Cheng, J.W., Yu, S.Y., Xiao, M., Wang, H., et al. (2016) Identification and antifungal susceptibility profile of *Candida guilliermondii* and *Candida fermentati* from a multicenter study in China. *Journal of Clinical Microbiology*. 54 (8), 2187–2189.

Available from: doi:10.1128/JCM.00938-16.

Chowdhary, A., Sharma, C. & Meis, J.F. (2017) *Candida auris*: A rapidly emerging cause of hospital-acquired multidrug-resistant fungal infections globally. *PLOS Pathogens*. 13 (5), 1–10. Available from: doi:10.1371/journal.ppat.1006290.

Cieslak, M., Szymanski, J., Adamiak, R.W. & Cierniewski, C.S. (2003) Structural rearrangements of the 10-23 DNAzyme to beta integrin subunit mRNA induced by cations and their relations to the catalytic activity. *Journal of Biological Chemistry*. 278(48), 47987–47996.Available from: doi:10.1074/jbc.M300504200.

Clancy, C.J. & Nguyen, M.H. (2018a) Diagnosing invasive candidiasis. *Journal of Clinical Microbiology*. 56 (5), 1–9. Available from: doi:10.1128/JCM.01909-17.

Clancy, C.J. & Nguyen, M.H. (2013) Finding the "Missing 50%" of invasive candidiasis: how nonculture diagnostics will improve understanding of disease spectrum and transform patient care. *Clinical Infectious Diseases*. 56 (9), 1284–1292. Available from: doi:10.1093/cid/cit006.

Clancy, C.J. & Nguyen, M.H. (2018c) T2 Magnetic Resonance for the diagnosis of bloodstream infections: Charting a path forward. *Journal of Antimicrobial Chemotherapy*. 73 (4), 2–5. Available from: doi:10.1093/jac/dky050.

Clements, D.N., Wood, S., Carter, S.D. & Ollier, W.E.R. (2008) Assessment of the quality and quantity of genomic DNA recovered from canine blood samples by three different extraction methods. *Research in veterinary science*. 85 (1), 74–79. Available from: doi:10.1016/j.rvsc.2007.09.009.

Colomba, C., Trizzino, M., Imburgia, C., Madonia, S., et al. (2014) *Candida glabrata* meningitis and endocarditis: A late severe complication of candidemia. *International Journal of Infectious Diseases*. 29, 174–175. Available from: doi:10.1016/j.ijid.2014.04.032.

Cubeta, M.A. (1991) Characterization of anastomosis groups of binucleate *Rhizoctonia* species using restriction analysis of an amplified ribosomal RNA gene. *Molecular Plant Pathology*. 81 (11), 1395–1400. Available from: doi:10.1094/phyto-81-1395.

Dhillon, R.H. & Clark, J. (2011) Fungal infections in the critically ill. *Trends in Anaesthesia and Critical Care*. 1 (4), 210–218. Available from: doi:10.1016/j.tacc.2011.05.007.

Dhiman, N., Hall, L., Wohlfiel, S.L., Buckwalter, S.P., et al. (2011) Performance and cost analysis of Matrix-Assisted Laser Desorption Ionization-Time of Flight Mass Spectrometry for routine identification of yeast. *Journal of Clinical Microbiology*. 49 (4), 1614–1616. Available from: doi:10.1128/JCM.02381-10.

Duettmann, W., Koidl, C., Krause, R., Lackner, G., et al. (2016) Specificity of mannan antigen and anti-mannan antibody screening in patients with haematological malignancies at risk for fungal infection. *Mycoses*. 59 (6), 374–378. Available from: doi:10.1111/myc.12482.

Eboigbodin, K.E. & Hoser, M.J. (2016) Multiplex strand invasion based amplification (mSIBA) assay for detection of *Chlamydia trachomatis* and *Neisseria gonorrhoeae*. *Scientific Reports*. 6 (2), 1–9. Available from: doi:10.1038/srep20487.

Eigl, S., Hoenigl, M., Spiess, B., Heldt, S., et al. (2017) Galactomannan testing and *Aspergillus* PCR in same-day bronchoalveolar lavage and blood samples for diagnosis of invasive aspergillosis. *Medical Mycology*. 55 (5), 528–534. Available from: doi:10.1093/mmy/myw102.

Ellis, M., Al-Ramadi, B., Bernsen, R., Kristensen, J., et al. (2009) Prospective evaluation of mannan and anti-mannan antibodies for diagnosis of invasive *Candida* infections in patients with neutropenic fever. *Journal of Medical*

Microbiology. 58 (5), 606–615. Available from: doi:10.1099/jmm.0.006452-0.

Enache-Angoulvant, A. & Hennequin, C. (2005) Invasive *Saccharomyces* infection: A comprehensive review. *Clinical Infectious Diseases*. 41 (11), 1559–1568. Available from: doi:10.1086/497832.

Farmakiotis, D., Kyvernitakis, A., Tarrand, J.J. & Kontoyiannis, D.P. (2015) Early initiation of appropriate treatment is associated with increased survival in cancer patients with *Candida glabrata* fungaemia: A potential benefit from infectious disease consultation. *Clinical Microbiology and Infection*. 21 (1), 79–86. Available from: doi:10.1016/j.cmi.2014.07.006.

Feldman, A.R. & Sen, D. (2001) A new and efficient DNA enzyme for the sequence-specific cleavage of RNA. *Journal of molecular biology*. 313 (2), 283–294. Available from: doi:10.1006/jmbi.2001.5058.

Fiammengo, R. & Jäschke, A. (2005) Nucleic acid enzymes. *Current Opinion in Biotechnology*. 16 (6), 614–621. Available from: doi:10.1016/j.copbio.2005.10.006.

Forsberg, K., Woodworth, K., Walters, M., Berkow, E.L., et al. (2019) *Candida auris* : The recent emergence of a multidrug-resistant fungal pathogen. *Medical Mycology*. 57 (1), 1–12. Available from: doi:10.1093/mmy/myy054.

Fraga, D., Meulia, T. & Fenster, S. (2014) Real-Time PCR. In: *Current Protocols Essential Laboratory Techniques*. 1–40. Available from: doi:10.1002/9780470089941.et1003s08.

Fredricks, D.N. & Relman, D.A. (1998) Improved amplification of microbial DNA from blood cultures by removal of the PCR inhibitor sodium polyanetholesulfonate. *Journal of clinical microbiology*. 36 (10), 2810–2816.

Froehlich, T., Sagner, G. & Tellmann, G. (2009) LightCycler® 480 and 1536 real-time PCR systems-powerful solutions for different throughput levels a cross-platform

comparison. *Gene Expression*. 4 (4), 17–19.

Fu, G., Miles, A. & Alphey, L. (2012) Multiplex detection and SNP genotyping in a single fluorescence channel. *PLoS ONE*. 7 (1). Available from: doi:10.1371/journal.pone.0030340.

Gao, J., Shimada, N. & Maruyama, A. (2015) MNAzyme-catalyzed nucleic acid detection enhanced by a cationic copolymer. *Biomaterial Science*. 3 (5), 716–720. Available from: doi:10.1039/C4BM00449C.

Gerasimova, Y. V. & Kolpashchikov, D.M. (2010) Nucleic acid detection using MNAzymes. *Chemical Biology*. 17 (2), 104–106. Available from: doi:10.1038/jid.2014.371.

Gosiewski, T., Flis, A., Sroka, A., K¸dzierska, A., et al. (2014) Comparison of nested, multiplex, qPCR; FISH; SeptiFast and blood culture methods in detection and identification of bacteria and fungi in blood of patients with sepsis. *BMC Microbiology*. 14 (313), 1–8. Available from: doi:10.1186/s12866-014-0313-4.

Gow, N.A.R., Van De Veerdonk, F.L., Brown, A.J.P. & Netea, M.G. (2012) *Candida albicans* morphogenesis and host defence: Discriminating invasion from colonization. *Nature Reviews Microbiology*. 10 (2), 112–122. Available from: doi:10.1038/nrmicro2711.

Gow, N.A.R. & Yadav, B. (2017) *Candida albicans*: A shape-changing, opportunistic pathogenic fungus of humans. *Microbiology*. 163 (8), 1145–1147. Available from: doi:10.1099/mic.0.000499.

Guarro, J., Gené, J. & Stchigel, A.M. (1999) Developments in fungal taxonomy. *Clinical Microbiology Reviews*. 12 (3), 454–500.

Guinea, J. (2014) Global trends in the distribution of *Candida* species causing candidemia. *Clinical Microbiology and Infection*. Available from: doi:10.1111/1469-0691.12539.

Halliday, C.L., Kidd, S.E., Sorrell, T.C. & Chen, S.C.A. (2015) Molecular diagnostic methods for invasive fungal disease: the horizon draws nearer? *Pathology*. 47 (3), 257–269. Available from: doi:10.1097/PAT.0000000000000234.

Hammond, S.P., Bialek, R., Milner, D.A., Petschnigg, E.M., et al. (2011) Molecular methods to improve diagnosis and identification of mucormycosis. *Journal of Clinical Microbiology*. 49 (6), 2151–2153. Available from: doi:10.1128/JCM.00256-11.

Hasseine, L., Cassaing, S., Robert-Gangneux, F., Fillaux, J., et al. (2015) High negative predictive value diagnostic strategies for the reevaluation of early antifungal treatment: A multicenter prospective trial in patients at risk for invasive fungal infections. *Journal of Infection*. 71 (2), 258–265. Available from: doi:10.1016/j.jinf.2015.04.005.

Hebert, P.D.N., Cywinska, A., Ball, S.L. & DeWaard, J.R. (2003) Biological identifications through DNA barcodes. *Proceedings. Biological sciences / The Royal Society*. 270 (1512), 313–321. Available from: doi:10.1098/rspb.2002.2218.

Hibbett, D.S., Binder, M., Bischoff, J.F., Blackwell, M., et al. (2007) A higher-level phylogenetic classification of the fungi. *Mycological Research*. 111 (5), 509–547. Available from: doi:10.1016/j.mycres.2007.03.004.

Hope, W.W., Walsh, T.J. & Denning, D.W. (2005) Laboratory diagnosis of invasive aspergillosis. *The Lancet Infectious Diseases*. 5 (10), 609–622. Available from: doi:10.1016/S1473-3099(05)70238-3.

Horvath, L.L., George, B.J., Murray, C.K., Harrison, L.S., et al. (2004) Direct comparison of the BACTEC 9240 and BacT/ALERT 3D automated blood culture systems for *Candida* growth detection. *Journal of Clinical Microbiology*. 42 (1), 115–118. Available from: doi:10.1128/JCM.42.1.115-118.2004.

Hsu, J.L., Binkley, J., Clemons, K. V., Stevens, D.A., et al. (2014) Application of a non-amplification-based technology to detect invasive fungal pathogens. *Diagnostic Microbiology and Infectious Disease*. 78 (2), 137–140. Available from: doi:10.1016/j.diagmicrobio.2013.11.013.

Hsu, J.L., Ruoss, S.J., Bower, N.D., Lin, M., et al. (2011) Diagnosing invasive fungal disease in critically ill patients. *Critical reviews in microbiology*. 37 (4), 277–312. Available from: doi:10.3109/1040841X.2011.581223.

Huang, Q., Liu, Z., Liao, Y., Chen, X., et al. (2011) Multiplex fluorescence melting curve analysis for mutation detection with dual-labeled, self-quenched probes Igor Mokrousov (ed.). *PLoS ONE*. 6 (4), 1–9. Available from: doi:10.1371/journal.pone.0019206.

Hube, B. (2009) Fungal adaptation to the host environment. *Current Opinion in Microbiology*. 12 (4), 347–349. Available from: doi:10.1016/j.mib.2009.06.009.

Irinyi, L., Lackner, M., de Hoog, G.S. & Meyer, W. (2016) DNA barcoding of fungi causing infections in humans and animals. *Fungal Biology*. 120 (2), 125–136. Available from: doi:10.1016/j.funbio.2015.04.007.

Jainlabdin, M.H., Chua, A.L., Nizam, T.M. & Santhanam, J. (2018) Dual panel multiplex PCR assay for rapid detection of medically important fungi and resistant species of *Candida* and *Aspergillus*. *Sains Malaysiana*. 47 (3), 489–498. Available from: doi:10.17576/jsm-2018-4703-08.

Jeffery-Smith, A., Taori, S.K., Schelenz, S., Jeffery, K., et al. (2018) *Candida auris*: A review of the literature. *Clinical Microbiology Reviews*. 31 (1), 1–18. Available from: doi:10.1128/CMR.00029-17.

Juskowiak, B. (2011) Nucleic acid-based fluorescent probes and their analytical potential. *Analytical and Bioanalytical Chemistry*. 399 (9), 3157–3176. Available from: doi:10.1007/s00216-010-4304-5.

Kajiura, L.N., Stewart, S.D., Dresios, J. & Uyehara, C.F. (2015) Simultaneous extraction of viral and bacterial nucleic acids for molecular diagnostic applications. *Journal of Biomolecular Techniques*. 26 (4), 118–124. Available from: doi:10.7171/jbt.15-2604-002.

Karageorgopoulos, D.E., Vouloumanou, E.K., Ntziora, F., Michalopoulos, A., et al. (2011) B-D-Glucan assay for the diagnosis of invasive fungal infections: A meta-analysis. *Clinical Infectious Diseases*. 52 (6), 750–770. Available from: doi:10.1093/cid/ciq206.

Kauffman, C.A., Pappas, P.G., Sobel, J.D. & Dismukes, W.E. (2011) *Essentials of Clinical Mycology*. 2nd edition. Springer New York.

Kauffman, C.A., Sobel, J.D., Pappas, P.G. & Dismukes, W.E. (2003) *Clinical Mycology: Second edition*. Available from: doi:10.1007/978-1-4419-6640-7.

Khot, P.D. & Fredricks, D.N. (2009) PCR-based diagnosis of human fungal infections. *Expert Review of Anti-Infective Therapy*. 7 (10), 1201–1221. Available from: doi:10.1586/eri.09.104.

Kolomeyer, A.M., Murphy, K.M., Traband, A., Frank, I., et al. (2018) Beta-d-glucan testing in patients with fungal endophthalmitis. *Retina*. 38 (4), 650–659. Available from: doi:10.1097/IAE.0000000000002049.

Kontoyiannis, D.P., Sumoza, D., Tarrand, J., Bodey, G.P., et al. (2000) Significance of aspergillemia in patients with cancer: A 10-year study. *Clinical Infectious Diseases*. 31 (1), 188–189. Available from: doi:10.1086/313918.

Kozel, T.R. & Wickes, B. (2014) Fungal diagnostics. *Cold Spring Harbor perspectives in medicine*. 4 (4), 1–14. Available from: doi:10.1101/cshperspect.a019299.

Kwiatkowski, N.P., Babiker, W.M., Merz, W.G., Carroll, K.C., et al. (2012) Evaluation of nucleic acid sequencing of the D1/D2 region of the large subunit of the 28S rDNA and the internal transcribed spacer region using smartgene IDNS

software for identification of filamentous fungi in a clinical laboratory. *Journal of Molecular Diagnostics*. 14 (4), 393–401. Available from: doi:10.1016/j.jmoldx.2012.02.004.

Landlinger, C., Preuner, S., Willinger, B., Haberpursch, B., et al. (2009) Species-specific identification of a wide range of clinically relevant fungal pathogens by use of Luminex xMAP technology. *Journal of Clinical Microbiology*. 47 (4), 1063–1073. Available from: doi:10.1128/JCM.01558-08.

Lau, A., Halliday, C., Chen, S.C.., Geoffrey Playford, E., et al. (2010) Comparison of whole blood, serum, and plasma for early detection of candidemia by multiplex-tandem PCR. *Journal of Clinical Microbiology*. 48 (3), 811–816. Available from: doi:10.1128/JCM.01650-09.

Lehmann, L.E., Hunfeld, K.P., Steinbrucker, M., Brade, V., et al. (2010) Improved detection of blood stream pathogens by real-time PCR in severe sepsis. *Intensive Care Medicine*. 36 (1), 49–56. Available from: doi:10.1007/s00134-009-1608-z.

Leslie, T.L., Chong, P.P., Ng, K.P. & Seow, H.F. (2012) Detection of 10 medically important *Candida* species by seminested Polymerase Chain Reaction. *Diagnostic Microbiology and Infectious Disease*. 72 (2), 196–198. Available from: doi:10.1016/j.diagmicrobio.2011.10.008.

Leung, A.Y.H., Chim, C.S., Ho, P.L., Cheng, V.C.C., et al. (2002) *Candida tropicalis* fungaemia in adult patients with haematological malignancies: clinical features and risk factors. *Journal of Hospital Infection*. 50, 316–319. Available from: doi:10.1053/jhin.2002.1194.

Loeffler, J., Henke, N., Hebart, H., Schmidt, D., et al. (2000) Quantification of fungal DNA by using fluorescence resonance energy transfer and the light cycler system. *Journal of Clinical Microbiology*. 38 (2), 586–590.

Lõoke, M., Kristjuhan, K. & Kristjuhan, A. (2011) Extraction of genomic DNA from

yeasts for PCR-based applications. *BioTechniques*. 50 (5), 325–328. Available from: doi:10.2144/000114497.

Ma, J., Hu, Y., Wu, M., Wang, X., et al. (2018) Timing determination of invasive fungal infection prophylaxis according to immune function in HSCT Patients. *Frontiers in Microbiology*. 9 (3), 1–7. Available from: doi:10.3389/fmicb.2018.00370.

Mackay, I.M. (2004) Real-time PCR in the microbiology laboratory. *Clinical Microbiology and Infection*. 10 (3), 190–212. Available from: doi:10.1111/j.1198-743X.2004.00722.x.

Mada, P.K. & Alam, M.U. (2019) *Cryptococcus (Cryptococcosis)*. StatPearls Publishing.

Makene, V.A. (2014) Identification of non-albicans *Candida* yeasts associated with vulvovaginal candidiasis in tanzania using a combination of multiplex PCR and DNA sequence divergence of the 26S LSU rDNA. *Scholars Academic Journal of Biosciences*. 2 (2), 124–131.

Marchetti, O., Lamoth, F., Mikulska, M., Viscoli, C., et al. (2012) ECIL recommendations for the use of biological markers for the diagnosis of invasive fungal diseases in leukemic patients and hematopoietic SCT recipients. *Bone Marrow Transplantation*. 47 (6), 846–854. Available from: doi:10.1038/bmt.2011.178.

Martín-Mazuelos, E., Zakariya-Yousef, I., García-Rey, S., Castro, C., et al. (2017) *Candida albicans* Germ-Tube Antibody: Evaluation of a new automatic assay for diagnosing invasive candidiasis in ICU patients. *Mycopathologia*. 182 (7–8), 645–652. Available from: doi:10.1007/s11046-017-0125-9.

Martin, R., Wächtler, B., Schaller, M., Wilson, D., et al. (2011) Host-pathogen interactions and virulence-associated genes during *Candida albicans* oral

infections. *International Journal of Medical Microbiology*. 301 (5), 417–422. Available from: doi:10.1016/j.ijmm.2011.04.009.

Martínez-Jiménez, M.C., Muñoz, P., Valerio, M., Vena, A., et al. (2015) Combination of *Candida* biomarkers in patients receiving empirical antifungal therapy in a Spanish tertiary hospital: A potential role in reducing the duration of treatment. *Journal of Antimicrobial Chemotherapy*. 70 (11), 3107–3115. Available from: doi:10.1093/jac/dkv241.

Martino, P. & Girmenia, C. (2000) Making the diagnosis of fungal infection: when to start treatment. *International journal of antimicrobial agents*. 16 (3), 323–329.

McMullan, B.J., Halliday, C., Sorrell, T.C., Judd, D., et al. (2012) Clinical utility of the cryptococcal antigen lateral flow assay in a diagnostic mycology laboratory Markus M. Heimesaat (ed.). *PLoS ONE*. 7 (11). Available from: doi:10.1371/journal.pone.0049541.

Miceli, M.H., Díaz, J.A. & Lee, S.A. (2011) Emerging opportunistic yeast infections. *The Lancet Infectious Diseases*. 11 (2), 142–151. Available from: doi:10.1016/S1473-3099(10)70218-8.

Mokany, E., Bone, S.M., Young, P.E., Doan, T.B., et al. (2010) MNAzymes, a versatile new class of nucleic acid enzymes that can function as biosensors and molecular switches. *Journal of American Chemical Society*. 132 (10), 1051–1059.

Mokany, E., Tan, Y.L., Bone, S.M., Fuery, C.J., et al. (2013) MNAzyme qPCR with superior multiplexing capacity. *Clinical Chemistry*. 59 (2), 419–426. Available from: doi:10.1373/clinchem.2012.192930.

Molenkamp, R., Ham, A. Van Der, Schinkel, J. & Beld, M. (2007) Real-Time multiplex PCR of five different dna targets using the LightCycler® 480 System. *Gene Expression*. 3 (3), 15–17.

Moreira-Oliveira, M.S., Mikami, Y., Miyaji, M., Imai, T., et al. (2005) Diagnosis of

candidemia by Polymerase Chain Reaction and blood culture: Prospective study in a high-risk population and identification of variables associated with development of candidemia. *European Journal of Clinical Microbiology and Infectious Diseases*. 24 (11), 721–726. Available from: doi:10.1007/s10096-005-0041-7.

Mpoza, E., Mukaremera, L., Kundura, D.A., Akampurira, A., et al. (2018) Evaluation of a point-of-care immunoassay test kit 'StrongStep' for cryptococcal antigen detection Ray Borrow (ed.). *PLoS ONE*. 13 (1), 1–8. Available from: doi:10.1371/journal.pone.0190652.

Mylonakis, E., Clancy, C.J., Ostrosky-Zeichner, L., Garey, K.W., et al. (2015) T2 Magnetic Resonance assay for the rapid diagnosis of candidemia in whole blood: A clinical trial. *Clinical Infectious Diseases*. 60 (6), 892–899. Available from: doi:10.1093/cid/ciu959.

Nadeem, S.G., Hakim, S.T. & Kazmi, S.U. (2010) Use of CHROMagar *Candida* for the presumptive identification of *Candida* species directly from clinical specimens in resource-limited settings. *Libyan Journal of Medicine*. 5 (1), 1–6. Available from: doi:10.3402/ljm.v5i0.2144.

Nalintya, E., Kiggundu, R. & Meya, D. (2017) Evolution of cryptococcal antigen testing: What is new?. *Current Fungal Infection Reports*. 10 (2), 62–67. Available from: doi:10.1007/s12281-016-0256-3.

Nelson, R.T. & Lodge, J.K. (2006) *Cryptococcus neoformans* Pathogenicity. In: *Fungal Genomics*. 237–266. Available from: doi:10.1007/3-540-30809-1_13.

Ng, K.P., Kuan, C.S., Kaur, H., Na, S.L., et al. (2015) *Candida* species epidemiology 2000-2013: A laboratory-based report. *Tropical Medicine & International Health*. 20 (11), 1447–1453. Available from: doi:10.1111/tmi.12577.

Nguyen, M.H., Wissel, M.C., Shields, R.K., Salomoni, M.A., et al. (2012)

Performance of *Candida* real-time Polymerase Chain Reaction, beta-d-glucan assay, and blood cultures in the diagnosis of invasive candidiasis. *Clinical Infectious Diseases*. 54 (9), 1240–1248. Available from: doi:10.1093/cid/cis200.

Niessen, L. (2015) Current state and future perspectives of Loop-Mediated Isothermal Amplification (LAMP)-based diagnosis of filamentous fungi and yeasts. *Applied Microbiology and Biotechnology*. 99 (2), 553–574. Available from: doi:10.1007/s00253-014-6196-3.

Nosanchuk, J.D. (2016) Endemic Mycoses. *Murray and Nadel's Textbook of Respiratory Medicine*. 646-660.e11. Available from: doi:10.1016/B978-1-4557-3383-5.00037-3.

Nurmi, J., Ylikoski, A., Soukka, T., Karp, M., et al. (2000) A new label technology for the detection of specific Polymerase Chain Reaction products in a closed tube. *Nucleic Acids Research*. 28 (8), 1–6.

O'Neill, J. (2016) *Tackling Drug-Resistant Infections Globally: Final Report and Recommendations*. Available from: doi:10.1016/j.jpha.2015.11.005.

Odabasi, Z., Mattiuzzi, G., Estey, E., Kantarjian, H., et al. (2004) Beta-D-glucan as a diagnostic adjunct for invasive fungal infections: Validation, cutoff development, and performance in patients with acute myelogenous leukemia and myelodysplastic syndrome. *Clinical Infectious Diseases*. 39 (2), 199–205.

Osei Sekyere, J. (2018) *Candida auris*: A systematic review and meta-analysis of current updates on an emerging multidrug-resistant pathogen. *MicrobiologyOpen*. 7 (4), 1–29. Available from: doi:10.1002/mbo3.578.

Ostrosky-Zeichner, L. (2012) Invasive mycoses: Diagnostic challenges. *The American Journal of Medicine*. 125 (1), 14–24. Available from: doi:10.1016/j.amjmed.2011.10.008.

Oz, Y. & Kiraz, N. (2011) Diagnostic methods for fungal infections in pediatric

patients: Microbiological, serological and molecular methods. *Expert review of anti-infective therapy*. 9 (3), 289–298. Available from: doi:10.1586/eri.10.168.

Page, B.T. & Kurtzman, C.P. (2005) Rapid identification of *Candida* species and other clinically important yeast species by flow cytometry. *Journal of Clinical Microbiology*. 43 (9), 4507–4514. Available from: doi:10.1128/JCM.43.9.4507.

Parida, M. & Sannarangaiah, S. (2008) Loop Mediated Isothermal Amplification (LAMP): a new generation of innovative gene amplification technique; perspectives in clinical diagnosis of infectious diseases. *Reviews in medical virology*. 18, 407–421. Available from: doi:10.1002/rmv.

Passos, A.I.M., Dertkigil, R.P., Ramos, M. de C., Busso-Lopes, A.F., et al. (2017) Serum markers as an aid in the diagnosis of pulmonary fungal infections in AIDS patients. *The Brazilian Journal of Infectious Diseases*. 21 (6), 606–612. Available from: doi:10.1016/J.BJID.2017.07.002.

Patterson, T.F. & Donnelly, J.P. (2019) New concepts in diagnostics for invasive mycoses: Non-culture-based methodologies. *Journal of Fungi*. 5 (1), 1–9. Available from: doi:10.3390/jof5010009.

De Pauw, B., Walsh, T.J., Donnelly, J.P., Stevens, D.A., et al. (2008) Revised definitions of invasive fungal disease from the european organization for research and treatment of cancer/invasive fungal infections cooperative group and the national institute of allergy and infectious diseases mycoses study group (EORTC/MSG) consensus group. *Clinical Infectious Diseases*. 46 (12), 1813–1821. Available from: doi:10.1086/588660.

Pegorie, M., Denning, D.W. & Welfare, W. (2017) Estimating the burden of invasive and serious fungal disease in the United Kingdom. *Journal of Infection*. 74 (1), 60–71. Available from: doi:10.1016/J.JINF.2016.10.005.

Pemán, J., Zaragoza, R., Quindós, G., Alkorta, M., et al. (2011) Clinical factors

associated with a *Candida albicans* Germ Tube Antibody positive test in Intensive Care Unit patients. *BMC infectious diseases*. 11 (1), 60. Available from: doi:10.1186/1471-2334-11-60.

Pérez-Torrado, R. & Querol, A. (2016) Opportunistic strains of *Saccharomyces cerevisiae*: A potential risk sold in food products. *Frontiers in Microbiology*. 6 (1), 1–5. Available from: doi:10.3389/fmicb.2015.01522.

Person, A.K., Kontoyiannis, D.P. & Alexander, B.D. (2011) Fungal infections in transplant and oncology patients. *Infectious Disease Clinics of North America*. 24 (2), 439–459. Available from: doi:10.1016/j.hoc.2010.11.013.

Pfaller, M.A. & Castanheira, M. (2016) Nosocomial candidiasis: Antifungal stewardship and the importance of rapid diagnosis. *Medical Mycology*. 54 (1), 1–22. Available from: doi:10.1093/mmy/myv076.

Pfaller, M.A., Diekema, D.J., Gibbs, D.L., Newell, V.A., et al. (2008) *Candida krusei*, a multidrug-resistant opportunistic fungal pathogen: Geographic and temporal trends from the ARTEMIS DISK Antifungal Surveillance Program, 2001 to 2005. *Journal of Clinical Microbiology*. 46 (2), 515–521. Available from: doi:10.1128/JCM.01915-07.

Preuner, S. & Lion, T. (2013) Species-specific identification of a wide range of clinically relevant fungal pathogens by the Luminex® xMAP technology. In: Louise O'Connor & Barry Glynn (eds.). *Humana Press*. Methods in Molecular Biology. Totowa, NJ, Humana Press. 119–139. Available from: doi:10.1007/978-1-62703-257-5_9.

Pryce, T.M., Palladino, S., Price, D.M., Gardam, D.J., et al. (2006) Rapid identification of fungal pathogens in BacT/ALERT, BACTEC, and BBL MGIT media using Polymerase Chain Reaction and DNA sequencing of the internal transcribed spacer regions. *Diagnostic Microbiology and Infectious Disease*. 54 (4), 289–

297. Available from: doi:10.1016/j.diagmicrobio.2005.11.002.

Public Health England (2017) Voluntary surveillance of candidaemia in England, Wales and Northern Ireland. *Health protection Report [serial online]*.12 (34).

Rautemaa-Richardson, R., Rautemaa, V., Al-Wathiqi, F., Moore, C.B., et al. (2018) Impact of a diagnostics-driven antifungal stewardship programme in a UK tertiary referral teaching hospital. *Journal of Antimicrobial Chemotherapy*. 73 (12), 3488–3495. Available from: doi:10.1093/jac/dky360.

Reinwald, M., Spiess, B., Heinz, W.J., Vehreschild, J.J., et al. (2012) Diagnosing pulmonary aspergillosis in patients with hematological malignancies: a multicenter prospective evaluation of an *Aspergillus* PCR assay and a galactomannan ELISA in bronchoalveolar lavage samples. *European Journal of Haematology*. 89 (2), 120–127. Available from: doi:10.1111/j.1600-0609.2012.01806.x.

Reyes-Montes, M., Duarte-Escalante, E., Frías-De-León, M., Martínez-Herrera, E., et al. (2018) Molecular diagnosis of invasive aspergillosis. In: *Molecular Medicine*. IntechOpen. 1–24. Available from: doi:10.5772/intechopen.78694.

Rhodes, J., Abdolrasouli, A., Farrer, R.A., Cuomo, C.A., et al. (2018) Genomic epidemiology of the UK outbreak of the emerging human fungal pathogen *Candida auris*. *Emerging Microbes and Infections*. 7 (1), 43. Available from: doi:10.1038/s41426-018-0045-x.

Robert, V., Szöke, S., Eberhardt, U., Cardinali, G., et al. (2011) The quest for a general and reliable fungal DNA barcode. *The Open Apllied Informatics Journal*. 5 (1), 45–61. Available from: doi:10.2174/1874136301105010045.

De Rosa, F.G., Aldieri, C., Cavallo, R., Petrolo, A., et al. (2015) The effect on mortality of fluconazole or echinocandins treatment in candidemia in internal medicine wards. *PLoS ONE*. 10 (5), 1–9. Available from:

doi:10.1371/journal.pone.0125149.

Ruhnke, M. (2014) Antifungal stewardship in invasive *Candida* infections. *Clinical Microbiology and Infection*. 20 (6), 11–18. Available from: doi:10.1111/1469-0691.12622.

Ruhnke, M., Behre, G., Buchheidt, D., Christopeit, M., et al. (2018) Diagnosis of invasive fungal diseases in haematology and oncology: 2018 update of the recommendations of the infectious diseases working party of the German society for hematology and medical oncology (AGIHO). *Mycoses*. 61, 796–813. Available from: doi:10.1111/myc.12838.

Ruiz-Herrera, J., Victoria Elorza, M., Valentín, E. & Sentandreu, R. (2006) Molecular organization of the cell wall of *Candida albicans* and its relation to pathogenicity. *FEMS Yeast Research*. 6 (1), 14–29. Available from: doi:10.1111/j.1567-1364.2005.00017.x.

Safavieh, M., Coarsey, C., Esiobu, N., Memic, A., et al. (2017) Advances in *Candida* detection platforms for clinical and point-of-care applications. *Critical Reviews in Biotechnology*. 37 (4), 441–458. Available from: doi:10.3109/07388551.2016.1167667.

Sanguinetti, M. & Posteraro, B. (2017) Identification of molds by Matrix-Assisted Laser Desorption Ionization-Time of Flight Mass Spectrometry. *Journal of clinical microbiology*. 55 (2), 369–379. Available from: doi:10.1128/JCM.01640-16.

Santoro, S.W. & Joyce, G.F. (1997) A general purpose RNA-cleaving DNA enzyme. *Proceedings of the National Academy of Sciences of the United States of America*. 94 (9), 4262–4266. Available from: doi:10.1073/pnas.94.9.4262.

Schabereiter-Gurtner, C., Selitsch, B., Rotter, M.L., Hirschl, A.M., et al. (2007) Development of novel real-time PCR assays for detection and differentiation of

eleven medically important *Aspergillus* and *Candida* species in clinical specimens. *Journal of Clinical Microbiology*. 45 (3), 906–914. Available from: doi:10.1128/JCM.01344-06.

Schelenz, S., Hagen, F., Rhodes, J.L., Abdolrasouli, A., et al. (2016) First hospital outbreak of the globally emerging *Candida auris* in a European hospital. *Antimicrobial Resistance and Infection Control*. 5 (35), 1–7. Available from: doi:10.1186/s13756-016-0132-5.

Schoch, C.L., Seifert, K.A., Huhndorf, S., Robert, V., et al. (2012) Nuclear ribosomal Internal Transcribed Spacer (ITS) region as a universal DNA barcode marker for Fungi. *Proceedings of the National Academy of Sciences of the United States of America*. 109 (16), 6241–6246. Available from: doi:10.1073/pnas.1117018109.

Sexton, D.J., Bentz, M.L., Welsh, R.M. & Litvintseva, A.P. (2018) Evaluation of a new T2 Magnetic Resonance assay for rapid detection of emergent fungal pathogen *Candida auris* on clinical skin swab samples. *Mycoses*. 61 (10), 786–790. Available from: doi:10.1111/myc.12817.

Shor, E. & Perlin, D.S. (2015) Coping with stress and the emergence of multidrug resistance in fungi. *PLoS Pathogens*. 11 (3), 1–7. Available from: doi:10.1371/journal.ppat.1004668.

da Silva Dantas, A., Lee, K.K., Raziunaite, I., Schaefer, K., et al. (2016) Cell biology of *Candida albicans*–host interactions. *Current Opinion in Microbiology*. 34, 111–118. Available from: doi:10.1016/j.mib.2016.08.006.

Silverman, S.K. (2008) Nucleic acid enzymes (ribozymes and deoxyribozymes): *In vitro* selection and application. *Wiley Encyclopedia of Chemical Biology*. 1–17. Available from: doi:10.1002/9780470048672.wecb406.

Spanu, T., Posteraro, B., Fiori, B., D'Inzeo, T., et al. (2012) Direct MALDI-TOF Mass Spectrometry assay of blood culture broths for rapid identification of *Candida*

species causing bloodstream infections: An observational study in two large microbiology laboratories. *Journal of Clinical Microbiology*. 50 (1), 176–179. Available from: doi:10.1128/JCM.05742-11.

Straub, J., Paula, H., Mayr, M., Kasper, D., et al. (2017) Diagnostic accuracy of the ROCHE Septifast PCR system for the rapid detection of blood pathogens in neonatal sepsis - A prospective clinical trial Brenda A Wilson (ed.). *PLoS ONE*. 12 (11), 1–12. Available from: doi:10.1371/journal.pone.0187688.

Sulaiman, I., Jacobs, E., Simpson, S. & Kerdahi, K. (2014) Molecular identification of isolated fungi from unopened containers of greek yogurt by DNA sequencing of internal transcribed spacer region. *Pathogens*. 3 (3), 499–509. Available from: doi:10.3390/pathogens3030499.

Taghizadeh-Armaki, M., Saber, S., Hedayati, M.T., Seyedmousavi, S., et al. (2017) Effect of involved *Aspergillus* species on galactomannan in bronchoalveolar lavage of patients with invasive aspergillosis. *Journal of Medical Microbiology*. 66 (7), 898–904. Available from: doi:10.1099/jmm.0.000512.

Thain, L., Greenman, J., Docker, P.T., Greenway, G.M., et al. (2009) The use of carrier RNA to enhance DNA extraction from microfluidic-based silica monoliths. *Analytica Chimica Acta*. 652 (1–2), 231–233. Available from: doi:10.1016/j.aca.2009.03.038.

Theel, E.S. & Doern, C.D. (2013) β-D-Glucan testing is important for diagnosis of invasive fungal infections. *Journal of Clinical Microbiology*. 51 (11), 3478–3483. Available from: doi:10.1128/JCM.01737-13.

Tirodker, U.H., Nataro, J.P., Smith, S., LasCasas, L., et al. (2003) Detection of fungemia by Polymerase Chain Reaction in critically ill neonates and children. *Journal of Perinatology*. 23 (2), 117–122. Available from: doi:10.1038/sj.jp.7210868.

Trovato, L., Astuto, M., Castiglione, G., Scalia, G., et al. (2019) Diagnostic surveillance by *Candida albicans* germ tube antibody in intensive care unit patients. *Journal of Microbiology, Immunology and Infection*. Available from: doi:10.1016/J.JMII.2019.02.001.

Trovato, L., Betta, P., Romeo, M.G. & Oliveri, S. (2012) Detection of fungal DNA in lysis-centrifugation blood culture for the diagnosis of invasive candidiasis in neonatal patients. *Clinical Microbiology and Infection*. 18 (3), E63-5. Available from: doi:10.1111/j.1469-0691.2011.03731.x.

Turner, S.A. & Butler, G. (2014) The *Candida* pathogenic species complex. *Cold Spring Harbor Perspectives in Medicine*. 4 (9), 1–17. Available from: doi:10.1101/cshperspect.a019778.

Valero, C., De La Cruz-Villar, L., Zaragoza, Ó. & Buitrago, M.J. (2016) New panfungal real-time PCR assay for diagnosis of invasive fungal infections. *Journal of Clinical Microbiology*. 54 (12), 2910–2918. Available from: doi:10.1128/JCM.01580-16.

Vanittanakom, N., Cooper, C.R., Fisher, M.C., Sirisanthana, T., et al. (2006) *Penicillium marneffei* infection and recent advances in the epidemiology and molecular biology aspects. *Clinical microbiology reviews*. 19 (1), 95–110. Available from: doi:10.1128/CMR.19.1.95-110.2006.

Ven, K., Safdar, S., Dillen, A., Lammertyn, J., et al. (2019) Re-engineering 10–23 core DNA- and MNAzymes for applications at standard room temperature. *Analytical and Bioanalytical Chemistry*. 411 (1), 205–215. Available from: doi:10.1007/s00216-018-1429-4.

Vergidis, P., Razonable, R.R., Wheat, L.J., Estes, L., et al. (2014) Reduction in false-positive *Aspergillus* serum galactomannan enzyme immunoassay results associated with use of piperacillin-tazobactam in the United States. *Journal of*

Clinical Microbiology. 52 (6), 2199–2201. Available from: doi:10.1128/JCM.00285-14.

Vijayakumar, R., Giri, S. & Kindo, A.J. (2012) Molecular species identification of *Candida* from blood samples of intensive care unit patients by Polymerase Chain Reaction - Restricted Fragment Length Polymorphism. *Journal of Laboratory Physicians*. 4 (1), 1–4. Available from: doi:10.4103/0974-2727.98661.

Vilgalys, R. & Hester, M. (1990) Rapid genetic identification and mapping of enzymatically amplified ribosomal DNA from several *Cryptococcus* species. *Journal of Bacteriology*. 172 (8), 4238–4246.

Walsh, T.J., Wissel, M.C., Grantham, K.J., Petraitiene, R., et al. (2011) Molecular detection and species-specific identification of medically important *Aspergillus* species by real-time PCR in experimental invasive pulmonary aspergillosis. *Journal of Clinical Microbiology*. 49 (12), 4150–4157. Available from: doi:10.1128/JCM.00570-11.

Wattal, C., Oberoi, J.K., Goel, N., Raveendran, R., et al. (2017) Matrix-assisted Laser Desorption Ionization Time of Flight Mass Spectrometry (MALDI-TOF MS) for rapid identification of micro-organisms in the routine clinical microbiology laboratory. *European Journal of Clinical Microbiology and Infectious Diseases*. 36 (5), 807–812. Available from: doi:10.1007/s10096-016-2864-9.

Webb, B.J., Ferraro, J.P., Rea, S., Kaufusi, S., et al. (2018) Epidemiology and clinical features of invasive fungal infection in a us health care network. *Open Forum Infectious Diseases*. 5 (8), 1–8. Available from: doi:10.1093/ofid/ofy187.

Welsh, R.M., Bentz, M.L., Shams, A., Houston, H., et al. (2017) Survival, persistence, and isolation of the emerging multidrug-resistant pathogenic yeast *Candida auris* on a plastic health care surface. *Journal of Clinical Microbiology*. 55 (10), 2996–3005. Available from: doi:10.1128/JCM.00921-17.

White, P.L., Perry, M.D. & Barnes, R.A. (2009) Polymerase Chain Reaction diagnosis of fungal disease: Finally coming of age. *Current Fungal Infection Reports*. 3 (4), 207–215. Available from: doi:10.1007/s12281-009-0029-3.

White, P.L., Perry, M.D., Loeffler, J., Melchers, W., et al. (2010) Critical stages of extracting DNA from *Aspergillus fumigatus* in whole-blood specimens. *Journal of Clinical Microbiology*. 48 (10), 3753–3755. Available from: doi:10.1128/JCM.01466-10.

White, T.J., Bruns, T., Lee, S. & Taylor, J. (1990) Amplification and direct sequencing of fungal ribosomal RNA genes for phylogenetics. In: *PCR Protocols: A Guide to Methods and Applications*. Academic Press. 315–322. Available from: doi:10.1016/b978-0-12-372180-8.50042-1.

Wickes, B.L. & Wiederhold, N.P. (2018) Molecular diagnostics in medical mycology. *Nature Communications*. 9 (1), 5135. Available from: doi:10.1038/s41467-018-07556-5.

Wisplinghoff, H., Ebbers, J., Geurtz, L., Stefanik, D., et al. (2014) Nosocomial bloodstream infections due to *Candida* spp. in the USA: Species distribution, clinical features and antifungal susceptibilities. *International Journal of Antimicrobial Agents*. 43 (1), 78–81. Available from: doi:10.1016/j.ijantimicag.2013.09.005.

Xu, J. (2016) Fungal DNA barcoding Sarah Adamowicz (ed.). *Genome*. 59 (11), 913–932. Available from: doi:10.1201/b18645-8.

Yuan, B.F., Xue, Y., Luo, M., Hao, Y.H., et al. (2007) Two DNAzymes targeting the telomerase mRNA with large difference in Mg2+ concentration for maximal catalytic activity. *International Journal of Biochemistry and Cell Biology*. 39 (6), 1119–1129. Available from: doi:10.1016/j.biocel.2007.03.004.

Zaragoza, R., Pemán, J., Quindós, G., Iruretagoyena, J.R., et al. (2009) Kinetic patterns

of *Candida albicans* germ tube antibody in critically ill patients: Influence on mortality. *Clinical and Vaccine Immunology*. 16 (10), 1527–1528. Available from: doi:10.1128/CVI.00183-09.

Zeller, I., Schabereiter-Gurtner, C., Mihalits, V., Selitsch, B., et al. (2017) Detection of fungal pathogens by a new broad range real-time PCR assay targeting the fungal ITS2 region. *Journal of Medical Microbiology*. 66 (10), 1383–1392. Available from: doi:10.1099/jmm.0.000575.

Zhang, S.S., Chen, D. & Lu, Q. (2012) An improved protocol and a new grinding device for extraction of genomic DNA from microorganisms by a two-step extraction procedure. *Genetics and Molecular Research*. 11 (2), 1532–1543. Available from: doi:10.4238/2012.May.21.10.

Zhou, W., Ding, J. & Liu, J. (2017) Theranostic DNAzymes. *Theranostics*. 7 (4), 1010–1025. Available from: doi:10.7150/thno.17736.

Zhou, W., Li, H., Zhang, Y., Huang, M., et al. (2017) Diagnostic value of galactomannan antigen test in serum and bronchoalveolar lavage fluid samples from patients with nonneutropenic invasive pulmonary aspergillosis. *Journal of Clinical Microbiology*. 55 (7), 2153–2161. Available from: doi:10.1128/jcm.00345-17.

Zuza-Alves, D.L., Silva-Rocha, W.P. & Chaves, G.M. (2017) An update on *Candida tropicalis* based on basic and clinical approaches. *Frontiers in Microbiology*. 8, 1–25. Available from: doi:10.3389/fmicb.2017.01927.